SYNTHESIS, CHARACTERIZATION, AND MAGNETIC PROPERTIES OF SUBSTITUTED PEROVSKITE-TYPE MANGANATES AND RELATED OXIDES

THESIS

SUBMITTED TO THE

UNIVERSITY OF PUNE

FOR THE DEGREE OF

DOCTOR OF PHILOSOPHY

IN CHEMISTRY

By

Joseph Joly V. L

Physical Chemistry Division

National Chemical Laboratory

Pune 411008

India

June 2004

CERTIFICATE

Certified that the work incorporated in the thesis

Synthesis, Characterization, and Magnetic Properties of Substituted Perovskite-type Manganates and Related Oxides

submitted by Mr. Joseph Joly V. L was carried out by the candidate under our supervision. Such material as has been obtained from other sources has been duly acknowledged in the thesis.

Dr. P. A. Joy
(Research Co-guide)

Dr. S. K. Date
(Research Guide)

Dedicated to

.....to each one, who cares and teaches.

Acknowledgements

I would like to express my irrefragable gratitude to Dr. S. K. Date for providing an incredible opportunity to pursue my career as a Ph. D. student, for his comely advice, concern, and encouragement which proved to inspire me, enliven me....

My heartfelt delectation is due to Dr. P. A. Joy for the extensive discussions on the splendiferous yet enigmatic world of magnetism, for his suggestions, for scrupulously reading this thesis, and setting me straight where i went wrong.....

Many thanks go to the director, National Chemical Laboratory, for allowing me to carry out my research in a prestigious and well equipped laboratory.

I owe special thanks to the head, physical chemistry division, to Dr. C. S Gopinath for the professional expertise in x-ray photoelectron spectroscopy studies and invaluable insights, to Dr. S. D. Kulkarni, Dr. N. R. Pawaskar, Dr. V. Ravi and Dr. K. Sreedhar for their timely help and support.

Dr. Joy and Indira teacher deserve special thanks for being very much supportive, affectionate and making me feel at home.

I would like to thank all my colleagues for their immense cooperation and providing an excellent working ambience.

Inexplicable admiration is felt to all my friends who have directly or indirectly supported and nudged me with my thesis work and left me with many admirable memories.....

UGC-India is acknowledged for the financial support.

It would be very thoughtless of me if I fail to honor my family members for the love and care they bestowed on me...

V. L. Joseph Joly

Contents

Abstract **1**

1 Introduction **3**

1.1 Chronicle 4

1.2 Structural aspects 6

1.2.1 Structural distortions from relative ionic sizes 8

1.2.2 Structural changes by localized electrons 11

1.2.3 Structural changes by collective electrons 13

1.2.4 Structural transformations due to B ion ordering 13

1.3 Magnetism: An introduction 14

1.3.1 Classical view of paramagnetism 15

1.3.2 Quantum mechanical approach 16

1.3.3 Cooperative magnetic phenomena 19

1.4 Magnetic and structural properties of Mn-site substituted $LaMnO_3$. . 26

1.4.1 The parent compound, $LaMnO_{3\pm\delta}$. 29

1.4.2 d^0, d^{10}- substituents 31

1.4.3 d^n- substituents 38

1.4.4 Conclusions 48

2 Experimental **51**

2.1 Material synthesis 51

2.1.1 Ceramic or solid-state reaction method 52
2.1.2 Low-temperature method 53
2.2 Estimation of Mn^{+4} content 55
2.3 Powder X-ray Diffraction (XRD) 56
2.4 X-ray Photoelectron Spectroscopy(XPS) 58
2.5 Magnetic measurements 59
2.5.1 Vibrating Sample Magnetometer (VSM) 60
2.5.2 AC-susceptometer 62

3 Co substituted $LaMnO_3$ **65**
3.1 La_2MnCoO_6 ($x = 0.5$) 68
3.1.1 Background 69
3.1.2 Powder XRD studies 70
3.1.3 Magnetic measurements 73
3.1.4 AC-susceptibility studies 79
3.1.5 Determination of Spin-states of Mn and Co 82
3.2 Mn-rich compositions ($0 < x < 0.5$) 94
3.2.1 Background 94
3.2.2 Magnetic measurements 95
3.2.3 Powder XRD studies 107
3.3 Co-rich compositions ($0.5 < x < 1$) 111
3.3.1 Background 112
3.3.2 Magnetic measurements 112
3.3.3 Powder XRD studies 117
3.4 Conclusions 118

4 Studies on La_2MnNiO_6 **124**
4.1 Background 124

4.2 Synthesis 126
4.3 Magnetic measurements 127
4.3.1 HT samples 128
4.3.2 LT samples 129
4.4 Powder XRD studies 132
4.4.1 HT samples 133
4.4.2 LT samples 135
4.5 Determination of Spin-states of Mn and Ni 136
4.5.1 Paramagnetic susceptibility 136
4.5.2 Non-magnetic substitution with isovalent ion 139
4.5.3 XPS studies 141
4.5.4 Origin of ferromagnetism in La_2MnNiO_6 147
4.6 Conclusions 150

5 Studies on $La_2MnCo_{1-x}M_xO_6$ 152

5.1 $La_2MnCo_{1-x}Ni_xO_6$ 153
5.1.1 Background 153
5.1.2 Synthesis 154
5.1.3 Magnetic measurements 155
5.1.4 Powder XRD studies 163
5.1.5 Origin of ferromagnetism in $La_2MnCo_{1-x}Ni_xO_6$ 167
5.1.6 Conclusions 171
5.2 $La_2MnCo_{1-x}Fe_xO_6$ 172
5.2.1 Background 172
5.2.2 Synthesis 173
5.2.3 Powder XRD studies 174
5.2.4 Magnetic measurements 175

5.2.5 Conclusions 185
5.3 $La_2MnCo_{1-x}Al_xO_6$ 185
5.3.1 Background 185
5.3.2 Synthesis 186
5.3.3 Powder XRD studies 186
5.3.4 Magnetic measurements 190
5.3.5 Conclusions 194

6 Studies on $RE_2\mathbf{Mn}M\mathbf{O}_6$ 195
6.1 Background 195
6.2 Synthesis 198
6.3 Powder XRD studies 199
6.4 Magnetic measurements 205
6.5 Conclusions 220

Bibliography 223

List of Publications 240

List of Tables

1.1 The ionic radii in Å and electronic configurations of the d^0, d^{10}-substituents. 32

1.2 The ionic radii in Å , and electronic configurations of the d^n-substituents. 39

3.1 Comparison of μ_{so} and μ_{eff} for various spin-states of Mn and Co in the high-T_c (HTC) and low-T_c (LTC) phases of La_2MnCoO_6 84

3.2 Experimental and calculated ferromagnetic moments of Al substituted La_2MnCoO_6, annealed at 700 °C. The values are for the simple perovskite formula $LaMn_{0.5}Co_{0.5}O_3$. 87

4.1 Spin-only moments (μ_{so}) for various spin-states of Mn and Ni in La_2MnNiO_6 (calculations are based on the simple perovkite formula, $LaMn_{0.5}Ni_{0.5}O_3$).138

4.2 Mn $2p_{3/2}$ and Ni $2p_{3/2}$ XPS BE in the two different ferromagnetic phases of La_2MnNiO_6 (LMN) and Nd_2MnNiO_6 (NMN). 146

List of Figures

1.1 The perovskite structure: (a) The B ions at the origin, in cubic basis, (b) the A ions at the origin, in cubic basis, (c) the A cation at the origin, in hexagonal basis. The anion is oxygen,O. 7

1.2 (a) Hexagonal unit cell, showing the direct correlation of c with cubic basis, (b) stacking of corner-shared octahedra. 9

1.3 (a) View along triad axis, (b) pure hexagonal stacking, (c) view along tetrad axis, (d) tetragonal tilt. 10

1.4 Generic temperature dependence of inverse susceptibility, in different types of magnetism. 20

1.5 (a) orthogonality of e_g and $p\pi$ orbitals, (b) orthogonality of t_{2g} and $p\sigma$ orbitals, (c) both e_g half filled, (d) one half filled and the other empty, (e) both e_g empty. 24

2.1 Diffraction represented in reciprocal space. 57

2.2 Vibrating Sample Magnetometer. 61

2.3 Schematic diagram of AC-susceptometer. 63

3.1 Powder XRD patterns of La_2MnCoO_6; (a) low-temperature synthesized sample annealed at different temperatures and (b) high-temperature synthesized sample annealed at 1000 °C for 96 h and 1300 °C for 96 h. 71

3.2 ZFC magnetization curves (H = 50 Oe) of x = 0.5, annealed in the temperature range 200-700 °C. 74

3.3 ZFC magnetization curves (H = 50 Oe) of x = 0.5, annealed in the temperature range 700-1350 °C. 74
3.4 FC and ZFC magnetization curves of the two phases of $x = 0.5$, H = 50 Oe. 75
3.5 Magnetic field dependence of isothermal magnetization of the La_2MnCoO_6 sample annealed at 200 °C. The numbers on the curves indicate the temperature in K. Inset: Temperature variation of the magnetization at 82 K of the low-T_c phase, measured at 15 kOe. 77
3.6 ZFC (H = 50 Oe) magnetization curves of the samples synthesized by the ceramic method and heated at different temperatures as indicated. 79
3.7 Comparison of the zero field cooled magnetization curves of the low-temperature synthesized La_2MnCoO_6 annealed at 200, 700 and 1300 °C, measured at 50 Oe. The dotted curve is the derivative of magnetization, dM/dT. 80
3.8 Temperature variation of the AC-susceptibility of the low-T_c phase of La_2MnCoO_6, measured at three different frequencies. 81
3.9 AC-susceptibility of Ni substituted La_2MnCoO_6, measured at 210 Hz and 2 Oe. 81
3.10 Temperature variation of inverse paramagnetic susceptibility of the two different phases of La_2MnCoO_6. 83
3.11 Temperature variation of magnetization (H = 5000 Oe) of La_2MnCoO_6 (LMC) and the Al-substituted samples, $La_2Mn_{0.8}Al_{0.2}CoO_6$ (LMAC), and $La_2MnCo_{0.8}Al_{0.2}O_6$ (LMCA). 86
3.12 XPS valence band spectra of La_2MnCoO_6, annealed at 700 and 1300 °C. Inset: XPS valence band spectra of the unscraped surface of the sample annealed at 700 °C. 88

3.13 Co2p XPS of La_2MnCoO_6, (a) high-T_c phase, (b) sample heated to 1200 °C, (c) sample heated to 1300 °C for 6 h, and (d) low-T_c phase. 89
3.14 Mn 2p XPS of La_2MnCoO_6, (a) high-T_c phase, (b) sample heated to 1200 °C, (c) sample heated to 1300 °C for 6 h, and (d) low-T_c phase. 90
3.15 Mn 2p XPS of La_2MnCoO_6 annealed at 200, 700, 1300 °C. 92
3.16 Co 2p XPS of La_2MnCoO_6 annealed at 200, 700, 1300 °C. 93
3.17 Comparison of the ZFC magnetization curves of samples annealed at 200 °C, for different compositions. 96
3.18 ZFC magnetization curves of $x = 0.125$, for samples annealed at different temperatures 97
3.19 ZFC magnetization curves of $x = 0.25$, for samples annealed at different temperatures 97
3.20 ZFC magnetization curves of $x = 0.375$, for samples annealed at different temperatures 98
3.21 ZFC magnetization curves of $x = 0.3$, for samples annealed at different temperatures 99
3.22 Comparison of the ZFC magnetization curves of all compositions, for samples annealed at 700 °C for 12 hours. 100
3.23 ZFC magnetization curves of all compositions, for samples annealed at 1000 °C 103
3.24 ZFC magnetization curves of all compositions, for samples annealed at 1300 °C 105
3.25 ZFC magnetization curves of $x = 0.2$ composition synthesized by the ceramic method and heated at different temperatures, as indicated. . 106
3.26 ZFC magnetization curves of $x = 0.3$ composition synthesized by the ceramic method and heated at different temperatures, as indicated. . 106
3.27 XRD patterns of Mn-rich $LaMn_{1-x}Co_xO_3$, annealed at 200°C. 108

3.28 XRD patterns of $x = 0.375$ in $LaMn_{1-x}Co_xO_3$ compositions, annealed at different temperatures. 108
3.29 XRD patterns of low-temperature synthesized $LaMn_{1-x}Co_xO_3$, annealed at 1000 °C. 109
3.30 XRD patterns of Mn-rich $LaMn_{1-x}Co_xO_3$ compositions, annealed at 1300°C. 110
3.31 Variation of orthorhombic cell parameters as a function of the concentration of Co, for Mn-rich compositions, for samples annealed at 1300 °C. 111
3.32 Comparison of the ZFC magnetization curves of $LaMn_{0.4}Co_{0.6}O_3$ samples prepared by ceramic (a) and low-temperature (b) methods and annealed at different temperatures. The magnetization curves of the two phases of La_2MnCoO_6 are shown as thick lines for comparison. . 113
3.33 Comparison of the ZFC magnetization curves of $LaMn_{0.2}Co_{0.8}O_3$ samples prepared by ceramic (a) and low-temperature (b) methods and annealed at different temperatures. The arrows indicate the Curie temperatures of the two phases of La_2MnCoO_6. 114
3.34 Comparison of the ZFC magnetization curves of $LaMn_{0.7}Co_{0.3}O_3$ samples prepared by ceramic (a) and low-temperature (b) methods and annealed at two different temperatures. The arrow indicate the T_c of the high-T_c phase of La_2MnCoO_6. 115
3.35 Magnetization curves for $x \leq 0.5$ (a) and $x > 0.5$ (b), synthesized by the low-temperature method and heated at 1000 °C. The curves of $x = 0.7$ and 0.8 are multiplied by 2 and 10, respectively, to show the weak magnetic transition at ∼230 K. 116
3.36 XRD patterns of $LaMn_{1-x}Co_xO_3$, annealed at or above 1300°C. . . . 118
3.37 Variation of cell parameters of Co-rich samples assigned rhombohedral. 119

3.38 Comparison of XRD patterns of ceramic (HT) and low-temperature (LT) synthesized samples, annealed at different temperatures 121
3.39 Variation of T_c and magnetization (measured at 82 K and 15 kOe) as a function of x in $LaMn_{1-x}Co_xO_3$. • - ceramic method, ∘ - low-temperature method, △ - from [Tro00]. For $x = 0.5$, T_c and M of the two phases of the compound are shown. 122
4.1 ZFC magnetization ($H = 50$ Oe) curves of La_2MnNiO_6 synthesized by the ceramic method, annealed at 1100, 1200 and 1300 °C. Inset: temperature variation of magnetization at $H = 5000$ Oe. 128
4.2 ZFC magnetization ($H = 50$ Oe) curves of the low-temperature synthesized La_2MnNiO_6, annealed in the temperature range 200–1300 °C. 129
4.3 ZFC magnetization ($H = 50$ Oe) curves of La_2MnNiO_6: HT sample annealed at 1300 °C (LMN-HT), LT samples annealed at 400 (LMN400) and 1300 °C (LMN1300), and a 2:1 physical mixture of LMN400 and LMN1300 (mix-2:1). 130
4.4 ZFC magnetization curves of the two phases of La_2MnNiO_6, LMN400 and LMN1300. Inset: ZFC magnetization curves of low-temperature synthesized Nd_2MnNiO_6, annealed at 400 (NMN400) and 1300 °C (NMN1300). 131
4.5 Powder XRD patterns of La_2MnNiO_6, annealed at different temperatures, after synthesized by ceramic and low-temperature methods. . . 134
4.6 Temperature variation of the inverse of the paramagnetic susceptibility of LMN400 and LMN1300. 137
4.7 Temperature variation of the magnetization of La_2MnNiO_6 (LMN), $La_2MnNi_{0.8}Al_{0.2}O_6$ (LMNA), and $La_2Mn_{0.8}Al_{0.2}NiO_6$ (LMAN), annealed at 1300 °C; $H = 5000$ Oe. 140
4.8 Mn $2p$ XPS of LMN400 and LMN1300. 142

4.9 Ni $2p$ XPS of LMN400 and LMN1300, along with the La $3d_{3/2}$ XPS of La_2MnCoO_6 (LMC). 143
4.10 Mn and Ni $3p$ XPS of LMN400 and LMN1300. 144
4.11 Mn $2p$ XPS of NMN400 and NMN1300. 145
4.12 Ni $2p$ XPS of NMN400 and NMN1300. 146
5.1 Comparison of the ZFC magnetization ($H = 50$ Oe) curves of the two different phases of La_2MnCoO_6 and La_2MnNiO_6. 156
5.2 ZFC magnetization ($H = 50$ Oe) curves of $La_2MnCo_{0.5}Ni_{0.5}O_6$ annealed at 200 °C. 157
5.3 ZFC magnetization ($H = 50$ Oe) curves of different compositions in $La_2MnCo_{1-x}Ni_xO_6$ annealed at 700 °C. 157
5.4 ZFC magnetization ($H = 50$ Oe) curves of $La_2MnCo_{0.5}Ni_{0.5}O_6$, annealed at different temperatures. 159
5.5 ZFC magnetization ($H = 50$ Oe) curves of different compositions in $La_2MnCo_{1-x}Ni_xO_6$ showing higher Curie temperatures. 159
5.6 ZFC magnetization ($H = 50$ Oe) curves of the different phases of $La_2MnCo_{1-x}Ni_xO_6$. The numbers on the curves indicate the annealing temperatures in °C. 161
5.7 Variation of T_cs of the two phases, with x, in $La_2MnCo_{1-x}Ni_xO_6$. The solid lines are the calculated values as discussed in the text. 162
5.8 Powder XRD patterns of $La_2MnCo_{0.5}Ni_{0.5}O_6$, synthesized by low-temperature method and annealed at 200, 900, and 1300 °C. 163
5.9 Powder XRD patterns of $La_2MnCo_{1-x}Ni_xO_6$,synthesized by low-temperature method and annealed at intermediate temperatures. 164
5.10 Powder XRD patterns of $La_2MnCo_{1-x}Ni_xO_6$, synthesized by low-temperature method and annealed at 1300-1350 °C. 165

5.11 Parts of the powder XRD patterns indicative of structural phase transition with increasing x in $La_2MnCo_{1-x}Ni_xO_6$, for samples annealed at 1300-1350 °C. a–e are the regions identified in the previous figure. . . 166
5.12 Variation of lattice parameters with Ni concentration in low-T_c phases. 167
5.13 Powder x-ray diffraction patterns of different compositions in $La_2MnCo_{1-x}Fe_xO_6$. 174
5.14 Variation of the lattice parameters as a function of x in $La_2MnCo_{1-x}Fe_xO_6$. 175
5.15 ZFC magnetization (H = 50 Oe) curves of different compositions in $La_2MnCo_{1-x}Fe_xO_6$. Inset: magnetic hysteresis of the x = 0.8 composition measured at 228 K. 176
5.16 Field cooled (FC) and zero field cooled (ZFC) magnetization for x = 0 and 0.6 in $La_2MnCo_{1-x}Fe_xO_6$. 177
5.17 Magnetic hysteresis, recorded at 82 K, for different values of x in $La_2MnCo_{1-x}Fe_xO_6$. 177
5.18 Variation of T_p (top), H_c (middle), and M (bottom) as a function of x in $La_2MnCo_{1-x}Fe_xO_6$. The solid line in the bottom panel is the estimated reduction in M from that of the x = 0 composition, $M_x = M_0(1-x)$. 179
5.19 Powder XRD patterns for different compositions in $La_2MnCo_{1-x}Al_xO_6$. 187
5.20 Evolution of peaks in two different 2θ regions (indicated by arrows in the previous figure) in the powder XRD patterns of $La_2MnCo_{1-x}Al_xO_6$, with x. 188
5.21 Variation of the lattice parameters, as a function of x in $La_2MnCo_{1-x}Al_xO_6$. inset: variation of monoclinic and rhombohedral angles, as a function of x. 189
5.22 Zero field cooled magnetization curves of different compositions in the series $La_2MnCo_{1-x}Al_xO_6$, measured at 50 Oe. 191

5.23 Magnetization as a function of field, measured at 82 K, for different compositions in $La_2MnCo_{1-x}Al_xO_6$. 192
5.24 Variation of Curie temperature and saturation magnetization at 82 K and 15 kOe, as a function of x in $La_2MnCo_{1-x}Al_xO_6$. 193
6.1 Powder XRD patterns of low-temperature synthesized RE_2MnCoO_6, including that of La_2MnCoO_6, annealed at 200 °C. 199
6.2 XRD patterns of low-temperature synthesized RE_2MnNiO_6,including that of La_2MnNiO_6, annealed at 200 °C. 200
6.3 Powder XRD patterns of low-temperature synthesized RE_2MnCoO_6, including that of La_2MnNiO_6, annealed at 700–1000 °C. * - Yb_2O_3. . 201
6.4 Powder XRD patterns of low-temperature synthesized RE_2MnCoO_6, including that of La_2MnCoO_6, annealed at 1300-1350 °C. * - Er_2O_3 and Yb_2O_3. 202
6.5 XRD patterns of low-temperature synthesized RE_2MnNiO_6, including that of La_2MnNiO_6, annealed at 1300-1350 °C. * - rare-earth oxides. . 203
6.6 Variation of lattice parameters, as a function of the nine-coordinated ionic radii of RE in RE_2MnCoO_6, annealed at 1300-1350 °C. 204
6.7 Variation of lattice parameters, as a function of the nine-coordinated ionic radii of RE in RE_2MnNiO_6, annealed at 1300-1350 °C. 204
6.8 ZFC magnetization curves of Pr_2MnCoO_6, annealed at different temperatures. 206
6.9 ZFC magnetization curves of Nd_2MnCoO_6, annealed at different temperatures. 207
6.10 ZFC magnetization curves of some RE_2MnCoO_6 compositions, annealed at 200 °C. Inset: comparison of La (labelled LaCo & LaNi) and Nd (labelled NdCo & NdNi) compounds of $RE_2Mn{M}O_6$ 208

6.11 ZFC magnetization of the high-T_c phases of RE_2MnCoO_6, obtained after annealing at 700 (for La–Eu), 1000 (for Gd–Er), and 1350 °C (for Yb). 209
6.12 Comparison of the ZFC magnetization curves of the high-T_c (thin lines) and low-T_c (thick lines) phases of RE_2MnCoO_6, H = 50 Oe and La_2MnCoO_6. 211
6.13 Variation of T_cs of the two phases of RE_2MnCoO_6 as a function of ionic radius of RE^{+3}, along with the difference in the T_cs (ΔT_c). . . . 212
6.14 Variation of the ionic radius of RE^{+3}, for nine-fold coordination [Sha76], with number of f-electrons. The inset shows the variation of the average Mn-O-Mn angle in $REMnO_3$ [Alo00] with the ionic radius of RE^{+3}. 213
6.15 Variation of T_cs of the two phases of RE_2MnCoO_6 with tolerance factor, t. 214
6.16 Comparison of ZFC magnetization curves of high-T_c phases RE_2MnCoO_6 and RE_2MnNiO_6, H = 50 Oe. 216
6.17 Variation of T_cs of the high-T_c phases RE_2MnCoO_6 and RE_2MnNiO_6 with the ionic radius of the rare-earth ions. 217
6.18 Variation of T_cs of high-T_c phases RE_2MnCoO_6 and RE_2MnNiO_6 with tolerance factor. 218
6.19 Variation of the one-electron spin-orbit coupling coefficient [The76], ζ, with the ionic radius of RE^{+3}. 219

Abstract

Substituted perovskite-type manganese oxides with the general formula $La_{1-x}D_xMnO_3$ (D = divalent alkaline-earth ion) have been studied since 1950. The antiferromagnetic $LaMnO_3$ becomes ferromagnetic by this type of substitution due to a concomitant change in the valency of manganese; from trivalent to tetravalent. The recent interest in these oxides stem from the observation of huge change in the electrical resistance, under a magnetic field, known as Colossal Magnetoresistance (CMR), in 1994. In the La-site substituted compounds, the interesting magnetic and electrical properties are derived from the difference in the spin-states of Mn ions when compared to that in $LaMnO_3$. Therefore, it can be expected that the effects derived from La-site substitution can be mimicked, to some extent, by the substitution of Mn, represented as $LaMn_{1-x}M_xO_3$ (M = Cr, Co, Ni, etc.). This latter class of compounds, which are equally important, but relatively underexplored is studied, in the present work. Similarly, a sub-class of Mn-site substituted compounds, called *double perovskites*, of the type RE_2MnMO_6 (RE = lanthanide ion), which can show a number of interesting properties like ordering of ions in specific lattice sites, charge disproportionation, etc., are also explored.

The major challenge in the study of $LaMn_{1-x}M_xO_3$ is the difficulty in underpinning the spin-states of the Mn-site ions, as evident from the contradicting reports in the literature. This ambiguity may be an intrinsic property of the compounds or can be due to inadequate processing or investigation. To understand and explain the observed properties – especially magnetic properties – of the Mn-site substituted manganate compositions, a meticulous and detailed investigation from the point of view of processing-structure-property correlation study is required. The thesis deals with these studies and is divided into six chapters.

A general introduction to the subject and a review of the previous studies on

Mn-site substitution of the perovskite-type manganates are treated in the first chapter. The finding that majority of the reports in the literature on these systems are contradictory, is illustrated.

Details of the methods of synthesis of the compounds studied in the present work and the principles of techniques and devices used for structural, electronic, and static/dynamic magnetic property studies are discussed in the second chapter.

Structural and magnetic properties of the $LaMn_{1-x}Co_xO_3$ compositions are presented in three sections of the third chapter; i) the double perovskite composition, La_2MnCoO_6 and its new ferromagnetic phases, which are synthesized in pure forms, for the first time, during this work, ii) the compositions in the region $0 < x < 0.5$, which showed an unprecedented magnetic behaviour, namely a 'melt-down' of ferromagnetic transition temperatures of all compositions to 150 K after annealing at higher temperatures, iii) the Co-rich region $0.5 < x < 1.0$, where all compositions are proved to be lacking long-range ferromagnetic order.

The fourth chapter describes detailed studies on two different ferromagnetic phases of La_2MnNiO_6, synthesized in single phase forms, by a low-temperature method, during this work. The origin of the mixed phase behaviour of La_2MnNiO_6, synthesized by the conventional solid-state method, is explained.

Structural and magnetic studies on $La_2MnCo_{1-x}M_xO_6$ (M= Ni, Fe, and Al) series are described in the fifth chapter. Interesting modifications in the magnetic properties of La_2MnCoO_6 are obtained on substitution, viz. Ni, reinforces the ferromagnetism of La_2MnCoO_6, Fe induces broadening of the magnetic transition, and Al results in a shift of the magnetic transition to lower temperatures.

The sixth chapter deals with the possible ferromagnetic phases of the rare-earth double perovskites RE_2MnMO_6 (RE = rare-earth ion, M = Co or Ni). The effect of ionic-size of RE^{+3} on the strength of the ferromagnetic exchanges in these substituted manganates is analyzed.

Chapter 1

Introduction

Material science is one of the oldest branches of science and its enormous influence sequels on various vistas of technological and biomedical advancements. From the time immemorial, materials have been used as the medium for aesthetic art, and later the proliferation of staple devices and articles, changed the face of this science. Now, the objectives of materials science can be abridged into two;

1. Understand structure-properties relationship.
2. Manipulate atomic and microstructural processes to create novel materials with desired structure and properties.

There are different methods of classification of materials in different contexts. From the research point of view, materials may be divided into three;

Functional materials: They have a function in a particular application, attributed to their crystallographic or electronic features. e.g. semiconductors, magnetic materials, etc.

Structural materials: Their applications are based on the mechanical properties and other features are not much relevant. e.g. steel, plastic, etc.

Smart materials: Similar to the functional materials, their electronic and crystallographic features are considered in applications, but their response while per-

forming a particular function is as smart as living organisms. e.g. shape-memory alloys, magnetostrictive materials, etc.

Functional materials always occupy the center stage of scientific research, owing to their ubiquity and usefulness. A class of such materials that has become increasingly interesting for electronic devices is the *perovskite-type* oxides. By structural and compositional tuning, these compounds can be made to exhibit any degree of conductivity including superconductivity and almost any kind of magnetic order like ferromagnetism, antiferromagnetism, etc. This type of materials are indispensable in one of the nascent technologies namely *spintronics*, where both the conductivity and magnetism are blended spectacularly.

1.1 Chronicle

One of the reasons, for the interest in perovskite oxides in the earlier times is the simplicity and flexibility of their structure. Structural flexibility facilitate the incorporation of a large number of metal ions into the perovskite lattice, giving rise to a plethora of exotic properties. Similarly, its simple structure compared to that of other ternary oxides (discussed in the following section), makes them model compounds to study and experiment with. Perovskite-type oxides derive their name from the mineral called *perovskite* with the chemical formula $CaTiO_3$. This mineral was named by the geologist Gustav Rose in the 1830s after the Russian mineralogist Count Lev Aleksevich von Perovski. Perovskite-type oxides, which have the crystal structure related to $CaTiO_3$ are the earth's most abundant minerals and have long been of the interest to the geologists for the information inscribed in their crystal structure and electrical properties, regarding the evolution of the planet earth [Haz88].

The observation of ferroelectric phenomena in $BaTiO_3$ in 1945 (by Arthur R. von Hippel in the United States), admitted perovskite oxides into the group of functional

materials. Following this discovery, the volume of research work carried out, on this oxides was so extensive that within a decade of time almost all possible members of this family were studied for their structural and electronic properties [Gal69]. Meanwhile, partial substitution of the metal ions by other suitable ions was found to generate interesting properties, which were not existing in the pristine compounds, and that initiated the whole gamut of *substituted* perovskite-type compounds. This lead to the discovery of many new ferromagnetic, ferroelectric, piezoelectric, and laser-host materials in the succeeding years.

In 1986 perovskite-type oxides became the most celebrated material, since the discovery of high-temperature superconductivity in the oxygen deficient, copper-containing substituted perovskite-type oxide, $Ba_xLa_{5-x}Cu_5O_{5(3-y)}$ ($x = 1$ and 0.75, $y > 0$) [Bed86]. Recently in 1994, once again substituted perovskite-type oxides came into the spotlight of rigorous materials research with the report of huge changes in electrical resistance in the presence of a magnetic field, called *Colossal Magnetoresistance* (CMR), in the compound $La_{0.67}Ca_{0.33}MnO_x$ (x varies with the oxygen pressure used during synthesis) [Jin94]. Material researchers around the globe are exploring this oxide system, to underpin the origin of its anomalous behaviour. Such substituted lanthanum manganates are studied, because if this effect is properly tuned, they may replace the metal layers currently used–since 1997–as read heads in modern computers, owing their superiority in structural stability and ease of manufacture. It is interesting to note that the above ferromagnetic metallic manganate is derived from an antiferromagnetic insulating parent, $LaMnO_3$, just by Ca substitution. Here the substitution by Ca generates an equivalent amount of Mn^{+4} ions for charge neutralization and thereby the novel properties. Such La-site substituted manganates have been studied extensively in the recent past after the discovery of CMR [Col98, Coe99, Che00, Col00]. Substitution of manganese ions in $LaMnO_3$ by other transition metal ions like Co, Ni, etc, also generates ferromagnetism, but they

are less exploited [Goo61, Bla65, Hav66, Jon66]. However, most of these characteristics in both types of substitutions can be explained in terms of the structural and electronic changes concomitant with the substitution in the perovskite lattice.

1.2 Structural aspects

Structurally, perovskites are included in the family of *ternary* crystal systems with two distinct cation sites ("A" and "B") and an anion site ("X") in the lattice [Mul74]. The ternary crystal systems encompasses the compounds with general formulae ABX_3, ABX_4, A_2BX_4, etc. Perovskites come under the class with the general molecular formula ABX_3, that also contains groups, viz. ilmenites, calcites, corundums, etc., of different crystal structures. Perovskite structure essentially consists of a framework of BX_6 octahedra linked by their corners, with large A cations (of comparable size as that of X anions), occupying cuboctahedral cavities (in oxides X = oxygen ions). This structure can also be envisaged as the smaller B cations occupying the octahedral voids formed by a 'cubic close packed' array of A cations and X anions in combination. In the ideal case, with proper sized ions, a cubic crystal structure is formed as in the aristotype, $SrTiO_3$. In Figure 1.1(a), the ideal perovskite structure in a cubic unit cell basis is shown. Here, the B ions are at the origin and A ions are in the twelve coordinated cuboctahedral cavity. The face centered cubic unit cell formed by A and X ions jointly, with A ions at the origin and B ions in the octahedral cavity, depicting the possible close packing, is shown in Figure 1.1(b).

But, the perovskite structures are rarely cubic, due to the unavoidable misfit in the packing of atoms, if the atoms A, B and X are not of the ideal relative sizes. This size-mismatch cannot be sidestepped by adjusting atomic position parameters so as to keep the symmetry intact (as in spinels), instead a *hettotype* with lower symmetry is formed. Such structural distortions can be easily visualized using a hexagonal basis

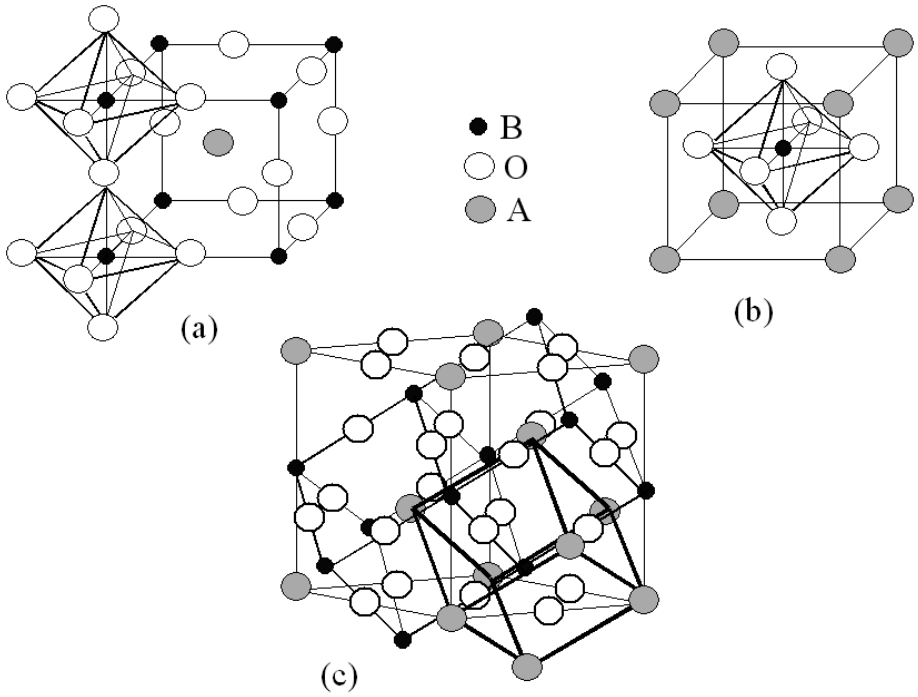

Figure 1.1: The perovskite structure: (a) The B ions at the origin, in cubic basis, (b) the A ions at the origin, in cubic basis, (c) the A cation at the origin, in hexagonal basis. The anion is oxygen,O.

as shown in Figure 1.1(c). In the hexagonal basis, the unit cell is constructed along the $< 111 >$ direction of the cube (in the figure some ions are avoided for clarity). In addition to the size effect, electronic effects also contribute towards structural distortion [Goo98]. The formation of a large variety of such hettotypes of perovskites can be grouped into four categories, as follows;

1. The BX_6 octahedra, while remaining regular, may tilt (rotate) relative to one another, reducing the cavity occupied by A cation and this is the most common case of structural distortion. This tilting of octahedra occurs if there is a mismatch in the ionic sizes of cations, especially when A cation is too small for the twelve coordination.

2. The localized electrons affect the structure, mainly by distorting the octahedra

of X ions around B cation, i.e. by displacing the X ions. This type of effects turn up at certain critical temperatures.

3. The B or A cation may be displaced from the center of the interstices surrounded by X ions, while the X ions retaining their original positions. Such phenomena, arising from the collective electrons, are temperature dependent.

4. When there is an ordering of B ions, by some means like charge disproportionation, electron transfer, etc., structural distortion occurs.

The structural distortions arising from distortion of octahedra due to electronic effects and tilting of octahedra due to smaller A cations are of interest to the present study of perovskite-type manganates of the general formula $A\mathrm{MnO_3}$.

1.2.1 Structural distortions from relative ionic sizes

From the structural point of view, the primary requirement for the perovskite oxide structure is the formation of stable $B\mathrm{O_6}$ octahedra. Hence the ions having suitable size and charge, for six coordination of oxygen ions, may be considered as candidates for B-site in perovskite-type oxides. Nevertheless, this is not a sufficient criteria for a stable perovskite structure, but the A cation should be capable of twelve coordination. In other words, a compromise between the sizes and charges of A and B ions is necessary.

With a cubic basis, the stability of perovskite structure can be expressed by an empirical parameter [Gol26, Goo70] called *tolerance factor, t* , which is related to the respective ionic sizes as;

$$t = \frac{r_A + r_O}{\sqrt{2}(r_B + r_O)} \tag{1.1}$$

where, r_A, r_B and r_O are the ionic radii of the A, B, and O ions, respectively. Assigning the effective ionic radius [Sha76] of $\mathrm{O^{-2}}$ as 1.4 Å, the ideal radii for A ion and B ion

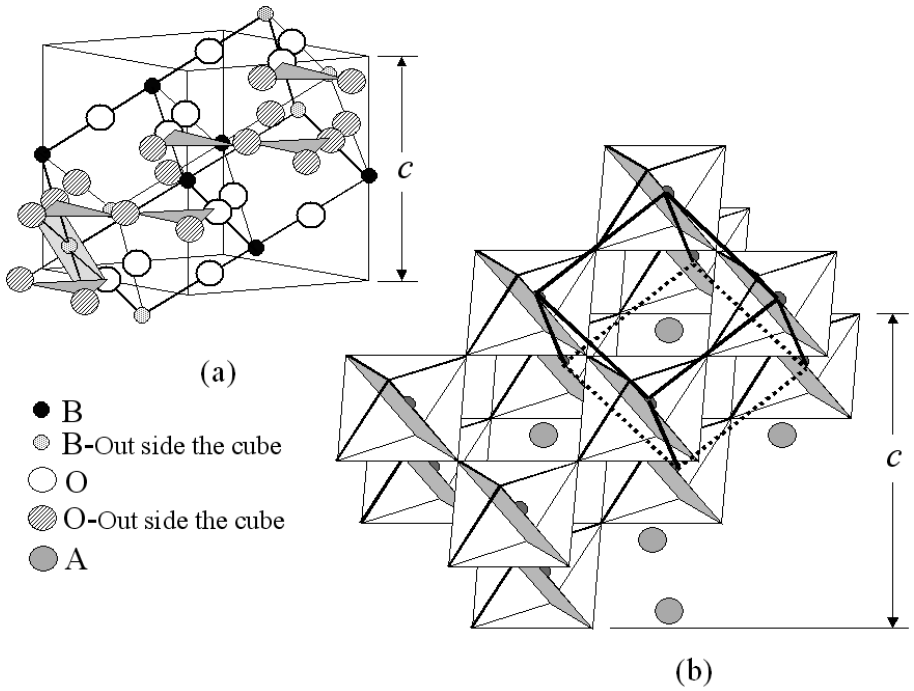

Figure 1.2: (a) Hexagonal unit cell, showing the direct correlation of c with cubic basis, (b) stacking of corner-shared octahedra.

will be 1.4 Å and 0.58 Å respectively, so that $t = 1$ for the cubic structure.Perovskite structure (with lower symmetry) occurs only within the $0.75 < t < 1.0$ range. In this range of t, a cooperative tilting of corner shared octahedra occurs, resulting in crystal structures like rhombohedral, orthorhombic, etc [Meg73].

The tilting of the BO_6 octahedra result in a new unit cell with larger volume because of the fact that the tilts alternate in direction for the successive octahedra. There are several complicated ways of tilting of octahedra in perovskites, but they can be represented as the sum of the component tilts along the symmetry axes. The triad axis of the BO_6 octahedra, with hexagonal basis, as illustrated in Figure 1.2(a), is more useful in this aspect. Also it depicts the direct correlation of hexagonal c with the cell parameters of cubic basis (the ions outside the hexagonal unit cell are shaded and some ions are avoided for clarity). The frame work of corner-shared octahedra in

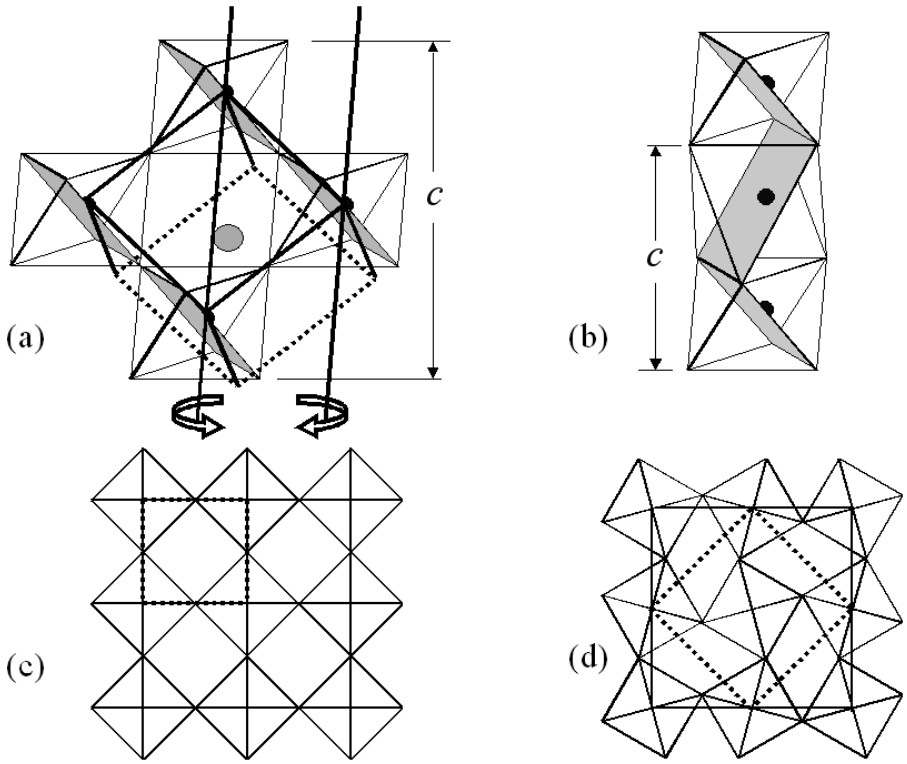

Figure 1.3: (a) View along triad axis, (b) pure hexagonal stacking, (c) view along tetrad axis, (d) tetragonal tilt.

the hexagonal basis is shown in Figure 1.2(b). As the size of the A ion decreases, the tilting increases and in the extreme cases, the perovskite structure with corner sharing collapses to hexagonal close packed structures such as corundum, ilmenite etc., where the octahedra are sharing their faces also. Similarly, if the A ion is too large, with $t > 1$, hexagonal close packing results, destroying the perovskite structure. In this case, depending up on the sizes and charges of A and B ions, a cubic-hexagonal mixed stacking is also possible, in addition to the pure hexagonal close packing [Mul74]. The pure hexagonal close packing, as shown in Figure 1.3 (b) may be obtained, by a tilt about the triad axis of cubic stacking given in Figure 1.3(a). The relationship between the cell parameters in the pure cubic and pure hexagonal stacking is also shown. One of the simplest types of tilting of octahedra, where the perovskite structure is retained,

is shown in Figure 1.3(d). Here, the resultant tetragonal crystal structure may be derived from the tilting of cubic-stacked octahedra, as in Figure 1.3(c), about the tetrad axis. The thick dotted line indicates the cubic (pseudo-cubic) unit cell in each case.

1.2.2 Structural changes by localized electrons

The two major phenomena originating from localized electrons of B ions that can alter the structure expected on the basis of pure ionic size and charge considerations are *spin-orbit coupling* and *Jahn-Teller effect*. In an octahedral crystal field, the atomic states derived from the atomic orbital angular momentum of the valence d electrons will be split into t_{2g} and e_g groups on the basis of symmetry. As an aftermath, the orbital angular momenta of the doubly degenerate e_g orbitals gets quenched ($m_l = 0$) and that of the triply degenerate t_{2g} orbitals gets reduced ($m_l = 0, \pm 1$). This splitting of energy levels depends on symmetry, and the symmetry-based term symbols such as T_{2g}, E_g, etc. are used to represent such ions, rather than the momentum-based terms such as D, F, etc. The ground states having an orbital degeneracy and $m_l \neq 0$, are split by spin-orbit coupling into $(2J + 1)$ states, where J is the resultant angular momentum quantum number. Spin-orbit coupling introduces an axial symmetry to the charge distribution, where the spin (atomic-moment) defines the axis. Coupling of this charge distribution with the crystal field leads to spin-lattice interaction, especially below the ordering temperature of the spins. This interaction is the origin of magnetic anisotropy and results in the distortion of octahedra, at certain temperature range.

The second important effect from localized electrons is the Jahn-Teller phenomena, which is generally observed in non-linear molecules. In perovskites, the B cation is in octahedral crystal field and if the ground state of this ion is an orbitally two-fold degenerate E_g state (but not a Kramers' doublet), e.g. Mn^{+3} with ^5E_g, with

the t_{2g} orbitals either full or half-filled , then there is no spin-orbit coupling available to remove this degeneracy. In this situation, the Jahn-Teller effect originates as a spontaneous local distortion of the octahedra around the B cation. The energy gained by this effect varies linearly with the distortion, whereas the energy lost against the elastic restoring forces of the crystal varies quadratically, setting a limit to the degree of distortion. This energy loss in elastic forces is minimized in the case of cooperative Jahn-Teller distortions, where the ions distort the BO_6 octahedra in synchronization. Such cooperative distortions are of significant magnitude and of interest to the perovskite manganates. At the same time, the normal vibrational modes that split the ground state, E_g, are themselves two-fold degenerate with symmetry E_g [Van39]. One mode gives a tetragonal distortion (Q_3 mode), and the other results in orthorhombic distortion (Q_2 mode). Therefore there is a dynamic coupling between electronic charge density and vibrational modes, resulting in a dynamic splitting of electronic E_g state, called dynamic Jahn-Teller distortion. However, below certain temperature, the dynamic distortions are frozen, giving rise to static Jahn-Teller distortion. The parent compound of manganates, which is relevant to the present study, namely stoichiometric $LaMnO_3$, is a Jahn-Teller distorted compound. Below 900 K, the rhombohedral structure of $LaMnO_3$ changes to O′-orthorhombic, associated with the freezing of dynamic distortion. Here, the O′-orthorhombic structure with $c/a < \sqrt{2}$ indicates that the Jahn-Teller distortions are superimposed on an O-orthorhombic crystal with $c/a > \sqrt{2}$, which is already distorted due to ionic-size mismatches [Goo61]. Nevertheless, the impact of these localized electronic effects on the structure is of ten times less, when compared to that from the ionic size/charge effects.

1.2.3 Structural changes by collective electrons

Here, the cations are moved out of their center of symmetry and that is the major difference from the structural distortions due to localized electrons. Collective electrons mainly affect the ferroelectric properties of perovskites by displacing the B or A ions from their symmetrical positions in the respective interstices. A cooperative displacement of the cationic sublattice, relative to the anionic sublattice, may increase the energy gap between the occupied, primarily anionic states and empty, primarily cationic states, thereby stabilizing the occupied states. Here, both electronic energy gained and the energy lost in elastic strain are dependent quadratically on the degree of displacement. Therefore, when the constant of proportionality for the electronic stabilization is greater than that of the elastic energy, an electronic stabilization may be possible by such displacements. For example, B cations having empty d orbitals can form more covalent-type bond, and show cation displacement. Here, depending upon the axis of displacement, different crystal structures are formed, e.g. $BaTiO_3$ is rhombohedral at the lowest temperatures (below 183 K) due to the displacement of Ti ions along the [111] axis. Nevertheless, the covalency of the A-O bond should be weak enough to avoid the cancellation of the effect due to the B-O bond covalency e.g. $CaTiO_3$, which is orthorhombic without any Ti ion displacement.

1.2.4 Structural transformations due to B ion ordering

There are four different situations, in which the ordering of B ions occur, resulting in a possible distortion of perovskite lattice;

1. When the A cation with two different valence states are present and if the B ion is capable of vary its valence state, inorder to maintain electrical neutrality B cations will be forced to present in two different valence states. Below certain temperature, these B ions will order by electron transfer resulting in a structural

transformation, e.g. $La^{+3}_{0.5}Ca^{+2}_{0.5}Mn^{+3}_{0.5}Mn^{+4}_{0.5}O_3$, below 150 K [Wol55].

2. When the energy difference between the high-spin and low-spin-states of B ion is nearly equal, their population approaches each other at higher temperatures. Therefore, above certain temperatures, ionic ordering and a structural transformation results, e.g. $LaCoO_3$ changes its symmetry from $R\overline{3}c$ to $R\overline{3}$, above 400 K [Goo70].

3. Disproportionation of the B^{+m} cation into $B^{+(m-1)}$ and $B^{+(m+1)}$ can create ions of different size and charge, facilitating their ordering and thereby a change in crystal structure, e.g. $\square PdF_3$, where A cation is missing, disproportionates into $Pd^{+2}Pd^{IV}F_6$.

4. When a fraction of the B ion is substituted by other ions, B', of different size or charge, an ordering between B and B' ions may occur, accompanied by a structural transition, e.g. double perovskite compositions, generally represented as $AB_{0.5}B'_{0.5}O_3$ or $A_2BB'O_6$.

1.3 Magnetism: An introduction

Magnetism is a universal property, present in any matter which is composed of charged particles, and is attributed to the relative motion of these particles. A material is said to be "magnetic", if it has a *response*, when it is kept in an external magnetic field. Depending on the nature of this response, magnetic matter can be grouped into two; *Diamagnetic*, if the matter is repelled from the external magnetic field and *Paramagnetic*, if it is attracted towards the field. The most important charged particle, which contributes to magnetism, is a *moving electron*. Therefore magnetism due to electrons is briefly described here. Diamagnetism is omnipresent and originates when an external magnetic field tries to deflect the path of the electron, according

to Lenz's law. However, the magnitude of diamagnetic response is meagerly small in most of the matter, except in the case of superconductors, which are the perfect diamagnets and hence diamagnetism is of less relevance here.

1.3.1 Classical view of paramagnetism

A paramagnetic material is composed of atoms (ions), with a magnetic moment, $\vec{\mu}$, due to unpaired electrons on each atoms. These moments will be forced to align parallel to an applied field, $\vec{H}$, to minimize the potential energy, given by the formula;

$$E_P = -\vec{\mu} \cdot \vec{H} \tag{1.2}$$

At the same time, thermal agitation prevents the moments from aligning in any direction. Thus a Maxwell-Boltzmann statistics can be applied to a paramagnetic system, with n atoms per unit volume, in an applied field, and expressed mathematically as [Cul72];

$$\frac{n\overline{\mu}}{n\mu} = \frac{M}{M_\circ} = coth\, a - \frac{1}{a} \tag{1.3}$$

The expression on right hand side of the above equation is called the *Langevin function*, expressed as a series;

$$L(a) = \frac{a}{3} - \frac{a^3}{45} + \frac{2a^5}{945} - \ldots \tag{1.4}$$

where $a = \mu H/kT$. When a is small, either because of a lower applied field or due to a higher temperature, Equation 1.4 reduces to $a/3$ and from Equation 1.3, the response of a paramagnetic substance at lower applied fields is derived as;

$$\chi = \frac{M}{\rho H} = \frac{N\mu^2}{3AkT} \text{ emu g}^{-1}\text{Oe}^{-1} \tag{1.5}$$

where, χ is called paramagnetic molar susceptibility, N is Avogadro's number, $\overline{\mu}$ is the average magnetic moment on each component atom of mass A, at a given temperature, T, and field, H, ρ is the density of the substance and k is Boltzmann's constant (here,

all the atoms of the magnetic substance are assumed to have a magnetic moment). Also, $\overline{\mu}$ become equal to μ, at very low temperatures and very high applied fields and then magnetization per gram, M, of the material is called saturation magnetization, $M_\circ$. In general, χ is a scalar quantity, if the material is magnetically isotropic and for anisotropic materials, χ is a tensor. Equation 1.5 can be written in a more compact form, by combining all the constants, to form the Curie's law, which is the first mathematical relation between temperature and magnetic susceptibility, as given by;

$$\chi = \frac{C}{T} \tag{1.6}$$

where, C is the Curie constant per gram of a given substance.

1.3.2 Quantum mechanical approach

If one goes in depth to the origin of paramagnetism, it leads to the orbital angular momentum, $\mid \vec{l} \mid = \hbar\sqrt{l(l+1)}$ and spin angular momentum, $\mid \vec{s} \mid = \hbar\sqrt{s(s+1)}$ (where, $\hbar = h/2\pi$, h is Plank's constant, s is the spin quantum number, and l is the azimuthal quantum number) [Cas76], of the unpaired electrons on the atoms (ions), of which the material is made. Each of these motions generates a magnetic moment, which is given by the product of the *gyromagnetic ratio* (the ratio of magnetic moment to angular momentum), and angular momentum. Gyromagnetic ratio for orbital momentum is equivalent to a unit Bohr magneton, μ_B, and that of spin, is $2.0023\mu_B(\approx 2\mu_B)$ [Abr70], where, $\mu_B = 9.2732 \times 10^{-21}$emu or erg Oe^{-1} in *cgs* units. Thus the magnetic moments are represented as;

$$\vec{\mu}_{orbital} = -\mu_B \vec{l} \ \text{ emu} \tag{1.7}$$

$$\vec{\mu}_{spin} = -2\mu_B \vec{s} \ \text{ emu} \tag{1.8}$$

But, these angular momenta, being vector quantities, can couple in four ways, viz. $\vec{l_i} - \vec{s_i}$, $\vec{l_i} - \vec{s_k}$, $\vec{l_i} - \vec{l_k}$, and $\vec{s_i} - \vec{s_k}$, where, the subscript indicates the i^{th} or k^{th} electron.

Out of these, $\vec{l_i} - \vec{s_k}$ coupling is very weak and hence may be neglected [Ear68]. There now exists two possibilities;

1. When the spin–orbit coupling is weak, $\vec{s_i} - \vec{s_k} > \vec{l_i} - \vec{l_k} > \vec{l_i} - \vec{s_i}$, so that the spin and orbital angular momenta couple individually to form the *total spin quantum number*, $S = \sum_i s_i$ and *total orbital quantum number*, $L = \sum_i l_i$. These L and S couple to form the *total angular momentum quantum number*, J and is called *Russell–Saunders coupling*. This coupling is generally observed in lighter transition metals ions and therefore of significance to the study of magnetism in perovskite manganates. But J, formed after this coupling can have different possible values $(L+S), (L+S-1), (L+S-2), \ldots, \mid L-S \mid$. Then the ground state of the total angular momentum of an atom, with a less than half filled or more than half-filled shell corresponds to the smallest or largest J value, respectively.

2. When spin-orbit coupling is strong, $\vec{l_i} - \vec{s_i} > \vec{s_i} - \vec{s_k} > \vec{l_i} - \vec{l_k}$, so that the spin and orbital momenta of each electron couple to form effective angular momentum quantum number, j, and they couple to give the *total angular momentum quantum number*, $J = \sum_i j_i$. This is known as *jj coupling* and is observed in rare-earth elements and other heavier elements.

Corresponding to each of the angular momentum quantum numbers, there is an angular momentum vector, having a magnitude greater than the respective quantum number, e.g. $\mid \vec{J} \mid = \sqrt{J(J+1)}$. So, practically, the magnetic moment of any atom or ion is originating from the total angular momentum vector and it is called *effective magnetic moment*, given as;

$$\vec{\mu}_{\vec{J}} = \vec{\mu}_{eff} = -g\mu_B \vec{J} \quad \text{emu} \tag{1.9}$$

$$\mu_{eff} = -g\mu_B \mid \vec{J} \mid = -g\mu_B \sqrt{J(J+1)} \quad \text{emu} \tag{1.10}$$

where, g, the Landé g-factor in the case of Russell-Saunders coupling, is given by;

$$g = 1 + \frac{J(J+1) - L(L+1) + S(S+1)}{2J(J+1)} \tag{1.11}$$

Interestingly, for an atom with unpaired electrons, Equation 1.9 reduces to $\vec{\mu}_{orbital}$, when $S = 0$ or $\vec{\mu}_{spin}$, when $L = 0$. The latter situation arises most frequently in the case of transition metal ions in a crystal field. Here, the orbital angular momentum is quenched, either partly or completely, by the coupling of electric field of the lattice with the orbitals so that the orbitals and the orbital magnetic moments are prevented from rotating towards the applied magnetic field. Unlike orbitals, the spins are only loosely bound to the orbitals, facilitating its contribution to magnetization. For most of the atoms, g-factor lies between 1 and 2, with some exceptions. Since the magnetic moment depends on g-factor, the experimentally determined g-factor, using magnetic resonance measurements, is helpful to calculate the atomic magnetic moment.

When a magnetic field is applied to determine the susceptibility of a paramagnetic material, the ground state, $\vec{J}$, undergoes space quantization (all the other $\vec{J}$s splits similarly) into $(2J + 1)$ directions. Then, corresponding magnetic quantum number, $m_J = \vec{J}_z$, has values $J, J-1, J-2, \ldots, -(J-2), -(J-1), -J$, where, $\vec{J}_z$ is the component of total angular momentum vector along z-axis. Each $\vec{J}_z$ generates a corresponding magnetic moment, which is the component of $\vec{\mu_{eff}}$ in the direction of applied field, H, given by;

$$\vec{\mu}_{\vec{H}} = -g\mu_B \vec{J}_z \quad \text{emu} \tag{1.12}$$

And the magnitude of the above component will be expressed as;

$$\mu_{\vec{H}} = -g\mu_B J_z = -g\mu_B m_J \quad \text{emu} \tag{1.13}$$

Here the maximum value of $\mu_{\vec{H}}$ is equal to $-g\mu_B J$ emu. The only difference between classical and quantum mechanical approaches is in the expression for potential energy (see Equation 1.2), which is given in the latter case as;

$$E_P = -g\mu_B m_J H \tag{1.14}$$

After the application of Maxwell-Boltzmann statistics to the above energy distribution into quantized levels, for a system of n atoms per unit volume, the quantum mechanical expression, similar to the classical one (see Equation 1.3), is obtained as;

$$\frac{n\overline{\mu}}{ng\mu_B J} = \frac{M}{M_\circ} = \frac{2J+1}{2J}\,coth\left(\frac{2J+1}{2J}\right)a^{'} - \frac{1}{2J}\,coth\frac{a^{'}}{2J} \tag{1.15}$$

where, $a^{'} = g\mu_B JH/kT$ and the expression on right side is called the *Brillouin function*, which is abbreviated as $B(J, a^{'})$. When $J = \infty$, the quantized levels become continuous and Brillouin function reduces to the classical situation given by the Langevin function. Similarly, at lower applied fields and ambient temperatures, i.e. at lower $a^{'}$, Equation 1.15 reduces to $a^{'}(J+1)/3J$, and therefore in practical situations, paramagnetic susceptibility is expressed as

$$\chi = \frac{M}{\rho H} = \frac{N\mu_{eff}^2}{3AkT}\ \text{emu}\,\text{g}^{-1}\text{Oe}^{-1} \tag{1.16}$$

This expression is now in the form of Curie law. Until now the paramagnetism originating from the localized electrons are only subjected to the discussion, but in solids, the collective electrons, also contribute to paramagnetism [Goo63]. Such effects are generally less significant for insulating compounds and is out of scope for an introduction to magnetism in manganates.

1.3.3 Cooperative magnetic phenomena

The essence of paramagnetism lies in the criterion that there is hardly any *interaction* between the individual magnetic moments. In order to achieve the saturation magnetization, $M_\circ$, of a paramagnet, where all the moments align parallel to the direction of the applied field, very high magnetic fields are required, simultaneously with very low temperatures. But there are systems which are paramagnetic only above a critical temperature. Such materials undergo spontaneous ordering of magnetic moments below the critical temperature, because of the 'interaction' between the moments.

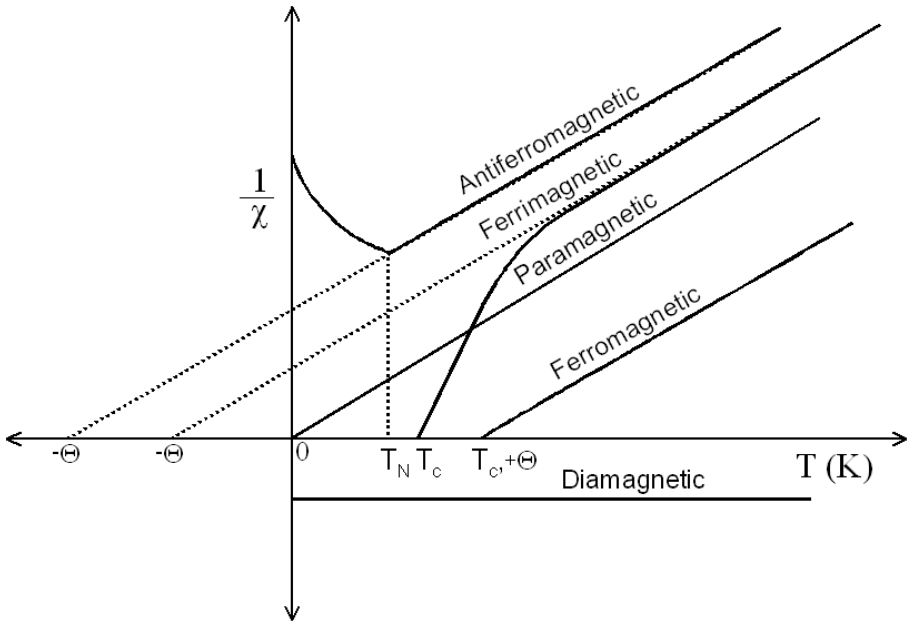

Figure 1.4: Generic temperature dependence of inverse susceptibility, in different types of magnetism.

Based on the types of ordering, such magnetic systems may be classified into four, viz. *ferromagnetic, antiferromagnetic, ferrimagnetic and helimagnetic.* In ferromagnetic materials, below Curie temperature, T_c, moments align parallel to each other. These materials will attain saturation magnetization, M_o, under relatively small applied magnetic fields and are of importance to the study of perovskite manganates. In the case of antiferromagnetism, moments cancel out each other by antiparallel alignment, below the Néel temperature, T_N. Ferrimagnetism is also a situation of antiparallel alignment of moments, but the moments are of unequal magnitudes, so that there is a net magnetization. All other types of alignments of magnetic moments, may be included in the class of helimagnetism, considering the angle between the magnetic moments in the range, $0° < \theta < 180°$($\theta = 0°$, corresponds to ferromagnetism and $\theta = 180°$, is antiferromagnetism or ferrimagnetism).

As discussed earlier the Curie low for paramagnets is based on the ideal condition,

where the individual moments do not interact with each other. But practically most of the paramagnets undergo a cooperative ordering of moments due to their mutual interaction. This lead to the modification of Curie law by Pierre Weiss, for the application to all types of paramagnets. Weiss incorporated an additional magnetic field, called *molecular field*, H_m, exerted by the individual moments themselves. This field is directly proportional to the magnetization, M and the modified form, known as Curie-Weiss law is expressed as;

$$\chi = \frac{M}{\rho(H + H_m)} = \frac{M}{\rho(H + \gamma M)} = \frac{C}{T - \rho C\gamma} = \frac{C}{T - \Theta} \tag{1.17}$$

where, γ is the molecular field constant and Θ is called the Weiss constant.

All the above classes of magnetic materials obey Curie-Weiss law in their paramagnetic state and it is illustrated in Figure 1.4. Generally, Weiss constant, Θ, for both ferrimagnetic and antiferromagnetic materials are negative, where as that for ferromagnetic substances are positive. Diamagnetic substances, except in a few cases, show temperature independent susceptibility. Similarly, for ideal paramagnetic substances, where there is no 'interaction' between moments, have $\Theta = 0$. In other words, Weiss constant gives some idea about the strength and nature of 'interaction' between moments. The response of a paramagnetic substance is most commonly measured as a function of either temperature at a constant field or applied magnetic field at a constant temperature.

Interaction of magnetic moments: Exchange phenomena

The first explanation for spontaneous ordering of moments given by Pierre Weiss, assumes a *molecular field*, acting on each atomic moment, which is proportional to the magnetization. Even though the concept of molecular field is useful in many contexts, its origin is unexplained. If magnetic dipolar interactions were considered as the origin of molecular field, cooperative magnetic ordering would not have been observed above

1 K, i.e. it is so weak to account for the observed magnetic transition temperatures. This difficulty is solved by considering the *exchange interaction* between electrons, attributed to their indistinguishable nature. The energy involved in these interactions, called *exchange energy*, is sufficiently high to explain the cooperative ordering of the magnetic moments, persisting up to quite high temperatures.

Electrons, being fermions, obey Pauli's principle, which states that the total wave function of an electron system should be antisymmetric. The total wave function has two parts, one corresponding to the space coordinates of electrons and the other to their total spin, S. So, either the space or the spin function has to be antisymmetric such that their product gives antisymmetric total wave function. Therefore, a symmetric space function (where the electrons exists closely in the space) combines with the antisymmetric spin function (where the spins are antiparallel), and vice versa. Thus for a two electron case, the possibilities, which may lead to either parallel (singlet) or antiparallel (triplet) alignment of electrons by exchange is expressed as;

$$\text{singlet, } \Psi_S = \frac{1}{\sqrt{2}}[\psi_i(1)\psi_j(2) + \psi_i(2)\psi_j(1)][\alpha(1)\beta(2) - \alpha(2)\beta(1)] \tag{1.18}$$

$$\text{triplet, } \Psi_T = \frac{1}{\sqrt{2}}[\psi_i(1)\psi_j(2) - \psi_i(2)\psi_j(1)][\alpha(1)\beta(2) + \alpha(2)\beta(1)] \tag{1.19}$$

where, ψ_i and ψ_j are wave functions for single electrons, moving in the potential V and belong to the i^{th} and j^{th} atom. The numbers 1 and 2 refer to the spacial coordinates of electrons. Spin-states of the electrons are designated by α and β.

The ground state - singlet or triplet - of a two electron system is decided by several factors like the inter-atomic separation, nature of the overlapping orbitals, etc. The magnetic exchanges represented by the above equations are called *direct* exchanges, where the respective orbitals having unpaired electrons interact directly and these exchanges are observed in metals, alloys etc. For a two electron case, the energy of singlet state is given as [Sma66];

$$E_S = E^\circ + \int \psi_i^*(1)\psi_j^*(2)\frac{e^2}{r_{12}}\ \psi_i(1)\psi_j(2)\ \ d\tau + \int \psi_i^*(1)\psi_j^*(2)\frac{e^2}{r_{12}}\ \psi_i(2)\psi_j(1)\ \ d\tau \quad (1.20)$$

Similarly, the energy of triplet state is expressed as

$$E_T = E^\circ + \int \psi_i^*(1)\psi_j^*(2)\frac{e^2}{r_{12}}\ \psi_i(1)\psi_j(2)\ \ d\tau - \int \psi_i^*(1)\psi_j^*(2)\frac{e^2}{r_{12}}\ \psi_i(2)\psi_j(1)\ \ d\tau \quad (1.21)$$

Where, asterisk mark indicates complex conjugate of the function, E° is the energy of two electron system in the absence of electron-electron interactions , e is the charge of electron, r_{12} is the separation of the two electrons and $d\tau$ is the integral over the co-ordinate space. The first integral on right hand side of the above equations represents coulomb interaction and the second integral gives exchange interaction, usually abbreviated as J_{ij}. A positive J_{ij} results in ferromagnetic exchange and a negative value results in antiferromagnetic exchange. For a many electron system, the exchange is represented by a generalized form, called Heisenberg exchange Hamiltonian,

$$\mathcal{H}_{ex} = -\sum_{ij} J_{ij} S_i \cdot S_j \quad (1.22)$$

where, J_{ij} is the effective exchange integral between atoms i and j having total spin S_i and S_j, respectively. The above expression is a starting point for several theoretical models of magnetism, which will not be discussed here. Nevertheless, in the compounds where the magnetic atoms are interspaced by 'non magnetic' anions, the orbitals of unpaired electrons can not interact directly, and then the *indirect exchanges* have to be considered.

Magnetic Superexchanges

In metal oxides, magnetic cations are intervened by oxygen ions, and therefore direct exchanges are impossible. There are several types of indirect coupling methods for magnetic moments, but the one which is relevant to perovskite manganates is the

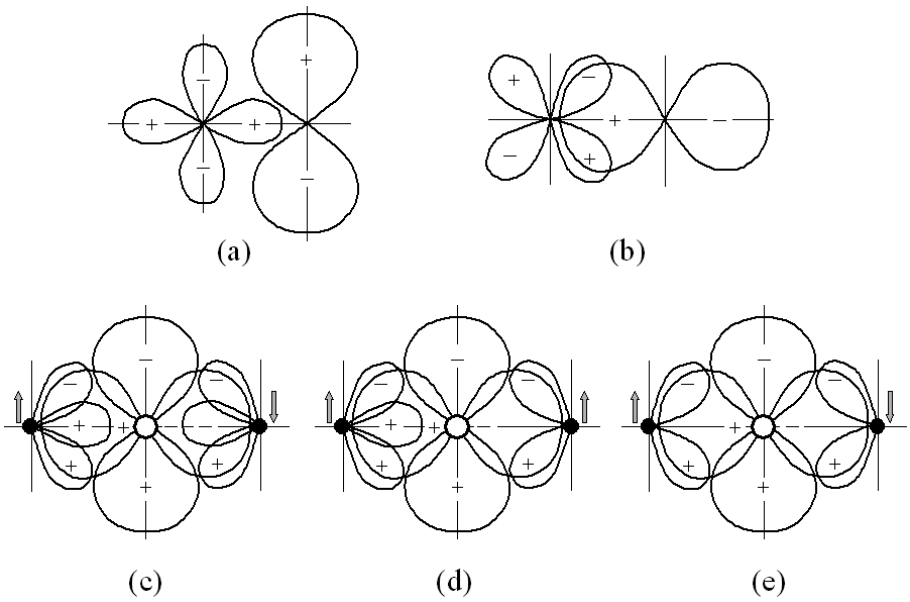

Figure 1.5: (a) orthogonality of e_g and $p\pi$ orbitals, (b) orthogonality of t_{2g} and $p\sigma$ orbitals, (c) both e_g half filled, (d) one half filled and the other empty, (e) both e_g empty.

180° *cation-oxygen-cation superexchange*. Here, anion orbitals mediate the exchange and cation-anion-cation bond angle is supposedly 180°, and hence the name. In superexchange, some sort of excited state is formed by the transfer of one p electron of O^{-2} to the d orbital of one of the neighbouring cations [And50]. This makes the oxygen ion paramagnetic and can take part in magnetic interaction. Depending upon the nature of e_g orbitals (considering an octahedral crystal field) of cations, the coupling results in different types of magnetic ordering, e.g. if both e_g orbitals are half-filled, then antiferromagnetic alignment and if one is empty with the other half-filled, then ferromagnetic alignment results [Goo63]. The underlying principles of these phenomenon are Pauli principle and Hund's rule.

The situations in which ferromagnetic or antiferromagnetic ordering occurs by superexchange is illustrated in Figure 1.5. Here, metal cations are considered in the octahedral interstices, in accordance with perovskite manganates. Figure 1.5(a)

and (b) depict the orthogonality between cation e_g and anion $p\pi$ orbitals and cation t_{2g} and anion $p\sigma$ orbitals, respectively. Therefore, two types of electron transfer or partial covalence (two bonds with three electrons) are possible, viz. between e_g and $p\sigma$ orbitals, known as σ transfer and between t_{2g} and $p\pi$ orbitals, called π transfer. Since the predominant contribution to superexchange comes from the covalency of σ bonds, the more ionic the bonds, the weaker the 180° superexchange. The major electronic effects controlling superexchange are *correlation* effect, which takes care of the simultaneous partial covalent bond formation on each side of the anion and *delocalization effect*, which considers the transfer of electron from one cation to the other through the anion. The delocalization effect depends sensitively on the extent of overlap of orbitals.

In the case represented in Figure 1.5(c), both the cation's e_g orbitals are half filled, so that the anion electrons of antiparallel spin to the cation spins couple on both sides. This results in strong antiferromagnetic interaction between the cations. Similarly, in the second situation as given in Figure 1.5(d), where one e_g is half filled and the other is empty, the anion electron couples parallel to the spin of the cation with empty orbital and antiparallel to the half filled cation. This results in moderate ferromagnetic interaction. In the third type as shown in Figure 1.5(e), there is no delocalization effect from σ transfer, but the correlation effect gives weak antiferromagnetic coupling similar to the first case. In all the above three cases, the π transfer adds a weak antiferromagnetic component, because of the half filled nature of t_{2g} orbitals. Similar superexchanges incorporating more than half filled orbitals are considerably weaker and may result in antiferromagnetic interaction.

It is necessary to understand the temperature and field dependence of magnetization of a ferromagnetic system. When a ferromagnet is cooled below its T_c, in the absence of an applied field, there develops a magnetization by the exchange coupling, called, spontaneous magnetization, M_s. Nevertheless, the material as a whole will be

unmagnetized because it will be split into several small regions of ferromagnetism, called *domains*, that are oriented in different directions such that their magnetization vectors cancel altogether. Domains are formed to minimize the magnetostatic energy due to the separation of magnetic poles. So the role of an applied magnetic field is to convert a multi-domain specimen to single-domain state, magnetized in the direction of the applied field. The nature of this field dependence is mainly controlled by magnetic anisotropy, which encourages the magnetization only in particular directions in the crystal, and also by exchange energies.

The spontaneous magnetization, M_s, of a ferromagnetic specimen is equal to the saturation magnetization $M_\circ$ at T = 0 K. Using Brillouin function (Equation 1.15), in the absence of an applied field, the magnetization behaviour below T_c can be understood from a plot of $M_s/M_\circ$ verses T/T_c, known as *reduced-scale plot*, for different total angular momentum values (J). Below T_c, applied field has not much effect on the spontaneous magnetization. Above T_c, the long-range ordering of moments collapses, but due to the persistence of short-range ordering, a deviation from the paramagnetic Curie-Weiss law is observed up to a certain higher temperatures. Therefore the straight line fit to the inverse-susceptibility intersects the abscissa at a higher temperature than T_c, called the paramagnetic curie temperature, θ_p, rather than weiss constant.

1.4 Magnetic and structural properties of Mn-site substituted $LaMnO_3$.

As already mentioned, the observation of Colossal Magnetoresistance (CMR), gave momentum to the studies on manganates from early nineties [Jin94] and the CMR effect still remains incompletely explained. CMR is the influence of a magnetic transition on the electronic conduction and is a superlative of Giant Magnetoresistance

(GMR). GMR is observed in the case of ferromagnetic/nonmagnetic multi-layers after switching on an external magnetic field and the read heads of modern computers make use of this effect. GMR effect is achieved by introducing interfaces in spin-polarized conductors and is restricted below the ferromagnetic ordering temperature, T_c. Whereas, CMR is a bulk property which originates from magnetic ordering and is usually confined to the vicinity of T_c. Unlike GMR, spin-polarized charge carriers and multi-layer geometry are not required for CMR, which makes it a highly tractable phenomenon for device manufacture.

The substituted lanthanum manganates of the general formula $La_{1-x}D_xMnO_{3\pm\delta}$ (D = Ca, Sr, etc.), usually exhibit CMR (oxygen content of these compounds can be non-stoichiometric, varying by an amount, δ moles). The magnetic, transport, and structural properties of such La-site substituted compounds have been studied extensively, for the CMR effect [Col98, Coe99, Col00]. But it is interesting to note that all these effects, after La-site substitution, are derived directly or indirectly from the structural-electronic changes of the Mn ions. This underpins the importance of studying the effects of direct substitution of Mn ion by other suitable ions. Also, if one wants to study the CMR effect as a function of Mn^{+4} or Mn^{+3} content, without affecting the pristine crystal structure, Mn-site substitution is the only solution. This is because, there are relatively large number of metal ions available for substituting Mn, with suitable ionic size or ionic charge or electronic structure. La-site substitution, even if by a trivalent ion, increases the structural distortion since La is the largest trivalent ion with nine or more than ninefold coordination (Bi^{+3} reported to have a maximum coordination of eight and is slightly larger than the eight coordinated La^{+3}) [Sha76]. Similarly, divalent ion substitution in the La-site also affects the crystal structure, in addition of changes in Mn^{+4} and Mn^{+3} content.

One more class of substituted manganates are also being investigated, which is represented as $La_{1-x}D_xMn_{1-y}M_yO_{3\pm\delta}$, where M is a smaller ion like transition metal

ions. These types of studies are aimed to explore the special type of ferromagnetic exchange called *Double Exchange* (DE) between Mn^{+4} and Mn^{+3} ions in systems without the complete ordering of these two types of ions [Zen51]. However, such substitutions destroy ferromagnetism of $La_{1-x}D_xMnO_3$ due to the suppression of DE [Ahn96, Li99]. In DE, unlike in superexchange, a real transfer of electron occurs from the partially filled e_g orbital of Mn^{+3} to the empty e_g orbital of Mn^{+4}, through the intervening oxygen ion. DE results in the initial and final states of the same energy. During DE, the spin of the hopping electron is kept intact via Hund's rule coupling. All these salient features of the DE were believed to be the reason for metallic conductivity and CMR effect of $La_{1-x}D_xMnO_{3\pm\delta}$ compounds below the ferromagnetic transition temperature.

But later, DE was found to be insufficient to explain the high resistivity of the substituted systems, with low amounts of divalent cation, above the ferromagnetic transition temperature [Mil95]. This triggered off the studies of other electronic effects like *Dynamic Jahn-Teller effect*, in these systems. Thus the systems with substitution only at Mn-site, with general formula $LaMn_{1-x}M_xO_{3\pm\delta}$, became more relevant. This is also because of the possibility of avoiding a DE background, so that the changes in the superexchange interaction and Static Jahn-Teller effect in the parent $LaMnO_3$ can be studied without much complications.

It is a fact that in perovskite oxides, ABO_3, ferromagnetism is observed only when the B-ions are *not all alike*. i.e., ferromagnetism originates in these class of compounds, if and only if the B ions are different either in their valency or atomic number (except $BiMnO_3$). This is again a testimony to the importance of Mn-site substitution studies. However, unlike the substitution of La by a divalent ion, the possibility of variable valency for the Mn-site substituted ions makes this system more challenging. The effects of these types of substitutions can be due to three factors;

1. Ionic size.

2. Ionic charge.

3. Electronic structure of the substituent ion.

where, ionic size and ionic charge effects predominantly determine the crystal structure of the new compound. These factors also decide whether the substituent atom occupies Mn-site in an ordered fashion or not. When the Mn and M ions order in the B-site of the perovskite lattice, a cooperative structural change is expected along with the changes in the properties. On the other hand, random occupancy of M ions in the lattice affects the physical properties much faster than the crystal structure. In the case of electronic effects, the ions can be grouped into, those having unpaired d-electrons, with d^n electronic configuration and those with full or empty d orbitals, represented as d^{10} or d^0. In principle, only the former group can take part in magnetic exchange interactions and can be called "magnetic". The other important aspect, generally applicable to all materials, is the methods of synthesis and processing conditions of the compounds. Formation of metastable phases and coexistence of more than one phases are some of the issues of this aspect.

1.4.1 The parent compound, $LaMnO_{3\pm\delta}$.

As discussed in Section 1.2.1, ionic size mismatch tilts the MnO_6 octahedra and thereby bypasses the "internal pressure", giving rise to orthorhombic crystal structure for stoichiometric $LaMnO_3$ (Mn-O-Mn bond angle = 157°) [Ter00]. Since Mn^{+4} can reduce the average Mn-site ionic size, the usual observation of Mn^{+4} content in $LaMnO_3$ can be argued to be for the purpose of reducing this internal pressure, persisting even after tilting of MnO_6 octahedra. This argument is corroborated by the observation of decrease in Mn^{+4} content abruptly, when Mn in $LaMnO_3$ is substituted by smaller ions like, Al^{+3} [Kri00b], Co^{+3} [Elf00], etc. The additional charge due to Mn^{+4} in $LaMnO_3$ is supposedly compensated by an excess of oxygen. In fact there is

no provision for accommodating excess oxygen in the perovskite structure. Therefore this actually corresponds to the cation deficiency and represented as $La_{1-x}Mn_{1-y}O_3$. In literature, oxygen non-stoichiometry is generally expressed as $LaMnO_{3\pm\delta}$, where positive δ indicates the "excess" and negative gives "deficiency" of oxygen. But oxygen deficient compounds are hardly reported, apparently because of the difficulty to compensate the charge by forming the bigger Mn^{+2} ions.

As discussed in Section 1.2.2, due to the Jahn-Teller distortion of MnO_6 octahedra in $LaMnO_3$, e_g orbitals loose their degeneracy. Also, two new e_g orbitals namely, $3x^2 - r^2$ and $3y^2 - r^2$ are formed by the linear combination of $x^2 - y^2$ and $3z^2 - r^2$ with the help of Q_2 mode of Jahn-Teller active lattice vibration [Cus01]. Now, hybridization with the oxygen $2p$ orbitals gives antibonding nature to these new orbitals. Thus, e_g orbital extending along the longer Mn–O bond has lower energy and results in the ordering of $3x^2-r^2$ and $3y^2-r^2$ orbitals in the *ab*-planes [Mit00]. In short, Mn^{+3}-O-Mn^{+3} exchange interactions become anisotropic and results in A-type antiferromagnetic spin ordering below 135 K, but with a positive Θ.

In the range $0 < \delta \leq 0.06$ of non-stoichiometric $LaMnO_{3+\delta}$, O′-orthorhombic structure persists at room temperature [Top97a]. The compound have ferromagnetic clusters rich in Mn^{+4} in an antiferromagnetic matrix, in this case. Therefore, the magnetic coupling between clusters and matrix, below 135 K, may create *spin-frustration* and a *Spin-Glass* behaviour can be resulted. The spin-glass state occurs when the magnetic moments are frozen randomly, before they reaches the ground state orientation [Zho01]. With higher δ, $0.10 < \delta \leq 0.18$, the room temperature structure is rhombohedral (the lower δ region transforms to O-orthorhombic structure below room temperature), which is less distorted compared to the O′-orthorhombic one. Since O-orthorhombic and rhombohedral structures do not support static cooperative Jahn-Teller distortions, Mn^{+3}-O-Mn^{+3} exchange interactions become isotropic and ferromagnetic, in addition to the Mn^{+3}-O-Mn^{+4} ferromagnetic exchanges. Con-

sequently, the matrix as such becomes ferromagnetic. The Mn^{+3}-O-Mn^{+4} exchange can be a superexchange, if the charge transfer is slow or a DE, if it is fast relative to the period of oxygen atom vibration along the Mn-O-Mn bond axis. The former results in the formation of *polaron*, which is the localized charge carrier by the vibration of oxygen atom. Thus, antiferromagnetic insulator, $LaMnO_3$, eventually become ferromagnetic and conducting with increasing Mn^{+4}. For $\delta \geq 0.14$, the transport is mainly by DE coupling below T_c [Top97a].

Here, the studies on Mn-site substitution is reexamined on the basis of the argument that the internal pressure increases if the average size of the Mn-site ions increases after substitution into Mn-site of $LaMnO_3$. Such an increase in internal pressure will be either accommodated by worsening the structural distortion, or may result in the collapse of perovskite lattice. The former situation may lead to a structural transition from rhombohedral to orthorhombic, or an increase in orthorhombic distortion of the parent $LaMnO_3$ and the latter may result in the formation of hexagonal phases.

1.4.2 d^0, d^{10}- substituents

The substituent ions with empty or full d orbitals as well as those do not have d orbitals, are included in this category. The electronic configuration and effective six coordination ionic radii [Sha76] of the various reported non-magnetic substituents are given in Table 1.1. The dopant ions are grouped into two, with reference to the ionic radius of high-spin (HS) Mn^{+3}. On the basis of ionic size considerations, those ions having ionic size greater than the high-spin (HS) Mn^{+3} are expected to destabilize the parent structure. However, mono and divalent substituents may oxidize Mn^{+3}, reducing the average Mn-site ionic radii. Such ions may reduce the internal pressure, irrespective of being bigger than Mn^{+3}.

In principle, these ions can not directly take part in the magnetic exchanges.

Table 1.1: The ionic radii in Å and electronic configurations of the d^0, d^{10}-substituents.

Mn^{+3} = 0.645 Å, $S = 2$, $t_{2g}^3 e_g^1$, and Mn^{+4} = 0.530 Å, $S = 3/2$, $t_{2g}^3 e_g^0$				
Substituent	*Larger than Mn^{+3}*		*Smaller than Mn^{+3}*	
Monovalent	Li^{+1}, $1s^2$	Na^{+1}, $2p^6$		
Å	0.76	1.02		
Divalent	Mg^{+2}, $2p^6$	Zn^{+2}, $3d^{10}$		
Å	0.720	0.740		
Trivalent	Sc^{+3}, $3p^6$		Ga^{+3}, $3d^{10}$	Al^{+3}, $2p^6$
Å	0.745		0.620	0.535
Tetravalent	Sn^{+4}, $4d^{10}$		Ti^{+4}, $3p^6$	
Å	0.690		0.605	

Nevertheless, they can affect the magnetism and crystal structure of the parent phase through the size effect. That is, depending upon the size of the substituent ion, Mn-O-Mn bond angle may change, which in turn affects the strength of the superexchange interactions. Similarly, if there is a considerable difference in either the ionic sizes or the ionic charges of Mn and the substituent ions, they may order in the B-site of the perovskite lattice, in order to minimize the elastic or electrostatic energies respectively. Conversely, if both ionic sizes and charges are similar, they may not show any site preference, resulting in a random distribution of ions. Fortunately, there is little room for ambiguity about the spin-states of the non-magnetic ions.

Li^{+1} substitution

Synthesis of the $LaMn_{1-x}Li_xO_3$ compounds by conventional solid-state method results in $LiMn_2O_4$ instead of the perovskite phase [Gon01]. Different methods like, using flux, wet-chemical method, etc. have been used for synthesis of these compounds and the annealing temperature used is in the range of 1100-1300 °C. All the reports show that a rhombohedral structure results with the increase in Li content [Kut00, Gon01, Heb02a]. At very low concentrations of Li, a positive δ is observed in $LaMn_{1-x}Li_xO_{3+\delta}$, which decreases quickly with increasing Li content. Even though

Li^{+1} substitution generates Mn^{+4}, the magnetic and transport properties are quite different from that of $La_{1-x}D_xMnO_3$ containing same amount of Mn^{+4}, i.e. mostly these compositions are insulating spin-glasses, due to the formation of small ferromagnetic clusters.

In Li^{+1} substitution, charge compensation requires the oxidation of twice the amount Mn^{+3} to Mn^{+4} for each Li^{+1}. This limits the maximum amount of Li^{+1}, which can be incorporated into the lattice, as equal to 33%. But, there are no studies to prove this limit and being a lighter element there are lack of neutron diffraction studies. The observation of rhombohedral structure and decrease in δ are suggestive of a relief in internal pressure with Li substitution.

Na^{+1} substitution

$LaMn_{1-x}Na_xO_3$ compositions have been synthesized from NaOH melt, at lower processing temperatures, because usual solid-state route results in alkali-metal evaporation [Was97, Was00]. The nominal composition, $LaMn_{0.8}Na_{0.2}O_3$, is reported to be of orthorhombic perovskite structure [Was00]. An increase in the lattice parameters after substitution is suggested as the proof for Na incorporation into the Mn-site. A weak and broad ferromagnetic transition, incipient around 300 K, is observed in $LaMn_{0.8}Na_{0.2}O_3$, measured at 10 kOe.

Unlike Li^{+1} substitution, the net effect of Na^{+1} substitution is structural instability, since the average Mn-site ionic size increases from that of $LaMnO_3$. And an increase in cell parameters occurs even if Na occupies the La-site (radius of nine coordinated Na^{+1} = 1.24 Å, and that of La^{+3} = 1.216 Å). Therefore, the structural analysis is not fully convincing. Adding to this doubt, powder XRD studies showed the presence of $La(OH)_3$, which can be attributed to the presence of excessive vacancy in Mn-site, when Na is not incorporated.

Mg^{+2} substitution

The $LaMn_{1-x}Mg_xO_{3+\delta}$ ($0.05 \leq x \leq 0.4$) compositions synthesized by wet chemical method show O-orthorhombic perovskite structure [Kut00]. An increase in T_c, up to 20% Mg substitution is observed and δ decreases with increase in the Mg content.

Mg^{+2} produces an equal amount of Mn^{+4} in order to neutralize the charge. This may lead to a structural stabilization, by the reduction in average Mn-site ionic size, irrespective of the larger size of Mg^{+2}. The reduction in orthorhombic distortion (with $c/a > \sqrt{2}$), and δ supports the relief in internal pressure. A maximum of 50% of divalent ion substitution is only possible in Mn-site, due to the restriction from charge neutralization.

Zn^{+2} substitution

Different reports say that, $LaMn_{1-x}Zn_xO_3$, prepared by ceramic method, is orthorhombic in the Mn-rich region [Heb02a, Hu03]. But, the reports on the magnetic properties of $LaMn_{1-x}Zn_xO_3$ contradict each other; T_c increases up to $x = 0.15$ and then decreases for $x = 0.2$ [Heb02a], whereas T_c decreases continuously with increase in x in the latter case [Hu03]. The continuous decrease in T_c with increasing x is interpreted as due to ferromagnetic cluster formation [Hu03]. And the initial increase in T_c with increasing x, in the other report, [Heb02a], is attributed to the destruction of orbital ordering of $LaMnO_3$ by Zn substitution.

The difference in the above reports may be coming from the difference in oxygen stoichiometry. Here, a slight stabilization of structure can be expected, due to a small decrease in average Mn-site ionic size after Zn incorporation.

Sc^{+3} substitution

In $LaMn_{1-x}Sc_xO_3$, O′-orthorhombic structure is retained till $x = 0.75$ and the O-orthorhombic structure results for $x > 0.75$ concomitant with the collapse of orbital ordering of the parent compound [Goo02]. Sc^{+3} is considered to occupy randomly in the Mn-site. A ferromagnetic behaviour is observed only for $0.75 < x \leq 0.8$, and the lower concentrations of Sc results in canted spin antiferromagnetism or spin-glass nature.

The larger size and isovalent nature of Sc^{+3} is expected to increases the structural distortion slightly. Ferromagnetism is obtained from Mn^{+3}-O-Mn^{+3} isotropic superexchanges, after the destruction of orbital ordering in $LaMnO_3$ by Sc substitution. Also, for trivalent ions such as Sc^{+3}, there is no limit for the amount of substitution, set by charge neutralization criterion.

Ga^{+3} substitution

All the reports on $LaMn_{1-x}Ga_xO_3$ show that the O′-orthorhombic structure is retained up to $x = 0.5$ [Goo61, Top97b, Cus01, Zho01, Heb02a, Ver02]. This is interpreted as the persistence of orbital ordering in the (001) planes, similar to the case of $LaMnO_3$. Generally, on Ga substitution, the collapse of orbital ordering commences for $x = 0.2$-0.3 compositional range, and simultaneously the compounds transform from spin-glass or canted spin-state to ferromagnetic state [Goo61, Top97b, Zho01, Heb02a, Ver02]. The isotropic Mn^{+3}-O-Mn^{+3} superexchange is suggested as the origin of ferromagnetism in these compounds. The magnetization values show an increasing trend with increasing x, at least up to 50% of Ga. At the same time, the magnetic ordering temperatures decreases with increasing x, especially in the orbital ordered compositions. There is no agreement among the reports on the composition up to which $LaMn_{1-x}Ga_xO_3$ is ferromagnetic.

Ga^{+3} is of slightly smaller, but of comparable size as that of Mn^{+3}. So, it is expected to stabilize the structure and occupy randomly in the B-site. On the contrary to the expectation, it was found to order in the alternate (001) planes. The driving force for this anomalous behaviour is suggested as the relief in elastic energy associated with the commencement of static orbital ordering in the O′-orthorhombic structure [Goo61]. Also, Ga^{+3} is more efficient than Sc^{+3}, in destroying the orbital ordering, most likely because of its stronger octahedral site preference, owing to its smaller size than that of Sc^{+3}.

Al^{+3} substitution

In the first report, $LaMn_{1-x}Al_xO_3$ is interpreted to have a monoclinic structure [Jon56], whereas the recent report shows O-orthorhombic structure, in the $0 \leq x \leq 0.2$ range [Goo02]. Studies indicate a rapid decrease in the Mn^{+4} content with the increase in Al content [Kri00a, Kri00b]. There is a second magnetic transition observed below T_c, in the range $0.075 \leq x \leq 0.2$, which shows frequency and field dependence. This behaviour is hypothesized as from the dynamics of the smaller ferromagnetic clusters arising from random occupancy of Al.

Al^{+3} is having almost the same size as that of Mn^{+4}, and is expected to stabilize the system considerably, in addition to the destruction of static Jahn-Teller distortion. However Al^{+3}, being a smaller ion, have a tetrahedral site preference than the required octahedral site. Therefore Al^{+3} offers a little effort to destroy the cooperative orbital ordering and this is the reason for the absence of ferromagnetic long-range ordering in $LaMn_{1-x}Al_xO_3$.

Sn^{+4} substitution

Studies on low-temperature synthesized $LaMn_{1-x}Sn_xO_3$ ($0 \leq x \leq 0.1$) report rhombohedral structure for all compositions [Mor01] and SnO_2 impurity is detected for

$x \geq 0.15$ [Mor02a]. Also, an oxygen excess of considerable amount ($\delta = 0.18$) is reported by the same authors [Mor02b]. The magnetization is found to decrease with the Sn content and is interpreted on the basis of superparamagnetic clusters separated by Sn-rich regions.

Charge neutralization is the key issue about tetravalent ion incorporation. In order to neutralize the charge, either Sn^{+4} should reduce Mn^{+3} to a bigger Mn^{+2} or create cation vacancies. The first possibility is excluded, since Mn^{+2} is hardly observed in the lanthanum manganates, probably due to its larger size. The remaining way is cation vacancy formation proportional to the tetravalent ion content. But, there is a limit for the extent of cation vacancy that can be tolerated by the perovskite and also it is not as simple as in the case of Mn^{+4} formation, where Mn^{+4} can be formed near the vacancy by a charge redistribution. Moreover, a decrease in Mn^{+4} concentration may also be considered as a means for charge neutralization in the cases of tetravalent ion substitution. Irrespective of all the above arguments, Sn^{+4} in the Mn-site is supposed to destabilize the system due to its slightly larger size. Thus, even the 10% substitution of Sn into $LaMnO_3$ is doubtful.

Ti^{+4} substitution

The $LaMn_{1-x}Ti_xO_3$ compositions are reported to have orthorhombic structure for $x \leq 0.07$, and impurity phases appear for higher concentrations of Ti [Jun97]. A decreasing Mn^{+4} content with increasing x is observed in this case. Similarly, an $x = 0.05$ composition prepared by a wet-chemical method also shows orthorhombic structure, but with high amount of Mn^{+4} [Kut00]. Another report shows that the structure is rhombohedral for $0 \leq x \leq 0.2$ [Sah03]. The magnetic moment and T_c are found to decrease with increasing Ti concentration. From the studies on frequency-dependence of magnetization, it is confirmed that $x = 0.2$, is a *reentrant spin-glass* (RSG), with the simultaneous presence of T_c and a frequency-dependent peak below

T_c [Won85]. This RSG behaviour originates when the longitudinal spin components (in the direction of the field) order at T_c, but the transverse components are random at T_c and freeze only at a lower temperature, T_f.

Even though Ti is in the tetravalent state, making it difficult to neutralize the charge after substituting for Mn in $LaMnO_3$, its size is in between that of Mn^{+4} and Mn^{+3}. So, ionic size does not create any threat to the structural stability in Mn-site substitution. To some extent, a decreasing Mn^{+4} content, as in the case of first report [Jun97], is supportive of Ti^{+4} incorporation. Observation of impurity phases, even for relatively lower concentrations of Ti, casts doubt on the phase purity of $LaMn_{1-x}Ti_xO_3$ samples.

1.4.3 d^n- substituents

The substituent ions with partly filled d orbitals are included in this category. The effective ionic radii of the substituent ions in six coordination [Sha76] and the electronic configurations corresponding to their relevant spin-states are given in Table 1.2. Here, most of the ions are reported to have more than one spin-state in the substituted perovskite manganates. The oxidation states of more than three for the substituent ions are excluded from the discussion, as there are no reports. This is not surprising because, in the case of tetravalent ion substitution, charge balancing require the formation of larger Mn^{+2} ions. This aggravates the internal pressure and destabilizes the perovskite structure.

V substitution

$LaMn_{1-x}V_xO_{3\pm\delta}$ $(0.1 \leq x \leq 0.9)$, synthesized in vacuum, shows orthorhombic structure [Tep00a] and the oxygen excess decreases with increase in x [Tep00b]. The double perovskite composition, La_2MnVO_6, prepared by arc-melting method, is reported to show cubic structure, with partial ordering of ions [And02]. None of the compositions

Table 1.2: The ionic radii in Å , and electronic configurations of the d^n-substituents.

Mn^{+3}, 0.645 Å, $S = 2$, $t_{2g}^3 e_g^1$				
Substituent	*Larger than* Mn^{+3}		*Smaller than* Mn^{+3}	
Divalent	V, $3d^3$	Cr, $3d^4$	Fe, $3d^6$	
Å	0.79	0.73(LS), 0.80(HS)	0.61(LS)	
	Fe, $3d^6$	Co, $3d^7$		
Å	0.780(HS)	0.65(LS), 0.745(HS)		
	Ni, $3d^8$	Cu $3d^9$		
Å	0.690	0.73		
Trivalent	Rh, $4d^6$	Ru, $4d^5$	V, $3d^2$	Fe, $3d^5$
Å	0.665	0.68	0.640	0.55(LS), 0.645(HS)
	Ir, $5d^6$		Cr, $3d^3$	Co, $3d^6$
Å	0.68		0.615	0.545(LS), 0.61(HS)
				Ni, $3d^7$
Å				0.56(LS), 0.60(HS)
Tetravalent			Mn, $3d^3$	Rh, $4d^5$
Å			0.530	0.60
			Ir, $5d^5$	Ru, $4d^4$
Å			0.625	0.620
Pentavalent			Ru, $4d^3$	Rh, $4d^4$
Å			0.565	0.55
			Ir, $5d^4$	
Å			0.57	

of this system shows long-range ferromagnetism, but a spin-glass behaviour coexisting with short-range magnetic order is reported.

All the above reports indicate that V ion is trivalent in the substituted manganates. The V^{+3} ion is slightly smaller than Mn^{+3}, which may help to reduce the internal pressure. Similarly, a destruction of the orbital ordering by the random occupancy of V ions can produce isotropic Mn^{+3}-O-Mn^{+3} exchange, in addition to the possible positive Mn^{+3}-O-V^{+3} superexchange [Goo63]. This may be the origin of short-range ferromagnetism in the above compositions.

Cr substitution

Even though the earlier reports on $LaMn_{1-x}Cr_xO_3$ showed a monoclinic structure for Mn-rich (especially for x around 0.3) compositions [Jon56, Ben57], most of the recent studies indicate a rhombohedral crystal structure in this region [Hro97, Tag99, Zha00, Elf00, Sun01]. However, O′-orthorhombic structure is also reported for this compositional region [Gun96, Dei02]. For higher concentrations of Cr, an orthorhombic structure is reported mostly [Ben57, Hro97, Tag99, Elf00, Sun01, Dei02]. Also, around $x = 0.5$, a mixed phase region is shown to exist [Hro97].

All the above reports on $LaMn_{1-x}Cr_xO_3$ agree with a trivalent ground state for the Cr ion. Majority of the reports indicate that $LaMn_{1-x}Cr_xO_3$ compositions are ferromagnetic at lower concentrations of Cr, with decreasing ordering temperature as x increases [Gun96, Sun01]. Concomitantly, the Weiss constant, Θ, also decreases from positive value and become negative [Jon56, Tag99]. Whereas, for the intermediate compositions, different magnetic behaviours are reported, viz. ferromagnetic cluster formation [Gun96, Sun01], ferrimagnetic behaviour [Ben57, Yan00b], etc.

The significance of Cr^{+3} is attributed to its similarity in electronic configuration with Mn^{+4} and therefore the possibility for a Mn^{+3}-O-Cr^{+3} 'double exchange' (DE) [Zha00, Sun01]. But the possibility for a DE is excluded by many researchers for the following reasons; First of all, Cr^{+3} is not as small as Mn^{+4}, and thus, the structural stabilization is relatively less. Second reason is that, once a specific composition is prepared, Cr^{+3} ionic distribution is fixed, where as Mn^{+4} distribution may change by electron transfer. The third reason is that, unlike Mn^{+3}-O-Mn^{+4}, the initial and final states are not identical for Mn^{+3}-O-Cr^{+3} after exchange. However, a positive Mn^{+3}-O-Cr^{+3} superexchange [Goo63] and isotropic Mn^{+3}-O-Mn^{+3} exchange may generate ferromagnetism in $LaMn_{1-x}Cr_xO_3$. The report indicating a constant amount, 28%, of Mn^{+4}, in the range $0 \leq x \leq 0.6$ gives evidence for the fact that the tendency $LaMnO_3$ to form excess Mn^{+4} is for the purpose of reduction of the internal pressure

due to ionic size mismatch [Elf00]. That is, here the average ionic radius of Mn-site ions remains almost constant after Cr^{+3} incorporation and thus has a constant Mn^{+4} content.

It is interesting to note that all the reports on Cr^{+3} substitution, in a broad sense, agree with the building up of antiparallel alignment of magnetic moments. This is evident from the decreasing ordering temperature and Θ values, with x. This can be due to an opposite alignment of moments through Mn^{+3}-O-Cr^{+3} exchange [Ben57, Yan00b, Dei02], instead of the predicted ferromagnetic exchange [Goo63]. Moreover, the building up of antiferromagnetic Cr^{+3}-O-Cr^{+3} exchanges also prevent ferromagnetic interactions, as evident from the studies on a thin film sample [Tan99]. Neutron diffraction study, confirming that the G-type antiferromagnetic structure of $LaCrO_3$ persists up to 60% of Mn^{+3} [Ben57], supports the antiparallel ordering of magnetic moments.

Fe substitution

$LaMn_{1-x}Fe_xO_3$ compositions are reported to show an orthorhombic structure for Fe-rich samples [Gil57, Wu94] and monoclinic structure for $0 \leq x \leq 0.1$ [Miw00]. In the lower concentration range of x in $LaMn_{1-x}Fe_xO_3$, a parallel alignment of magnetic moments are not obtained [Miw00, Oda02]. And the magnetic ordering temperature decreases and the magnetic transition broadens to a wide temperature range, as x increases. A thin film $LaMn_{0.5}Fe_{0.5}O_3$, prepared by laser molecular beam epitaxy with the 1/1 stacking periodicity of $LaMnO_3/LaFeO_3$, gave ferromagnetic ordering only in the <111> superlattice [Tan99, Ued99]. This is explained as due to the fact that a maximum number of Fe-Mn interactions are possible only in <111> superlattice. Similarly, a thin film sample of $x = 0.5$, prepared from bulk $LaMn_{0.5}Fe_{0.5}O_3$ target, is also reported to be ferromagnetic [Ued01].

All the above reports on $LaMn_{1-x}Fe_xO_3$ compositions indicate a trivalent high-

spin (HS) state for Fe, when substituted in perovskite manganates. Fe^{+3} (HS) has the same ionic size as that of Mn^{+3}, giving the possibility for a random occupancy of Fe^{+3} and thereby increasing the probability of Fe^{+3}-O-Fe^{+3} antiferromagnetic exchange interactions. Nevertheless, the structural stress associated with static Jahn-Teller distortion may be relieved by this substitution. Mn^{+3}-O-Fe^{+3} (HS) exchange is predicted to be strongly ferromagnetic [Goo63]. The influence of antiferromagnetic Fe^{+3}-O-Fe^{+3} exchange on the above ferromagnetic exchange and the random occupancy of Fe^{+3} in the Mn-site of the manganate are evident from the studies on a thin film sample of $LaMn_{0.5}Fe_{0.5}O_3$, where Mn and Fe ions are found to be ordered to a considerable extent [Tan99, Ued99, Ued01]. In the bulk samples, the random occupancy of Fe destroys a long-range ferromagnetic ordering.

Co substitution

Almost all the structural reports on $LaMn_{1-x}Co_xO_3$ show a rhombohedral perovskite structure for the Co-rich ($x > 0.5$) compositions [Jon66, Nar85, Jia94, Wu94, Aru00, Elf00]. Similarly, an orthorhombic structure is proposed for Mn-rich compositions ($0.1 \leq x \leq 0.4$) [Gil57, Nar85, Elf00], in addition to pseudocubic structures [Jon66, Aru00]. For $x = 0.5$ composition, earlier reports indicated cubic [Nar85, Tro97] or rhombohedral [Bar02] perovskite structures, but recent neutron [Bul01, Bul03], and x-ray diffraction [Das03] studies show that a monoclinic structure, which permits ion ordering in the Mn-site, is the best suiting structure for $x = 0.5$. Nevertheless, there are reports on the existence of more than one crystallographic phases for compositions near to $x = 0.5$ [Goo61, Kyo03].

The reports in the literature about the spin-states of Co and Mn are contradicting to each other. Majority of the reports indicate a Co^{+2} ground state for Co in $LaMn_{1-x}Co_xO_3$ compositions [Bla65, Jon66, Nar85, Nis95, Par97, Par99, Aru00, Tro00, Bul01, Bar02, Heb02a, Bul03, Das03, Kyo03]. But there are several reports,

which show a low-spin Co^{+3} [Goo61, Dey67, Elf00, Tan02], mixture of low-spin and high-spin Co^{+3} [Jia94], mixture of Co^{+2} and intermediate-spin Co^{+3} [Van99, Tro97], as the spin-state of Co after substitution into $LaMnO_3$. In the reports, where the Co^{+2} is given as the ground state of Co, the charge neutralization requires the presence of all the three ions, viz. Mn^{+4}, Mn^{+3} and Co^{+2} in the Mn-rich region. Due to the same reason, the Co-rich region should have Mn^{+4}, Co^{+3} and Co^{+2}, i.e. a perfect Mn^{+4}/Co^{+2} state is possible only for the $x = 0.5$ composition. There are reports indicating that the amount of Mn^{+4} or Co^{+2} ions depends on the heat treatment conditions, e.g. quenched sample has higher amount of trivalent Co/Mn ions than the annealed ones [Jon66, Das03, Kyo03]. The fact that, the conversion of low-spin Co^{+3} to high-spin state requires only 10 meV energy, makes situation more complicated [Jon66]. Therefore, the differences in the reports on the spin-states of Co may be due to the variation in the heat treatment conditions of the compositions.

All the reports agree to the point that the magnetic transition temperature increases at least up to $x = 0.5$, with the increase in x [Jon66, Heb02a]. Beyond this concentration of Co, the reports contradict on the composition up to which this series is ferromagnetic. Depending on the spin-states, there are three positive superexchanges reported for the ferromagnetic behaviour of $LaMn_{1-x}Co_xO_3$, viz. Mn^{+3}-O-Mn^{+3}, Mn^{+4}-O-Mn^{+3}, and Mn^{+4}-O-Co^{+2}. A double exchange mechanism is also suggested for the origin of the magnetic properties [Par97, Par99].

The composition $x = 0.5$ is the most studied composition of $LaMn_{1-x}Co_xO_3$. The interest in this composition originates from the observations of mixed crystallographic and magnetic phases around this composition [Goo61, Tro00, Das03, Kyo03]. These phases are explained to be formed due to the changes in the spin-states of Mn and Co depending upon the heat treatment history. In some of the reports a low-temperature anomaly is observed, below the T_c of the $x = 0.5$ composition. This anomalous magnetic transition, which shows frequency dependence, is interpreted as due to the

dynamic oscillations of pinned domain wall [Mah03] or lack of long-range Mn/Co order [Kyo04].

Co substitution is one of the most studied among all Mn-site substitutions. The interest in this substitution stem from the continuously increasing magnetic transition temperature up to 50% of Co in $LaMnO_3$. On the other hand, for most of the substituents, except Ni, the magnetic transition temperature decreases with increasing substituent concentration. Moreover, the ambiguity in the spin-state of Co is more than that found for any other Mn-site substituents, which also make the system studied repeatedly. All trivalent Co ions (low-spin, intermediate-spin, and high-spin) are of smaller size than Mn^{+3}, but larger than Mn^{+4}. Also, the low-spin Co^{+3} is the smallest among these ions and its size is close to that of Mn^{+4}. Co^{+2} of high-spin as well as low-spin state are larger than Mn^{+3}, but they reduce the average Mn-site ionic size and therefore may relieve internal pressure. Similarly, a collapse of orbital ordering by Co substitution also helps to induce ferromagnetism in $LaMnO_3$. The report about a quick decrease in the amount of Mn^{+4}, with increasing x, may be considered as the proof for the relief of internal pressure, present in $LaMnO_3$, by Co substitution [Elf00]. The formation of trivalent Co is opposed by the reports which show that the reaction, $Mn^{+4}+ Co^{+2} \rightleftharpoons Mn^{+3}+ Co^{+3}$, is biased to left by about 0.2 eV [Nar85, Par97, Par99, Das03]. But, as suggested by Jonker [Jon66], the trivalent ion formation is possible if there is some kind of ordering between Mn and Co ions. This argument is supported by the study on a thin film of $x = 0.5$, prepared by laser molecular beam epitaxy, as a <001> superlattice with the 1/1 stacking periodicity of $LaMnO_3/LaCoO_3$, which gave a T_c of 190 K [Tan99]. This indicate that an inter-layer exchange between trivalent Mn and Co ions induces ferromagnetism in the $LaMnO_3$ layer.

Ni substitution

Most of the reports on $LaMn_{1-x}Ni_xO_3$ show an orthorhombic structure for Mn-rich compositions [Wol58, Wol59, Goo61, Heb02a, Min03, Bla02a, Bla02b]. The Ni-rich compositions ($x > 0.5$) are reported to be unstable with a perovskite lattice, especially when prepared by the ceramic method, and thus a mixed phase behaviour is observed in this region [Wol59, Goo61, Vas84, Vas89, Min03]. Nevertheless, the Ni-rich compositions are reported to be synthesized using low-temperature methods. Such Ni-rich compositions are found to have a rhombohedral structure [Vas84, Vas89, Bla01, Bla02a, Bla02b]. Similar to the case of Co substitution, here also the $x = 0.5$ is found to have more than one crystallographic and magnetic phases. There are reports on orthorhombic [Vas84, Vas89], rhombohedral [Tro97] and coexistence of both orthorhombic and rhombohedral phases [Bla02a, Bla02b], for this composition, from x-ray diffraction studies. Whereas, more accurate analysis, using neutron diffraction studies prove the existence of ion ordering in Mn-site of $x = 0.5$ composition. A monoclinic $P2_1/n$ space group, which allows the ordering of ions, is suggested for this compound [Bla02a, Bla02b, Bul03].

Different probable spin-states of the Mn and Ni ions are reported in the literature for the $LaMn_{1-x}Ni_xO_3$ compositions. However, most of the reports show Ni^{+2} as the ground state of Ni ion, in this series [Bla65, Fuj67, Asa79, Son92, Tro97, Bla01, Bla02a, Bla02b, Heb02a, San02, Yam02]. Similarly, a trivalent low-spin (LS) state is also reported [Wol58, Goo61, Sar94, Yan00a, Bul03, Min03]. At the same time, some reports show that both trivalent and divalent states of Ni coexist [Vas84, Vas89, San01]. Here, depending on the spin-states of ions, four different types of positive exchanges are reported, viz. Mn^{+3}-O-Mn^{+3}, Mn^{+3}-O-Ni^{+3}, Mn^{+4}-O-Mn^{+3}, and Mn^{+4}-O-Ni^{+2}. Even though the reaction Mn^{+3} + $Ni^{+3} \rightleftharpoons$ Mn^{+4} + Ni^{+2} is naturally to be biased to the left hand side [Das03], depending upon the Mn concentration, temperature and the degree of ionic ordering, this bias can change its

direction [Vas84, Vas89]. This can be a possible reason for the observation of trivalent ions when Ni is incorporated into $LaMnO_3$.

In AC-susceptibility measurements of $LaMn_{1-x}Ni_xO_3$, an additional transition is observed below T_c [Bla01, Bla02a, Bla02b]. This anomalous cusp, observed at lower temperatures, is attributed to the pinning of domain wall to the crystal defects, or to the spin-glass nature.

In $LaMn_{1-x}Ni_xO_3$, the ferromagnetic ordering temperature increases with x and a maximum T_c is obtained for the $x = 0.5$ composition. Ni^{+2} ($S = 1$) is larger than Mn^{+3}, but it reduces the average Mn-site ionic size, in combination with Mn^{+4} and may reduce the internal pressure present in $LaMnO_3$. Whereas, trivalent ion can be either in low-spin Jahn-Teller active state ($S = 1/2$) or high-spin state ($S = 3/2$). Both the trivalent ions are smaller than Mn^{+3} and the stabilization can be more for low-spin Ni^{+3}, being the smallest. The stability of the perovskite structure of Ni-rich compositions are doubtful, as many of the above reports on the structural [Wol59, Goo61, Vas84, Vas89, Min03] and magnetic [Asa79] studies show a mixed phase behaviour in this compositional region. Moreover, the local spin density calculations show that $LaMn_{1-x}Ni_xO_3$ is ferromagnetic only in the range $0.25 \leq x \leq 0.5$ [Yan00a]. Similarly a collapse of the orbital ordering, as evident from extended x-ray absorption fine structure (EXAFS) spectra [San01], may also lead to the generation of ferromagnetism. The studies showing that a thin film of $x = 0.5$ prepared by laser molecular beam epitaxy as a <001> superlattice, with 1/1 stacking periodicity of $LaMnO_3/LaNiO_3$, has the tendency to become ferromagnetic [Tan99], serves as evidence for the positive exchange between trivalent Mn and Ni ions.

Cu substitution

The Mn-rich compositions of $LaMn_{1-x}Cu_xO_3$ are reported to have rhombohedral [Gal77, Vog77, Tab98, Por99] or orthorhombic structures [Kni98, Sun00]. But all the

reports indicate that, similar to the case of Ni substitution, the perovskite structure of Cu-rich ($x > 0.5$) compositions are unstable, especially when synthesized by ceramic method [Gal77, Vog77, Kni98, Tab98, Por99]

The magnetic ordering temperature of the $LaMn_{1-x}Cu_xO_3$ compositions decreases with increase in x. Owing to the divalent state of Cu, two types of positive superexchanges are reported, namely Mn^{+3}-O-Mn^{+4} [Sun00] and Mn^{+4}-O-Cu^{+2} [Bla65]. At the same time, the Cu^{+2}-O-Cu^{+2} antiferromagnetic interaction also increases with x and forbids the building up of a long-range ferromagnetic order. Generally divalent Cu^{+2} ($S = 1/2$) is reported in the literature for different compositions and the Jahn-Teller activity of this ion is not considered in any of them. Even though Cu^{+2} is larger than Mn^{+3}, it reduces the average Mn-site radius and so may decrease the internal pressure.

Rh substitution

The nominal composition, $LaMn_{0.85}Rh_{0.15}O_3$, is reported to have an orthorhombic structure with trivalent Rh ions [Heb02a]. Similarly, $LaMn_{0.5}Rh_{0.5}O_3$ is shown to be orthorhombic and has a positive Weiss constant [Sch00]. Nevertheless, AC-susceptibility measurements indicate that in $LaMn_{0.5}Rh_{0.5}O_3$, the ferromagnetic interactions are of short-range nature. A spin-state combination of Mn^{+2}/Rh^{+4} is suggested from paramagnetic susceptibility studies, for this compound. Since Mn^{+2} is an uncommon spin-state for Mn in manganates, further confirmation studies are necessary.

In the above reports, Rh^{+3}, is less likely to stabilize the structure, due to its larger size than Mn^{+3}. Whereas, the smaller Rh^{+4} may stabilize the structure in a similar way as in the case of Ti^{+4}.

Ru substitution

The first report assigns a cubic structure for $x = 0.5$ composition of $LaMn_{1-x}Ru_xO_3$ [Gal65]. But the recent reports indicate an orthorhombic structure for this composition [Gon02, Kam00]. A trivalent spin-state is speculated to be the ground state of Ru ion in $LaMn_{1-x}Ru_xO_3$ [Gon02, Kam00]. A decrease in T_c is found with the increase in Ru content. Another report on $LaMn_{0.95-x}Ru_xO_3$ speculates that, for $x \leq 0.2$, both Ru and Mn are mixed valent as Mn^{+3}/ Mn^{+4} and Ru^{+4}/Ru^{+5} [Sah02]. Surprisingly, this report does not tell how the excess positive charge generated by Ru ions is neutralized.

Similar to the case of Rh substitution, except Ru^{+3}, all other higher valency ions are smaller than Mn^{+3}, but larger than Mn^{+4}. Therefore, Ru^{+3} is less likely to stabilize the structure.

Ir substitution

$LaMn_{0.5}Ir_{0.5}O_3$ is reported to show a cubic unit cell with a trivalent state of Ir ion [Gal65]. The same composition synthesized by a high-pressure-high-temperature route is shown to have a pseudo-orthorhombic and speculated to be of Mn^{+2}(high-spin)/Ir^{+5} spin-states [Dem94].

The same arguments, as that of Rh and Ru substitutions, can be applied to the size effects of trivalent and tetravalent Ir ions.

1.4.4 Conclusions

In $LaMn_{1-x}M_xO_3$, none of the stoichiometric-substituted compounds result in a metallic transport. In almost all the cases, the calculated magnetic moment of the Mn-site ions, are reported to be less than the theoretical spin-only values, due to various reasons like, non-magnetic nature of substituent, randomness in the occupancy

of substituent, negative superexchanges, grain boundaries and spin-frustration. Co and Ni substitutions are the most studied among the Mn-site substitutions, but unfortunately the reports have a little agreement with each other. Only Co and Ni substitutions results in ferromagnetic behaviour, with an increasing T_c persisting up to the 50% of x. These two systems show structural and magnetic phase multiplicity around $x = 0.5$. Compositions with $x > 0.5$ not only show noticeable decrease in magnetization but all of them have the same T_c as that of the respective $x = 0.5$ composition. This particular magnetic behaviour of $x > 0.5$ compositions is common for almost all other M ion substitutions. In other words, the M-rich compositions generally do not have long-range ferromagnetic ordering. The phase ambiguities around the $x = 0.5$ composition of different M ions are yet to be sorted out.

Almost all the substitutions, except Co and Ni cases, lead to short-range ferromagnetic interactions, in the Mn-rich compositional region, most likely due to a canting of the antiparallel moments of $LaMnO_3$. The extent of this canting can be even 180°, where a pure ferromagnetic alignment occur, or in the other extreme with 0° canting, a ferrimagnetic alignment of moments is also possible. The canting of moments in a stoichiometric compound is controlled by the size or charge or electronic structure of the substituents. The impact of above factors are manifested as the destruction of the static cooperative Jahn-Teller distortion of $LaMnO_3$ or as the changes in the B-O-B bond angle, in addition to the changes in the exchange interactions. Here, the amount of substituent ion required to destroy the orbital ordering in $LaMnO_3$ is inversely proportional to the octahedral site-preference of the same ion. In many of the cases of Mn-site substitutions, antiferromagnetic interactions also increase proportional to x, which compete with the ferromagnetic interactions and therefore beyond certain concentration of x, ferromagnetic cluster formation or spin-glass nature results.

The strength of ferromagnetic superexchange interaction increases with the de-

crease in interionic distances [Hav66]. In the case of rhombohedral and orthorhombic structures, of ABO_3, the B–O distances are almost independent of lattice parameters, but the interionic B-O-B angle changes. Hence, the changes in Weiss constant, Θ, for these non-cubic compounds are due to the changes in bond angles. The Mn^{+3}-O-Mn^{+3} interactions are antiferromagnetic, when the interionic angle is 90°, and at 180°, it is ferromagnetic. Based on the reported trend of Θ with interionic angle, this superexchange interaction is expected to change from ferromagnetic to antiferromagnetic, when B-O-B angle is in the range 135-150°. In general, any substitution which destroy the cooperative static Jahn-Teller distortion (orbital ordering) of $LaMnO_3$, makes Mn^{+3}-O-Mn^{+3} superexchange to be isotropic and ferromagnetic.

Chapter 2

Experimental

There are various tools and techniques, which played a vital role in the present study of Mn-site substituted manganates and helped to discover the many new phases and interesting properties of this family of compounds. Such techniques include the methods of synthesis of the oxide compounds, nondestructive characterization techniques like powder XRD, XPS, and the measurements of magnetic properties by VSM and AC-susceptometer. However, the Mn^{+4} content of the samples were determined in a destructive manner. In the following discussions and all other chapters, the unit of the temperature of magnetic measurements is expressed in Kelvin (K) as most of the measurements are done below room temperature and the synthesis and processing temperatures of the samples are expressed in degree centigrade (°C), for practical convenience.

2.1 Material synthesis

There are several types of methods commonly used for the synthesis of oxide materials, such as ceramic, sol-gel, combustion, and co-precipitation, etc [Rao94]. The most commonly used method of synthesis is the solid-state reaction or the ceramic method. In the present study, majority of the compounds are synthesized by a combustion method which is a soft chemical route (*Chimie Douce*) [Jon89]. The soft chemical

(low-temperature) method was adopted for making sure of the phase homogeneity - a serious issue in ceramic synthesis - of the oxide samples. At the same time, most of the reports in the literature about the manganates are based on the compounds prepared by solid-state method. Therefore, those compositions, that required a comparison of the properties with the literature report, were synthesized by the ceramic method also. All the chemicals used for the synthesis of the compounds in the present study were of purity $\geq 99.9\%$. Similarly, for the synthesis and annealing of different compounds, a maximum temperature of 1350 °C was used and all the samples were furnace cooled in air.

2.1.1 Ceramic or solid-state reaction method

In the ceramic or solid-state reaction method of synthesis of oxides, the components in the form of oxides, carbonates, oxalates, etc. are weighed accurately in the required stoichiometric ratio and mixed thoroughly in an agate mortar with a pestle. This mixture is pre-fired at a comparatively lower temperature to facilitate the decomposition of the component carbonates, etc. After the pre-firing, the powder samples are ground well and heated repeatedly at different temperatures, with many intermediate grindings, till the pure compound is formed. In many cases, after mixing, the powders are compacted into the form of pellets and heated for better reactivity.

In the solid-state reaction method, the rate of the reaction is considerably low, due to several factors like, the energy required for the nucleation of the product especially when a large structural reorganization is needed, the difficulty in diffusion of different components to the reaction site, etc. Therefore, very high reaction temperatures and repeated heatings are required to get the desired product in single phase form. In addition to this, homogeneity of the product is doubtful, because of the diffusion controlled nature of the reaction. This is especially true when multi-component oxides or compositions in a solid solution series are synthesized. However, the solid-state or

ceramic method is very simple and is the preferred method when larger quantities of the products are required.

In this work, for example, the compound La_2MnCoO_6 is synthesized from La_2O_3, MnO_2 and $CoC_2O_4.2H_2O$. Initially, La_2O_3 is pre-heated at 1000 °C, for 6 hours, to remove any carbonate or moisture present and stored in a desiccator. The components are then weighed in the stoichiometric ratio of 1 : 1 : 1, to get about 10 g of the final product. Finally, these components are mixed together in an agate mortar, with the help of acetone (CH_3COCH_3) as a mixing agent. The mixed powder is then heated in a furnace, in air, at 1000 °C for 12 hours and furnace cooled. The resulting powder is further heated under the same conditions after grinding for 30 minutes. The grinding and heating at 1000 °C are repeated four times for 12 hours each, at 1100 °C for 24 hours, at 1200 °C for 24 hours and at 1300 °C for 96 hours with three intermediate grindings. The powders after each heating and grinding are characterized for verifying the completeness of the reaction.

2.1.2 Low-temperature method

The combustion method is very useful for synthesizing highly homogenous oxides at very low temperatures and hence it is included in the category of the low-temperature methods for the synthesis of oxides [Pat02]. In the combustion method, a fuel and an oxidizer is required for the completeness of the reaction. For preparing metal oxides, usually metal nitrates are used as the oxidizer and different fuels like urea, glycine, carbohydrazide, oxalic dihydrazide, etc., are used. The oxidizer and fuel are made into a solution, individually using water as the solvent, and finally mixed together. This ensures a unform mixing of the components in a molecular level, and therefore better homogeneity of the products are expected.

If a fuel and oxidizer are intimately mixed, burning reaction is self-sustaining, requiring only a small amount of heat to ignite the mass. Theoretically, the reaction

products of a stoichiometric fueloxidizer mixture combustion reaction (burn) are N_2, H_2O, CO_2 and the fine agglomerated particles of the desired oxide composition. In practice, however, lab scale reactions do not proceed perfectly, resulting in noxious gasses, fuel residue, and multi-phase product (individual metal oxides, carbonates, hydroxides, even nitrates). Interference from the ambient environment (O_2 and CO_2 in the air) and insufficient reaction temperatures result in incomplete combustion, producing various solid phases (e.g., carbonates, oxides) and potentially NO_x or CO gasses. By using proper fuels and oxidizers the reaction can be significantly altered without producing toxic gases or requiring environmental controls. During combustion, the temperature of the flame can be very high, for a short time, which is sufficient to produce metal oxides. Therefore, at molecular level, sufficient heat energy is available for the formation of oxides, from the oxidation of the fuel. The availability of such amount of energy and the homogeneity of the precursor solution make their formation easy.

The low-temperature method used in this study is a solution-combustion method, using glycine as the fuel [Chi90]. Glycine ($H_2NCH_2CO_2H$), an amino acid, is used here as a fuel because it is abundant in elements like carbon, hydrogen and nitrogen, which can burn in the presence of the oxidizing agent, namely nitrate ions (NO_3^-) belonging to the metal salts. More importantly, being a bi-dentate ligand, glycine binds metal ions, which not only prevents selective precipitation during evaporation of solvent, but facilitates a molecular level mixing of the components also.

In this method, for example, for the synthesis of La_2MnCoO_6, the nitrates of La, Mn and Co are taken in the 2 : 1 : 1 ratio and dissolved individually in minimum amount of distilled water. The individual nitrate solutions are then mixed together with a water solution of glycine, such that two moles of glycine is available to each mole of metal cation in the composition. The metal to glycine ratio of 1 : 2 is maintained for the synthesis of all the compositions studied in this work, since this

ratio is reported to give better efficiency [Chi90]. The final solution is taken in a 5 L glass beaker and heated on a laboratory hot plate, at a temperature of ∼200 °C and the beaker is covered with a stainless steel wire gauze. Auto-ignition of the precursor solution occurs immediately after the evaporation of the solvent. Finally, the combustion reaction results in an amorphous oxide ash. This powder is then annealed at higher temperatures in the range 200-1350 °C and the formation of the required phase is analyzed, after each annealing, by different methods.

2.2 Estimation of Mn^{+4} content

The parent compound, $LaMnO_3$, of the present study has a tendency to form Mn^{+4}, making the compound non-stoichiometric in oxygen content. Similarly, oxygen non-stoichiometry may persist, even after Mn is replaced by other ions, due to the creation of mixed valency. Therefore, it is necessary to monitor the oxygen stoichiometry or the amount of Mn^{+4} in the final compound. Oxygen stoichiometry, in the present work, is determined by a redox titration [Yak55, Jef89] method, which is generally used for the perovskite manganates. This is based on the reduction of Mn^{+3} and Mn^{+4} to Mn^{+2} in an acidic solution in the presence of Fe^{+2} which is oxidized to Fe^{+3}.

A nearly 0.02 N ferrous ammonium sulphate ($FeSO_4.(NH_4)_2SO_4.6H_2O$) solution is prepared for the titration, and standardized using a standard solution of potassium permanganate, $KMnO_4$, which in turn was standardized using a primary standard, oxalic acid ($H_2C_2O_4.2H_2O$). About 20 mg of the powder sample is weighed accurately and dissolved in sufficient quantity of a known volume of ferrous ammonium sulphate solution. The unreacted amount of Fe^{+2} after the reduction process is determined by titrating against standard potassium permanganate solution. From the titre values, the total amount of Fe^{+2} consumed for the reduction of Mn ions is back-calculated. Thus the amount of Mn^{+4} is determined by assuming that exactly one mole of Fe^{+2}

is required per mole of the stoichiometric compound.

2.3 Powder X-ray Diffraction (XRD)

X-ray diffraction (XRD) is a useful nondestructive method of structure analysis. When an electromagnetic wave enters a crystal it will be scattered by the electrons inside. But due to the periodicity associated with the arrangement of atoms of a crystal, for certain angles of incidence (θ), there will be constructive interference between the different scatterers (planes of atoms). Nevertheless, for most of the angles, destructive interference leads to the cancellation of the diffracted beams. With the knowledge of the wavelength (λ) of the radiation and by measuring at which angles the constructive interference occurs (called Bragg angle, θ_B), it is possible to understand the geometrical ordering of the atoms inside the crystal. The relation of crystal structure with the above two parameters is expressed by the Bragg equation $n\lambda = 2dsin\theta$, where d is the spacing between any two parallel planes of atoms inside the crystal and n is an integer [Klu54, Cul56]. Whenever constructive interference occurs for a given set of planes, the angle of incidence θ is taken as θ_B of that planes. Bragg equation puts a limit to the maximum wavelength that can be used for diffraction as $\lambda \leq 2d$. This is the reason for using x-rays for crystal structure studies, as the d values are typically in the range of few angstroms.

Corresponding to each crystal lattice there is an imaginary lattice called *reciprocal lattice* present, such that a plane in the crystal lattice is represented by a point in the reciprocal lattice [Kit03]. Also, the reciprocal lattice point is at a perpendicular distance of $1/d$ from the given plane. In fact the diffraction pattern of a crystal is a map of the reciprocal lattice of the crystal. In Figure 2.1 the diffraction of an incident wave, given by a vector $\mathbf{k}$, is represented in reciprocal lattice and condition

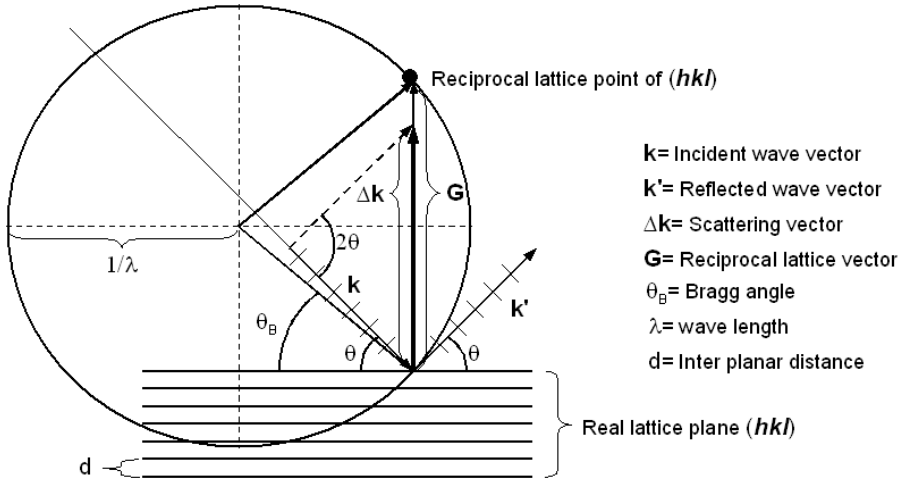

Figure 2.1: Diffraction represented in reciprocal space.

of constructive interference is given as;

$$\Delta\mathbf{k} = \mathbf{G} \tag{2.1}$$

where $\Delta\mathbf{k}$ is called the scattering vector and is equivalent to $\mathbf{k}' - \mathbf{k}$. And $\mathbf{k}'$ is the wave vector corresponding to the reflected radiation and has the same magnitude as $\mathbf{k}$. Here $\mathbf{G}$ is the reciprocal lattice vector for a given (hkl) plane and expressed as $\mathbf{G} = ha^* + kb^* + lc^*$, where $a^*, b^*, \& c^*$ are axis vectors of reciprocal lattice. As illustrated in the Figure 2.1, $\Delta\mathbf{k}$ can take any value, but the complete constructive interference for a given plane occurs only when it becomes equal to the reciprocal lattice vector of that plane. At this situation, the reciprocal lattice point will lie on an imaginary sphere of radius $1/\lambda$ and the magnitude of $\mathbf{k}$ becomes equal to the radius of this sphere called Ewald's sphere of reflection. This is nothing but the Bragg's condition of diffraction.

In addition to the information about the crystal geometry, the size of the particles in a given diffracting system can also be determined from an XRD profile. This is based on the fact that, if the number of planes in a diffracting particle is less than that is required for the complete constructive interference at θ_B, a small spread of

angles, $\theta_B \pm \delta$, also gives considerable constructive interference. This results in the broadening of the XRD peaks. The dependence of broadening of a diffraction peak at θ_B, on the particle size D, is expressed by Scherrers formula;

$$D = \frac{0.9\lambda}{\sqrt{\sigma^2 - \sigma_0^2} cos\theta} \tag{2.2}$$

where λ denotes the wave length of x-ray radiation (here, Cu Kα), σ is the measured full width at half maximum of the diffraction peak at θ_B, expressed in radians, and σ_0 represents a scan aperture of the diffractometer [Klu54]

Powder x-ray diffraction (XRD) patterns of the present work are recorded on a Philips PW1830 diffractometer. The x-ray source of this diffractometer emits Cu Kα radiation with a wavelength of 1.5418 Å. The diffractometer is calibrated with reference to a standard oriented Si wafer. For usual structural phase analysis, a scan rate of 4°/minute is used and slow-scans are done at 0.25°/minute. For the determination of lattice parameters by least-squares method, from powder diffraction data, different computer programmes are used, viz. *Lazy Pulverix* (Yvon, K., Jeitschko, W., and Parthe, E.), *Powder Diffraction Package* 1.1 (Calligaris, M. and Geremia, S.), and *PowderCell* 2.3 (Kraus, W. and Nolze, G.).

2.4 X-ray Photoelectron Spectroscopy(XPS)

When a material is irradiated with a photon having energy greater than that of an electron in a given orbital of an atom in the sample, there is a finite probability that the incident photon is absorbed by the atom and an atomic electron is promoted to an unoccupied level or ejected as a photoelectron. The latter mechanism is the underlying principle of x-ray photoelectron spectroscopy (XPS). Here, x-ray is used for the study of core-level electrons owing to its higher value of energy, which is sufficient to eject the core electrons. However, the kinetic energy of the photoelectron

depends upon both the energy of the incident photon and the binding energy [Hol70]. This can be expressed mathematically as;

$$E_{h\nu} - E_{Binding} = E_{Kinetic} \tag{2.3}$$

Thus, knowing the energy of the incident photon, $E_{h\nu}$ and the kinetic energy of the photoelectron, $E_{Kinetic}$, the binding energy, $E_{Binding}$ of the electron in a particular orbital can be determined.

In the present study, photoemission spectra are recorded on a VG Microtech Multilab ESCA 3000 spectrometer equipped with a twin anode of Al and Mg. All measurements are made at room temperature using non-monochromatized Mg Kα x-ray source ($h\nu$ = 1253.6 eV). Base pressure in the analysis chamber is generally 4×10^{-10} Torr. Extreme care has been taken to minimize the surface contamination problem by scraping the samples thoroughly and repeatedly over the surface with a stainless steel blade *in situ* under high vacuum. The scraping is repeated until the higher binding energy shoulder in the O 1s XPS showed a minimum and no further decrease in intensity, as reported in the literature [Cha92, Sai95]. Sample surface cleanliness is also confirmed by the absence of any impurity signal in the valence band spectra. The energy resolution of the spectrometer is determined from the full width at half maximum of metallic gold and the value obtained is better than 0.8 eV for Mg Kα radiation at a pass energy of 20 eV. Adventitious carbon on gold surface shows a C 1s core-level peak at 284.9 eV and all binding energies (BE) are referenced to this peak at 284.9 eV. The errors in all the BE values are within 0.1 eV.

2.5 Magnetic measurements

All the samples in this study, after annealing at each temperature, are explored for their magnetic behaviour. The static magnetic properties are studied at various magnetic field strengths and in different ranges of temperatures, to get information on

the magnetic transition temperature, saturation magnetization, paramagnetic susceptibility, etc. AC-susceptibility measurements are also made, in certain cases, as a function of temperature at different frequencies to get information on the dynamic magnetic behaviour. The general techniques for the measurement of magnetic moment involves the detection of force, torque, or induction from the magnetic moment, where, the induction techniques are the most commonly used ones. Generally, all the magnetic induction measurements involve observation of a voltage induced in a detection coil associated with a flux change, when the applied magnetic field, coil position or sample position is changed.

2.5.1 Vibrating Sample Magnetometer (VSM)

VSM involves the measurement of magnetic induction in the vicinity of the sample [Bus03]. According to Faraday's law of electromagnetic induction, an emf (V) will be generated in a coil when there is a change in flux linked to coil. For a given coil, with n turns and cross-sectional area, a;

$$V = -na\frac{dB}{dt} \tag{2.4}$$

where B, magnetic induction is equal to the product of the constant applied field, H, and the permeability, μ_0. But when a sample with magnetization M is introduced into the coil, the magnetic induction becomes;

$$B = \mu_0(H + M) \tag{2.5}$$

Incorporating the corresponding flux change, $\Delta B = \mu_0 M$, into the Equation 2.4, the output signal of the coil is obtained as

$$Vdt = -na\mu_0 M \tag{2.6}$$

That is the output signal is independent of the magnetic field, H,in which the measurement has been carried out.

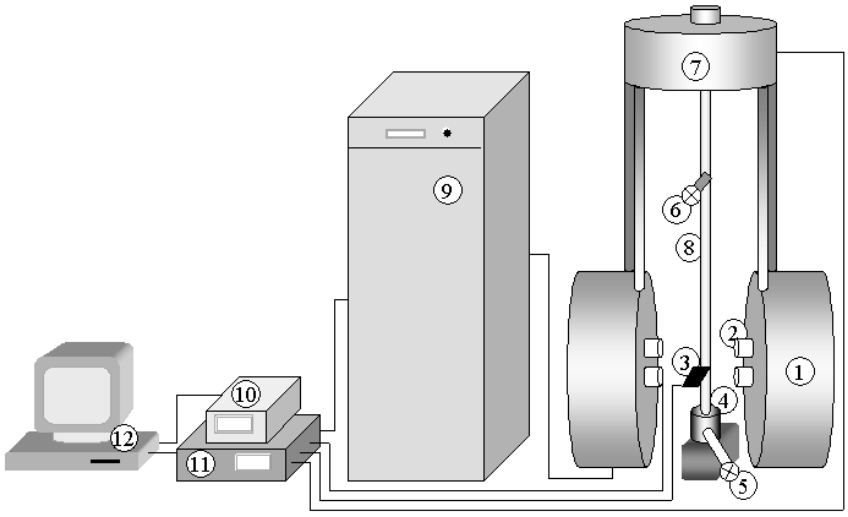

Figure 2.2: Vibrating Sample Magnetometer.

Vibrating Sample Magnetometer (VSM) measures the voltage induced by a sinusoidal motion of the sample, produced with the help of a transducer assembly, in vertical direction with respect to the magnetic field. The sample is centered in the region between the magnetic poles and the stationary pick-up coils are suitably located on the magnetic pole pieces. Here, the frequency of the output signal is the same as the vibrational frequency of the sample. Whereas, the intensity of the signal is determined by the magnetic moment as well as the frequency and amplitude of sample vibration. Therefore, in order to avoid any errors due to variations in the amplitude or frequency of vibration, usually a reference technique is employed. This is done by using a vibrating capacitor which generates a reference signal that is sensitive to the vibrational amplitude and frequency. A schematic diagram of the VSM is given in Figure 2.2.

Magnetic measurements of the present work are performed on a PAR EG&G 4500

vibrating sample magnetometer. Calibration of this VSM is done by using a standard nickel sample which gives a saturation magnetization value of 490 emu/g, in a wide range of temperatures around room temperature. The sample holder used is made of a non-magnetic a polymeric material, Kel-F (poly(chlorotriflouro)ethylene). Field dependence of magnetization is done using a maximum magnetic field of ±15000 Oe. The temperature range in which magnetic properties are studied is 10–873 K. Most of the measurements are carried out in the 80–300 K temperature range, using a liquid nitrogen cryostat. A closed cycle helium cryostat is used for measurements in the 10–300 K range and an oven assembly is used for measurements above room temperature.

Temperature variation of magnetization is measured by two methods. The first one involves cooling the samples in zero magnetic field from room temperature to the lowest measuring temperature and then the magnetization is recorded while warming the sample in a lower field (generally 50 Oe). This method is called zero field cooled, ZFC, magnetization measurement. In the second method, the sample is cooled under an applied magnetic field itself and the magnetization is monitored while heating in the same field. This method is called the field cooled (FC) magnetization measurement. Zero field cooled (ZFC) magnetization measurements, using very low magnetic fields, are found to be useful for the identification of different magnetic phases co-existing in a given sample of R-site substituted manganates [Ani98]. Therefore ZFC magnetization curves are recorded for all the samples at a lower field of 50 Oe. Curie temperature (T_c) is determined as the temperature at which a maximum is observed in the dM/dT versus T curves.

2.5.2 AC-susceptometer

AC-susceptibility is a simple and best method for probing the magnetization dynamics of materials [van82]. Compared with the DC techniques (like VSM), AC-susceptibility

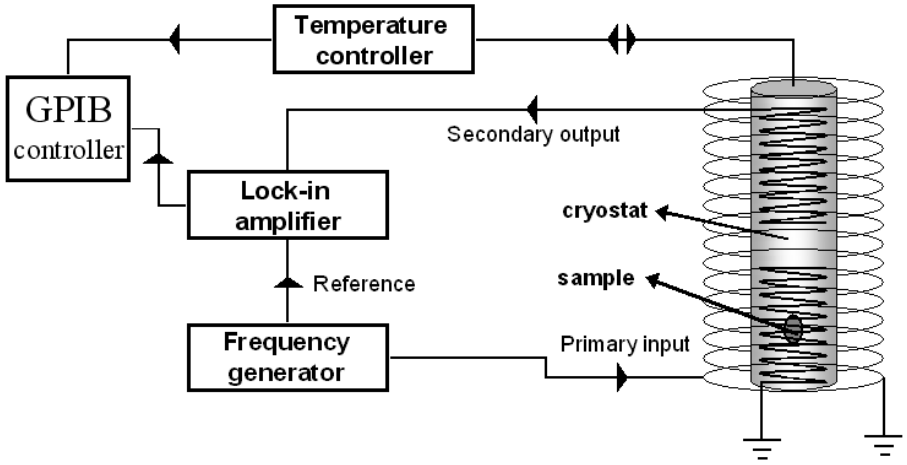

Figure 2.3: Schematic diagram of AC-susceptometer.

is the only technique where the actual susceptibility (dM/dH) is measured directly, instead of measuring the gradient of the initial magnetization curve. Also, the magnitude of the applied field is usually smaller with AC-susceptometer than used in the DC techniques and therefore the state probed by AC-susceptibility is much closer to the ground state, which is important in the study of systems like spin glasses. The measurement of AC-susceptibility relies on the change of the mutual inductance of a set of two coils or the self-inductance of a single coil, when a magnetic sample is inserted. Experimentally, the AC-susceptometer operates as; a primary coil produces a small ac AC field and the resulting emf, directly proportional to the derivative of the magnetization of the sample, induced in the secondary (pick-up) coil wound around the sample, is analyzed. The in-phase and out-of-phase components of the output signal with respect to the driving current of the primary coil is proportional to the real χ' and imaginary χ'' components of the susceptibility, χ, respectively. Mathematically, this situation is expressed as;

$$\chi = \sqrt{\chi'^2 + \chi''^2} \tag{2.7}$$

where $\chi' = \chi cos\phi$ and $\chi'' = \chi sin\phi$, with ϕ as the phase shift to the imaginary component with respect to the drive signal. For separating the real and imaginary components, a lock-in amplifier is used. A schematic diagram of the AC-susceptometer is shown in Figure 2.3.

During the present study, the AC-susceptibility measurements are done in the temperature range of 10-300 K, using an APD cryogenics closed cycle helium cryostat. An AC magnetic field of 0.5 to 2 Oe is applied in different measurements with a maximum frequency of 5 kHz.

Chapter 3

Co substituted $LaMnO_3$

Ferromagnetism can be induced in the antiferromagnetic lanthanum manganate, $LaMnO_3$, by substituting La (La-site) or Mn (Mn-site) by suitable ions. Extensive studies have been made on the magnetic properties of $La_{1-x}D_xMnO_3$ (D = Ca, Sr, etc.) after the discovery of CMR in this class of compounds and the results are well documented in the literature [Col98, Coe99, Col00]. Nevertheless, the ferromagnetic properties of the La-site substituted compounds arise because of the changes in the valence state of Mn and the associated structural variations. Therefore, studies on the Mn-site substituted manganates also can provide a wealth of information in terms of the origin of ferromagnetic properties and the relevance of substitution is expatiated in Section 1.4. Even though there are many studies, reported by several groups, on the substitution of Mn by Co, there are severe disagreements among the reports regarding the magnetic phases, structural features, etc. The striking fact is that most of the reports are on compounds synthesized by different methods and processing conditions. These ambiguities on the structural and magnetic properties can therefore be associated with the difference in synthetic methods/conditions, which is one of the indispensable problems inherent in multicomponent solid oxides. Even the studies on $LaMn_{1-x}Co_xO_3$ series synthesized under similar conditions, report different origins for ferromagnetism. Thus it is necessary to study this system in detail to

have a cessation to these contradictions in a convincing manner.

Most of the studies reported in the literature on the Co-substituted compositions, $LaMn_{1-x}Co_xMnO_3$, are on $x = 0.5$. This indicates the relevance of this particular composition when compared to the others. It may exhibit certain novel properties because of the parity in the amount of Mn and Co in the composition. Hence, the studies on $LaMn_{1-x}Co_xMnO_3$ are divided into three sections, such that the composition, $x = 0.5$ ($LaMn_{0.5}Co_{0.5}O_3$ or the double perovskite formula La_2MnCoO_6), is treated exclusively in the first section, followed by studies on the Mn-rich compositions, $0 < x < 0.5$, and Co-rich compositions, $0.5 < x \leq 1.0$, in the next two sections, respectively.

Synthesis

Conventional solid-state reaction method of synthesis of the oxides may end up with misleading results if the compounds are not processed properly. Therefore all the compositions in the $LaMn_{1-x}Co_xO_3$ series were prepared by a low-temperature method, called the solution-combustion method [Chi90]. And these compositions were processed further under identical conditions, whenever it was required to avoid changes in processing conditions. Some of the compositions were also synthesized by the conventional solid-state reaction route for a direct comparison of the properties. To exploit the possibility of long-range magnetic interactions at different proportions of Co and Mn, the concentration of Co in the compositions were selected as the whole number multiples of 1/16. The other conventional compositions, where Co concentration varying as the multiples of 1/10, were also synthesized.

In the low-temperature method of synthesis, the nitrates of La, Mn and Co were taken in the required stoichiometric ratio and dissolved in water along with glycine (2 moles of glycine per mole of metal ion) and on slow evaporation on a hotplate at 200 °C, this precursor spontaneously burnt and formed a black powder. The powder

samples, thus obtained following the above procedure were annealed in air, in the temperature range 200–1300 °C at intervals of 100 °C for 12 hours each and furnace-cooled to room temperature. The low-temperature synthesized samples are denoted by the abbreviation 'LT'.

In the ceramic method of synthesis, a solid-mixture containing La_2O_3 (pre-heated at 1000 °C), MnO_2 and $CoC_2O_4.2H_2O$, taken in the required stoichiometry, were heated initially at 1000 °C for 12 hours and then heated at the same temperature for 96 hours with five intermediate grindings. The powders obtained were further heated at 1100 and 1200 °C for 24 hours each and then at 1300 °C for 120 hours with intermediate grindings. The samples synthesized by the ceramic method are demarcated as 'HT'.

Oxygen Stoichiometry

Reports on the oxygen stoichiometry studies show that the parent compound, $LaMnO_3$, always form with excess Mn^{+4}, $LaMnO_{3+\delta}$, and Mn^{+4} content decreases on the substitution of Mn by different elements; Cr [Gun96], Cu [Por99], Al [Kri00a, Kri00b], Co [Elf00, Tro00], and Mg [Kut00]. This phenomenon observed, independent of the type and charge of metal ions, can be due to the decrease in internal pressure concomitant with the decrease in the average Mn-site ionic radius, after substitution.

In $LaMn_{1-x}Co_xO_{3+\delta}$, the samples synthesized by the ceramic method were found to be nearly stoichiometric, with $\delta = \pm 0.02$. In the case of the low-temperature synthesized compounds, the as-prepared samples always showed slight amounts of residual carbon, making the oxygen estimation erroneous. When these samples were annealed in air at 700 °C, δ decreased quickly with increasing x and compounds became oxygen stoichiometric for $x > 0.3$. Similarly after annealing in the range 1300-1350 °C, δ reduced much faster with x.

3.1 La_2MnCoO_6 ($x = 0.5$)

Mixed valency of the transition metal ions, charge disproportionation, existence of two different crystallographic forms, etc., appear to be some of the common features of the perovskite-type magnetic oxides $A_2BB'O_6$ (or $AB_{0.5}B'_{0.5}O_3$) [Fal97, Ram00, Ued01, Wak01]. The double perovskites became very important after the observation of large tunnelling magnetoresistance, at room temperature, in the *half-metallic* compound, Sr_2FeMoO_6 [Kob98]. Half-metallicity is a situation in which all the charge carriers of a conductor have the same spin. Such compounds find application in intergrain-tunnelling magnetoresistance devices. The above compound has two crystallographic phases with different Curie temperatures, viz. a cubic phase with $T_c \approx 390$ K and a tetragonal phase with $T_c = 415$ K [Kob98, Goo00, Tom00]. Here, majority of the ions are present as Fe^{+3} and Mo^{+5} [Nak68, Gre01]. It has been predicted that the perfect alternating order of Fe and Mo ions promotes the equilibrium $Fe^{+3} + Mo^{+5} \rightleftharpoons Fe^{+2} + Mo^{+6}$ and the overlapping of the redox energies of Fe^{+3}/Fe^{+2} and Mo^{+6}/Mo^{+5} couple to produce half-metallicity and ferromagnetism in Sr_2FeMoO_6 [Sle72, Goo00].

La_2MnCoO_6 ($LaMn_{0.5}Co_{0.5}O_3$) is reported to possess the highest T_c among all the other possible compositions of $LaMn_{1-x}Co_xO_3$ series. Magnetic properties of the manganese oxides, $La_2Mn\mathit{M}O_6$, where M = Co, Ni, Cr, etc., were first studied in the 1960s (both the perovskite formula $LaMn_{0.5}M_{0.5}O_3$ and the double perovskite formula $La_2Mn\mathit{M}O_6$ were commonly used by the earlier workers), to understand the nature of the magnetic exchange interactions in these compounds [Wol58, Goo61, Bla65, Jon66, Dey67, Fuj67]. The interest in this composition is because of its similarity with other double perovskites like Sr_2FeMoO_6. Moreover, the local-spin-density calculations predict that La_2MnCoO_6 can be half-metallic [Pic98, Yan99].

3.1.1 Background

Because of the different structures of the end members, $LaMnO_3$ (orthorhombic) and $LaCoO_3$ (rhombohedral), phases with two different crystallographic structures may be possible for La_2MnCoO_6. The mixed phase behaviour of La_2MnCoO_6 was first reported by Goodenough *et* al. in 1961 [Goo61]. Mixed ferromagnetic phase behaviour of La_2MnCoO_6, with orthorhombic and rhombohedral structures, was found in the above samples prepared by the conventional solid-state reaction method. After a gap of more than three decades, electronic structure calculations on La_2MnCoO_6 showed that orthorhombic structure, with rock-salt type ordering of Mn and Co, is more stable than the rhombohedral structure [Yan99]. This indirectly tells that a metastable phase with rhombohedral structure is plausible for this compound.

A brief description of the reports on the studies of Co-substituted $LaMnO_3$ is given in Section 1.4. Most of these reports are on the samples synthesized using the solid-state method. There are no reports on the synthesis or isolation of the possible different ferromagnetic or crystallographic phases of this compound, in the pure forms. Even though there are reports about samples synthesized by low-temperature methods, different studies are carried out on samples treated at higher annealing temperatures and none of the studies have looked into the possibility of metastable ferromagnetic phase formation at lower temperatures. All the possible oxidation/spin-states like Mn^{+3}, Mn^{+4}, Co^{+2}, and Co^{+3} and positive superexchanges like Mn^{+3}-O-Mn^{+3}, Mn^{+4}-O-Co^{+2}, and Mn^{+4}-O-Mn^{+3} are reported by different groups, for La_2MnCoO_6. Similarly, there are reports on crystal structures with orthorhombic, rhombohedral, pseudocubic, and monoclinic symmetries. Therefore, it is necessary to sort out the issues of multiple phases of La_2MnCoO_6 and need to understand how and when these phases are formed.

3.1.2 Powder XRD studies

Powder x-ray diffraction patterns of the low-temperature synthesized La_2MnCoO_6 samples, annealed at 200, 400, 600, 700, and 1300 °C, are shown in Figure 3.1. A perovskite phase is obtained at lower annealing temperatures itself, with a pseudo-cubic lattice parameter $a \approx 3.90$ Å. All the reflections in the XRD pattern of the sample annealed at 200 °C are weak and broad due to fine particle nature of the low-temperature synthesized sample. The average particle size is obtained as ∼15 nm from x-ray profile broadening, using the Scherrer formula given by Equation 2.2 [Klu54, Cul56]. The average particle size is found to be almost independent of annealing temperature below 700 °C. An additional weak and broad reflection is observed at $2\theta \approx 29.4°$, in the XRD patterns of samples annealed below 500 °C. This extra reflection does not belong to the nitrates, oxides, carbonates or hydroxides of the individual starting metal ions and it is neither of glycine, the fuel used for the synthesis. Similarly, this peak is not matching with that of other perovskite related A_2BO_4 or the $A_2B_2O_7$ (pyrochlore) structures. This weak and broad peak, disappearing after annealing at 500 °C, may be due to small amounts of some unknown metastable phase of the mixed oxides. Moreover, such small amounts of impurity phase does not have any effect on the magnetic transition observed for this sample of La_2MnCoO_6 (see the following section). This argument is supported by the observation that La_2MnNiO_6, prepared under identical conditions as that of the above sample and having identical transition temperatures, does not show any impurity phase in the x-ray diffraction pattern (as discussed in the following chapter). Since this peak is very broad, most likely due to the lower particle size of the corresponding phase, it is extremely difficult to refine it reliably with any crystal structures.

In the case of sample annealed at 700 °C, broadness of all the peaks persists to certain extent and there are no traces of the weak reflections observed in the samples annealed at lower temperatures. Due to the ambiguity associated with the

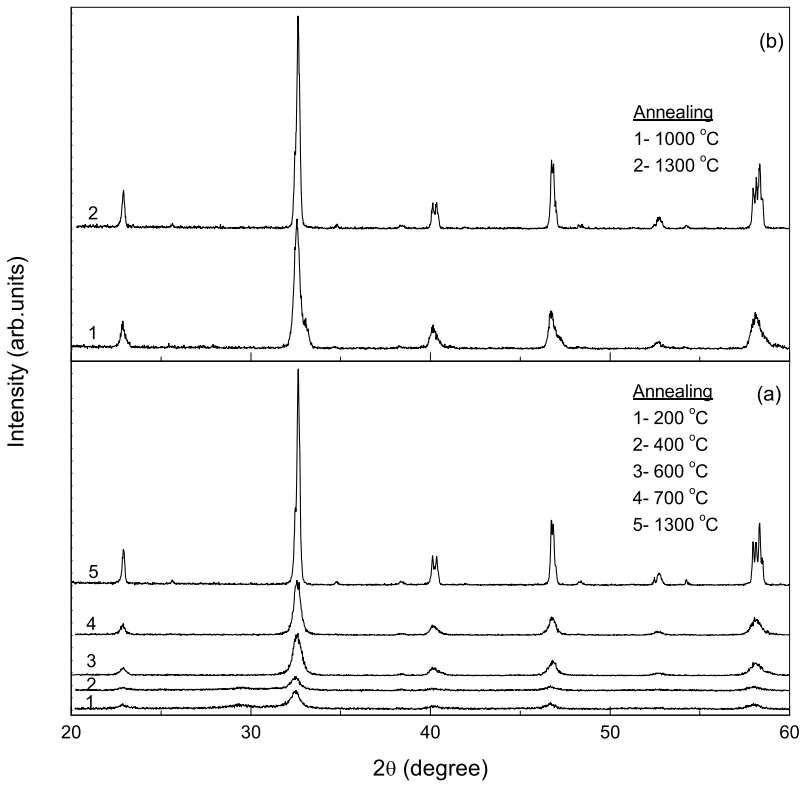

Figure 3.1: Powder XRD patterns of La_2MnCoO_6; (a) low-temperature synthesized sample annealed at different temperatures and (b) high-temperature synthesized sample annealed at 1000 °C for 96 h and 1300 °C for 96 h.

broadening of diffraction profile, refinement of the XRD pattern is done with both the crystal structures of the end members, which are the most likely structures in this case. The refinement of the lattice parameters, using least-squares method, give comparable goodness of fit in both the cases (orthorhombic space group $Pbnm$, a = 5.458 Å, b = 5.525 Å, c = 7.780 Å ,and rhombohedral space group $R\bar{3}c$, a = 5.488 Å, $\alpha = 60.2°$). At the same time, this compound may have an ordering of B-site ions, owing to the equality in concentration of Mn and Co ions and because of the difference in charge/size of Co and Mn ions. However, the above space groups do

not allow two crystallographically distinct positions for Mn-site ions, so as to account for the ion ordering. Therefore, instead of $Pbnm$ space group, its subgroup $P2_1/n$, having monoclinic structure, is also considered ($a = 5.522$ Å, $b = 5.459$ Å, $c = 7.779$ Å, $\beta = 89.8°$). Similarly in the place of $R\bar{3}c$, $R\bar{3}$ space group is considered ($a = 5.478$ Å, $\alpha = 60.4°$). According to the previous reports, such ion ordering can be distinguished clearly from neutron diffraction spectral studies [Bul03, Das03]. Our refinements of the x-ray diffraction spectra, with these new space groups, did not lead to a sizeable betterment.

Those samples annealed above 700 °C eventually become more and more crystalline after annealing at higher temperatures. Structure refinements with $Pbnm$ ($a = 5.466$ Å, $b = 5.510$ Å, $c = 7.748$ Å) or $P2_1/n$ ($a = 5.510$ Å, $b = 5.465$ Å, $c = 7.749$ Å, $\beta = 89.9°$) symmetry gave noticeable betterment than with using the rhombohedral space groups, and better refinement is obtained with the orthorhombic space group $Pbnm$ for the sample annealed at 1300 °C. This indicates clearly that the sample annealed at high temperatures has orthorhombic structure. But, the possibility that the compound has an ion ordered structure with monoclinic symmetry, can not be discerned from powder x-ray diffraction studies. It may be seen that there is only a slight difference between the corresponding lattice parameters of the samples annealed at 700 and 1300 °C. XRD patterns of the samples annealed between these temperatures also gave similar lattice parameters.

The powder XRD patterns of the sample synthesized by the ceramic method (HT sample) and annealed at 1000 and 1300 °C, for 96 h each, are also shown in Figure 3.1. There are no impurity reflections observed in the patterns, indicating the formation of a perovskite phase, even at 1000 °C. However, all the reflections in the pattern of the sample annealed at 1000 °C are some what broader, as if the particle sizes are smaller, and an additional shoulder is observed for all reflections at the right side of the main peaks. Smaller particle sizes are unlikely for the sample synthesized by

the ceramic method and therefore, the broadening of the peaks and the additional shoulders may be due to some compositional inhomogeneity [Ani98] or mixed phase behaviour. If different compositions close to $x = 0.5$ in $LaMn_{1-x}Co_xO_3$ are formed, or if the sample contains more than one phase of the same composition, having the perovskite structure, then the individual peaks will be a sum of the reflections of different compositions/phases having slightly differing lattice parameters, so that the reflections may appear broad. The XRD patterns of the HT and LT samples, annealed at 1300 °C, are identical, indicating the formation of single phase compositions. Almost identical orthorhombic lattice parameters are obtained for these two samples.

3.1.3 Magnetic measurements

LT samples

The temperature variation of the zero field cooled (ZFC) magnetization of the samples annealed between 200 and 700 °C is compared in Figure 3.2. The onset of a magnetic transition, at ∼150 K, and the broadness of magnetic transition are identical for the samples annealed up to 300 °C. An increase in the magnetic transition temperature and further broadening of the magnetic transition is observed with increase in the annealing temperature up to 500 °C. Onset of a magnetic transition below ∼230 K, with a slightly broad nature, is obtained for the sample annealed at 600 °C and this magnetic transition becomes sharper without any change in the T_c (Curie temperature) on further annealing at 700 °C. A maximum T_c of ∼230 K is obtained for the sample annealed at 700 °C, henceforth called as the high-T_c phase of $x = 0.5$ in $LaMn_{1-x}Co_xO_3$. The increase in T_c, with increasing annealing temperature between 200 and 700 °C, is not due to any particle size effect, as the average particle size was found to be almost constant for samples annealed in this temperature range. Moreover, the magnetic transition is expected to become sharper, instead of becoming

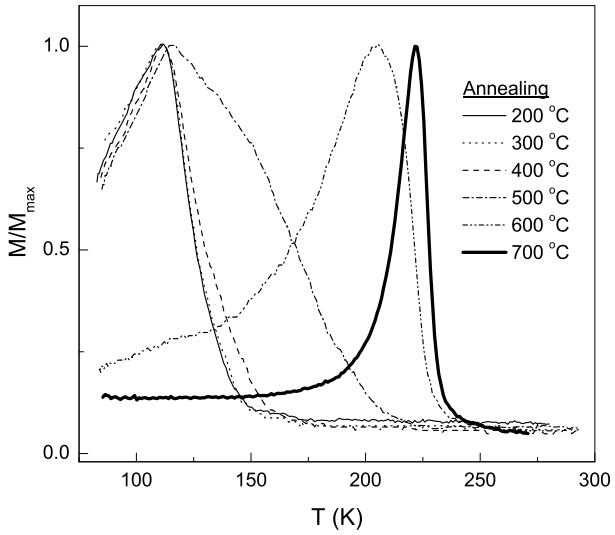

Figure 3.2: ZFC magnetization curves ($H = 50$ Oe) of $x = 0.5$, annealed in the temperature range 200-700 °C.

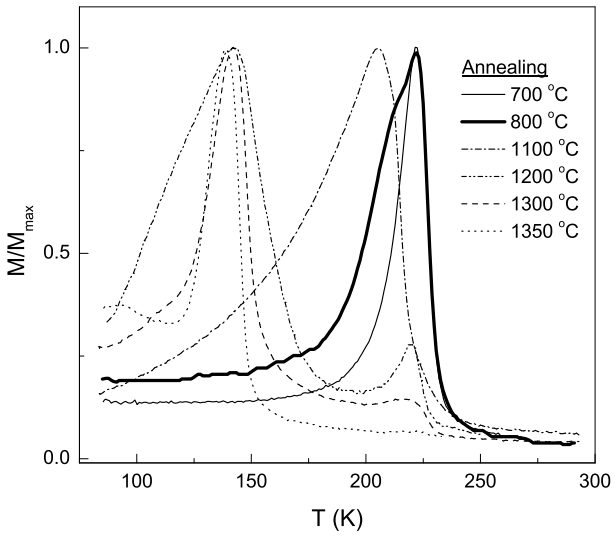

Figure 3.3: ZFC magnetization curves ($H = 50$ Oe) of $x = 0.5$, annealed in the temperature range 700-1350 °C.

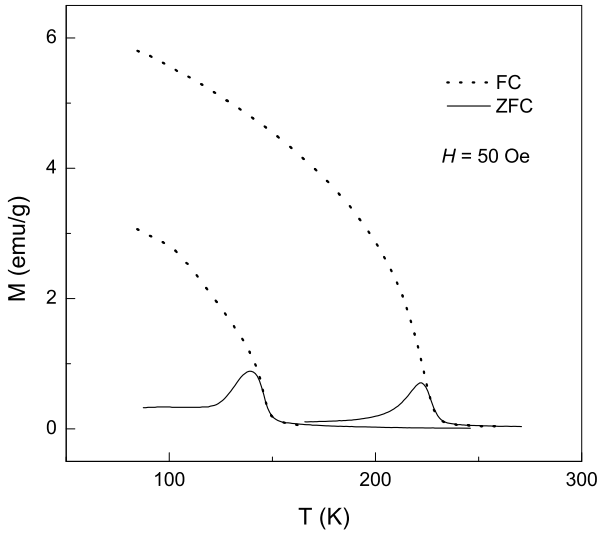

Figure 3.4: FC and ZFC magnetization curves of the two phases of $x = 0.5$, $H = 50$ Oe.

broad, if there is a real effect of increasing particle size.

The temperature dependence of ZFC magnetization of the samples annealed between 700 and 1350 °C is shown in Figure 3.3. The collapse of the high-T_c phase commences with the increase of the annealing temperature just by 100 °C. Here, an interesting observation is that stability of the high-T_c phase is limited to the annealing temperature range of 700±50°C. The sample annealed at 1100 °C shows a major magnetic transition temperature corresponding to the T_c of the high-T_c phase, with significant broadening towards lower temperatures. After annealing at higher temperatures, the contribution due to this magnetic transition decreases and a second broad magnetic transition appears close to 150 K. Finally, a single sharp magnetic transition is observed at ∼150 K for the sample annealed above 1300 °C. Henceforth this phase formed at 1350 °C is called the low-T_c phase. Interestingly, the temperature at which the initial increase in magnetization observed for the sample annealed

at 200 °C, is at the T_c of the low-T_c phase. But, the former sample shows a broad magnetic transition below 150 K, with a peak in M_{ZFC} at $T_p = 110$ K, whereas T_p is close to the T_c for the low-T_c phase. The broadness of magnetic transition and large difference between T_c and T_p may be ascribed to the superparamagnetic nature of the extremely fine (15 nm) particles of the sample annealed at 200 °C. In superparamagnetism, the ferromagnetic transition of a given sample is broadened due to the thermal fluctuation of the total moment on each particles of the sample, attributed to their single domain nature. This situation arises usually when the size of the particle is lower than certain critical value [Cul72].

Figure 3.4 shows the temperature variation of the zero field cooled (ZFC) and field cooled (FC) magnetization curves of the two different phases of La_2MnCoO_6. Even though a bifurcation in the magnetization occurs between the FC and the ZFC curves, below the transition temperature, this phenomenon, called thermomagnetic irreversibility, is not due to a spin-glass behaviour [Myd93], as interpreted in some reports [Gon01]. This is evident from the dynamic magnetization studies, which show no frequency dependence for the magnetic transition (see Section 3.1.4), unlike the spin-glasses. Nevertheless there are reports opposing the spin-glass nature of such systems showing thermomagnetic irreversibility [And02]. Instead, this behaviour in La_2MnCoO_6 may be due to the strong uniaxial anisotropy of the Co ions [Kum98a, Kum00].

Magnetic field dependence of the magnetization, as shown in Figure 3.5, confirms that the magnetic transition of the sample annealed at 200 °C corresponds to a ferromagnetic phase. The numbers on the curves represent the temperature at which the magnetization is measured. At 147 K, the M-H curve shows a linear behaviour, characteristic of a paramagnetic state. A continuous decrease in the magnetization with increasing temperature is obtained up to the T_c at higher magnetic fields. At low magnetic fields, the magnetizations are lower at lower temperatures than at some

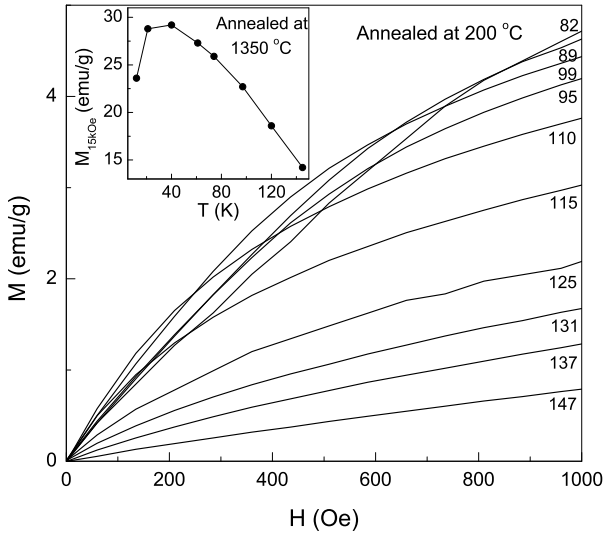

Figure 3.5: Magnetic field dependence of isothermal magnetization of the La_2MnCoO_6 sample annealed at 200 °C. The numbers on the curves indicate the temperature in K. Inset: Temperature variation of the magnetization at 82 K of the low-T_c phase, measured at 15 kOe.

higher intermediate temperatures. This corresponds to the magnetization drop in the low-field ZFC magnetization curves below T_p, as reported for different ferromagnetic compounds [Joy00]. Also, this excludes the possibility of an antiferromagnetic transition. Magnetic saturation is not attained even at 15 kOe (the maximum field used in this study), due to the insufficiency of the field as well as the anisotropy contribution from Co. The effect of anisotropy of Co ion is evident from the temperature dependence of magnetization at 82 K of the low-T_c phase of the compound, measured at a field of 15 kOe, as given in the inset of Figure 3.5. The magnetization increases with decreasing temperature, and below 50 K it starts decreasing, most likely due to the dominance of the anisotropy of Co. A large increase in the coercivity was observed at low temperatures, justifying the above conclusion. The magnetization was found to be unsaturated at 12 K and 15 kOe probably due to the same reason. It has been

reported that extremely low temperature and high magnetic fields are required for magnetic saturation for such Co incorporated compounds [Mah03].

HT samples

Based on the observation of two distinct ferromagnetic transition temperatures for the LT samples annealed at 700 and 1350 °C, it can be concluded that there are two different ferromagnetic phases for La_2MnCoO_6. Also, the LT samples annealed in the temperature range 800-1200 °C have both the above phases coexisting, where the amount of a given phase depends on the temperature of annealing. This gives some insight into the reported phase ambiguities associated with the samples of La_2MnCoO_6 synthesized by conventional solid-state method [Goo61], since the usual range of heat treatment in this method is 1000-1300 °C. Therefore, the magnetic properties of La_2MnCoO_6, synthesized by the ceramic method, are also explored.

ZFC magnetization curves of the sample prepared by the ceramic method and heated in air in the temperature range 1000-1300°C are compared in Figure 3.6. The samples heated at 1000 and 1100 °C show a major ferromagnetic transition at ∼230 K with the indication for the presence of another magnetic phase with a lower transition temperature below 200 K. On the other hand, the samples heated at 1200 °C and 1300 °C for a shorter duration show a major broad ferromagnetic transition below 200 K with a weak ferromagnetic transition at ∼230 K. After heating at 1300 °C for a longer period, a sharp ferromagnetic transition is observed at ∼150 K and still a minor rise in the magnetization is observed at ∼230 K. The results indicate that it is hardly possible to get the high-T_c phase of La_2MnCoO_6 in single phase form, if prepared by the usual ceramic method. However, pure low-T_c phase can be obtained by repeated heating of the sample at or above 1300 °C. The magnetic behaviour of the ceramic samples are sensitively dependent on the heating history. In most of the reports in the literature, the magnetization measurements are done in comparatively

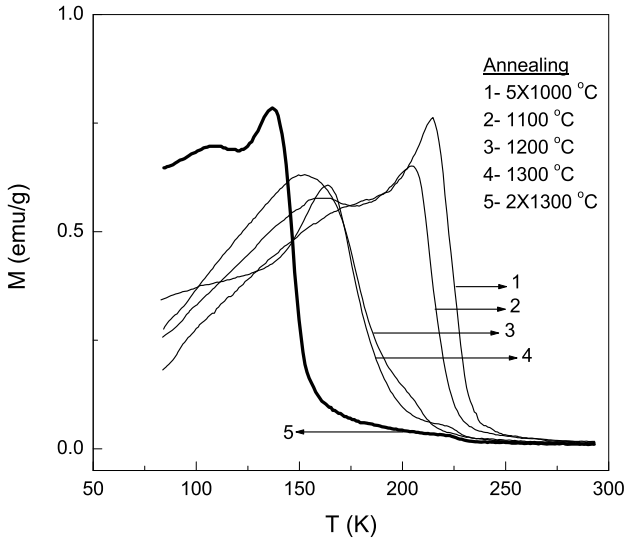

Figure 3.6: ZFC (H = 50 Oe) magnetization curves of the samples synthesized by the ceramic method and heated at different temperatures as indicated.

larger applied magnetic fields, which obscure the small contributions from the minor amounts of other magnetic phases. This unveils the cause of the contradictions in the reported magnetic behaviour of the compound.

3.1.4 AC-susceptibility studies

The ZFC magnetization curves of La_2MnCoO_6 samples annealed at 200, 700, and 1300 °C, measured in the temperature range 10-300 K, are compared in Figure 3.7. The Curie temperature is obtained as the temperature at which dM/dT is maximum, as shown in the figure for the sample annealed at 700 °C (high-T_c phase). Thus, for the high-T_c and low-T_c phases, T_cs are obtained as 225 K and 145 K, respectively. Interestingly the low-T_c phase obtained after high-temperature annealing, shows a cusp at 73 K. The sample annealed at 200 °C, though shows almost the same magnetic transition temperature, has no such well-resolved features and instead a broad decreasing

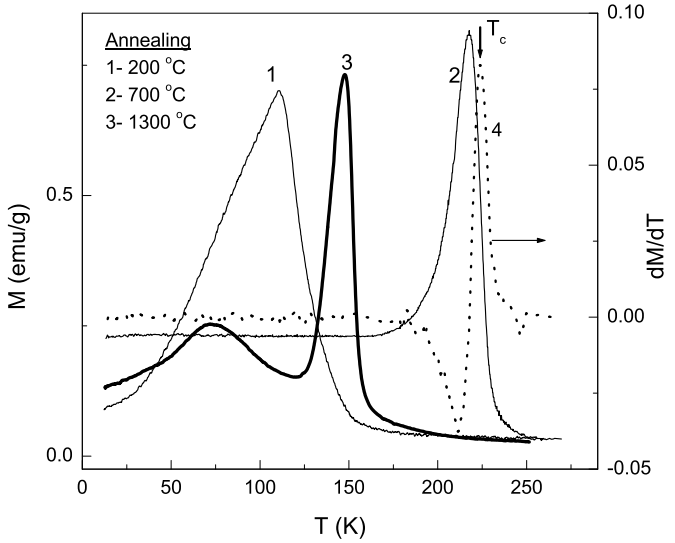

Figure 3.7: Comparison of the zero field cooled magnetization curves of the low-temperature synthesized La_2MnCoO_6 annealed at 200, 700 and 1300 °C, measured at 50 Oe. The dotted curve is the derivative of magnetization, dM/dT.

magnetization encompassing this cusp-region is observed. Neither the high-T_c phase has any such anomalous cusp below T_c. Such additional features, below T_c, have been reported for some Mn-site substituted systems. This has been explained in terms of small ferromagnetic clusters in the case of Al-substituted compounds [Kri00a, Kri00b]; due to Mn/Co disorder [Kyo03] and dynamic freezing of nanosized superparamagnetic domains or oscillations of pinned domain walls [Mah03] for Co-substituted compositions; from ferromagnetic clusters [Bla01] and domain wall pinning due to local anisotropy or structural defects [Bla02b] in the case of Ni substituted compounds. Measurement of the frequency dependence of AC-susceptibility is commonly practiced to understand the dynamics of domain wall motion in ferromagnets and spin freezing behaviour in spin-glasses. As observed in the ZFC magnetization curves, the cusp below Curie temperature is observed only in the low-T_c phase obtained after

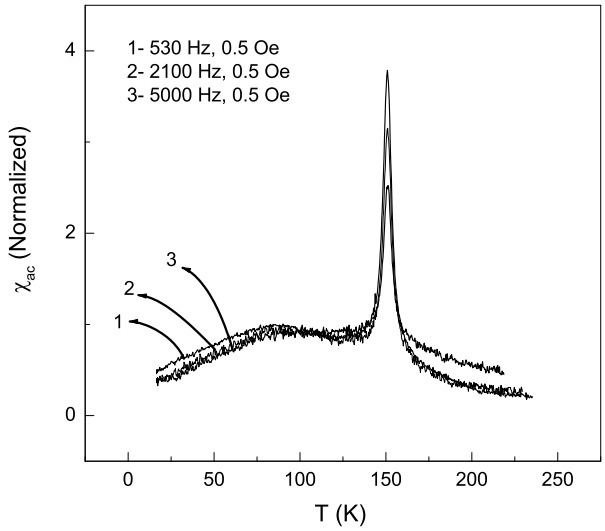

Figure 3.8: Temperature variation of the AC-susceptibility of the low-T_c phase of La_2MnCoO_6, measured at three different frequencies.

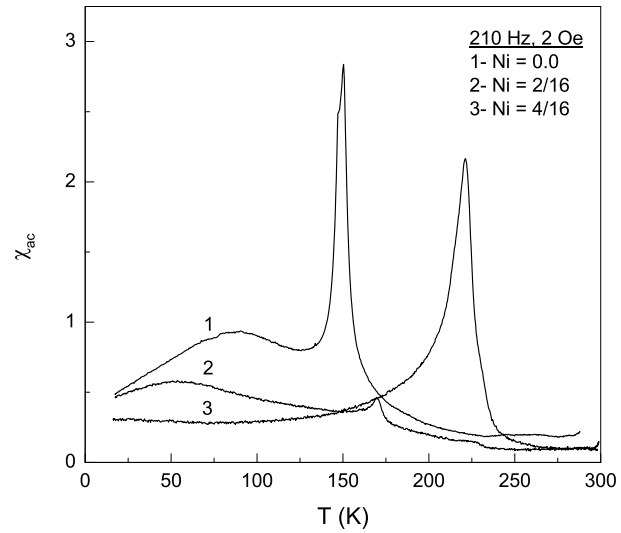

Figure 3.9: AC-susceptibility of Ni substituted La_2MnCoO_6, measured at 210 Hz and 2 Oe.

annealing at 1300 °C. AC-susceptibility measurements show that the ferromagnetic transition is independent of the frequency of the applied AC-magnetic field (See Figure 3.8). At the same time, the maximum of the cusp shifts to higher temperatures with the increase in frequency. This observation proves that the dynamics of magnetization is not related to a spin-glassy nature, because spin-glasses cannot have a magnetic transition, which is independent of frequency. Moreover, La_2MnCoO_6 shows all the features of a typical ferromagnet. Therefore, in the present case, the cusp as well as its frequency dependence can be because of the domain wall pinning effects, especially due to the strong uniaxial anisotropy of Co. However, it is difficult to demarcate the contributions from other effects, which leads to the pinning of domain walls. Evidence for the contribution of Co ion is obtained from those compositions (processed under identical conditions), where Co ions are partially replaced by Ni. The cusp broadens and shifts to lower temperatures and finally disappears for the case where more than 50% of Co is replaced by Ni (See Figure 3.9).

3.1.5 Determination of Spin-states of Mn and Co

It is confirmed that there are two possible ferromagnetic phases for La_2MnCoO_6, along with the high probability for the formation of mixed phases depending upon the heat treatment conditions. Also, the conditions of formation of the two phases are optimized. Therefore, it is the right opportunity for settling the issues regarding the spin-states of Co and Mn in the two different phases, by determining it meticulously. Three different methods are used here to get information on the spin-states; paramagnetic susceptibility measurements, x-ray photoelectron spectroscopic studies, and studies on the magnetic properties after substitution of a non-magnetic, isovalent ion.

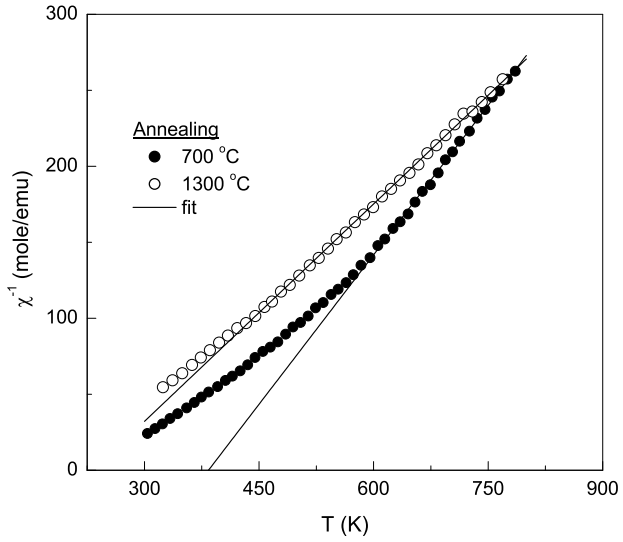

Figure 3.10: Temperature variation of inverse paramagnetic susceptibility of the two different phases of La_2MnCoO_6.

Paramagnetic susceptibility

Temperature variation of the inverse of the paramagnetic susceptibilities of the two pure phases of La_2MnCoO_6, obtained after annealing at 700 and 1300 °C are shown in Figure 3.10. Effective paramagnetic moment (μ_{eff}) is calculated from linear least-squares fit to the data at high temperatures. For the high-T_c phase, μ_{eff} is obtained as 3.52 μ_B (Bohr magneton) and paramagnetic Curie temperature, $\Theta = 378$ K. For the low-T_c phase, $\mu_{eff} = 4.01$ μ_B and $\Theta = 236$ K. Deviation from Curie-Weiss behaviour is observed below 600 K for the high-T_c phase and below 450 K for the other phase. In $LaCoO_3$ and $La_{1-x}Sr_xCoO_3$, existence of various possible spin-states (high-spin, intermediate-spin, and low-spin) of both trivalent and tetravalent Co ions have been predicted from magnetic and spectroscopic measurements [Tag78, Sai97a, Sai97b]. However, in $LaMnO_3$, and the La-site substituted manganates, paramagnetic susceptibility and ferromagnetic saturation magnetization measurements have indicated

Table 3.1: Comparison of μ_{so} and μ_{eff} for various spin-states of Mn and Co in the high-T_c (HTC) and low-T_c (LTC) phases of La_2MnCoO_6

Spin-states	$\mu_{so}(\mu_B)$	$\mu_{eff}(\mu_B)$
Mn^{+3} (S=2), Co^{+3} (S=2)	4.90	
Mn^{+3} (S=2), Co^{+3} (S=1)	4.00	4.01(LTC)
Mn^{+3} (S=2), Co^{+3} (S=0)	3.46	3.52(HTC)
Mn^{+4} (S=3/2), Co^{+2} (S=3/2)	3.88	4.01(LTC)
Mn^{+2} (S=5/2), Co^{+4} (S=5/2)	5.92	
Mn^{+2} (S=5/2), Co^{+4} (S=3/2)	5.00	
Mn^{+2} (S=5/2), Co^{+4} (S=1/2)	4.36	

that the trivalent Mn ions are present in their high-spin state [Jon50]. The theoretical spin-only values of the magnetic moment per Mn-site ion, μ_{so}, in the paramagnetic state, is calculated using the following equations (simple perovskite formula, $LaMn_{0.5}Co_{0.5}O_3$ is considered while calculating and comparing with the experimental values).

$$\mu_{Mn/Co} = [4S(S+1)]^{1/2} \tag{3.1}$$

$$\mu_{so} = [0.5\mu_{Mn}^2 + 0.5\mu_{Co}^2]^{1/2} \tag{3.2}$$

where, S is the total spin on the metal ion. For La_2MnCoO_6, the spin-only value of the paramagnetic moment, (μ_{so}), for various possible combinations of spin-states of Mn and Co are compared with the experimental μ_{eff} values in Table 3.1.

The μ_{eff} obtained for the high-T_c phase is comparable to the spin-only moment calculated for high-spin Mn^{+3} and low-spin Co^{+3}. Then it may be concluded that ferromagnetism arises in the high-T_c phase of the compound from Mn^{+3}-O-Mn^{+3} superexchange interactions alone, as the low-spin Co^{+3} ions are non-magnetic ($S = 0$). A previous report [Goo61], on ceramic samples also have suggested that this is the origin of ferromagnetism in $LaMn_{1-x}Co_xO_3$, though the $x = 0.5$ sample contained mixed phases. In the above report, the compound is prepared at 1100 °C, so that it is possible to have the high-T_c phase in relatively larger amount, and hence a majority

of trivalent ions, as observed for the sample heated at 1100 °C in the present work (see Figure 3.3). Another report on a sample synthesized by the decomposition of the freeze-dried acetate salts, and annealed in air at 1100 °C, also shows the predominance of high-spin Mn^{+3} and low-spin Co^{+3} [Elf00].

For the low-T_c phase (LTC), μ_{eff} is comparable to the spin-only moments calculated for a combination of high-spin Mn^{+3} and intermediate-spin Co^{+3} ($t_{2g}^5 e_g^1$) as well as for Mn^{+4} and high-spin Co^{+2}. This phase of La_2MnCoO_6 can be compared to the one reported, where the sample is heated above 1300 °C and have Mn^{+4} and Co^{+2} ions, as confirmed by electrical resistivity and seebeck coefficient measurements [Jon66]. Moreover, Θ and μ_{eff} in the above report are also comparable to that obtained for LTC in the present study. Similarly, there are many more reports on the $x = 0.5$ compositions, heated at or above 1300 °C, showing that Mn^{+4}/Co^{+2} combination is the ground state [Par97, Bul01, Kyo03]. Based on these arguments, it may be concluded that the Mn and Co ions are present as Mn^{+4} and Co^{+2} in the low-T_c phase of La_2MnCoO_6. The slightly larger value of μ_{eff} for LTC, when compared to μ_{so}, can be understood in terms of the contribution from spin-orbit coupling of Co^{+2} as has been generally observed for Co^{+2} containing compounds [Mul76]. Therefore, ferromagnetism in the low-T_c phase of La_2MnCoO_6 is from the Mn^{+4}-O-Co^{+2} superexchange interactions, in agreement with the previous report [Jon66].

Non-magnetic substitution with isovalent ion

Magnetic properties of La_2MnCoO_6 after substitution of Al for Mn or Co have been studied to obtain information on the spin-state of Co in the high-T_c phase. Al^{+3} ion (0.535 Å) is comparable in size with low-spin Co^{+3} (0.545 Å), but smaller than high-spin Mn^{+3} (0.645 Å). That is the structural strain in La_2MnCoO_6 (LMC) is already lower than that of $LaMnO_3$, as discussed in Section 1.4. Thus, replacing Mn or Co by Al in LMC may not help to increase the ferromagnetic strength, by improving the

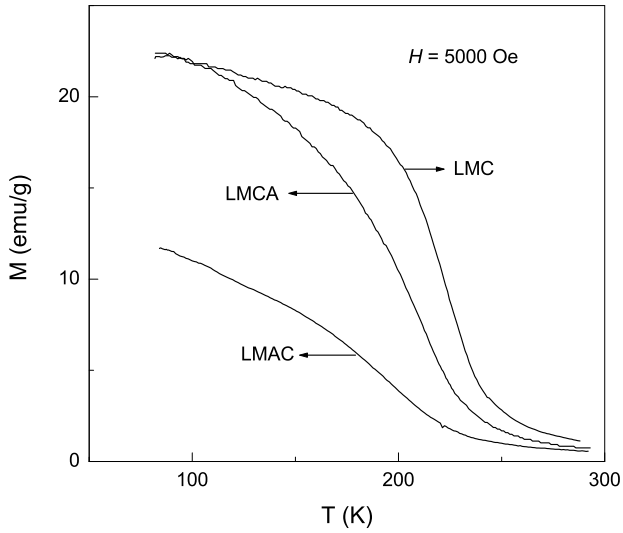

Figure 3.11: Temperature variation of magnetization (H = 5000 Oe) of La_2MnCoO_6 (LMC) and the Al-substituted samples, $La_2Mn_{0.8}Al_{0.2}CoO_6$ (LMAC), and $La_2MnCo_{0.8}Al_{0.2}O_6$ (LMCA).

B-O-*B* angle to a noticeable extent. Therefore, a sizeable change in the magnetic exchange strength, due to size effect is not expected. It was expected that if Co^{+3} is present in the low-spin state and ferromagnetism is due to Mn^{+3} alone, then there will not be much effect on the T_c or magnetization when Co is partially replaced by Al^{+3}. On the other hand, relatively large effects are expected on replacement of Mn^{+3} by Al^{+3}. Under identical conditions as that was used for the high-T_c phase of La_2MnCoO_6, two Al-substituted compositions, $La_2Mn_{0.8}Al_{0.2}CoO_6$ (LMAC) and $La_2MnCo_{0.8}Al_{0.2}O_6$ (LMCA) were prepared by the low-temperature method and annealed at 700 °C. Temperature variation of the magnetization of La_2MnCoO_6 (LMC), LMAC, and LMCA are compared in Figure 3.11. When Al is substituted for Co, it is found that the T_c or magnetization is not much affected, whereas when Al is substituted for Mn, the low temperature magnetization is drastically decreased and T_c is

Table 3.2: Experimental and calculated ferromagnetic moments of Al substituted La_2MnCoO_6, annealed at 700 °C. The values are for the simple perovskite formula $LaMn_{0.5}Co_{0.5}O_3$.

	LMC (μ_B)	LMAC (μ_B)	LMCA (μ_B)
Experimental (82 K, 15 kOe)	1.39	0.91	1.36
Mn^{+3} + Co^{+3} (S = 0)	2.0	1.6	2.0
Mn^{+3} + Co^{+3} (S = 1)	3.0	2.6	2.8
Mn^{+3} + Co^{+3} (S = 2)	4.0	3.6	3.6

shifted to lower temperatures considerably. The saturation magnetization, measured at 82 K and 15 kOe, for the three compositions are compared with the expected theoretical ferromagnetic moments in Table 3.2, assuming contributions from Mn^{+3} and different spin-states of Co^{+3}. Though the experimental values are much less than that of the theoretical values, due to the lower magnetic field and higher temperature of measurement, it may be seen that the experimental values are comparable for the unsubstituted and Co-site substituted compositions. La_2MnCoO_6 attains full magnetic saturation only at very low temperatures and under very high magnetic fields [Goo61]. The drastic drop in the observed saturation magnetization when Mn is replaced by Al is in accordance with the decrease in the expected ferromagnetic saturation moment when Co^{+3} is in the low-spin state. This clearly indicates that the Co^{+3} ions do not contribute much to magnetism in the high-T_c phase of La_2MnCoO_6 and that the contribution to ferromagnetism is mainly from Mn^{+3} ions.

XPS studies

The identical Curie temperatures of the low-temperature synthesized La_2MnCoO_6, annealed at 200 °C (LMC200) and 1300 °C (LMC1300) is an indication for the formation of the low-T_c phase of the compound at low temperatures, containing Mn^{+4} and Co^{+2} ions. If this phase is formed initially at low temperatures, then it is con-

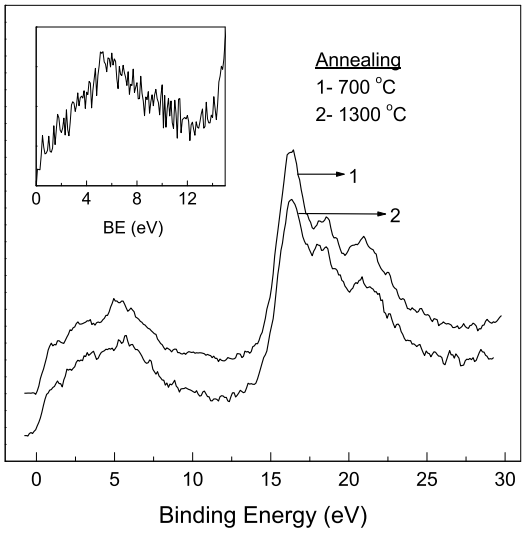

Figure 3.12: XPS valence band spectra of La_2MnCoO_6, annealed at 700 and 1300 °C. Inset: XPS valence band spectra of the unscraped surface of the sample annealed at 700 °C.

verted to the high-T_c phase after heating to 700 °C (LMC700) because of a possible charge disproportionation Mn^{+4}+Co^{+2} → Mn^{+3}+Co^{+3} and further converted back to the low-T_c phase after annealing at higher temperatures due to the charge disproportionation Mn^{+3}+Co^{+3} → Mn^{+4}+Co^{+2}. To verify these arguments, XPS studies were made on the three samples annealed at 200, 700, and 1300 °C.

The valence band x-ray photoelectron spectra (XPS) of the two different phases of La_2MnCoO_6, LMC700 and LMC1300 are shown in Figure 3.12. A broad peak around 10 eV, which was observed in the unscraped samples (see inset of Figure 3.12) is absent in the spectra indicating that the sample surface is free from contamination. Identical valence band features are observed for both the phases and the features are similar to those reported for $LaCoO_3$ [Cha92].

The $2p$ core-level XPS of the transition metal ions is known to be very sensitive

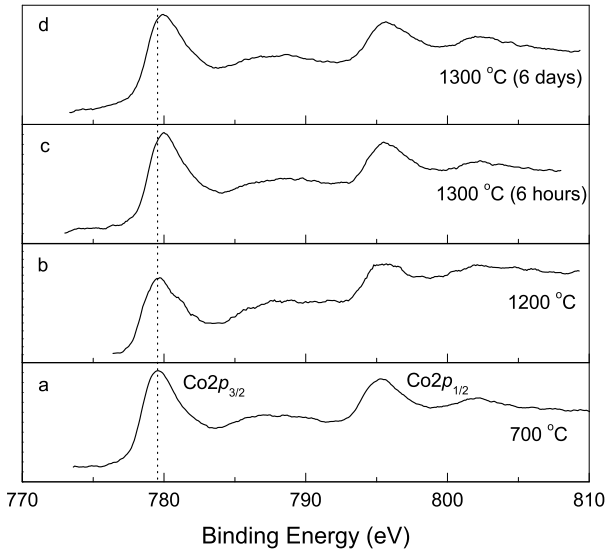

Figure 3.13: Co2p XPS of La_2MnCoO_6, (a) high-T_c phase, (b) sample heated to 1200 °C, (c) sample heated to 1300 °C for 6 h, and (d) low-T_c phase.

to their 3d electron content. However, under the same octahedral coordination environment, Co 2p binding energy (BE) is lower for low-spin Co^{+3}, when compared to that of high-spin Co^{+2}, contrary to what is observed for other transition metal ions [Bri74]. 2p core-level XPS of Co in the two different phases of La_2MnCoO_6 are shown in Figure 3.13 (curves a & d). 2p core-level XPS of Co in two mixed phase samples (see Figure 3.3) showing magnetic transitions between 150 and 230 K are also compared in the figure (curves b & c). The spectra are almost identical, the $2p_{3/2}$ peak of the low-T_c phase (curve d) is observed at a slightly higher BE compared to that of the high-T_c phase (curve a). The mixed phase sample undergoing a major magnetic transition close to the T_c of the high-T_c phase of the compound shows a Co $2p_{3/2}$ XPS peak (curve b) at the BE of the peak of the high-T_c phase, whereas the mixed phase sample undergoing a major magnetic transition close to the T_c of the low-T_c phase of the compound shows the Co $2p_{3/2}$ XPS peak (curve c) at the BE of

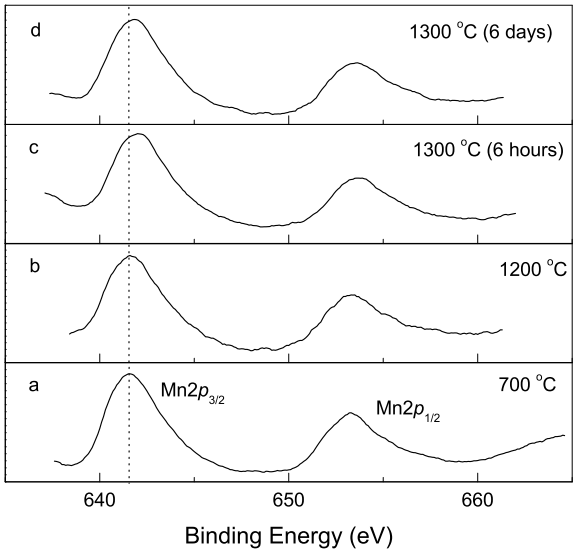

Figure 3.14: Mn 2p XPS of La_2MnCoO_6, (a) high-T_c phase, (b) sample heated to 1200 °C, (c) sample heated to 1300 °C for 6 h, and (d) low-T_c phase.

the peak of the low-T_c phase. This indicates that the observed difference in the BEs of the two single phase compounds is not due to any experimental error and that the spin-states of Co are different in the two different phases of La_2MnCoO_6.

The Co $2p_{3/2}$ peaks are observed at 779.6 and 780.1 eV, respectively, for the high-T_c and low-T_c phases of La_2MnCoO_6. These values are comparable to that observed for Co^{+3} in $LaCoO_3$ and $LiCoO_2$, in which the trivalent Co ions are reported to be in the low-spin configuration and for Co^{+2} in CoO with high-spin Co^{+2}, respectively [Lom83, Van91]. Majority of the cobalt ions in the two mixed phase samples have their spin-states closer to that of the spin-state of Co in either one of the two single phases. Recent XPS studies and electronic structure calculations [Kor96, Sai97b, Fla99, Tho00] have indicated that the intermediate-spin state ($t_{2g}^5 e_g^1$) is the most probable spin-state of trivalent Co ions in $LaCoO_3$ and $La_{1-x}Sr_xCoO_3$ at room temperature. On the other hand, x-ray absorption spectroscopic (XAS) studies

indicate a low-spin state of Co^{+3} in $LaCoO_3$, at room temperature [Abb93]. Hence, it is possible that the Co ions are present as low-spin and/or intermediate-spin Co^{+3} in the high-T_c phase of La_2MnCoO_6. In the low-T_c phase of La_2MnCoO_6, cobalt ions are present as high-spin Co^{+2}.

XPS of Mn $2p$ in the two phases of La_2MnCoO_6 (curves a & d) and in the samples containing mixed phases (curves b & c), shown in Figure 3.14, are also indicative of different spin-states of Mn in the two different phases. The $2p_{3/2}$ peaks of Mn in the high-T_c and low-T_c phases of the compound are observed at 641.6 eV and 641.9 eV, respectively. The BE of the Mn $2p_{3/2}$ peak of the mixed phase sample showing a higher magnetic transition temperature is close (curve b) to that of the high-T_c phase and for the second mixed phase sample the BE is close (curve c) to that of the low-T_c phase of the compound. This is similar to that observed in the Co $2p$ XPS of the mixed phase samples, indicating a difference in the oxidation state of Mn in the two different phases of La_2MnCoO_6. The observed difference in the BE of the $2p_{3/2}$ peak in the two phases is comparable to that reported for Mn_2O_3 and MnO_2 where the Mn ions are present as Mn^{+3} and Mn^{+4}, respectively [Oku75] or that observed in the Mn $2p$ XPS of $La_{1-x}Sr_xMnO_3$, [Sai95] where a maximum difference of 0.4 eV is obtained for $x = 0$ (Mn^{+3}) and $x = 0.9$ (predominantly Mn^{+4}). The present observation indicates lower valence state of Mn (as Mn^{+3}) in the high-T_c phase and higher valence state of Mn (as Mn^{+4}) in the low-T_c phase of La_2MnCoO_6 and the BE values are in-line with the reported values. These valence states of Mn in the two phases are in accordance with that found for Co in the same phases (trivalent Mn when Co is trivalent and tetravalent Mn when Co is divalent), which take care of oxygen stoichiometry and preserve charge neutrality.

The XPS results give evidence for the different valence states of Mn and Co in the two different phases of La_2MnCoO_6. It is very difficult to distinguish the actual spin-state of Co^{+3} from XPS studies. It is possible that in the case of La_2MnCoO_6

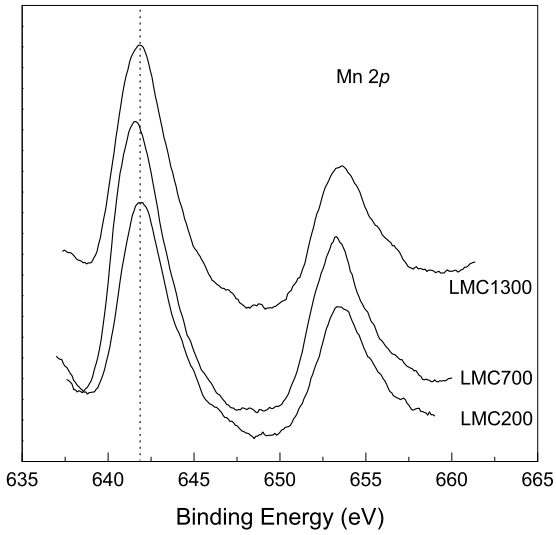

Figure 3.15: Mn $2p$ XPS of La_2MnCoO_6 annealed at 200, 700, 1300 °C.

also Co^{+3} may be in the low or intermediate spin-state as observed in $LaCoO_3$ from XAS and XPS studies. However, the effective paramagnetic moment (calculated from Curie-Weiss fit to the paramagnetic susceptibility at high temperatures) of the phase with $T_c \approx 230$ K is comparable to the spin-only value calculated for Mn^{+3} and low-spin Co^{+3} ($\mu_{eff} = 3.52\ \mu_B$, $\mu_{so} = 3.46\ \mu_B$). The effective moment is comparatively less than the spin-only moment calculated for Mn^{+3} and intermediate-spin Co^{+3} ($\mu_{so} = 4.0\ \mu_B$). This implies that the trivalent cobalt ions are likely to be present in their low-spin state in the high-T_c phase of La_2MnCoO_6. If this is correct, then it may be expected that ferromagnetism in this phase arises only from Mn^{+3}-O-Mn^{+3} superexchange interactions.

Evidence for the identical spin-states of Mn and Co in LMC200 and LMC1300, showing identical Curie temperatures, is also obtained from core-level XPS studies. The $2p$ core-level XPS of Mn and Co in La_2MnCoO_6 are compared in Figure 3.15 and Figure 3.16, respectively, for LMC200, LMC700, and LMC1300. The Mn and

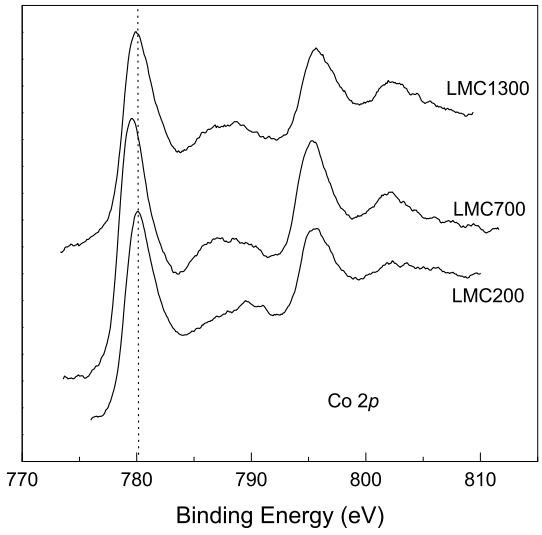

Figure 3.16: Co $2p$ XPS of La_2MnCoO_6 annealed at 200, 700, 1300 °C.

Co $2p_{3/2}$ peaks are observed at the same binding energies for LMC200 and LMC1300 whereas these peaks are observed at lower binding energies for LMC700. The identical Mn and Co $2p_{3/2}$ XPS binding energies of LMC200 and LMC1300 then indicates that the spin-states of Mn and Co are identical in the samples processed at very low temperatures (200 °C) and at very high temperatures (1300 °C). This then explains why the magnetic transition temperatures are almost identical for LMC200 and LMC1300, ignoring the relatively broader magnetic transition of LMC200 which is due to the smaller particle sizes of the sample. This also confirms a double charge disproportionation $Mn^{+4} + Co^{+2} \rightarrow Mn^{+3} + Co^{+3} \rightarrow Mn^{+4} + Co^{+2}$, as occurring when the samples are annealed in the temperature range 200–1300 °C.

3.2 Mn-rich compositions ($0 < x < 0.5$)

Studies on Mn-rich compositions are important to understand the origin of ferromagnetism when Mn in the A-type antiferromagnetic $LaMnO_3$ is replaced by other ions. Even though different transition metal ions can be substituted in the Mn-site, ferromagnetism does not result in all the cases. In many of the cases, the incipient ferromagnetic behaviour vanishes quickly with the increase in the concentration of the substituent in the Mn-rich region (see Section 1.4). However, as it is evident that $LaMn_{1-x}Co_xO_3$ is ferromagnetic when $x = 0.5$, it is possible that other compositions in the Mn-rich region are also ferromagnetic. Therefore, detailed studies on these Mn-rich compositions are expected to give information on the evolution of ferromagnetism in $LaMnO_3$ on partial replacement of Mn by Co.

3.2.1 Background

In the case of Mn-rich $LaMn_{1-x}Co_xO_3$ ($x < 0.5$) compounds, the magnetic data in various reports accede to the fact that all compositions are ferromagnetic and Curie temperature increases with the increasing concentration of Co. As it is elaborated in Section 3.1, the nominal composition, La_2MnCoO_6, show unprecedented magnetic behaviour, due to its metastable ferromagnetic phases. This underpins the relevance of studying the $x < 0.5$ region also, to look for the plausibility for any metastable phases in this compositional region. The most important issue about the Mn-rich compositions is another one; that is the contradicting reports about the spin-states of Mn and Co ions. Therefore, it is expected that the knowledge about the metastable phases of $x = 0.5$ may shed light on the underlying cause for these conflicts.

There are as many contradicting reports about the origin of ferromagnetism, as that about the spin-states of Co and Mn. Some reports stick to the divalent nature of Co and the positive Mn^{+4}-O-Co^{+2} superexchange or the Mn^{+3}-O-Mn^{+4} double

exchange as the origin of ferromagnetism. Also, trivalent nature of Co is equally reported, with positive isotropic Mn^{+3}-O-Mn^{+3} superexchange. However, the crystal structure is reported to be orthorhombic in the range $0.1 \leq x \leq 0.4$, in most of the cases [Gil57, Nar85, Elf00]. The orthorhombic structure of these compositions is not unexpected, when compared to that of stoichiometric $LaMnO_3$. The Mn-rich compositions in $LaMn_{1-x}Co_xO_3$ ($x < 0.5$) are studied in this work, based on the understanding of the influence of the processing conditions on the properties of $x = 0.5$, to gain information on the spin-states of Co and Mn, crystal structure and ferromagnetic phases. Temperature variation of the zero field cooled magnetization of the samples, synthesized by the low-temperature and the ceramic methods, annealed at different temperatures, for all compositions, are measured first to optimize the conditions at which the ferromagnetic phases of different compositions are formed in single phase forms.

3.2.2 Magnetic measurements

Figure 3.17 shows the ZFC magnetization curves of the low-temperature synthesized $LaMn_{1-x}Co_xO_3$ ($0 < x \leq 0.5$) samples annealed at 200 °C. All the compositions behave almost identical in terms of the magnetic transition temperature. This indicate that the magnetic transition is hardly dependent on the amount of Co. It was difficult to determine the Mn^{+4} content in the 200 °C annealed samples, using oxygen estimation, because of the high carbon content. From XPS studies, it was found that Mn and Co ions are present as Mn^{+4} and Co^{+2} (high-spin) in La_2MnCoO_6, i.e., for the samples annealed at 200 °C of $x = 0.5$ (see Section 3.1.5). Therefore, it can be assumed that all the 200 °C annealed Mn-rich $LaMn_{1-x}Co_xO_3$ compositions may contain at least an equivalent amount of Mn^{+4} as that of Co [Heb02a]. And the identical magnetic transition temperatures for all compositions may be originating from the ion common to them, i.e. Mn^{+4}. So, there are two possible positive superexchanges, viz.,

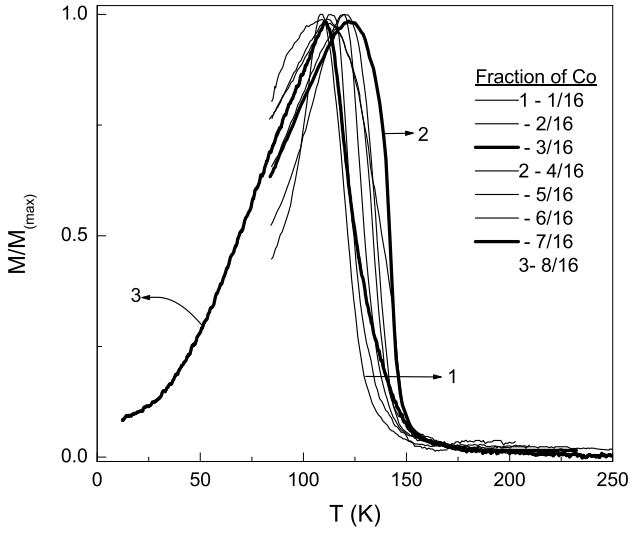

Figure 3.17: Comparison of the ZFC magnetization curves of samples annealed at 200 °C, for different compositions.

Mn^{+4}-O-Co^{+2} and Mn^{+3}-O-Mn^{+4}, capable of generating ferromagnetism, depending up on the concentration of Co. Since, both these exchanges are moderately ferromagnetic [Goo63], their strengths can be considered to be equal. Therefore, at lower Co concentrations, Mn^{+3}-O-Mn^{+4} will be the dominating superexchange mechanism and the Mn^{+4}-O-Co^{+2} superexchange for higher Co content. As a result of this, all the Mn-rich ($0 < x \leq 0.5$) compositions behave magnetically almost identical. Here, the contribution from Mn^{+3}-O-Mn^{+3} superexchange will be negligible, even at lower Co concentrations, due to the randomness in the distribution of Mn^{+3} and Mn^{+4} ions.

Figures 3.18, 3.19 and 3.20 show the effect of annealing of the low-temperature synthesized samples at different temperatures, for $x = 0.125$ (2/16), 0.25 (4/16) and 0.375 (6/16), respectively. In the case of $x = 0.125$, the sample annealed at 700 °C shows multiple magnetic transitions, one at ∼180 K and the second one at the same temperature as in the case of the sample annealed at 200 °C. Again, a single sharp

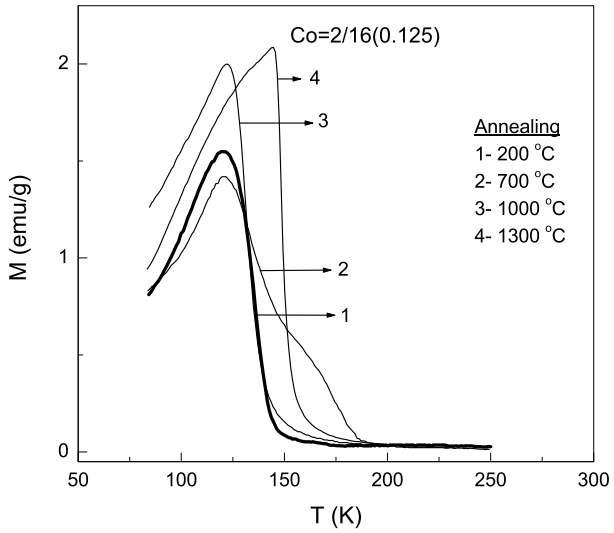

Figure 3.18: ZFC magnetization curves of $x = 0.125$, for samples annealed at different temperatures

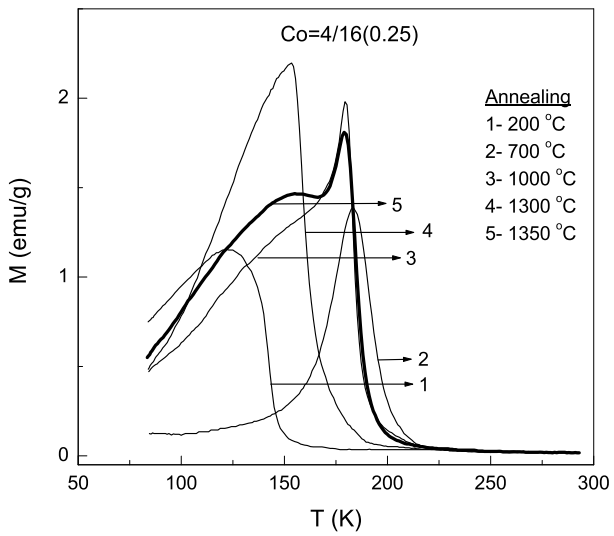

Figure 3.19: ZFC magnetization curves of $x = 0.25$, for samples annealed at different temperatures

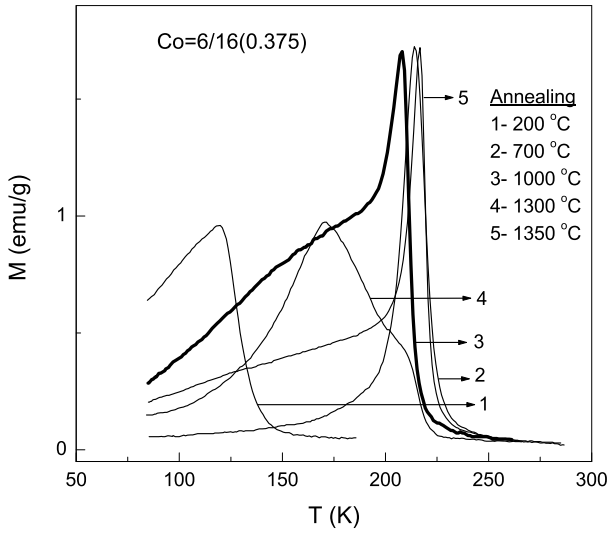

Figure 3.20: ZFC magnetization curves of $x = 0.375$, for samples annealed at different temperatures

magnetic transition is obtained below 140 K after annealing at 1000 °C and the T_c is further increased to 150 K after annealing at 1300 °C. Almost similar behaviour is observed for the other two compositions also. For $x = 0.25$, a single, but relatively broad, magnetic transition close to ∼200 K is observed for the sample annealed at 700 °C and the magnetic transition temperature decreases with increasing annealing temperature. However, after increasing the annealing temperature from 1300 to 1350 °C, the T_c increases and becomes identical to that of the sample annealed at 700 °C. It is interesting to note that one of the transition temperatures observed for $x = 0.125$ for the sample annealed at 700 °C is at the T_c of $x = 0.25$ annealed at 1000 °C. On the other hand, for $x = 0.375$, the T_c s are highest and identical for the samples annealed at 700 and 1350 °C, a sharp magnetic transition with a T_c lower by 25 K is observed for the samples annealed at 1000 °C and mixed phase behaviour is observed for the sample annealed at 1300 °C.

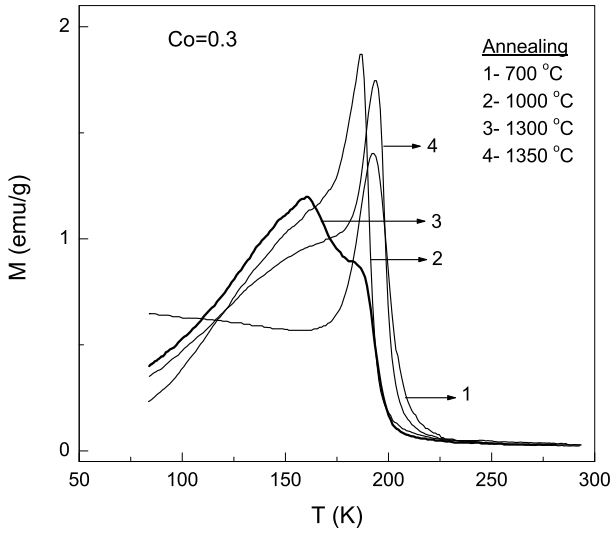

Figure 3.21: ZFC magnetization curves of $x = 0.3$, for samples annealed at different temperatures

Similar annealing temperature dependence of the magnetic transition is observed when the concentration of Co is varied by fractions of 10, as shown in Figure 3.21 for one of the compositions. As shown in the figure, for $x = 0.3$, multiple phase-like behaviour is observed when annealed at 1300 °C and T_c increases and become identical to the sample annealed at 700 °C, upon annealing at 1350 °C.

For all the compositions containing larger amounts of Co ($x > 0.125$), highest magnetic transition temperature is observed for the samples annealed at 700 °C. Figure 3.22 compares the ZFC magnetization curves of all samples in the Mn-rich region of $LaMn_{1-x}Co_xO_3$, annealed at 700 °C. The corresponding curve of a composition with $x > 0.5$ is also shown in the figure for comparison. The magnetic transitions are very broad for $x = 1/16$ and $2/16$, with the onset of a magnetic transition below $\sim$185 K. The sharpness of the magnetic transition as well as the magnetic transition temperature increases with increasing concentration of Co. The highest transition

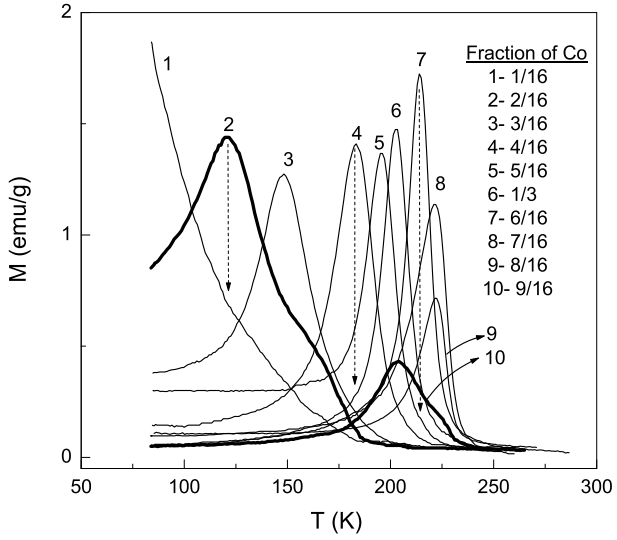

Figure 3.22: Comparison of the ZFC magnetization curves of all compositions, for samples annealed at 700 °C for 12 hours.

temperature is observed for x close to 0.5. Further increasing the concentration of Co above $x = 0.5$ causes the formation of multiple ferromagnetic phases (as discussed in Section 3.3). Interestingly, all the Mn-rich samples show the tendency to form a new ferromagnetic phase with a higher and different T_cs (compared to the identical T_cs observed for the samples annealed at 200 °C). Those Mn-rich compositions for which x is close to zero show an incipient high temperature magnetic transition whereas, those near to $x = 0.5$ form pure phases with sharp magnetic transitions. By comparing with the results obtained for the $x = 0.5$ composition annealed at 700 °C, it is possible that, in all the compositions, Mn and Co may undergo either a redistribution of charges or a redistribution of ions, in common. The fact that an increase in the Curie temperature is observed in all the Mn-rich compounds, the observed anomalies are expected to be due to the reduction of Mn^{+4} to Mn^{+3} after annealing at ≈ 700°C. This argument is supported by the fact that the ground state

of Mn and Co ions in the high-T_c phase of La_2MnCoO_6, formed at 700 °C, is Mn^{+3} and low-spin Co^{+3} (Section 3.1.5). But, this observation is opposed by the reports showing that the reaction Mn^{+4}+ Co^{+2}⇌Mn^{+3}+ Co^{+3} is biased to left by 0.2–0.3 eV [Jon66, Nar85, Par97, Par99, Das03]. The reduction in energy corresponds to the difference in the ionization energies of Mn^{+3} and Co^{+2}. The thermal energy corresponding to an annealing temperature of 700 °C is only 0.08 eV and therefore, the trivalent ion formation is energetically unfavorable. Nevertheless, there are reports indicating that, in spite of this energy bias, such a charge redistribution can reduce the elastic energy [Das03]. Neutron diffraction studies on the $LaMn_{1-x}Ga_xO_3$ series give information about the retention of the alternate-ferromagnetic (001) planes of $LaMnO_3$, even though the trivalent Ga and Mn ions are of similar sizes, i.e., the Mn and Ga ions occupy alternate (001) planes. For 50% Ga, the *B*-site ions are randomly distributed, but the ferromagnetic sheets in the (001) planes of the A-type $LaMnO_3$ are retained [Cus01]. For $0 < x < 0.4$, Ga orders into the alternate (001) ferromagnetic planes [Goo61]. Here, the driving force for the ion ordering is suggested to be the relief in elastic energy associated with the static orbital ordering in the O′-orthorhombic structure. Similarly, in the case of Ni-substituted $LaMnO_3$, it is predicted that the reaction Mn^{+3}+ Ni^{+3}⇌Mn^{+4} + Ni^{+2} can be biased either to the right or to left depending up on the Mn concentration, the temperature and the degree of ionic-ordering [Vas84]. This is most likely happening in the present case also.

Therefore, an ordering of Mn and Co ions in the alternate (001) planes, facilitating a cooperative Jahn-Teller distortion, may be the reason for the formation of the trivalent ions at 700 °C. In short, it may be concluded that, Mn^{+3}, Mn^{+4} and Co^{+2} ions are somewhat randomly distributed in the samples annealed at 200 °C, showing similar magnetic transition temperatures. While increasing the annealing temperature to 700 °C, gradually these ions become more ordered in the lattice. This

ordering is most likely by the charge redistribution, $Mn^{+4} + Co^{+2} \rightarrow Mn^{+3} + Co^{+3}$,in such a way that the trivalent Mn ions are present mostly in the alternate (001) planes and trivalent Co in the remaining (001) planes. The ion ordering by an ion redistribution may not be possible at a comparatively lower temperature such as 700 °C. Another supporting fact for the trivalent ion formation is that, the average ionic size of the Mn-site ions decreases considerably by this process and thereby decreasing the structural stress. This can be understood from the effective average ionic radii of the two possibilities, viz., 0.6375 Å = (0.745 Å for Co^{+2}(HS) + 0.530 Å for Mn^{+4})/2 and 0.595 Å = (0.545 Å for Co^{+3}(LS) + 0.645 Å for Mn^{+3}(HS)).

The ZFC magnetization behaviour of $LaMn_{1-x}Co_xO_3$ is highly peculiar after annealing at 700 °C (See Figure 3.22). The samples with $x = 1/16$ and 2/16 (curves 2 and 3) show a sharp rise in magnetization at a temperature which is matching with the T_c of $x = 4/16$ (curve 5), 183 K. Similarly there is an incipient rise in the magnetization of 3/16, at ∼185 K. This temperature is at the magnetic transition temperature for $x = 4/16$. The compositions with $x = 1/16$, 2/16, and 3/16 are therefore under the influence of a composition $x = 4/16$ which can be formed more easily (may be because of the possible ordering of Mn and Co at this concentration). All the compositions in the range $3/16 \leq x \leq 8/16$ show only one transition, whose broadness decreases with the increase in x. Similar to the behaviour of the lower Co concentrations, which are affected by the presence of $x = 4/16$ in the samples, the compositions in the higher range, close to $x = 0.5$, are also affected by the preferential formation of this composition. The extreme Mn-rich compositions ($x = 6/16$ and 7/16; curves 8 and 9) are showing the initial-rise in the magnetization coinciding with that of the T_c of $x = 8/16$ at 225 K. Another noticeable feature is that the magnetization curve of $x = 9/16$ is a replica of the curve of $x = 1/16$.

The ZFC magnetization curves of the Mn-rich $LaMn_{1-x}Co_xO_3$ samples, annealed at 1000 °C, are shown in Figure 3.23. Unlike in the case of annealing at 700 °C,

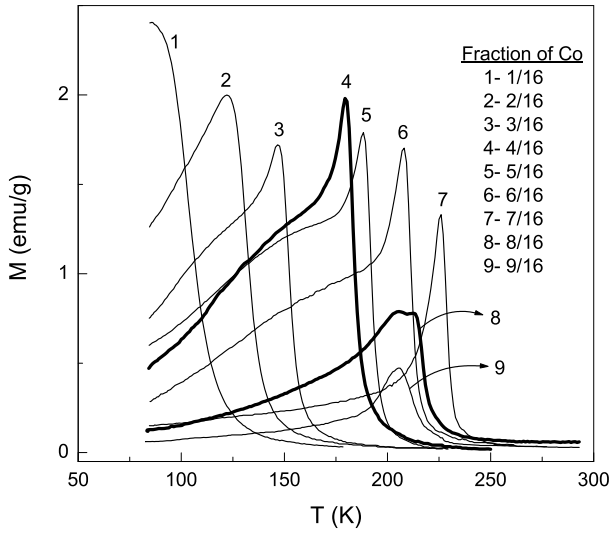

Figure 3.23: ZFC magnetization curves of all compositions, for samples annealed at 1000 °C

all the Mn-rich samples, except x =8/16 and 9/16 show relatively sharp magnetic transitions. The high-T_c ferromagnetic phase of $x = 8/16$, as already discussed in the Section 3.1.3, is formed only when annealed in a narrow temperature range close to 700 °C and it starts showing the signature of a mixed phase character on annealing above 700 °C. Similarly, the 9/16 samples even after annealing at 1000 °C does not show a single ferromagnetic phase character.

The magnetic transition temperature increases with the increase in the Co concentration for the samples annealed at 700 and 1000 °C, though the T_cs are slightly different for the corresponding compositions. Higher T_cs are observed for the 700 °C annealed samples. However, the magnetic transitions of these samples are some what broader than those of the 1000 °C annealed samples. This is probably because of the conversion of the Mn^{+4} and Co^{+2} present (equivalent to the amount of substituted Co) in the samples annealed at 200 °C to Mn^{+3} and Co^{+3}, as observed in the case

of La_2MnCoO_6. For La_2MnCoO_6, a high-T_c phase with Mn^{+3} and Co^{+3} is formed after annealing at this temperature. As discussed, there is a tendency to form the $x = 0.5$ compositions, in which Mn and Co ions are ordered in specific lattice sites, for those compositions close to $x = 0.5$. Therefore, the higher T_cs and broader magnetic transitions observed for these compositions, formed at 700 °C, can be due to this influence, i.e. the compounds are not truly single phasic. Further annealing at 1000 °C converts all compositions to single phase forms with the Mn^{+3} and Co^{+3} ions in the proper lattice sites.

The most surprising observation is that the Curie temperatures of all the Mn-rich samples, after annealing at 1300 °C, decreases to a narrow temperature range of 145-150 K, irrespective of the Co content, as shown in Figure 3.24. This is analogous to the case of the samples annealed at 200 °C, where transition temperatures of all the samples lie in the range 120-140 K. This shows that a second redistribution of charge or ion is occurring in $LaMn_{1-x}Co_xO_3$ when annealed at higher temperatures. The studies on the spin-states of La_2MnCoO_6 samples annealed at 1300 °C showed that the ground state for the ions is Mn^{+4}/Co^{+2} and it is supported by many of the reports in the literature (see Section 3.1.5).

For samples annealed at 1300 °C, unlike in the case of the samples annealed at 700 °C, an ion redistribution is most likely driving the reaction, $Mn^{+4} + Co^{+2} \rightleftharpoons Mn^{+3} + Co^{+3}$, to the left hand side. This argument is supported by the fact that the miscibility gap between the two end members, in $LaMn_{1-x}Co_xO_3$, disappears at 1100 °C [Kyo04] or 1300 °C [Jon66]. Therefore, a redistribution of ions into alternating (111) planes results. This happens because, in the case of (001) ordering, a given (001) face of a unit cell with one type of ion will have a different dimension from that of the opposite (001) face with a different ion, generating stress in the bonds. Whereas, in the case of (111) ordering, opposite faces contain different ions, avoiding a difference in dimensions. Thus, when the ions are (111) ordered, the need for a structural

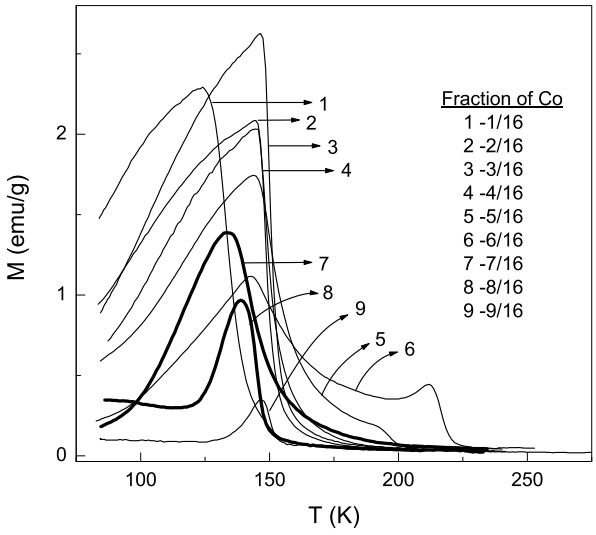

Figure 3.24: ZFC magnetization curves of all compositions, for samples annealed at 1300 °C

stabilization by cooperative Jahn-Teller ordering is less. Hence the Mn^{+3} is oxidized to Mn^{+4}, with a concomitant reduction of Co^{+3} to Co^{+2}, which also is favorable by ionization energy considerations. This tendency for ordering is visible from the variation of lattice parameters with the concentration of Co (as discussed in next section with respect to Figure 3.31).

This ordering is probably because of the increasing Mn^{+3}-O-Co^{+3} superexchange across the (001) planes and isotropic Mn^{+3}-O-Mn^{+3} superexchange within the Mn-rich (001) planes. Naturally, the Co-rich (001) planes will not contribute to the ordering of the moments, owing to its low-spin state and instead it supports the inter planar superexchange. The common T_c of the compositions in the samples annealed at 200 and 1300 °C are probably due to Mn^{+4}-O-Mn^{+3} superexchange at lower x and Mn^{+4}-O-Co^{+2} superexchange at higher x, in the Mn-rich limit, even though the latter samples will have a (111) ordering.

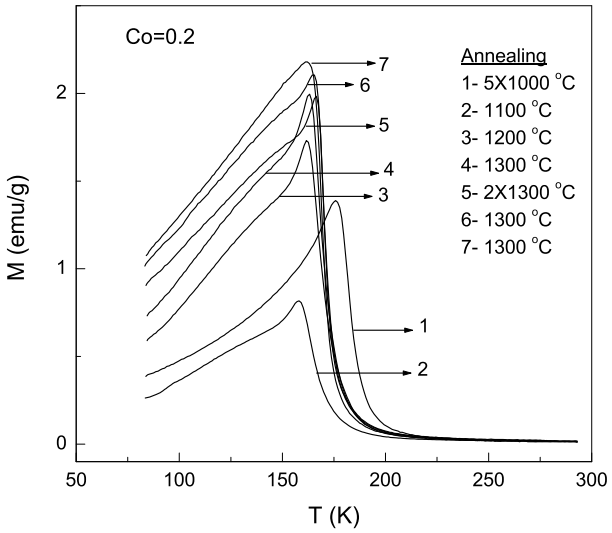

Figure 3.25: ZFC magnetization curves of $x = 0.2$ composition synthesized by the ceramic method and heated at different temperatures, as indicated.

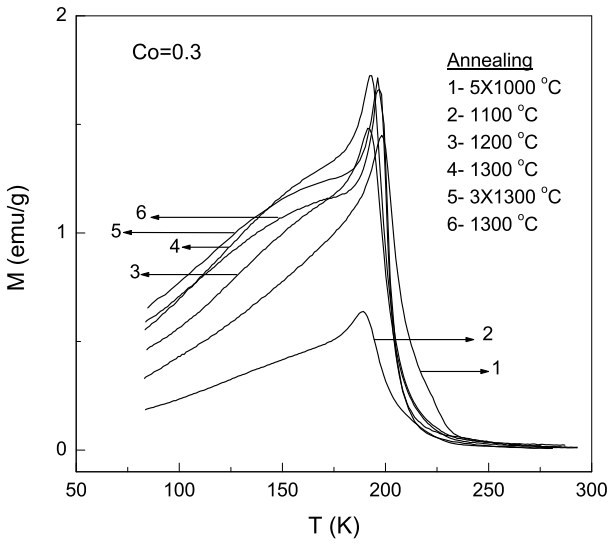

Figure 3.26: ZFC magnetization curves of $x = 0.3$ composition synthesized by the ceramic method and heated at different temperatures, as indicated.

In the case of $LaMn_{1-x}Co_xO_3$ samples synthesized by the high-temperature ceramic method, a different scenario is observed. Figures 3.25 and 3.26 show the ZFC magnetization curves of the ceramic samples of $x = 0.2$ and 0.3, respectively, heated at different temperatures in the range 1000–1300 °C. In both cases, the samples heated at 1000 °C show higher magnetic transition temperatures which are decreased after heating at 1100 °C. Further heatings at higher temperatures or at the highest temperature (1300 °C) for longer durations increase the sharpness of the magnetic transition. The magnetic transition temperatures observed for the ceramic samples after final annealing at 1300 °C and the low-temperature synthesized samples annealed at 1000 °C are comparable. However the magnetic transition temperatures are sharper for the low-temperature synthesized samples.

Thus the studies on different Mn-rich compositions in $LaMn_{1-x}Co_xO_3$, synthesized by a low-temperature method as well as the high-temperature method and annealed at different temperatures show that the magnetic transition temperatures depend on the annealing temperatures and methods of synthesis. It is very difficult to define the magnetic transition temperatures of different compositions in the Mn-rich region.

3.2.3 Powder XRD studies

All the compositions prepared by the low-temperature method, after annealing at 200 °C, show similar characteristics in the powder XRD patterns, as shown in Figure 3.27. As observed in the case of the $x = 0.5$ composition (La_2MnCoO_6), a weak and broad reflection is observed in all cases below the most intense peak, as indicated by the arrow in the figure. This feature is found to disappear after annealing above 500 °C. The perovskite feature is predominant in all the spectra. Refinement of the diffraction patterns were not successful due to the broadness of the profiles.

Figure 3.28 compares the powder XRD patterns of the $x = 0.375$ composition, after annealing at 700, 1000, 1300 and 1350 °C. From magnetization studies, it was

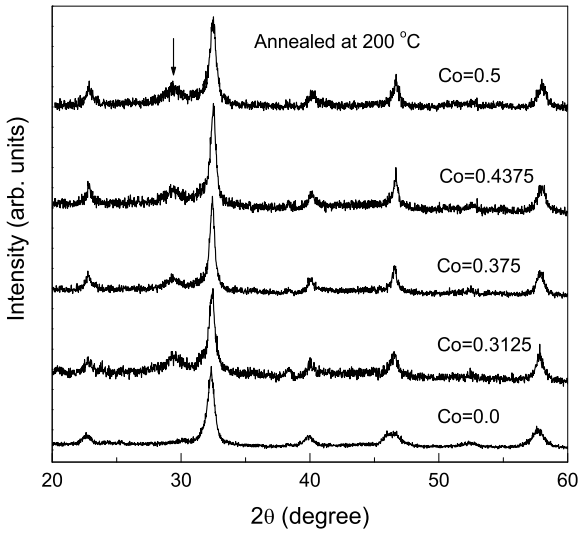

Figure 3.27: XRD patterns of Mn-rich $LaMn_{1-x}Co_xO_3$, annealed at 200°C.

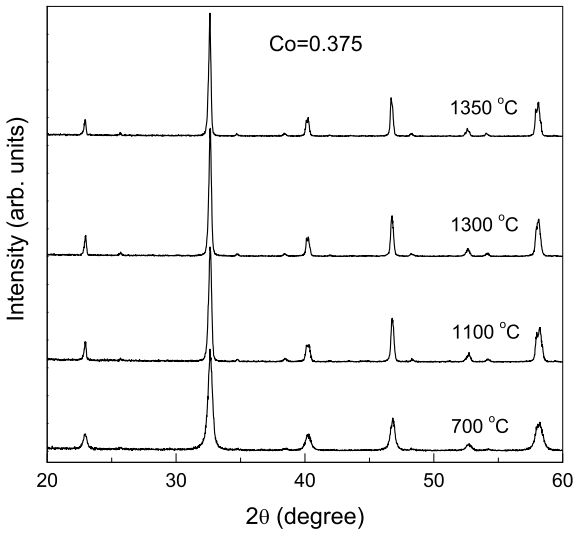

Figure 3.28: XRD patterns of $x = 0.375$ in $LaMn_{1-x}Co_xO_3$ compositions, annealed at different temperatures.

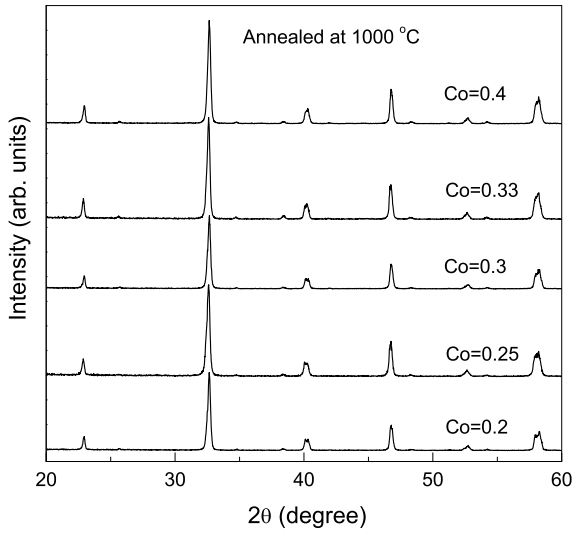

Figure 3.29: XRD patterns of low-temperature synthesized $LaMn_{1-x}Co_xO_3$, annealed at 1000 °C.

found that the T_cs are comparable for the samples annealed at 700 and 1350 °C, having the highest T_c. The sample annealed at 1000 °C showed a sharp magnetic transition at a lower temperature and mixed phase behaviour was observed after annealing at 1300 °C. The XRD figures show that there is not much difference in the nature of the patterns. All XRD patterns correspond to that of orthorhombic perovskite phases with comparable lattice parameters. No indication for any mixed phase behaviour is observed for the 1300 °C annealed sample. The samples annealed in the temperature range of 700-1350 °C, for all other compositions, showed similar XRD patterns as that of the respective high-temperature annealed samples and there was no evidence for any structural phase transitions after high temperature annealing.

Figure 3.29 compares the powder XRD patterns of some samples annealed at 1000 °C. All the patterns are alike and could be indexed to an orthorhombic unit cell. The unit cell parameters were found to be varying randomly, indicating a possible ordering

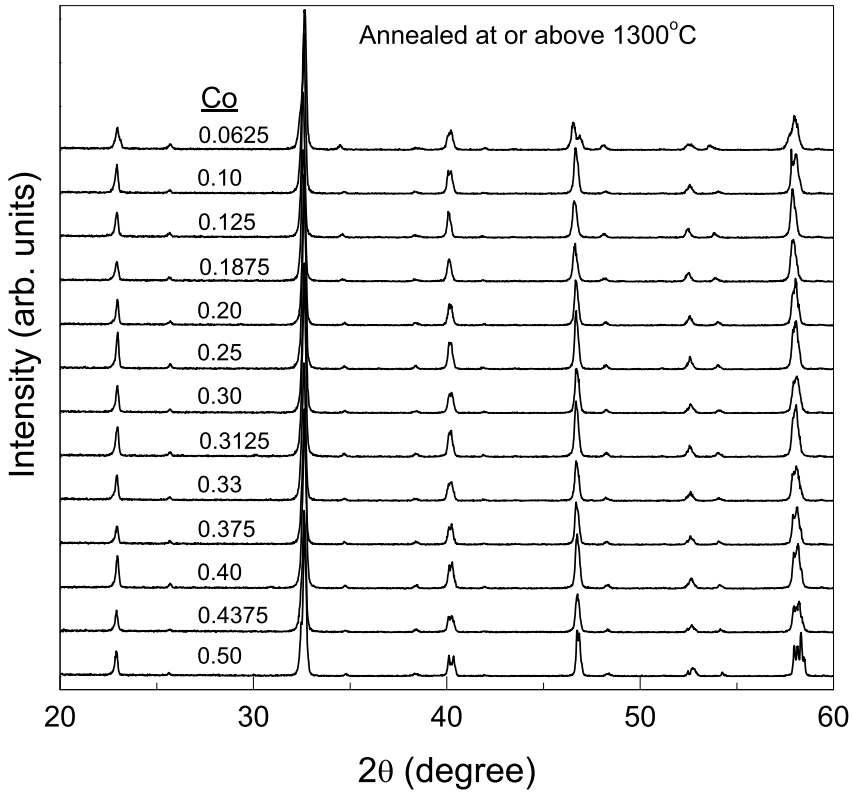

Figure 3.30: XRD patterns of Mn-rich $LaMn_{1-x}Co_xO_3$ compositions, annealed at 1300°C.

of Mn and Co ions in the lattice (Végard's law).

The XRD patterns of the low-temperature synthesized samples, formed after annealing at 1300 °C are compared in Figure 3.30. ZFC magnetization measurements showed that some of these sample contain mixed ferromagnetic phases. However, all the patterns show clear orthorhombic perovskite nature without any impurity phases and are refined well with orthorhombic *Pbnm* space group. The variation of the orthorhombic lattice parameters with the concentration of Co is given in Figure 3.31. An apparent decrease in the lattice parameters on increasing the concentration of Co

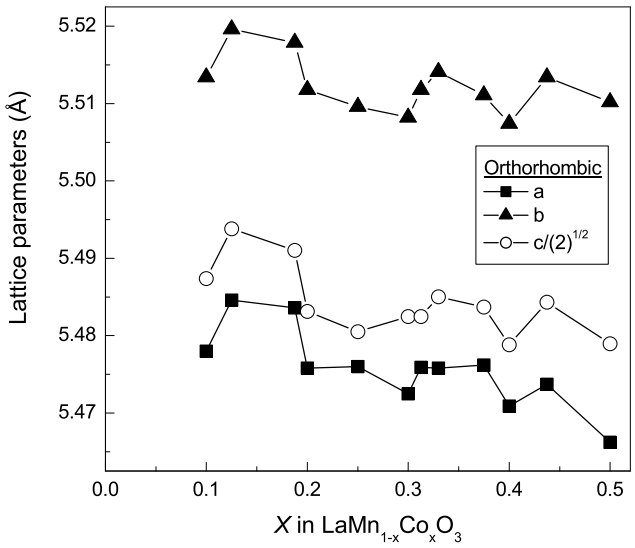

Figure 3.31: Variation of orthorhombic cell parameters as a function of the concentration of Co, for Mn-rich compositions, for samples annealed at 1300 °C.

is observed.

The overall results from powder XRD studies indicate that it is not possible to get any information on the formation of a particular phase from powder XRD studies.

3.3 Co-rich compositions ($0.5 < x < 1$)

Usually, studies on Mn-site substituted $LaMnO_3$ neglect the region containing more than 50% of the substituent ion. One of the reasons for the lack of interest in this compositional region is that in all the cases of more than 50% substitution, ferromagnetism is considerably weak, lacking the characteristics of a well defined ferromagnetic transition. However, a study of $LaMn_{1-x}M_xO_3$ solid solution series is never complete without the studies on the M-rich compounds ($x > 0.5$). Such studies help to understand the concentration up to which the structural and magnetic features of the end members $LaMnO_3$ and $LaMO_3$ persists. e.g. A-type magnetic order of $LaMnO_3$ is

found to disappear at 15% Cr^{+3} substitution, whereas the G-type structure of $LaCrO_3$ is found to persist up to 60% of Mn^{+3} [Ben57].

3.3.1 Background

In comparison with the crystal structure of the end member $LaCoO_3$, the Co-rich compounds in $LaMn_{1-x}Co_xO_3$ are reported to have a rhombohedral structure [Jon66, Nar85, Wu94, Aru00, Elf00]. The most important issue to be sorted out in the case of Co-rich $LaMn_{1-x}Co_xO_3$ (x >0.5) compositions is whether they show genuine ferromagnetic behaviour or not. All the reports indicate that $x = 0.5$ composition has the highest T_c. However, there are no agreements among the reports on the concentration of Co, up to which ferromagnetism exists. For example, there are different reports on the existence of ferromagnetism up to $x = 0.7$ [Nar82], up to $x = 0.8$ [Tro00], up to $x = 0.9$ [Dey67], etc. According to these reports, there is a significant decrease in magnetization with increasing Co concentration, in this compositional region. This observation gives some indication on the weakening of ferromagnetism beyond a particular concentration of Co. The contradictions about spin-states and magnetic exchanges persists in the Co-rich region as well. In short, it is necessary to examine the magnetic behaviour of Co-rich compositions meticulously.

3.3.2 Magnetic measurements

The zero field cooled (ZFC) magnetization curves of $LaMn_{0.4}Co_{0.6}O_3$ ($x = 0.6$) and $LaMn_{0.2}Co_{0.8}O_3$ ($x = 0.8$) samples, synthesized by the ceramic and low-temperature methods and annealed at different temperatures, are compared in Figure 3.32 and Figure 3.33, respectively. The magnetization curves of the two phases of La_2MnCoO_6 are also shown in Figure 3.32 for comparison. For both the ceramic and the low-temperature synthesized samples of $x = 0.6$ and 0.8, a magnetic transition is observed

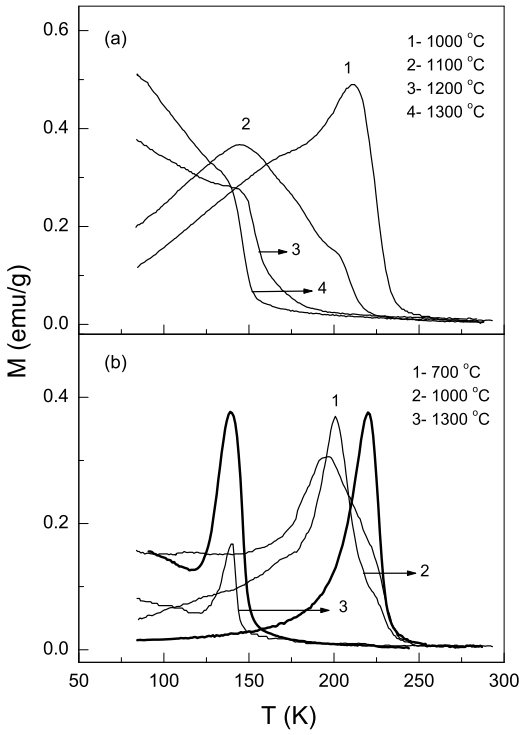

Figure 3.32: Comparison of the ZFC magnetization curves of $LaMn_{0.4}Co_{0.6}O_3$ samples prepared by ceramic (a) and low-temperature (b) methods and annealed at different temperatures. The magnetization curves of the two phases of La_2MnCoO_6 are shown as thick lines for comparison.

at the T_c (∼230 K) of the high-T_c phase of La_2MnCoO_6, when processed below 1100 °C. Similarly, the samples processed at higher temperatures show a magnetic transition at the T_c (∼150 K) of the low-T_c phase of La_2MnCoO_6. For $x = 0.8$, no magnetic transition is observed for the low-temperature synthesized sample processed at higher temperatures though the corresponding ceramic sample shows a weak magnetic transition at ∼150 K. For $x = 0.8$, $T_c \approx 140$ K is reported by Troyanchuk it et.al [Tro00]. The value of magnetization is lower for $x = 0.8$ when compared to that of $x = 0.6$ and the magnetization is relatively lower for the low-temperature synthesized sam-

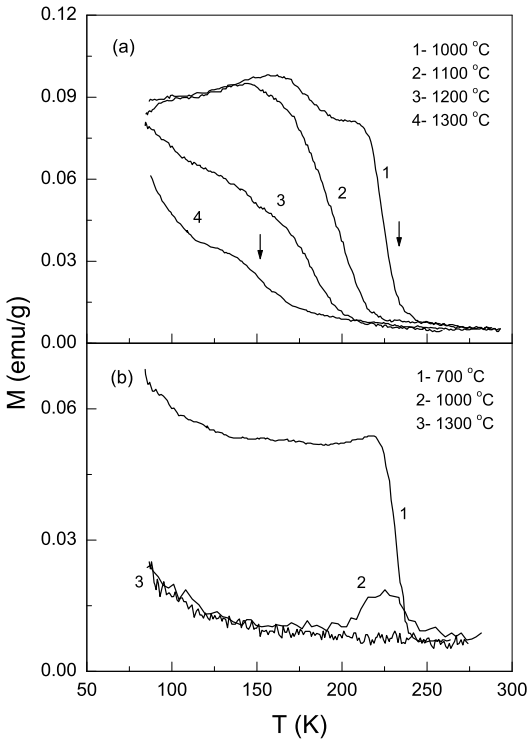

Figure 3.33: Comparison of the ZFC magnetization curves of $LaMn_{0.2}Co_{0.8}O_3$ samples prepared by ceramic (a) and low-temperature (b) methods and annealed at different temperatures. The arrows indicate the Curie temperatures of the two phases of La_2MnCoO_6.

ples. Similarly, the magnitude of magnetization is an order of magnitude less for this compositions, when compared to those in the Mn-rich region (see Section 3.2.2).

To show the effect of preparation conditions on the magnetic properties of Mn-rich compositions, the magnetization curves of $LaMn_{0.7}Co_{0.3}O_3$, prepared by the two different methods and processed at low- and high-temperatures are compared in Figure 3.34. The ceramic sample processed at lower temperatures shows a small increase in magnetization at the T_c of the high-T_c phase of La_2MnCoO_6 whereas no such mixed phase behaviour is observed for the sample prepared by the low-temperature method.

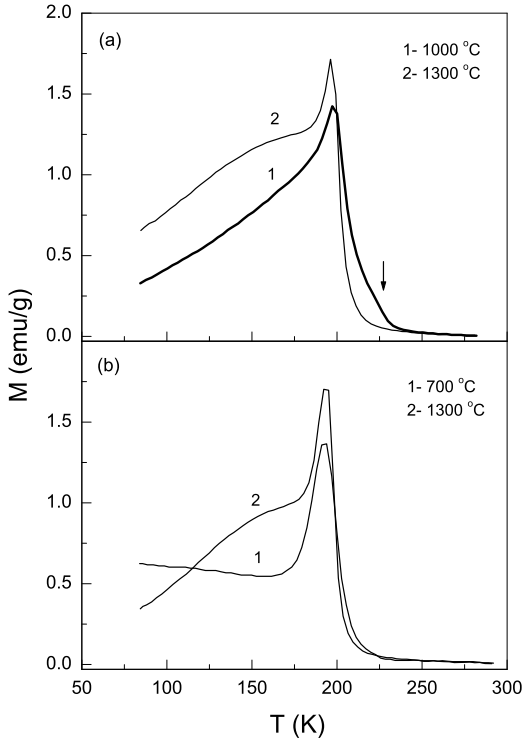

Figure 3.34: Comparison of the ZFC magnetization curves of $LaMn_{0.7}Co_{0.3}O_3$ samples prepared by ceramic (a) and low-temperature (b) methods and annealed at two different temperatures. The arrow indicate the T_c of the high-T_c phase of La_2MnCoO_6.

The two sets of samples show magnetic transitions at almost identical temperatures, but different from that of the T_cs of the two phases of La_2MnCoO_6. Similar results were obtained for other compositions for $x < 0.5$.

For $x > 0.5$, samples processed at different temperatures show weak and broad magnetic transitions. The magnetic transitions of these compositions processed at low temperatures are at the T_c (225 K) of the high-T_c phase of $x = 0.5$ and at the T_c (145 K) of the low-T_c phase of $x = 0.5$ when processed at high temperatures. Magnetic transitions are observed at intermediate temperatures, between 150 and 230 K, for the

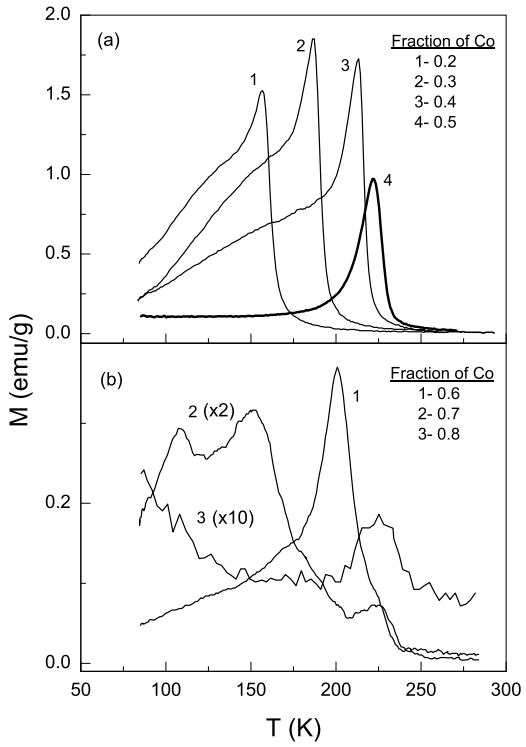

Figure 3.35: Magnetization curves for $x \leq 0.5$ (a) and $x > 0.5$ (b), synthesized by the low-temperature method and heated at 1000 °C. The curves of $x = 0.7$ and 0.8 are multiplied by 2 and 10, respectively, to show the weak magnetic transition at ∼230 K.

samples annealed in the temperature range 700–1300 °C, similar to that observed for $x = 0.5$. For $x > 0.5$ compositions the observed T_cs cannot be considered as the true magnetic transition temperature. The magnetization curves of some compositions for $x \leq 0.5$ and $x > 0.5$, synthesized by the low temperature method and annealed at 1000 °C are compared along with that of $x = 0.5$, in Figure 3.35. For $x < 0.5$, single sharp magnetic transitions are observed at different temperatures and the Curie temperature varies with x. On the other hand, for $x > 0.5$, a weak magnetic transition, with decreasing magnitude of magnetization with increasing x, is observed

at the T_c of the high-T_c phase of $x = 0.5$. This suggests that the $x > 0.5$ samples are not truly homogeneous and the broad and multiple magnetic transitions suggest mixed phase behaviour.

Thus, the results show that, in all samples for $x > 0.5$ in $LaMn_{1-x}Co_xO_3$, fractions of one of the phases of La_2MnCoO_6 is present, depending on the annealing temperature. The amount of the ferromagnetic phase decreases with increasing x and multiple magnetic transitions are observed when both the phases of $x = 0.5$ are present together, showing an apparent value of magnetization for higher values of x due to mixed phase behaviour. From these results, it may be concluded that the Co-rich compositions ($x > 0.5$) in $LaMn_{1-x}Co_xO_3$ are not truly ferromagnetic.

3.3.3 Powder XRD studies

There is not much relevance for the studies on the structural characteristics of the compositions in the Co-rich region, after observing from the magnetization studies that all compositions in this region are not truly single phase and show magnetic transitions at the T_cs of the $x = 0.5$ composition. However, it would be interesting to look at the powder XRD patterns of some of the samples to see if the mixed phase behaviour can be detected from such studies. Such studies in the Mn-rich region did not give sufficient information on the mixed phase behaviour. Figure 3.36 shows the powder x-ray diffraction patterns of the low-temperature synthesized Co-rich compositions ($0.5 \leq x \leq 1$), after annealing in the temperature range 1300-1350 °C. For $x = 0.5$, the crystal structure is orthorhombic and the structure of $x = 1$ is rhombohedral. It may be seen that just by increasing the Co content from 0.5 to 0.56 the crystal structure changes from orthorhombic to rhombohedral (as observed in by the splitting of the most intense peak). All the XRD patterns of the Co-rich compositions are refined well with rhombohedral $R\bar{3}c$ symmetry. The variation of the rhombohedral lattice parameter, a, with the concentration of Co, is shown in

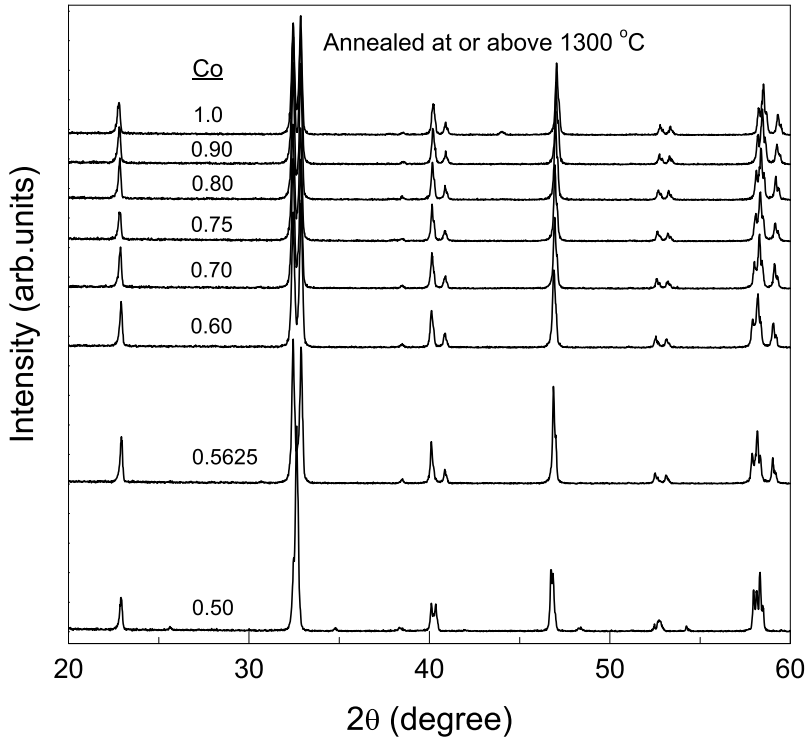

Figure 3.36: XRD patterns of $LaMn_{1-x}Co_xO_3$, annealed at or above 1300°C.

Figure 3.37. More importantly, it is not possible to get any information from the XRD patterns about the multiple phase behaviour, as evidenced from the magnetic measurements.

3.4 Conclusions

Magnetic and structural properties on different concentrations in the Mn-site substituted manganate system, $LaMn_{1-x}Co_xMnO_3$, have been studied to understand the evolution of ferromagnetism on substitution of Co for Mn in $LaMnO_3$. Different compositions were synthesized by the conventional solid state or ceramic method and a

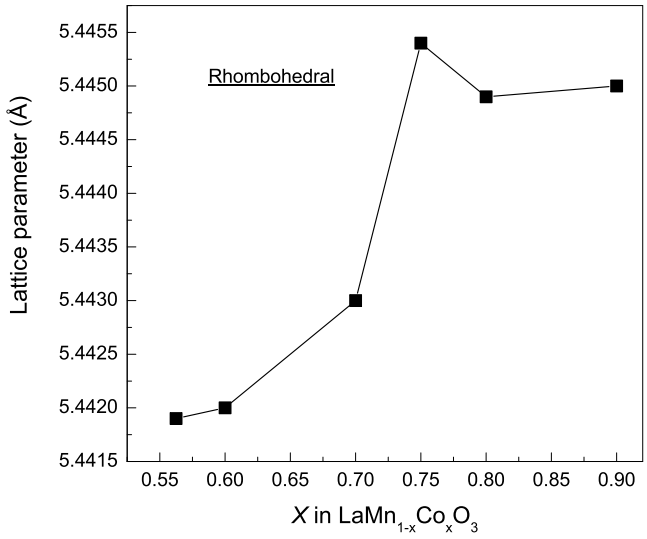

Figure 3.37: Variation of cell parameters of Co-rich samples assigned rhombohedral.

low-temperature method, to understand the differences in the properties of the compositions arising from the difference in the processing conditions. This is expected, because contradicting reports are made in the literature on the properties of some compositions processed under different conditions. The present studies showed that there are two possible ferromagnetic phases for $x = 0.5$, i.e. $LaMn_{0.5}Co_{0.5}O_3$ or the double perovskite formula, La_2MnCoO_6, which is generally used to represent this composition. Studies on the low-temperature synthesized sample indicated that one of the phases is stable only below 800 °C and is converted to a second phase if heated to higher temperatures. The compound synthesized by the ceramic method yielded a mixed phase when heated in the temperature range 1000–1300 °C and only the second phase, in single phase form, is obtained when heated at 1300 °C for a prolonged duration.

X-ray photoelectron spectroscopic and magnetic susceptibility studies on the single phase compositions obtained by the low-temperature method of synthesis indicated

that the spin-states of Mn and Co ions are different in the two different phases of La_2MnCoO_6. Mn and Co ions are present in their trivalent states with Co^{+3} in the low-spin configuration in the high-T_c phase, and as Mn^{+4} and high-spin Co^{+2} in the low-T_c phase. Origin of ferromagnetism in the phase showing a higher Curie temperature is therefore from superexchange interactions between Mn^{+3} ions where as superexchange interaction between Mn^{+4} and Co^{+2} ions is responsible for ferromagnetism in the phase showing a lower Curie temperature. When the high-T_c phase of the compound is heated to higher temperatures, the Mn^{+3}-Co^{+3} equilibrium is shifted to Mn^{+4}-Co^{+2}, i.e., a charge disproportionation Mn^{+3} + $Co^{+3}\rightarrow$ Mn^{+4} + Co^{+2}. Complete conversion from Mn^{+3}-Co^{+3} to Mn^{+4}-Co^{+2} takes place only at a higher temperature and therefore mixed phase behaviour is observed for samples heated in the temperature range 700-1300 °C. Then it is possible that samples heated in this temperature range will have different spin-states of Mn and Co (Mn^{+3}, Mn^{+4}, Co^{+2}, Co^{+3}).

In the case of Mn-rich compositions in $LaMn_{1-x}Co_xO_3$ ($0 < x < 0.5$) sharp magnetic transitions are obtained for the low-temperature synthesized compounds when annealed at 1000 °C. Samples annealed above or below this temperature showed mixed phase behaviour. The mixed phase behaviour is possibly due to the different spin-states of Mn and Co ions, due to the charge disproportionation as observed for $x = 0.5$. The samples synthesized by the ceramic method show broad magnetic transitions indicating co-existence of different compositions in the same sample, even for samples heated at higher temperatures. That is, it is difficult to get single phase compositions in this compositional range for the samples synthesized by the ceramic method. For Co-rich compositions ($x > 0.5$), synthesized by the low-temperature as well as the ceramic methods, weak ferromagnetism is observed for all compositions. Magnetic transitions are observed at the T_cs of either of the two phases of the $x = 0.5$ compound. This shows that, for $x > 0.5$, different compositions form mixed phases

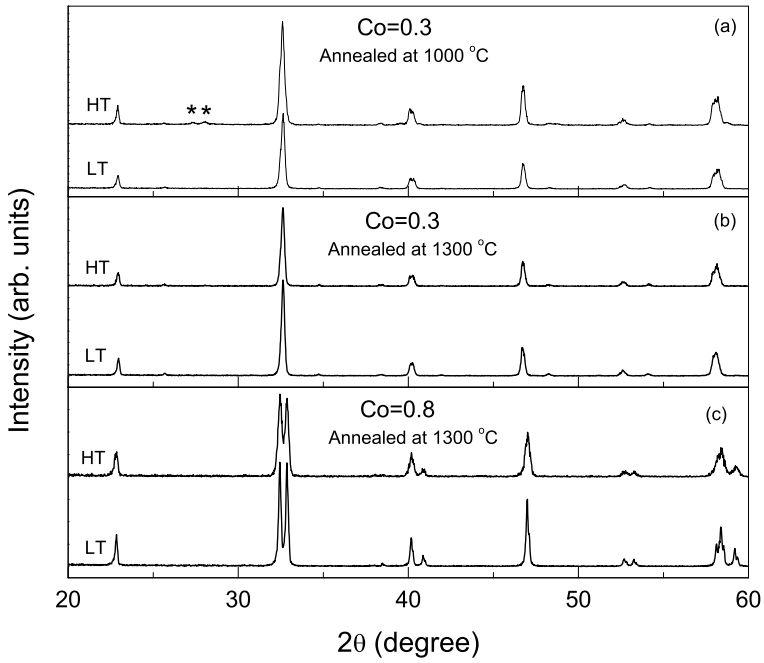

Figure 3.38: Comparison of XRD patterns of ceramic (HT) and low-temperature (LT) synthesized samples, annealed at different temperatures

and the different compositions are truly not ferromagnetic.

The ease of formation of pure perovskite phases, in $LaMn_{1-x}Co_xO_3$, prepared using the low-temperature method, in comparison with ceramic method of synthesis, is illustrated in the powder XRD patterns shown in Figure 3.38. The XRD patterns of $x = 0.3$, synthesized by the ceramic method, after heating at 1000 °C for 4 days, with five intermediate grindings and by the low temperature method, after a single heating at 1000 °C are compared in the top part of Figure 3.38.The XRD pattern of the ceramic sample is slightly broader than that of the low-temperature sample, whereas the reverse is generally expected. This is probably due to the formation of other compositions close to $x = 0.3$, in the ceramic sample, with slightly different lattice parameters, so that the observed XRD peaks contain contributions from these

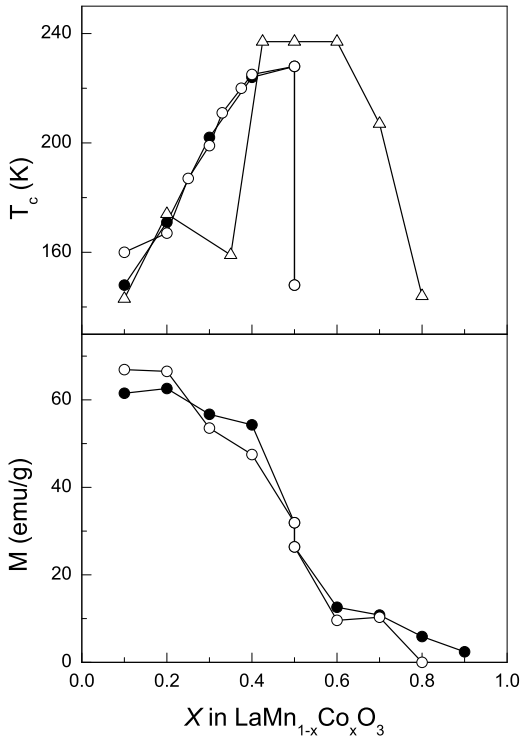

Figure 3.39: Variation of T_c and magnetization (measured at 82 K and 15 kOe) as a function of x in $LaMn_{1-x}Co_xO_3$. • - ceramic method, ∘ - low-temperature method, △ - from [Tro00]. For $x = 0.5$, T_c and M of the two phases of the compound are shown.

compositions and therefore the peaks are broad. This is further confirmed by the observation of residual $La(OH)_3$ diffraction peaks at 2θ values, 28.10° and 27.40° (marked with '*'), in the ceramic sample indicating incomplete reaction. The broader ferromagnetic transitions of the ceramic samples is an evidence for the formation of different close compositions within the same sample. On the other hand, the low-temperature synthesized sample shows a clean pattern, free of impurities as well as peak broadening, due to the formation of the required composition. After annealing at 1100 and 1200 °C for 1 day each and 1300 °C for 5 days, with intermediate

grindings, the ceramic sample shows identical orthorhombic pattern as that of the low-temperature synthesized sample obtained after a single annealing at 1300 °C (see middle part of Figure 3.38). Similarly, the ceramic Co-rich sample, $x = 0.8$, after sufficient heat treatment show identical rhombohedral pattern as that of the low-temperature synthesized sample, as shown in the bottom part of Figure 3.38. Here also, the reflections are broader for the ceramic sample, even after treatment at high temperatures and for longer durations. In other words, the low-temperature method of synthesis help the formation of the pure and homogenous compositions at lower temperatures.

The magnetic transition temperature as well as the magnetization measured at 82 K and 15 kOe, as a function of x in $LaMn_{1-x}Co_xO_3$, are shown in Figure 3.39, for samples synthesized by the two different methods. For $x = 0.5$, the phase with the higher T_c and larger magnetization is processed at 700 °C. T_c is shown only up to $x = 0.5$, because of the mixed phase behaviour and processing temperature dependence of the transition temperature for $x > 0.5$. The Curie temperatures obtained by Troyanchuk *et.al* [Tro00] are also shown in the figure for comparison. The lower value of the maximum T_c in the present work (for $x = 0.5$) may be due to the difference in the definition of the transition temperature. In the present work, the magnetic transitions are very sharp due to phase purity and the low magnetic fields used for the measurements, and T_c is taken as the temperature at which dM/dT is maximum. The T_cs are slightly higher at lower values of x for the low-temperature synthesized samples and this may be due to the presence of excess Mn^{+4} as generally observed in the case of $La_{1-x}A_xMnO_3$. The Curie temperature increases up to $x = 0.5$, contrary to the very low value of T_c reported for $x = 0.35$ [Tro00]. Moreover, the same Curie temperature is reported for $0.4 \leq x \leq 0.6$ and this may be due to the mixed phase behaviour, with relatively larger amount of the high-T_c phase of La_2MnCoO_6 present in the samples due to insufficient processing.

Chapter 4

Studies on La_2MnNiO_6

As explained in Section 3.1, the double perovskites, represented generally as $A_2BB'O_6$, show some highly peculiar phenomena, which make them potential candidates for future technological applications. The underlying reason for such properties are the possibility of different valence states, crystal structures, charge disproportionation, ionic ordering, etc. The most important issue in the study of the double perovskite compositions is the determination of the spin-states of the B and B′ions, because the spin-states of these ions in turn decide the structural, magnetic and transport properties.

4.1 Background

La_2MnMO_6 has been reported as a ferromagnet, unlike the non-ferromagnetic nature of the end members, e.g. antiferromagnetic $LaMnO_3$ and paramagnetic $LaNiO_3$. Similarly, the structures of the end members are also different e.g. the structure of stoichiometric $LaMnO_3$ is orthorhombic whereas stoichiometric $LaNiO_3$ is rhombohedral [Goo70]. There is little room for any ambiguity about the spin-states of the transition metal ions in the end members. However, when a second transition metal is incorporated into the B-site, there can be different possible combinations of the spin/oxidation states of the B-site ions.

There are many reports in the literature on the studies on La_2MnNiO_6. The earlier attempts to synthesize Mn-site ionic ordered $LaMn^{+4}_{0.5}M^{+2}_{0.5}O_3$ or La_2MnNiO_6 were not successful, since the cations were found to favor trivalent states [Wol58, Goo61], in spite of the fact that the reaction Mn^{+4}+ Ni^{+2}⇌Mn^{+3}+ Ni^{+3} is biased to left hand side by 0.8 eV [Das03]. On the other hand, it is also a fact that the above reaction can be biased either to the right or to the left depending up on the Mn concentration, the temperature and the degree of ionic ordering [Vas84]. This is because, the position of the energy level of Mn^{+3} e^1_g depends on the Mn concentration, e.g. for smaller Mn concentrations, it lies above the fermi-level and hence cannot be occupied, stabilizing Mn^{+4}, but for higher Mn concentration the energy level becomes overlapped by the fermi-energy, stabilizing Mn^{+3}. Therefore, the energy change of the above reaction cannot be generalized.

A higher $T_c \approx 280$ K has been reported for La_2MnNiO_6 [Goo61] when compared to the $T_c = 225$K of La_2MnCoO_6, despite the very small size difference between Co^{+3} (0.545 Å) and Ni^{+3} (0.56 Å) ions in their low-spin states. The striking similarity between the above Co and Ni containing double perovskite compositions is that both are having the highest Curie temperatures among the other compositions of their respective solid-solution series $LaMn_{1-x}M_xO_3$ (M = Co, Ni). This shows the fact that these compounds have similarity in the origin of ferromagnetism. Similar to that reported for the Co containing compositions, the corresponding Ni containing compositions are also reported to be of different combinations of spin-states like Mn^{+3}/Ni^{+3}, Mn^{+4}/Ni^{+2}, and correspondingly various superexchange mechanisms, for the origin of ferromagnetism, have been proposed by different groups [Wol58, Goo61, Bla65, Son92](detailed review is given in Section 1.4). Moreover, the crystal structures like orthorhombic [Wol59], a superposition of orthorhombic and rhombohedral [Son92], a mixture of monoclinic and rhombohedral [Bla02a, Bul03], etc. are also reported by different groups. This implies that La_2MnNiO_6 may form in

more than one crystallographic modifications, as expected from the different crystal structures of the end members $LaMnO_3$ and $LaNiO_3$.

As described in Section 3.1, two different ferromagnetic phases of La_2MnCoO_6 are prepared in single-phase forms by a low-temperature method of synthesis. A high-T_c phase is found to be stable only below 700 °C and a low-T_c phase, in single phase form, is obtained only after heating at 1300 °C. The high-T_c phase has Mn^{+3} and low-spin Co^{+3}, with ferromagnetic Mn^{+3}-O-Mn^{+3} superexchange interactions. On the other hand, the low-T_c phase consists of Mn^{+4} and Co^{+2} with positive Mn^{+4}-O-Co^{+2} superexchange interactions. An unusual charge disproportionation of the type $Mn^{+4} + Co^{+2} \rightarrow Mn^{+3} + Co^{+3} \rightarrow Mn^{+4} + Co^{+2}$ is found to be operative in the low-temperature synthesized La_2MnCoO_6, annealed at different higher temperatures and this is the origin of the controversy about the spin-states of Mn and Co in samples prepared by the ceramic method.

In view of the reports on the co-existence of different spin-states of Mn and Ni, different crystallographic forms, and ferromagnetic exchanges in La_2MnNiO_6, the compound is synthesized by the ceramic and low-temperature methods and the structural and magnetic properties of the samples annealed in air at different temperatures are studied. The studies are aimed at resolving the problem of the spin-states of Mn and Ni, and thereby to verify the nature of the magnetic exchange interactions in the compound.

4.2 Synthesis

La_2MnNiO_6 (LMN) samples were synthesized by the conventional high-temperature (referred as HT samples in the text) solid-state reaction (ceramic) method and a low-temperature (referred as LT samples in the text) method. In the ceramic method, a stoichiometric mixture of pre-heated La_2O_3, MnO_2 and NiO was heated at 1000

°C for 12 hours initially and further heated at the same temperature for 48 hours with an intermediate grinding. The powder sample obtained was then annealed at 1100 and 1200 °C for 24 hours each and then at 1300 °C for 96 hours with four intermediate grindings. All the heatings were made in air and then furnace-cooled to room temperature. La_2MnNiO_6 and a sample of Nd_2MnNiO_6 were prepared by a low-temperature glycine-nitrate method [Chi90]. In the low-temperature method, a water solution containing the nitrate salts of La, Mn, Ni, and Glycine in the 2:1:1:8 ratio were prepared. The powder samples obtained after initial decomposition of this metal nitrate-glycine mixture at ∼200 °C was then annealed at different temperatures in the range 200–1300 °C for 12 hours each, in air, and furnace-cooled to room temperature.

Oxygen stoichiometry

Oxygen stoichiometry is determined by redox titration, using potassium permanganate and ferrous sulphate. The oxygen stoichiometry of the sample heated at 1300 °C was found to be 3±0.01. This shows that the sample is stoichiometric and the properties exhibited will be free from any cation vacancy effects. The sample heated at 400 °C was found to be slightly oxygen deficient (2.95). This could be due to the error in the calculation (actual weight of the sample taken for measurement will be less due to the high carbon content in the sample, as evidenced from XPS studies, discussed later in this chapter).

4.3 Magnetic measurements

As discussed, a magnetic transition below ∼280 K is reported in the literature from studies on the magnetic properties of La_2MnNiO_6 using high magnetic fields. It has been shown that magnetic measurements using very low magnetic fields can detect the presence of different phases of ferromagnetic compounds, if they coexist in the

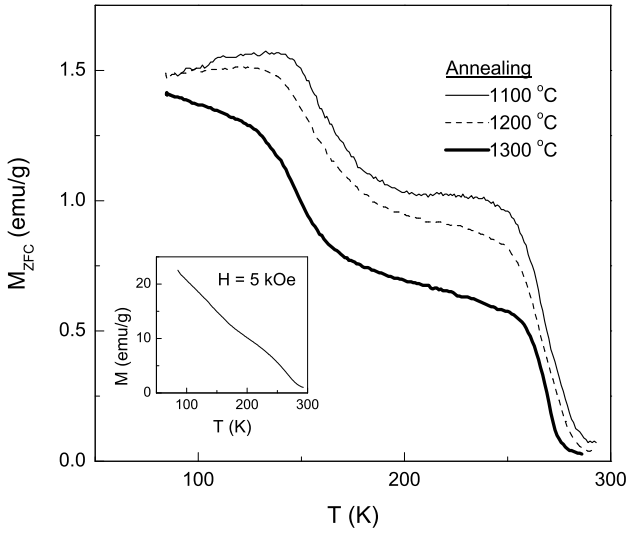

Figure 4.1: ZFC magnetization ($H = 50$ Oe) curves of La_2MnNiO_6 synthesized by the ceramic method, annealed at 1100, 1200 and 1300 °C. Inset: temperature variation of magnetization at $H = 5000$ Oe.

samples [Joy97, Joy98, Joy02]. Therefore, zero field cooled magnetization, M_{ZFC}, measurements were made at a low magnetic field of 50 Oe, to look for the possible existence of different phases of La_2MnNiO_6, in the HT and LT samples, annealed at different temperatures.

4.3.1 HT samples

Figure 4.1 shows the ZFC magnetization curves of La_2MnNiO_6, synthesized by the ceramic method and annealed at 1100, 1200, and 1300 °C. Two well-defined magnetic transitions, at ∼150 and ∼280 K, are clearly visible in all the curves. There is no change in the onset of the magnetic transition temperatures or relative heights of the individual magnetic transitions even after heating at higher temperatures. From the two clear magnetic transitions at different temperatures, and when compared with

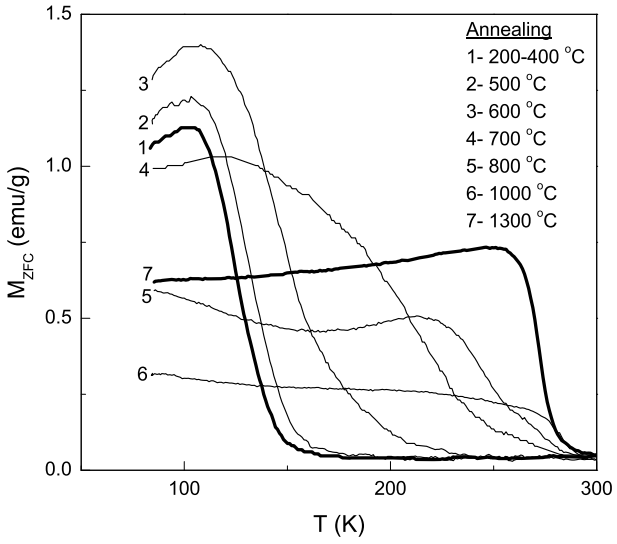

Figure 4.2: ZFC magnetization (H = 50 Oe) curves of the low-temperature synthesized La_2MnNiO_6, annealed in the temperature range 200–1300 °C.

the similar results obtained on La_2MnCoO_6 (see Section 3.1) samples prepared under identical conditions, it appears that there are two possible ferromagnetic phases for La_2MnNiO_6. The inset in the Figure 4.1 shows the temperature variation of the magnetization of the sample heated at 1300 °C, measured at 5000 Oe. The high-field magnetization curve do not show clearly the two different magnetic transitions. The magnetic transition appears very broad, with the onset of the magnetic transition below 280 K. This high-field magnetization curve is similar to that reported by Sonobe and Asai for one of their samples measured at 18 kOe [Son92].

4.3.2 LT samples

Temperature variation of the zero field cooled magnetizations of La_2MnNiO_6 samples, synthesized by the low-temperature method and annealed between 200 and 1300 °C, are shown in Figure 4.2. Magnetization curves of the samples annealed between 200

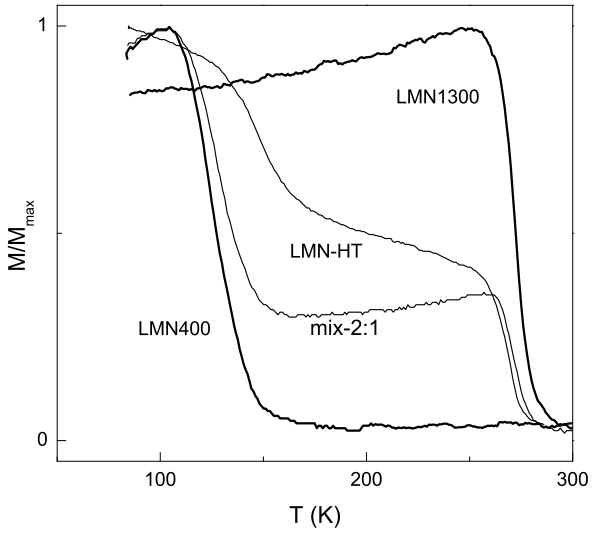

Figure 4.3: ZFC magnetization (H = 50 Oe) curves of La_2MnNiO_6: HT sample annealed at 1300 °C (LMN-HT), LT samples annealed at 400 (LMN400) and 1300 °C (LMN1300), and a 2:1 physical mixture of LMN400 and LMN1300 (mix-2:1).

and 400 °C are identical, onset of a broad magnetic transition is observed below 150 K. Increasing the annealing temperature above 500 °C causes a broadening of the magnetic transition, in such a way that the value of the temperature at which the magnetization picks up from its paramagnetic nature, is increased. A sharp magnetic transition at 273 K is observed for the sample annealed at 1300 °C. By comparing the results on the LT samples with that obtained on the HT samples, as shown in Figure 4.3, it may be seen that the magnetic transition observed for the LT sample annealed at 400 °C is at the temperature of the first magnetic transition of the HT sample (∼150 K). Similarly, the magnetic transition observed for the LT sample (273 K) annealed at 1300 °C is at the temperature of the second magnetic transition of the HT sample. This indicates that two different ferromagnetic phases of La_2MnNiO_6 can be obtained in single phase forms by a low-temperature method of

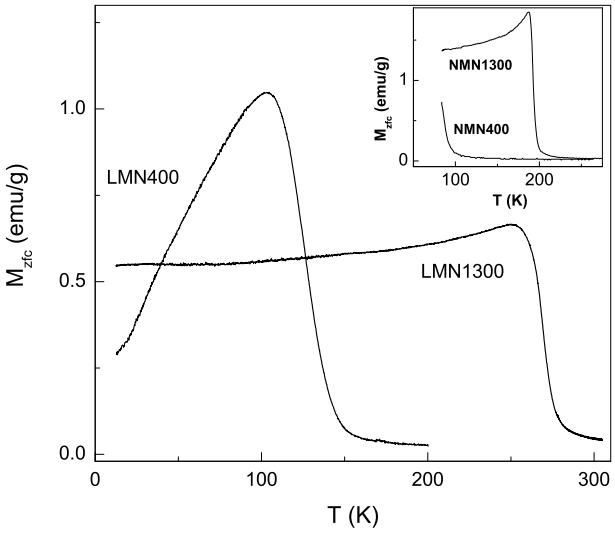

Figure 4.4: ZFC magnetization curves of the two phases of La_2MnNiO_6, LMN400 and LMN1300. Inset: ZFC magnetization curves of low-temperature synthesized Nd_2MnNiO_6, annealed at 400 (NMN400) and 1300 °C (NMN1300).

synthesis and when the samples are heated below 500 °C and above 1200 °C. The ZFC magnetization curve of a physical mixture of the samples annealed at 400 and 1300 °C (2:1 weight ratio) is almost identical to that of the HT sample, suggesting that the HT sample contains almost one-third of the phase showing a higher magnetic transition temperature. On the other hand, the broad magnetic transitions of the LT samples annealed between 600-1000 °C are indicative of a slow conversion of one phase in to the other.

The ZFC magnetization curves of the two different phases of La_2MnNiO_6, measured in the temperature range of 10–300 K are shown in Figure 4.4. Unlike in the case of La_2MnCoO_6, where an additional broad cusp at 73 K was observed for the low-T_c phase obtained after annealing at 1300 °C, no such anomalous behaviour below the Curie temperature is obtained for both phases of La_2MnNiO_6. However, the phases of

the corresponding Co and Ni compounds, obtained at lower annealing temperatures, show exactly identical magnetic transition temperatures and behaviour below T_c, indicating that the origin of the magnetic transition is common for them. Moreover, as discussed in Section 3.2, this magnetic transition temperature is independent of Mn or Co concentrations in the Mn-rich $LaMn_{1-x}Co_xO_3$ compounds.

A nominal composition with Nd instead of La, Nd_2MnNiO_6 (NMN), is also synthesized using the low-temperature method and processed under similar conditions as in the case of La_2MnNiO_6, to compare and confirm the multi-phase behaviour exhibited by La_2MnNiO_6. ZFC magnetization curves of NMN samples annealed at 400 and 1300 °C show magnetic transitions below 90 and 195 K, respectively, as shown in the inset of Figure 4.4, indicating the possible formation of two different ferromagnetic phases of this compound as in the case of the La compound. The decrease in the magnetic transition temperatures, for both phases, when La^{+3} is replaced by Nd^{+3} having a lower ionic size, may be due to the increased structural distortion, as discussed in detail in Chapter 6.

4.4 Powder XRD studies

There are contradicting reports in the literature on the crystal structure of different compositions in the $LaMn_{1-x}Ni_xO_3$ series. It has been reported that the Ni-rich compositions are not structurally stable, especially when synthesized by ceramic method [Wol59, Goo61, Asa79, Vas84, Min03]. Nevertheless, none of the reports indicate any structural instability for the $x = 0.5$ composition, i.e. La_2MnNiO_6. Some previous reports show that compositions up to $x = 0.5$ are orthorhombic, and a rhombohedral structure for $x > 0.5$ [Wol58, Vas84, Tro97]. For $x = 0.5$, slight monoclinic distortion is also reported [Wol58, Bla02a, Bul03]. However, considering the reports that the structure is orthorhombic for $x < 0.5$ including the end member $LaMnO_3$ and rhombo-

hedral for $x > 0.5$ including the end member $LaNiO_3$, it is possible for $x = 0.5$ to have two different phases with the above two crystal structures. As mentioned previously, the reports showing mixed crystallographic phases for La_2MnNiO_6 [Son92, Bla02a], support the above argument. There is one more factor which adds to the ambiguity in the crystal structure, namely the ionic ordering in the B-site. Though it is known that superlattice reflections due the ionic ordering in the B-site, which contain more than one type transition metal ions, is less likely to be observed in the x-ray diffraction pattern when their scattering powers are similar [Bla65], there are some reports on the observation of superlattice reflections in the x-ray diffraction pattern of La_2MnNiO_6 [Fuj67, Son92]. However, neutron diffraction studies have shown that there is ionic ordering in La_2MnNiO_6 [Bul03, Bla02b]. In the cases when ionic ordering is observed, monoclinic $P2_1/n$ or rhombohedral $R\overline{3}$ space groups are used instead of the usual orthorhombic $Pbnm$ or rhombohedral $R\overline{3}c$, respectively. Neutron diffraction studies also show a structural phase transition from a rhombohedral to monoclinic structure below 375 °C [Bul03] or below room-temperature [Bla02b] and in the latter case it has been proposed that only the monoclinic phase is ferromagnetic.

4.4.1 HT samples

The powder XRD patterns of the different samples of La_2MnNiO_6 are shown in Figure 4.5. For the HT sample, annealed at 1300 °C, no impurity peaks are observed and the reflections correspond to that of a perovskite phase. Wold *et al.* [Wol58] and Troyanchuk *et al.* [Tro97] found that the crystal structure of La_2MnNiO_6, synthesized by the ceramic method, as orthorhombic. The powder XRD pattern of LMN-HT could be indexed on an orthorhombic structure with lattice parameters $a = 5.477$ Å, $b = 5.464$ Å, and $c = 7.670$ Å. These lattice parameters are almost comparable to those reported previously [Wol58, Tro97]. However, the magnetic measurements have already indicated the presence of two ferromagnetic phases in this sample. Therefore,

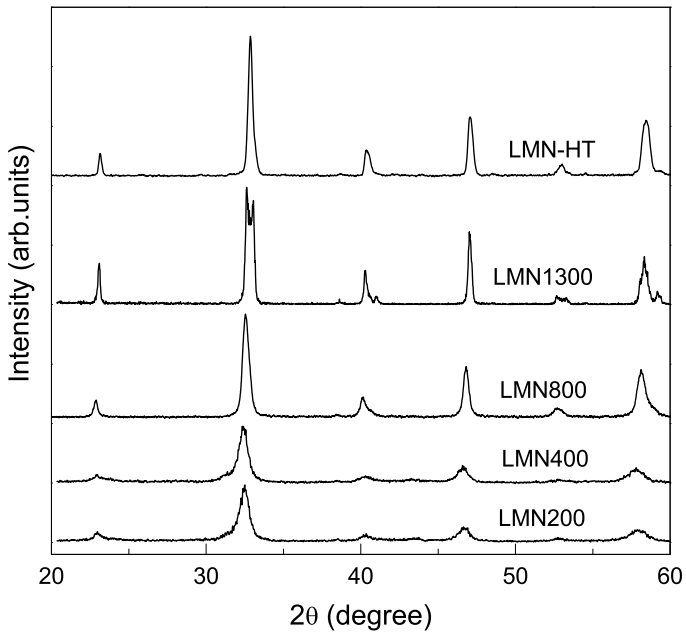

Figure 4.5: Powder XRD patterns of La_2MnNiO_6, annealed at different temperatures, after synthesized by ceramic and low-temperature methods.

it is reasonable to assume that the observed pattern comprises of the contributions from these two different phases. The observed pattern could be fitted to ∼70% of an orthorhombic phase (a = 5.478 Å, b = 5.460 Å, and c = 7.672 Å) and ∼30% of a rhombohedral phase (a = 5.426 Å and $\alpha = 60.9°$). These lattice parameters are comparable to that reported by Sonobe and Asai [Son92], where the authors found a major orthorhombic phase along with nearly 10-25% of a rhombohedral phase. The ratio of the two phases present, found from powder XRD, in the HT sample, is in agreement with the results from the magnetic measurements. The magnetic measurements on a physical mixture of the two individual phases obtained by the low-temperature method of synthesis showed that the HT sample constitutes the two phases in the ratio of approximately 2:1 (see Figure 4.3).

4.4.2 LT samples

Powder XRD patterns of the LT samples of La_2MnNiO_6, annealed at 200 (LMN200), 400 (LMN400), 800 (LMN800) and 1300 °C (LMN1300) are compared in Figure 4.5. All the reflections of LMN200 correspond to that of a perovskite phase, without any impurities, indicating the formation of the compound at 200 °C. The XRD patterns of LMN200 and LMN400 are identical, and the reflections are very broad indicating the fine particle nature of the compound obtained at low temperatures. Average particle size is obtained as 13 nm from x-ray line broadening, calculated using the Scherrer formula, given by the Equation 2.2. Even though the reflections in the XRD patterns of LMN200 and LMN400 are broader, the patterns could be approximately indexed to an orthorhombic unit cell with lattice parameters, $a = 5.50$ Å, $b = 5.65$ Å, and $c = 7.78$ Å. On the other hand, the XRD pattern of LMN1300 corresponds to the reflections from a rhombohedral lattice. The rhombohedral lattice parameters are obtained as a = 5.428 Å, and $\alpha = 60.9°$. The powder XRD pattern of the sample LMN800, which shows multiple magnetic transitions below ∼280 K, is almost identical to that of the sample prepared by the ceramic method showing two magnetic transitions. The XRD pattern of LMN800 also is found to be a mixture of an orthorhombic phase (∼60%) and a rhombohedral phase (∼40%). This indirectly tells that LMN200 is most likely having an orthorhombic structure, which eventually transforms to a rhombohedral structure up on annealing at higher temperatures.

In the case of perovskite type compounds, which are magnetic, it is known that the magnetic transition temperature depends on the structure of the compound. Highest Curie temperature is found for cubic phases and the Curie temperature decreases when the structure is distorted to rhombohedral and then to orthorhombic [Coe99]. This is because, the strength of the magnetic exchange interactions in the perovskites depend on inter-ionic distances and bond angles. The B-O-B bond angle (in ABO_3) is decreased when the structure is distorted from cubic → rhombohedral → orthorhom-

bic. This distortion modifies the magnetic transition temperature because T_c is determined by the strength of the exchange interactions, which in turn is decided by the orbital overlap between B and oxygen ions. Therefore, for a given composition, rhombohedral phase will have a larger Curie temperature than that of the phase with an orthorhombic structure. Similar results are observed here for La_2MnNiO_6 also, which is in accordance with the expected structural dependence of T_c. Here, the interpretation that only the low-temperature monoclinic phase is ferromagnetic [Bla02b], is questionable.

4.5 Determination of Spin-states of Mn and Ni

From zero field cooled magnetization measurements using low magnetic fields and powder XRD measurements, it is now obvious that La_2MnNiO_6 can form two different crystallographic forms with different magnetic transition temperatures. Having found that La_2MnNiO_6 synthesized by the high-temperature ceramic method is multiphasic due to the presence of two different phases of the compound and single phase compounds are obtained from samples synthesized by the low-temperature method and annealed at 400 and 1300 °C, the spin-states of Mn and Ni in the two phases are explored, to understand the origin of the different magnetic transition temperatures for the two phases. The x-ray photoelectron spectroscopy (XPS) and high-temperature paramagnetic susceptibility studies along with studies on the magnetic properties of the compound after substitution of Mn and Ni by the non-magnetic ion, Al^{+3}, were used to deduce information on the spin-states.

4.5.1 Paramagnetic susceptibility

The temperature dependence of the inverse of the paramagnetic susceptibility (> 300 K) of LMN400 and LMN1300 is shown in Figure 4.6. The simple perovskite

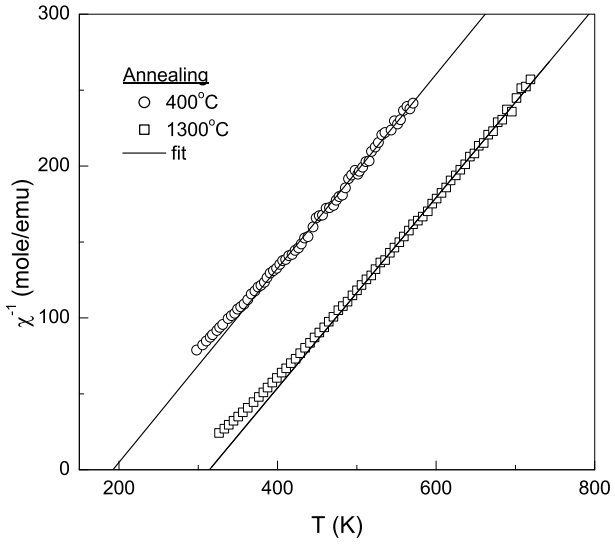

Figure 4.6: Temperature variation of the inverse of the paramagnetic susceptibility of LMN400 and LMN1300.

formula, $LaMn_{0.5}Ni_{0.5}O_3$, is used for the calculation of the molar susceptibilities. The susceptibility of LMN400 is measured up to 573 K (300 °C) only which is well within the stability temperature of this phase. Susceptibility of LMN1300 is measured up to 723 K (450 °C) as this phase is stable in this temperature range. Curie-Weiss behaviour, $\chi = C/(T - \Theta)$, is observed for both samples. The effective paramagnetic moment, $\mu_{eff} = 2.828\sqrt{C}$, where C is the Curie constant, is obtained from least-squares fit to the experimental data in the linear region at high temperatures. Almost identical slopes with different intercepts on the temperature axis are obtained for both samples. μ_{eff} is obtained as 3.54 μ_B and 3.57 μ_B for the two samples LMN400 and LMN1300, respectively, and the corresponding paramagnetic Curie temperatures (Θ) are obtained as 192 and 313 K.

The spin-only values of the moment, μ_{so}, for various possible combinations of different spin-states of Mn and Ni in La_2MnNiO_6 (calculations are based on the simple

Table 4.1: Spin-only moments (μ_{so}) for various spin-states of Mn and Ni in La_2MnNiO_6 (calculations are based on the simple perovkite formula, $LaMn_{0.5}Ni_{0.5}O_3$).

Spin-states	$\mu_{so} = [0.5\mu_{Mn}^2 + 0.5\mu_{Ni}^2]^{1/2}$ (μ_B)
Mn^{+3} (S=2), Ni^{+3} (S=3/2)	4.41
Mn^{+3} (S=2), Ni^{+3} (S=1/2)	3.67
Mn^{+4} (S=3/2), Ni^{+2} (S=1)	3.39
Mn^{+2} (S=5/2), Ni^{+4} (S=2)	5.43
Mn^{+2} (S=5/2), Ni^{+4} (S=1)	4.64
Mn^{+2} (S=5/2), Ni^{+4} (S=0)	4.18

perovskite formula, $LaMn_{0.5}Ni_{0.5}O_3$) are compared in Table 4.1. The experimental μ_{eff} values (3.54 and 3.57 μ_B) are almost comparable to the spin-only moments calculated for a combination of high-spin Mn^{+3} and low-spin Ni^{+3} as well as for Mn^{+4} and Ni^{+2}. Therefore, it is possible that the spin-states of Mn and Ni in LMN400 and LMN1300 are either identical or the above two different combinations. However, the different values of the paramagnetic Curie temperatures obtained from Curie-Weiss fit to the susceptibility data and the two different ferromagnetic Curie temperatures indicate a difference in the strength of the magnetic exchange interactions and therefore, a possible difference in the spin-states of Mn and Ni in LMN400 and LMN1300.

Compared to the high-T_c phase of La_2MnCoO_6, which contain Mn^{+3} and low-spin Co^{+3}, LMN1300 (the phase of La_2MnNiO_6 having a higher Curie temperature) may be assumed to be containing Mn^{+3} and low-spin Ni^{+3} (μ_{eff} = 3.57 μ_B and μ_{so} = 3.67 μ_B). Similarly, LMN400, showing the same magnetic transition temperature as that of the La_2MnCoO_6 sample annealed at 200 °C, can be assumed to be containing Mn^{+4} and Ni^{+2}. The higher value of μ_{eff} of LMN400 when compared to μ_{so} calculated for a combination of Mn^{+4} and Ni^{+2} can be accounted for, considering the contribution from spin-orbit coupling of Ni^{+2}. A slightly larger value of μ_{eff} can be expected for Ni^{+2} due to the contribution from spin-orbit coupling, as generally observed [Cas76]. The average magnetic moment, incorporating spin-orbit coupling

contribution, is expressed by the equation;

$$\bar{\mu}_e = \mu_{so}(1 - 4\lambda/10Dq) \tag{4.1}$$

where λ is the spin-orbit coupling coefficient and Dq is the crystal-field splitting parameter. Therefore, for Ni^{+2} having the ground term $^3A_{2g}$ and $\mu_{so} = 2.83\ \mu_B$, the average magnetic moment calculated using the above equation is $\sim$3.25 μ_B. Using this value of $\bar{\mu}_e$ for Ni^{+2}, the calculated moment for the Mn^{+4} and Ni^{+2} combination in $LaMn_{0.5}Ni_{0.5}O_3$ would be 3.58 μ_B which is comparable to the experimental value of 3.54 μ_B for LMN400. Therefore, if the contribution from the spin-orbit coupling of Ni^{+2} is taken into account, it may be considered that the combination of the spin-states Mn^{+4} and Ni^{+2} is possible in the low-T_c phase of the compound.

4.5.2 Non-magnetic substitution with isovalent ion

It is evident from temperature dependence of magnetization and paramagnetic susceptibility data that the phase formed after annealing at 1300 °C most likely has high-spin Mn^{+3} and low-spin Ni^{+3} ions. Nevertheless, the Curie temperature of $La_2Mn^{+3}Ni^{+3}O_6$ (273 K) is larger than that of the corresponding phase of the Co-containing composition $La_2Mn^{+3}Co^{+3}O_6$ (225 K). This is possibly due to the contribution from additional Mn^{+3}-O-Ni^{+3} or Ni^{+3}-O-Ni^{+3} superexchange interactions [Wol58, Goo61]. It may be noted that the low-spin Ni^{+3}, with electronic configuration $t_{2g}^6 e_g^1$, contains one unpaired electron ($S = 1/2$), when compared to the diamagnetic ($S = 0$), low-spin, Co^{+3} ion ($t_{2g}^6 e_g^0$). Therefore, the magnetic exchange interaction of the type Mn^{+3}-O-M^{+3}-O-Mn^{+3} would be stronger when M = Ni than when M = Co. Assuming trivalent states for Mn and Ni, the role of Ni in the magnetic exchange interactions in La_2MnNiO_6 is explored by substituting part of Mn^{+3} or Ni^{+3} by the non-magnetic ion, Al^{+3}. $La_2MnNi_{0.8}Al_{0.2}O_6$ (LMNA) and $La_2Mn_{0.8}Al_{0.2}NiO_6$ (LMAN) were prepared by the low-temperature method and heated at 1300 °C.

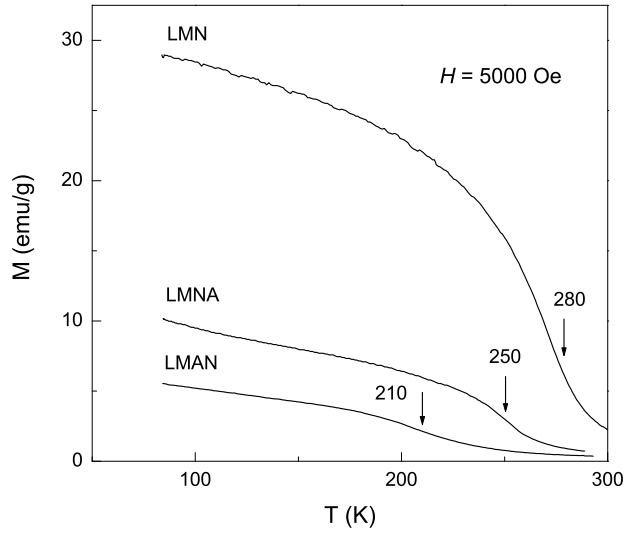

Figure 4.7: Temperature variation of the magnetization of La_2MnNiO_6 (LMN), $La_2MnNi_{0.8}Al_{0.2}O_6$ (LMNA), and $La_2Mn_{0.8}Al_{0.2}NiO_6$ (LMAN), annealed at 1300 °C; $H = 5000$ Oe.

Temperature dependence of the magnetization of LMN, LMNA and LMAN, measured using a field of 5000 Oe, is compared in Figure 4.7. Measurements are made using a high magnetic field to compare the effect of substitution of Al^{+3} on the magnitude of magnetization as well as on the Curie temperature. There is a drastic reduction in the magnetization when both Mn^{+3} and Ni^{+3} are partially replaced by Al^{+3}. Magnetization at the lowest temperature is reduced to 36% when 20% of Ni is substituted by Al and to 19% when 20% of Mn is substituted by Al. Similarly, Curie temperature (the temperature at which a sharp transition is observed in M_{ZFC} measurements using $H = 50$ Oe) is reduced from 273 K to 250 K when Ni is substituted and to 210 K when Mn is substituted by Al. When a similar substitution is made on the corresponding Co composition La_2MnCoO_6, it was found that magnetization and T_c is not much affected on replacing Co by Al. The reduction in both magnetization

and Curie temperature when Ni is replaced by Al indicates the direct role of Ni^{+3} in determining the higher T_c of La_2MnNiO_6 when compared to that of La_2MnCoO_6. Similarly, the large reductions in magnetization and T_c, when Mn is substituted by Al, indicate that major role is played by Mn^{+3} in the magnetic exchange interactions.

4.5.3 XPS studies

Core-level x-ray photoelectron spectroscopic studies are performed on LMN400 and LMN1300 to understand the results obtained from high temperature magnetic susceptibility studies. All the photoemission spectra are recorded at room temperature. As a measure to check the surface contamination problem, the samples are scraped thoroughly and repeatedly over the surface with a stainless steel blade *in situ* under high vacuum. The scraping is repeated until the higher binding energy (BE) shoulder in the O 1s XPS showed a minimum and no further decrease in intensity. In the case of the LT samples heated at 400 °C, on which XPS measurements are made, excess carbon is found. Perovskite manganates synthesized by low-temperature methods are known for carbon contamination [Bay82, Chi90]. Repeated scraping of the samples did not remove the carbon contamination in the LT samples, indicating the presence of carbon in the bulk. However, very good improvement in the spectral quality of O 1s, C 1s, and valence band spectra of LT samples after scraping, clearly indicates that the bulk carbon contamination do not significantly affect the overall results presented here. Further, core-level XPS measurements are made on three different LT samples each to make sure that the results are reproducible.

Core-level XPS of the transition metal ions are known to be sensitive to their spin-states and $3d$-electron contents. There is a general trend that the core-level binding energy increases with increasing oxidation state of a given ion, provided that the ions are located in similar coordination environment in different compounds [Bri74]. However, this rule breaks down when the number of unpaired electrons changes due

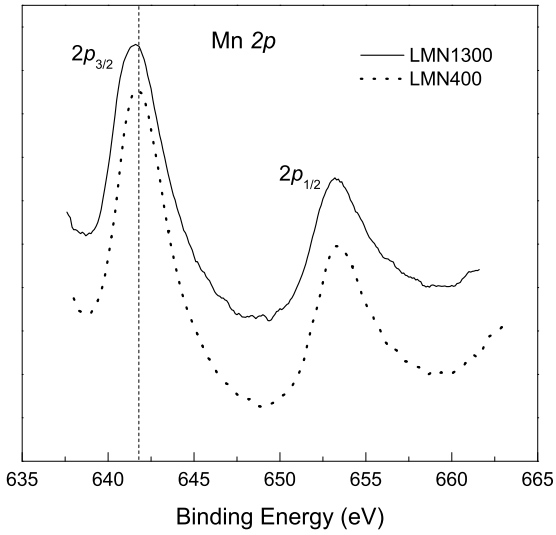

Figure 4.8: Mn $2p$ XPS of LMN400 and LMN1300.

to a change in the spin-state of a given ion. It has been reported earlier that under identical octahedral coordination environment, the $2p_{3/2}$ binding energy of low-spin Co^{+3} is lower than that of Co^{+2} [Fro72, Bri74]. Similarly, it is found that the Ni $2p_{3/2}$ BE of Ni_2O_3 containing low-spin Ni^{+3} is lower than that of NiO containing Ni^{+2} [Jor71, Ng76].

The $2p$ core-level XPS of Mn in LMN400 and LMN1300 are compared in Figure 4.8. The binding energy of Mn $2p_{3/2}$ is obtained as 641.8 eV for LMN400 and as 641.5 eV for LMN1300. Generally $2p_{3/2}$ BE is found to be lower for Mn^{+3} than for Mn^{+4} when the ions are situated in identical environments (as in $LaMn^{+3}O_3$ and $CaMn^{+4}O_3$) by 0.3-0.4 eV. The difference in the BEs of Mn $2p_{3/2}$ obtained for the two samples of La_2MnNiO_6 is identical to that found for the two different phases of La_2MnCoO_6 having different spin-states of Mn, Mn^{+3} for the high-T_c phase and Mn^{+4} for the low-T_c phase (see Section 3.1.5). In the case of La_2MnNiO_6 also, a lower BE is obtained for the sample with a higher T_c, indicating that the spin-state of Mn

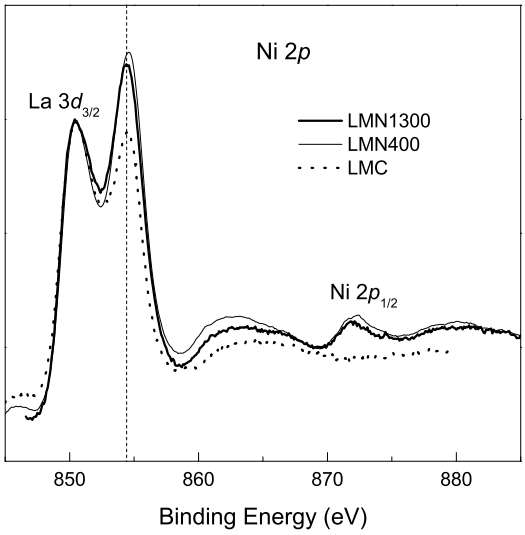

Figure 4.9: Ni $2p$ XPS of LMN400 and LMN1300, along with the La $3d_{3/2}$ XPS of La_2MnCoO_6 (LMC).

is Mn^{+3} in LMN1300 and Mn^{+4} in LMN400.

Figure 4.9 shows the $2p$ core-level XPS of Ni in LMN400 and LMN1300. Unfortunately the BE of the satellite peak of La $3d_{3/2}$ is almost identical to that of $2p_{3/2}$ of Ni in oxides and therefore these peaks overlap for compounds containing both La and Ni. The main and satellite peaks of La $3d_{3/2}$ in La_2O_3 and other perovskite-type oxides are observed with approximately 1:1 intensity ratio (see for La_2MnCoO_6 in Figure 4.9) [Sto97]. Therefore, larger intensity of peak in the BE region of satellite peak of La $3d_{3/2}$ may be considered as the contribution of Ni $2p_{3/2}$ for both LMN400 and LMN1300. Since the La^{+3} ion is situated in the same environment in both LMN400 and LMN1300, and the BE of the La $3d_{3/2}$ main peak is identical for both samples (the intensities of this peak is normalized for all samples in the figure), it may be assumed that the small difference in the BE of the peak in the region of the La $3d_{3/2}$ satellite peak is due to the difference in the BE of Ni $2p_{3/2}$ in the two samples. This

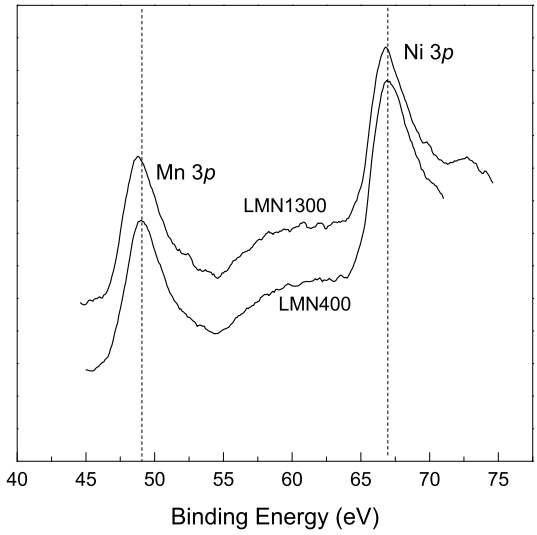

Figure 4.10: Mn and Ni $3p$ XPS of LMN400 and LMN1300.

comparison gives a Ni $2p_{3/2}$ BE of 854.6 eV for LMN400 and 854.3 eV for LMN1300. A similar difference in the BE is observed for the Ni $2p_{1/2}$ peaks also for the two compounds. The difference in the binding energies of Ni $2p_{3/2}$ and $2p_{1/2}$ are ΔE = 17.8 eV for LMN400 and ΔE = 17.6 eV for LMN1300, respectively. The lower value of ΔE for LMN1300 by 0.2 eV may be taken as evidence for one unpaired electron less for Ni in this sample. This fact, when combined with the lower BE of the Ni $2p_{3/2}$ peak, then corresponds to the spin-state of Ni as low-spin Ni^{+3} ($S = 1/2$) in LMN1300 and as Ni^{+2} ($S = 1$) in LMN400. These spin-states of Ni in the two samples are similar to that observed for Co in the nanocrystalline and high-temperature heated samples of La_2MnCoO_6. A lower BE is expected for low-spin Ni^{+3} when compared to the higher BE of Ni^{+2}, due to the less number of unpaired electrons in the former. Moreover, these spin-states of Ni in the two samples are in accordance with the spin-states of Mn, which will take care of charge neutrality and oxygen stoichiometry.

A comparison of Mn and Ni $3p$ XPS, shown in Figure 4.10, of LMN400 and

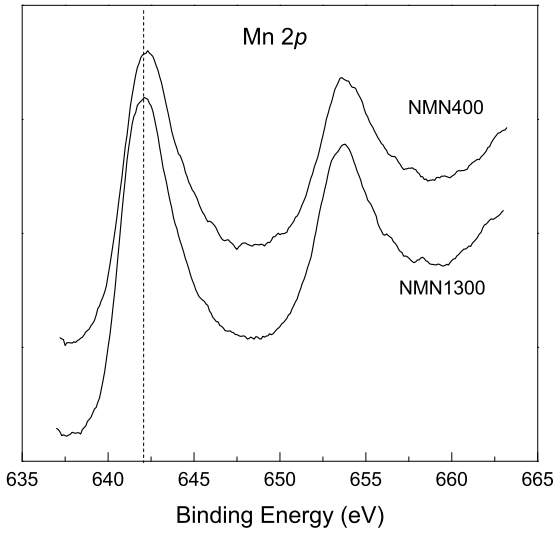

Figure 4.11: Mn $2p$ XPS of NMN400 and NMN1300.

LMN1300 also shows the same trend in the binding energies. Mn $3p$ XPS peaks are observed at 49.1 and 48.8 eV and Ni $3p$ peaks are observed at 66.9 and 66.7 eV, respectively, for LMN400 and LMN1300. This gives further evidence for the different spin-states of Mn and Ni in the two samples, as concluded from the analysis of the $2p$ XPS of Mn and Ni.

The overlapping of the Ni $2p_{3/2}$ XPS peaks with that of La $3d_{3/2}$ satellite peak for compounds containing both La and Ni can be taken care of by selecting a rare earth ion, instead of La, whose XPS peaks will not interfere with that of Ni $2p_{3/2}$, in the same composition. To compare the differences in the Ni $2p_{3/2}$ XPS binding energies of the compounds heated at 400 and 1300 °C, and to further confirm the observations made on La_2MnNiO_6, core level XPS studies are made on Nd_2MnNiO_6 (NMN) samples processed under identical conditions. Mn and Ni $2p$ XPS of the two samples of NMN, heated at 400 and 1300 °C (NMN400 and NMN1300), and showing magnetic transitions at different temperatures, are shown in Figure 4.11 and

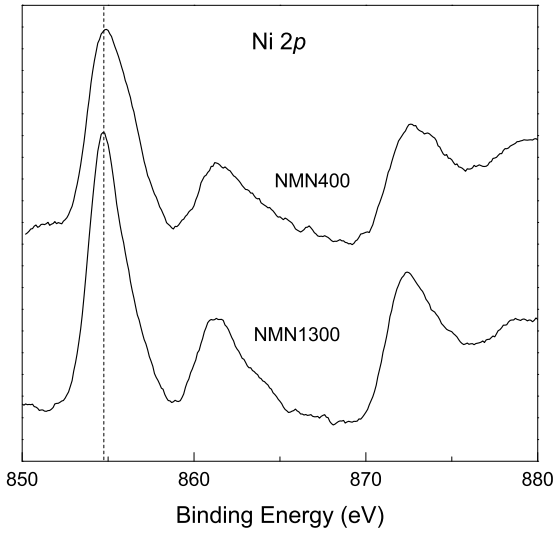

Figure 4.12: Ni $2p$ XPS of NMN400 and NMN1300.

Table 4.2: Mn $2p_{3/2}$ and Ni $2p_{3/2}$ XPS BE in the two different ferromagnetic phases of La_2MnNiO_6 (LMN) and Nd_2MnNiO_6 (NMN).

Compound	Sample	T_c (K)	Mn $2p_{3/2}$ (eV)	Ni $2p_{3/2}$ (eV)
La_2MnNiO_6	LMN400	150	641.8	854.6
	LMN1300	273	641.5	854.3
Nd_2MnNiO_6	NMN400	90	642.4	854.9
	NMN1300	195	642.1	854.7

Figure 4.12, respectively. The Mn $2p_{3/2}$ and Ni $2p_{3/2}$ XPS binding energies of Mn and Ni in LMN and NMN are compared in Table 4.2. There is a small shift in the BEs of the XPS peaks to higher values by ∼0.5 eV when La is replaced by Nd. Similar effects have been generally observed in the XPS studies on different rare earth compounds [Kan96, Mah96, Tal01].

As expected, there is a difference in the binding energies of the Mn as well as Ni $2p$ XPS peaks of NMN400 and NMN1300. Similar to the corresponding LMN samples, Ni $2p_{3/2}$ binding energy is lower by 0.2 eV for NMN1300 showing a magnetic transition

at a higher temperature when compared to NMN400, confirming that the spin-state of Ni is Ni^{+2} in the sample showing a lower magnetic transition temperature and low-spin Ni^{+3} for the high-T_c phase with rhombohedral symmetry. Similar difference in Mn $2p_{3/2}$ BE energy is observed for the two NMN samples also, indicating the presence of Mn^{+4} and Mn^{+3} in the samples heated at 400 and 1300 °C, respectively.

4.5.4 Origin of ferromagnetism in La_2MnNiO_6

Both the end members of La_2MnNiO_6, namely $LaMnO_3$ and $LaNiO_3$, are having Jahn-Teller active transition metal ions, but the former is antiferromagnetic with ferromagnetically ordered (001) planes whereas the latter is paramagnetic. In spite of the same e_g orbital electronic configuration, this drastic difference in the magnetic properties of the two end members stems from the difference in the electronic configuration of Mn^{+3} ($t_{2g}^3 e_g^1$) and low-spin Ni^{+3} ($t_{2g}^6 e_g^1$) in the t_{2g} orbitals . The low-spin Ni^{+3} does not have any localized moment to correlate the exchange electron with and hence the Ni-Ni interaction does not result in any particular spin ordering. In other words, there is no exchange splitting in low-spin Ni^{+3}. Due to the same reason, the Mn^{+3}-O-Ni^{+3} superexchange is ferromagnetic. Similarly, Mn^{+4}-O-Ni^{+2} exchange is also predicted to be ferromagnetic. If the Mn^{+3}-O-M^{+x} interaction is antiferromagnetic, the magnetic moment of the ordered compound formed by partly substituting Mn by M will correspond to a ferrimagnetic coupling, and the ferrimagnetic compositional range will be narrow too [Wol58]. On the other hand, if Mn^{+3}-O-M^{+x} interaction is ferromagnetic, the ferromagnetic compositional region may be extended up to 50% of M, provided ionic ordering is present. This indirectly tells that the magnetic exchange in La_2MnNiO_6 is likely to be ferromagnetic and with a possible ionic ordering.

The results from high-temperature paramagnetic susceptibility and core-level XPS studies confirm that the spin-states of Mn and Ni are different in the two ferromagnetic phases of La_2MnNiO_6 obtained at different processing temperatures. The dif-

ferent spin-states of Mn and Ni as Mn^{+4} and Ni^{+2} in LMN400 (low-T_c phase) and as Mn^{+3} and low-spin Ni^{+3} in LMN1300 (high-T_c phase) explain the different magnetic transition temperatures of these two phases of La_2MnNiO_6. In other words, a charge redistribution is the reason for the formation of the second magnetic phase, rather than an ionic redistribution. Nevertheless, there is no evidence to exclude a concomitant ion redistribution.

The changes in the spin-states of Mn and Ni in LMN400 and LMN1300 occur through a charge disproportionation $Mn^{+4} + Ni^{+2} \rightarrow Mn^{+3} + Ni^{+3}$ when the low-temperature synthesized sample is heated to higher temperatures. But the reaction $Mn^{+4} + Ni^{+2} \rightleftharpoons Mn^{+3} + Ni^{+3}$ is predicted to be biased to left by about 0.8eV [Das03]. However, this prediction is based on the studies on some binary structured oxides [Pau00]. Moreover, the above reaction can be biased either to right or to left depending up on the Mn concentration, the temperature and the degree of ionic-ordering [Vas84]. In short, the energy change accompanied by the formation of trivalent ions from Mn^{+4}/Ni^{+2} system is not convincingly clear.

Similar to that observed for the phase of La_2MnCoO_6 obtained at low-annealing temperatures, LMN400 has a majority of Mn^{+4}-O-Ni^{+2} ferromagnetic exchange, which is equivalent in strength to the Mn^{+4}-O-Co^{+2}. The similarity of the electronic configuration in the e_g orbitals – which take part in hybridization with oxygen orbitals – of Co^{+2} ($t_{2g}^5 e_g^2$) and Ni^{+2} ($t_{2g}^6 e_g^2$) can be the reason for such equivalence in magnetic exchange strengths and transition temperatures of the above two compositions. In the case of the high-T_c phase of La_2MnNiO_6, both the trivalent ions are Jahn-Teller active, with a single electron in the e_g orbital. Therefore, unlike in La_2MnCoO_6, an ordering of Jahn-Teller active ions into (001) planes is not necessary to achieve a cooperative effect and thereby a structural stabilization. In other words, there is no driving force from a possible (001) ordering for the reaction $Mn^{+4} + Ni^{+2} \rightleftharpoons Mn^{+3} + Ni^{+3}$ which is biased to left by about 0.8eV (for the Co system it is only 0.2 eV)

[Das03]. Moreover, the energy gain from such an ordering, if at all present, may not be sufficiently high to cope with the comparatively higher bias towards left hand side, making the (001) ordering unfavorable. There can be slight assistance from the ionic size effect towards the above reaction, since a reduction in the average Mn-site ionic radius is resulted by the same reaction. Thus the system depends mostly on the thermal energy for the formation of trivalent ions. This explains the higher formation temperature of the high-T_c phase of La_2MnNiO_6 than for its Co counterpart. A higher Curie temperature observed for a phase containing trivalent ions, for both Co and Ni compounds, suggests that Mn^{+3}-O-M^{+3} superexchange interactions are stronger than that of the Mn^{+4}-O-M^{+2} (M = Mn, Co, Ni) interactions. One of the possible reasons for this is that in the trivalent ion cases, the average ionic size of the Mn-site ions decreases, thereby strengthening the ferromagnetic exchange.

There is a double charge disproportionation $Mn^{+4} + Co^{+2} \rightarrow Mn^{+3} + Co^{+3} \rightarrow Mn^{+4} + Co^{+2}$, in La_2MnCoO_6, indicating the stability of the low-T_c phase of the compound having an orthorhombic structure. On the other hand, in the case of La_2MnNiO_6, there is no formation of a different phase of this compound after heating at intermediate temperatures and the rhombohedral phase containing Mn^{+3} and Ni^{+3} is not reverted back to the low-T_c phase even after annealing at 1300 °C. That is, there is only one step of charge disproportionation as $Mn^{4+} + Ni^{2+} \rightarrow Mn^{3+} + Ni^{3+}$ in La_2MnNiO_6. The phenomenal difference in the evolution of the different phases when M = Co and Ni, in $La_2Mn$$M$$O_6$, may be due to the difference in the stability of the different possible crystal structures in these two systems. Density functional theoretical calculations show that rhombohedral phase of La_2MnNiO_6 is energetically more stable than the orthorhombic phase [Yan00a] and contrary to this, orthorhombic phase of La_2MnCoO_6 is shown to be more stable compared to its rhombohedral form [Yan99].

The broader or multiple magnetic transitions observed for those samples heated

in the temperature range 400-1200 °C are then due to the mixed valence states of Mn and Ni (due to slow and partial charge disproportionation when sufficient thermal energy is not available) and therefore, due to the different types of superexchange interactions in these samples.

4.6 Conclusions

The properties of La_2MnNiO_6, synthesized by the ceramic and the low-temperature methods have been studied in detail to understand the origin of ferromagnetism in this compound. Two magnetic transitions are observed in the sample synthesized by the high-temperature ceramic method, due to the presence of two different phases of the compound. The two phases are obtained in single phase forms by a low-temperature method of synthesis. One phase showing a magnetic transition below 150 K is found to be stable only below 500 °C and is converted to the second phase having a higher magnetic transition temperature (273 K) after heating at higher temperatures, so that both phases coexist in samples processed in the temperature range 500–1300 °C. This explains why two magnetic transitions are observed in the samples synthesized by the ceramic method. The crystal structures of the two phases are also found to be different. Even though the reflections in the XRD pattern of the low-T_c phase are broader due to lower particle size, an orthorhombic symmetry can be assigned to this phase and a rhombohedral structure is observed for the high-T_c phase. High-temperature paramagnetic susceptibility studies on samples annealed at 400 and 1300 °C gave comparable values for the effective magnetic moment with a large difference in the paramagnetic Curie temperature, indicating the different strengths of magnetic exchange interactions in the two samples. The effective paramagnetic moment values obtained for the two phases are comparable to the spin-only moments calculated for a combination of different spin-states of Mn and Ni; Mn^{+3} and low-spin Ni^{+3} for

one phase and Mn^{+4} and Ni^{+2} for the other phase. A comparison of the results obtained on the similar compound La_2MnCoO_6 and core-level x-ray photoelectron spectroscopic studies give conclusive evidence for different spin-states of Mn and Ni in the two phases; Mn^{+4} and Ni^{+2} in the nanocrystalline material showing a magnetic transition at a lower temperature and Mn^{+3} and low-spin Ni^{+3} in the high-T_c phase. These results indicate a possible charge disproportionation, Mn^{+4} + Ni^{+2} $\rightarrow$ Mn^{+3} + Ni^{+3}, when the low-temperature synthesized sample is heated in the temperature range 400-1300 °C.

Chapter 5

Studies on $La_2MnCo_{1-x}M_xO_6$

Substitution in the *B*-site of double perovskite manganate compositions by a third element is hardly studied. One of the reasons is the added complexity which may arise due to the combinations of the spin-states of Mn and the other ions. But that is not a sufficiently discouraging factor for deserting such systems from scientific investigations. The studies centered on the double perovskite compositions, which show novel properties like magnetoresistance, half-metallicity, etc., are indispensable for technological advancements based on spintronics. In fact, substitution studies can give better information about the ionic ordering, magnetic exchange interactions, and spin-states of the ions in the parent compounds. For example, such studies on the double perovskite oxide, Sr_2FeMoO_6, showing tunnelling magnetoresistance, have been performed to gain knowledge about ionic ordering, magnetic interactions, etc [Das01, Pen01, Sam01, Bla02c, Dou02].

Having studied the structural and magnetic properties of the double perovskite compositions La_2MnCoO_6 and La_2MnNiO_6, further studies are made on a solid solution of these two compositions, $La_2MnCo_{1-x}Ni_xO_6$, to understand the role of Co and Ni in determining the properties. Similarly, Co^{+3} in La_2MnCoO_6 is partially substituted by the trivalent magnetic ion Fe^{+3} and the non-magnetic ion Al^{+3}, whose ionic sizes are comparable to those of Mn^{+3} and Co^{+3}, respectively, to obtain additional

information on the role the Co^{+3} ion in determining the magnetic properties of the parent compound.

5.1 $La_2MnCo_{1-x}Ni_xO_6$

5.1.1 Background

Studies on La_2MnCoO_6 (Section 3.1) and La_2MnNiO_6 (Chapter 4) indicate that two different spin-states are possible for each of the constituent B-site ions, in the two different ferromagnetic phases of the compounds. Conventional ceramic method of synthesis yields either mixed phases or only one of the phases in the pure form. This shows that the other phase (metastable) is formed and stable only at low temperatures and converted to a second phase on treating at higher temperatures. Different combinations of spin-states of Mn and M (Co, Ni) are possible when the two phases are present together in samples synthesized by the usual ceramic route. However, single phase forms of these compositions could be obtained when they are synthesized by a low-temperature method.

When La_2MnCoO_6 is synthesized by low-temperature method and annealed at different temperatures in the range 200–1300 °C, it is found that a ferromagnetic phase, initially formed, with a magnetic transition temperature of ∼150 K, is converted to another ferromagnetic phase with T_c = 225 K when annealed in air at 700 °C and converted back to the initial phase on further annealing at higher temperatures. These changes could be explained on the basis of a change in the spin-states of Mn and Co, in terms of the charge disproportionation Mn^{+4} + Co^{+2} → Mn^{+3} + Co^{+3} → Mn^{+4} + Co^{+2}. Therefore ferromagnetism in the phase with a low magnetic transition temperature (low-T_c phase) is due to Mn^{+4}-O-Co^{+2} exchange interactions and in the phase with a higher T_c (high-T_c phase), it is from Mn^{+3}-O-Mn^{+3} interactions, since Co^{+3} is present in its low-spin state ($S = 0$). On the other hand, in the

case of La_2MnNiO_6, a ferromagnetic phase formed at low temperatures is slowly converted into another phase with a higher Curie temperature when the low-temperature synthesized sample is annealed in air in the temperature range 200–1300 °C. In this case, the charge disproportionation, $Mn^{+4} + Ni^{+2} \rightarrow Mn^{+3} + Ni^{+3}$, could explain the formation of the phase with a higher T_c. In both cases, higher Curie temperatures are obtained when the transition metal ions are present in their trivalent states.

It is interesting to note that the high-T_c phase of La_2MnCoO_6 is formed at a relatively lower temperature of 700 °C, whereas that of La_2MnNiO_6 is obtained after processing at higher temperatures (> 1200 °C), even though both contain trivalent metal ions. On the other hand, the high temperature treated La_2MnCoO_6 comprises of Mn^{+4} and Co^{+2}. Hence, it would be interesting to study the properties of a solid-solution of the two compounds, i.e., $La_2MnCo_{1-x}Ni_xO_6$, to look for the possibility of formation of novel single phase compositions with different magnetic transition temperatures and spin-states of Mn, Co and Ni. Moreover, among La_2MnCoO_6 and La_2MnNiO_6, the high-T_c phase of Ni compound has a higher magnetic transition temperature by 50 K, probably due to contributions from additional ferromagnetic exchange interactions involving Mn^{+3} and low-spin Ni^{+3} (low-spin Co^{+3} is a diamagnetic ion). To understand the role of this additional magnetic interaction, the magnetic properties of $La_2MnCo_{1-x}Ni_xO_6$ is studied by replacing Co, in steps of 1/8, with Ni.

5.1.2 Synthesis

Different compositions in $La_2MnCo_{1-x}Ni_xO_6$ were synthesized by the low-temperature method as followed for the synthesis of the end members La_2MnCoO_6 (LMC) and La_2MnNiO_6 (LMN). The compounds obtained at a lower synthesis temperature is annealed in air at different temperatures in the range 200–1300 °C for 12 hours each and furnace cooled to room temperature. Since the high-T_c phase of La_2MnCoO_6 is

formed at 700 °C, all the compositions are annealed at this temperature to detect any magnetic phase formation. Similarly, all the samples are annealed at 1300-1350 °C because the high-T_c phase of La_2MnNiO_6 and the low-T_c phase of La_2MnCoO_6 are formed after annealing at this temperature. The fact that the temperature of formation of the high-T_c phases of the parent compounds are different, indicates that perhaps the high-T_c phases of the intermediate compositions, may be formed in the temperature range of 700–1300 °C. Therefore, the compositions after annealing in the above temperature range are closely observed for any metastable phase formation. Compared with the stoichiometric phases of the parent compounds, these compositions are also considered as stoichiometric in oxygen content.

5.1.3 Magnetic measurements

All the compositions, after annealing at each temperatures, were measured for the evolution of magnetic phases by zero field cooled (ZFC) magnetization measurements at a lower field of 50 Oe. ZFC magnetization curves of different phases of the end-members of the series $La_2MnCo_{1-x}Ni_xO_6$, viz., La_2MnCoO_6 (LMC) and La_2MnNiO_6 (LMN) are shown in Figure 5.1 for comparison. For both LMC and LMN, broad ferromagnetic transitions are observed below 150 K, when annealed at 200 °C. Similar to that observed for the end members, all the samples of $La_2MnCo_{1-x}Ni_xO_6$ annealed at 200 °C show a commensurate ferromagnetic transition below $\sim 150K$, as shown in Figure 5.2. This is indicative of a common mechanism for the origin of ferromagnetism in these low-temperature synthesized samples. The broadness of this magnetic transition is due to fine particle nature (∼20 nm) of the compounds synthesized at very low temperatures. Since the magnetic transition temperatures of all the compositions are broad, their T_cs are taken as that of the sharp transition of the magnetically equivalent phase of LMC obtained after annealing at 1300 °C, which is obtained as 145 K from the dM/dT curve. It is already described that the parent

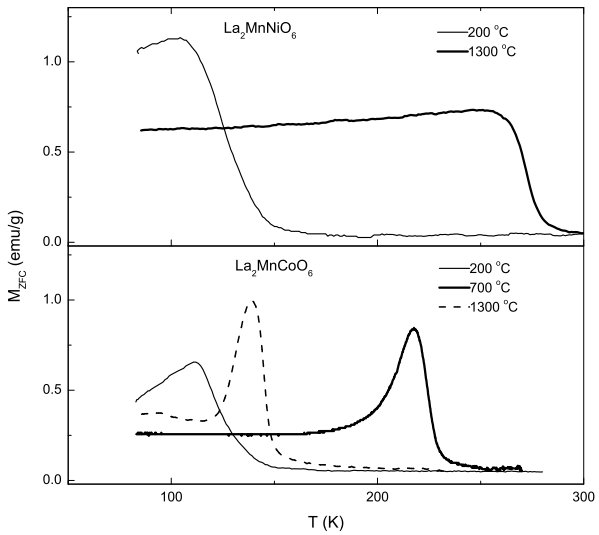

Figure 5.1: Comparison of the ZFC magnetization (H = 50 Oe) curves of the two different phases of La_2MnCoO_6 and La_2MnNiO_6.

compounds (LMC and LMN) when annealed at 200 °C have Mn^{+4}/Co^{+2} (Ni^{+2}) combination of spin-states. Therefore, it is sound to assume here also that tetravalent Mn and divalent Co and Ni ions combination would be present in the low-temperature annealed compositions. The identical magnetic transition temperatures, irrespective of the concentration of Co or Ni, are because the major contribution to ferromagnetism comes from Mn^{+4}-O-M^{+2} superexchange. The strength of Mn^{+4}-O-Co^{+2} and Mn^{+4}-O-Ni^{+2} superexchanges can be considered as almost the same, since both Co^{+2} ($t_{2g}^5e_g^2$) and Ni^{+2} ($t_{2g}^6e_g^2$) have the same number of e_g electrons, which take part in σ exchange interaction. Here, the other possible Mn^{4+}-O-Mn^{4+} exchange interaction is neglected owing to its antiferromagnetic nature.

For LMC, the high-T_c phase, in single phase form, is obtained when the low-temperature synthesized sample is annealed at 700 °C. On the other hand, for LMN, there is no pure phase formation at this annealing temperature, instead it exhibit

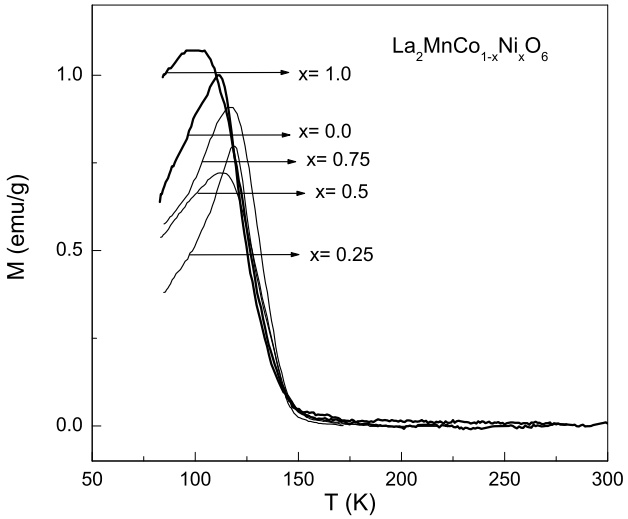

Figure 5.2: ZFC magnetization ($H = 50$ Oe) curves of $La_2MnCo_{0.5}Ni_{0.5}O_6$ annealed at 200 °C.

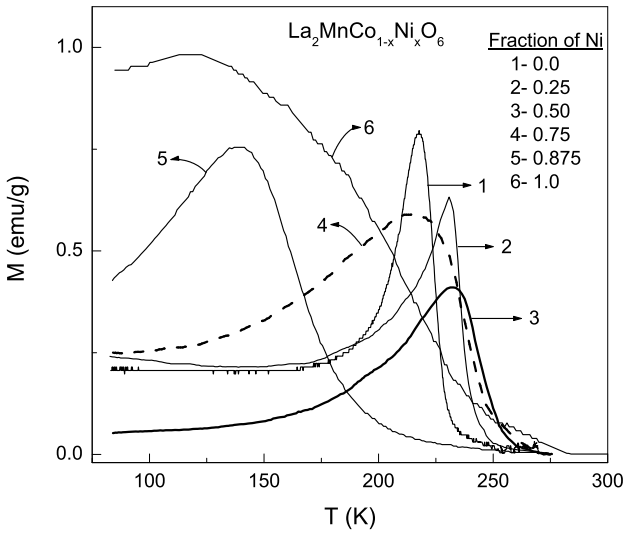

Figure 5.3: ZFC magnetization ($H = 50$ Oe) curves of different compositions in $La_2MnCo_{1-x}Ni_xO_6$ annealed at 700 °C.

a broad magnetic transition (see Figure 4.2). Hence, all the compositions in the $La_2MnCo_{1-x}Ni_xO_6$ series were annealed at 700 °C, initially, to look for the formation of any single phases. The ZFC magnetization curves of the samples annealed at 700 °C are shown in Figure 5.3. A trend of gradual broadening of the magnetic transition and increasing T_c, with the increase in Ni content, in addition to the smearing of the peak in the magnetization curve, is observed. The latter phenomenon is possibly due to the decreasing contribution of high uniaxial anisotropy of the Co ion, which leads to the pinning of domain walls. The broadening of the magnetic transition clearly tells that the long-range exchange interaction present in La_2MnCoO_6, which shows a sharp magnetic transition, is broken down concomitant with a possible charge disproportionation. This assumption can be understood from the behaviour of the end-members under similar conditions, where a charge redistribution at certain annealing temperature ranges result in such behaviours (see Section 3.1 and Chapter 4).

Before proceeding with the entire series, the nominal composition with $x = 0.5$ was investigated initially to have a better ground. The zero field cooled magnetization (M_{ZFC}, at 50 Oe) curves of $La_2MnCo_{0.5}Ni_{0.5}O_6$, annealed at different temperatures in the range 200–1300 °C are shown in Figure 5.4. The sample annealed at 200 °C shows the same transition temperature as that of the other compositions in the $La_2MnCo_{1-x}Ni_xO_6$ series. It is found that a high-T_c phase with a sharp magnetic transition at 248 K (when compared to the T_cs of high-T_c phases of LMC (225 K) and LMN (273 K) is formed after annealing at 900 °C. It is observed that the same magnetic transition temperature is observed for the sample annealed at 700°C also, but with a broader magnetic transition. Here, the striking point is that the annealing temperature required to get the high-T_c phase of $La_2MnCo_{0.5}Ni_{0.5}O_6$, with a sharp magnetic transition, is in between that of the corresponding phases of the end-members. That is, the charge disproportionation $Mn^{+4} + Co^{+2} \rightarrow Mn^{+3} + Co^{+3}$ is completed at a higher temperature when compared to that in LMC and the

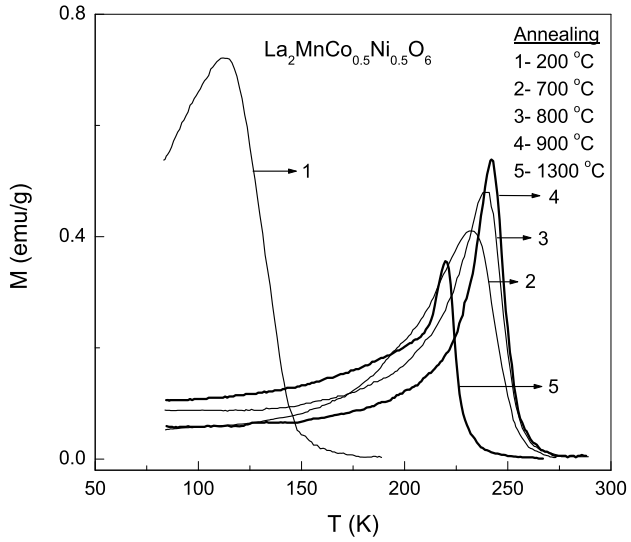

Figure 5.4: ZFC magnetization ($H = 50$ Oe) curves of $La_2MnCo_{0.5}Ni_{0.5}O_6$, annealed at different temperatures.

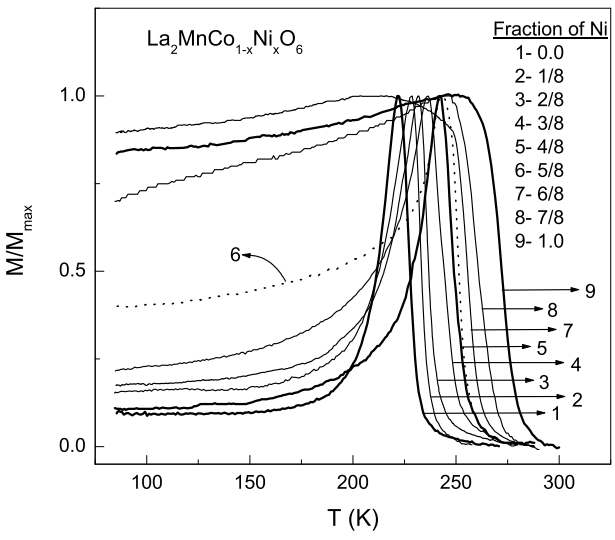

Figure 5.5: ZFC magnetization ($H = 50$ Oe) curves of different compositions in $La_2MnCo_{1-x}Ni_xO_6$ showing higher Curie temperatures.

charge disproportionation Mn^{+4} + Ni^{+2} → Mn^{+3} + Ni^{+3} is completed at a lower temperature when compared to that in LMN. Similarly, the sample annealed at 1300 °C undergo a ferromagnetic transition at 226 K (from the dM/dT curve), i.e., the Curie temperature is reduced from 248 K and this corresponds to an intermediate-T_c phase (considering that the sample annealed at 200 °C showing a magnetic transition below ∼150 K is the low-T_c phase).

Figure 5.5 illustrates the magnetization behaviour of the of different compositions in $La_2MnCo_{1-x}Ni_xO_6$ showing highest T_cs, formed at successively increasing annealing temperatures. For $x = 0.625$ (dotted curve, 6) the transition temperature is not much distinct from that of $x = 0.5$ (curve 5), indicating the influence of the latter composition – that has equal amounts of Co and Ni – on the former. A preferential formation of the phase containing equal amounts of Co and Ni is expected when x is close to 0.5 due to the possibility for better and easy ordering of the ions in the lattice. The cross over from Co dominant compositional region to Ni dominant region is clearly visible from the concomitant change in the nature of the curve immediately below T_c. The Co rich compositions show a peak whereas the Ni rich ones show a plateau below T_c.

Figure 5.6 shows temperature variation of the magnetization of the single phase compounds of some compositions in $La_2MnCo_{1-x}Ni_xO_6$, including that of the end-members La_2MnCoO_6 ($x = 0$) and La_2MnNiO_6 ($x = 1$).The magnetization curves of x = 0.25, 0.5 and 0.75, annealed at different temperatures, indicate that different phases are possible when Co and Ni are present together. As soon as Co is incorporated in place of Ni, in La_2MnNiO_6, the magnetic transition temperature of the samples heated at 1300-1350 °C decreases and another phase with a higher transition temperature is obtained when annealed between 700 and 1100 °C. This annealing temperature, to get a single phase compound with higher T_c, decreases with decreasing the Ni content. For higher Co concentrations studied (x = 0.125, 0.25, 0.375), a weak magnetic

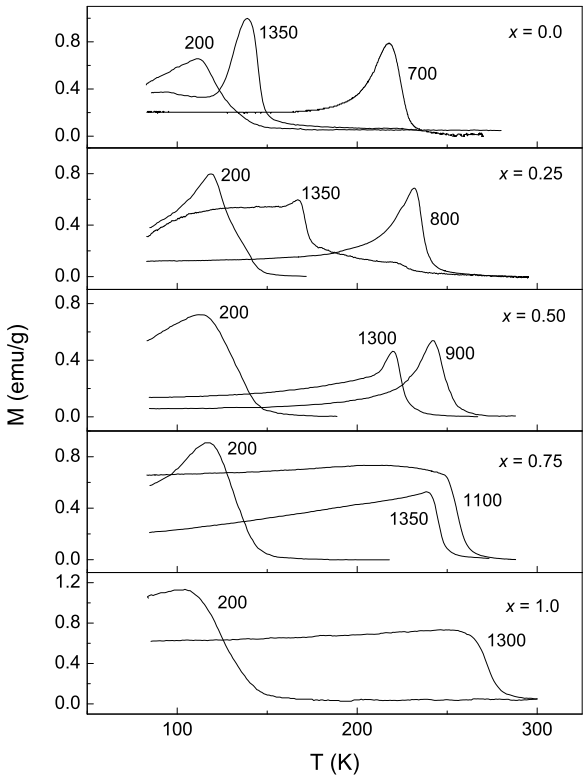

Figure 5.6: ZFC magnetization ($H = 50$ Oe) curves of the different phases of $La_2MnCo_{1-x}Ni_xO_6$. The numbers on the curves indicate the annealing temperatures in °C.

transition is observed at ≈ 226 K, for the samples annealed at 1350 °C. This transition temperature corresponds to the T_c of $x = 0.5$ annealed at the same temperature,and also is near to the high-T_c phase of La_2MnCoO_6. Since both these phases are found to influence the neighbouring compositions, because of their preferential formation, the compositions near to $x = 0$ may be stabilizing slight amounts of La_2MnCoO_6 and those adjacent to $x = 0.5$ forms a phase of the same. This observation is analogous to the case of the high-T_c phase of $x = 0.625$, whose T_c is not clearly distinct from

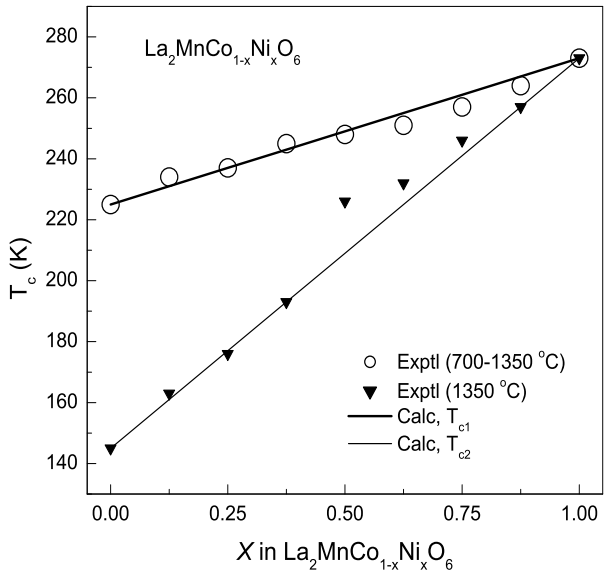

Figure 5.7: Variation of T_cs of the two phases, with x, in $La_2MnCo_{1-x}Ni_xO_6$. The solid lines are the calculated values as discussed in the text.

that of a phase corresponding to $x = 0.5$.

Figure 5.7 shows the variation of the magnetic transition temperatures of the two different phases (intermediate-T_c and high-T_c) of $La_2MnCo_{1-x}Ni_xO_6$, as a function of x. For the phase of La_2MnCoO_6 showing a higher magnetic transition temperature, the rate of increase in the T_c with decreasing Co concentration is less than that observed for the phase showing a lower T_c where the samples are heated to 1300-1350 °C. In both cases, the change in T_c with x is almost linear, except for a deviation from linearity for the phase with the lower T_c when $x = 0.5$. The possible reason for this deviation is an additional ordering of Mn, Co, and Ni ions in the perovskite lattice when they are present in equal amounts. This in turn can give rise to additional magnetic exchange interactions, other than those present in the remaining compositions.

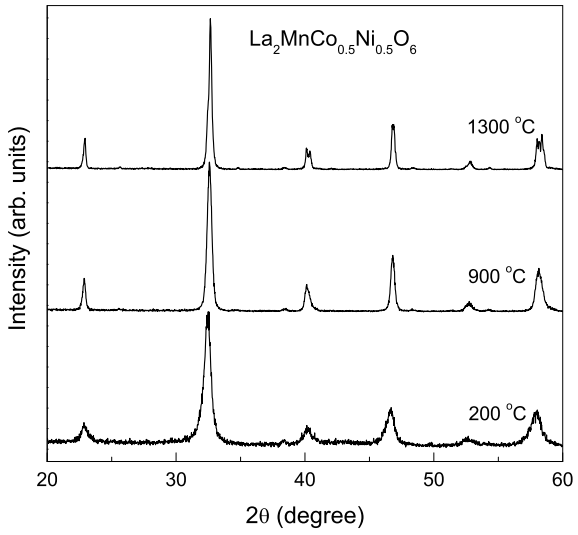

Figure 5.8: Powder XRD patterns of $La_2MnCo_{0.5}Ni_{0.5}O_6$, synthesized by low-temperature method and annealed at 200, 900, and 1300 °C.

5.1.4 Powder XRD studies

All the compositions in the $La_2MnCo_{1-x}Ni_xO_6$ series annealed at 200 °C were found to form perovskite phases. The powder XRD patterns of the $x = 0.5$ composition, $La_2MnCo_{0.5}Ni_{0.5}O_6$, annealed at 200, 900 and 1300 °C are compared in Figure 5.8. A single phase perovskite phase is formed in the 200 °C annealed sample and the broad reflections are indicative of fine particle nature of the compound formed. Except for the decreasing broadness of the reflections and splitting of the weak reflections due to this effect, no other noticeable features are observed when samples are annealed in the 200–1300 °C temperature range, though magnetic measurements on these samples showed different T_cs. Similar behaviour was observed for other compositions also in the series. It was found from magnetic measurements that the temperature of formation of the phase with the highest Curie temperatures – counterparts of the high-T_c phase of La_2MnCoO_6 – in the pure form, increases with the increase in the

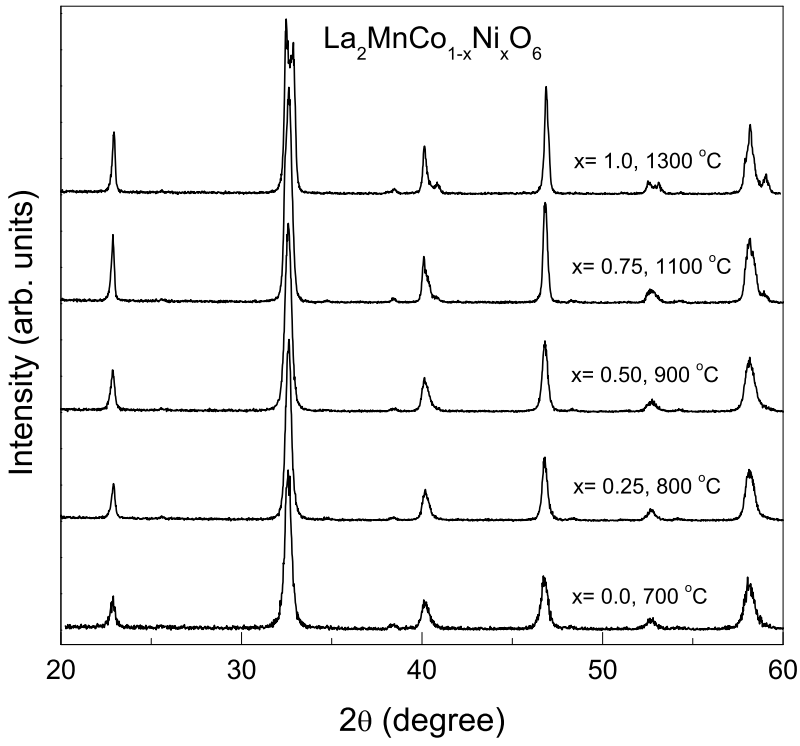

Figure 5.9: Powder XRD patterns of $La_2MnCo_{1-x}Ni_xO_6$,synthesized by low-temperature method and annealed at intermediate temperatures.

Ni content, from 700 °C for the Co end-member to 1300 °C for Ni end-member. The XRD patterns of these high-T_c phases, obtained after annealing in the temperature range 700-1300 °C for different compositions are compared in Figure 5.9. Compared to the structures of the end-members, the two most probable structures for this series are orthorhombic (for Co-rich compositions) and rhombohedral (for Ni-rich compositions). Refinement of the XRD patterns of the samples annealed below 1100 °C, with monoclinic $P2_1/n$ (subgroup of orthorhombic for ionic ordering) and rhombohedral $R\overline{3}$ space groups did not give a noticeable difference in the goodness of the fit. One of the reasons for this is the broad reflections due to smaller particles of the samples

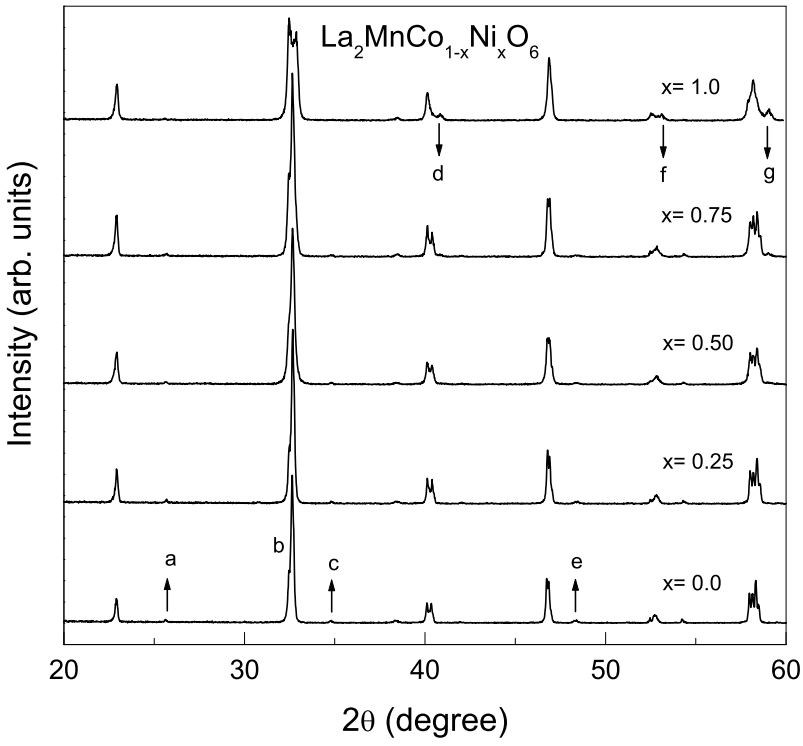

Figure 5.10: Powder XRD patterns of $La_2MnCo_{1-x}Ni_xO_6$, synthesized by low-temperature method and annealed at 1300-1350 °C.

annealed at lower temperatures. Nevertheless, all the compositions are obtained in the single phase forms without any impurity phases. For those samples annealed above 1100 °C, a better agreement is obtained with the rhombohedral structure.

The powder XRD patterns of the different compositions in $La_2MnCo_{1-x}Ni_xO_6$, formed after annealing in the temperature range 1300-1350 °C are shown in Figure 5.10. All the compositions are perovskite phases and they exhibit a systematic evolution of the rhombohedral structure of La_2MnNiO_6 from the orthorhombic structure of La_2MnCoO_6. The peaks in the XRD pattern, which undergo noticeable changes with the change in the concentration of Ni, are indicated with letters in

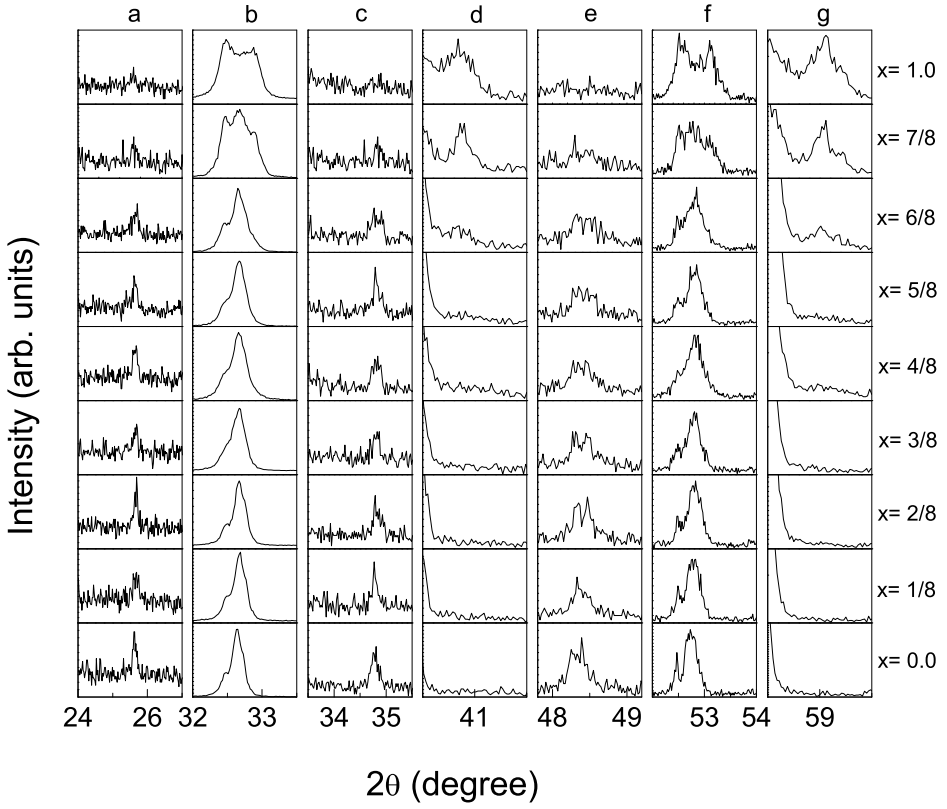

Figure 5.11: Parts of the powder XRD patterns indicative of structural phase transition with increasing x in $La_2MnCo_{1-x}Ni_xO_6$, for samples annealed at 1300-1350 °C. a–e are the regions identified in the previous figure.

Figure 5.10. The structural phase transition is continuous with respect to the concentration of Ni, a demarcation into orthorhombic (monoclinic) and rhombohedral compositional regions is difficult. Therefore the different XRD patterns are refined using both the monoclinic $P2_1/n$ and rhombohedral $R\bar{3}$ space groups. In the middle compositional region, both these space groups give almost similar goodness of the fit in refinement, whereas, the Co-rich region and the Ni-rich region showed better refinement with monoclinic and rhombohedral structures, respectively. This is in agreement with the structures of the end-members.

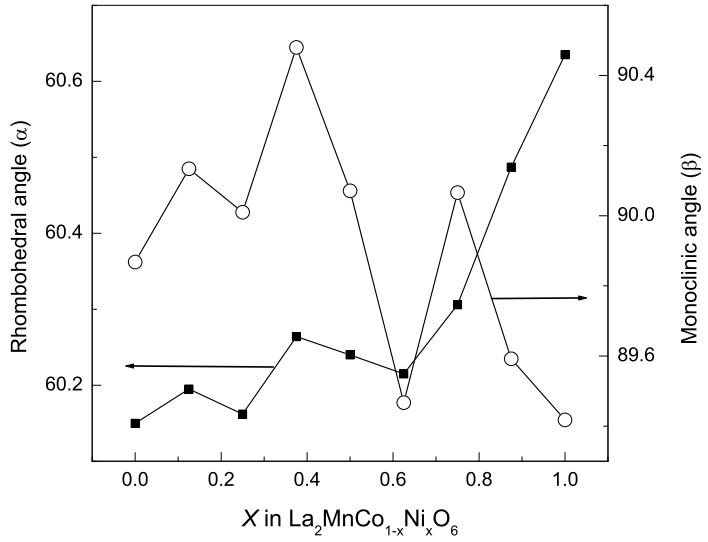

Figure 5.12: Variation of lattice parameters with Ni concentration in low-T_c phases.

The waxing of the new peaks corresponding to the rhombohedral structure and waning of the peaks corresponding to the monoclinic structure, with the increase in Ni concentration, is illustrated in the Figure 5.11 (the reflections marked by letters in Figure 5.10). The peaks at $2\theta = 25.6$, 32.6, 34.8, and 48.3, disappear and new peaks at 32.4, 32.9, 40.9, 53.1, and 59.0 appear eventually. Variations of the rhombohedral angle, α, and the monoclinic angle, β, with the concentration of Ni in $La_2MnCo_{1-x}Ni_xO_6$ are shown in Figure 5.12.Since there is a structural transition, application of Végard's law to the variation of lattice parameters is not much sensible. However, since the end-members are ion ordered, it is expected that in $La_2MnCo_{1-x}Ni_xO_6$ also Ni goes into the Co-site selectively, instead of a random distribution.

5.1.5 Origin of ferromagnetism in $La_2MnCo_{1-x}Ni_xO_6$

When Ni is substituted by Co in La_2MnNiO_6 (end-member of $La_2MnCo_{1-x}Ni_xO_6$, $x = 1$), the "magnetic status quo" is changed and the compounds start behaving

like La_2MnCoO_6 ($x = 0$). That is, when annealed between 700 and 1200 °C, the Co-containing compositions show the formation of a phase with a higher Curie temperature and further annealing at ≥1300 °C give a phase with a lower T_c. The only difference is that the phase with the higher T_c, showing a sharp magnetic transition, is obtained at higher temperatures for higher concentrations of Ni. For example, high-T_c phase of $x = 0.75$ is formed only after annealing at 1100 °C; whereas for $x = 0.25$, this phase is obtained at a lower annealing temperature of 800 °C. Hence, it may be assumed that the compounds behave similar to the end members, depending on the Co and Ni concentrations. That is, a double charge disproportionation $Mn^{+4} + Co^{+2} \rightarrow Mn^{+3} + Co^{+3} \rightarrow Mn^{+4} + Co^{+2}$ involving Mn and Co takes place corresponding to the concentration of Co and a single charge disproportionation $Mn^{+4} + Ni^{+2} \rightarrow Mn^{+3} + Ni^{+3}$ taking place corresponding to the concentration of Ni, when these compositions are annealed in the temperature range 200-1350 °C, in air.

Based on the above arguments, for $x = 0.25$, that is, for $La_2MnCo_{0.75}Ni_{0.25}O_6$, the phase showing a higher T_c (sample annealed at 800 °C) would contain Mn as Mn^{+3}, 0.75 Co as Co^{+3} and 0.25 Ni as Ni^{+3}. When this phase is further annealed at 1350 °C, 0.25 Mn and 0.25 Ni remain as Mn^{+3} and Ni^{+3} (as in La_2MnNiO_6), respectively, whereas, 0.75 Mn is converted to Mn^{+4} and 0.75 Co is converted to Co^{+2} (as in La_2MnCoO_6). Now, for La_2MnCoO_6 and La_2MnNiO_6, when the T_c = 145 K, the strength of the ferromagnetic interactions, Mn^{+4}-O-Co^{+2} and Mn^{+4}-O-Ni^{+2}, can be taken as 145 K. Similarly, for the high-T_c phase of La_2MnCoO_6 with T_c = 225 K, containing Mn^{+3} and low-spin Co^{+3} ($t_{2g}^6 e_g^0$) ions, the strength of the Mn^{+3}-O-Mn^{+3} ferromagnetic interactions can be taken as 225 K. For La_2MnNiO_6, the T_c of the high-T_c phase is 273 K. The difference between the T_cs of the high-T_c phases of La_2MnCoO_6 and La_2MnNiO_6, 273 - 225 K = 48 K, can be considered as the additional strength of Mn^{+3}-O-Ni^{+3} interactions in La_2MnNiO_6. Based on these arguments, the T_c of the high-T_c phase of $La_2MnCo_{0.75}Ni_{0.25}O_6$ can be calculated as

T_{c1} = 0.75 × 225 + 0.25 × 225 + 0.25 × 48 = 237 K. Similarly, for the sample annealed at 1350 °C, the T_c can be calculated as T_{c2} = 0.75 × 145 + 0. 25 × 225 + 0.25 × 48 = 177 K. The experimental T_cs obtained for these phases are 237 and 176 K, respectively. The experimental and calculated values are identical, indicating that the above assumptions are correct. Hence, the T_cs of the two phases, for different values of x in $La_2MnCo_{1-x}Ni_xO_6$, obtained after annealing in the temperature range 700–1350 °C, can be calculated as

$$T_{c1}(x) = (1-x)Q + xQ + xR \tag{5.1}$$

$$T_{c2}(x) = (1-x)P + xQ + xR \tag{5.2}$$

where P, Q, and R are the strengths of the ferromagnetic exchange interactions, Mn^{+4}-O-Co^{+2}/Ni^{+2} (145 K), Mn^{+3}-O-Mn^{+3} (225 K), and Mn^{+3}-O-Ni^{+3} (48 K), respectively.

The calculated T_c values of all compositions are shown in Figure 5.7. The experimental and calculated values are almost comparable for all compositions, except for the phase of x = 0.5 obtained after annealing at 1300 °C. According to the Equation 5.2, T_c is calculated as (225+48)/2 + 145/2 = 209 K, which is less by 17 K from the experimental value. There is another possibility that Ni and equivalent amount of Mn are present as in the high-T_c phase of LMN (Mn^{+3} and Ni^{+3}) and out of total Co and the rest of Mn, half of Mn and Co are present in an environment as in the high-T_c phase of LMC (Mn^{+3} and Co^{+3}) and the other half as in the low-T_c phase of LMC (Mn^{+4} and Co^{+2}). This is possible due to some kind of ordering of Mn, Co, and Ni ions in specific lattice sites. This will give a calculated T_c of $\frac{x}{2}P + (x + \frac{x}{2})Q + xR$ = 229 K, which is very close to the observed T_c of 226 K. The latter condition may arise when those Co ions close to Ni are remaining as Co^{+3} and the remaining Co ions are converted back to Co^{+2} ions because of a charge disproportionation involving the Mn ions. Also an ordering of Mn^{+3}, Mn^{+4}, Co^{+2} and Ni^{+3}, that are present in

equal amounts, can give rise to additional ferromagnetic exchange interactions like Mn^{+3}-O-Mn^{+4}, leading to higher T_c.

In La_2MnCoO_6, the high-T_c phase has the trivalent Mn and Co ions ordered into alternate (001) planes. On the other hand, the low-T_c phase of La_2MnCoO_6 and high-T_c phase of La_2MnNiO_6, which are obtained after annealing at 1300 °C, Mn and Co/Ni ions ordered into alternate (111) planes. In the solid-solution series, $La_2MnCo_{1-x}Ni_xO_6$, the so called high-T_c phases formed after annealing in the temperature range, 700-1200 °C, also contain all trivalent ions. The magnetization curves of the Co-rich samples annealed at 700 °C (see Figure 5.3) are sharper like that of La_2MnCoO_6 indicating the retention of the (001) ordering up to $x = 0.5$. Whereas, the Ni-rich compositions show significant broadening of the magnetic transition and a shift of the magnetic transition temperature to lower temperatures. The probable reason is that, unlike low-spin Co^{+3}, Ni^{+3} is a Jahn-Teller ion, and thus can not exert (001) ordering. This leads to a competition between (001) and (111) ionic ordering in the *B*-site for samples annealed at temperatures close to 700 °C. Naturally, in the Ni-rich region, this competition will be severe leading to broadening of the magnetic transition temperature. The formation of trivalent Ni from Ni^{+2} from the as-prepared phase requires more energy and thus these phases are formed in pure form at successively higher temperatures. At the same time Ni^{+3} enhances the ferromagnetic interaction, thereby increasing the T_c. At this point of time, it can be assumed that in the Co-rich compositions, the (001) ordering and in the Ni-rich compositions a (111) ordering of ions are present in high-T_c phases. The fact that a (111) ordering is materialized at a higher annealing temperature can be the reason for the increased temperature of formation of the high-T_c phases in the Ni-rich compositions. As the annealing temperature is increased, both the end-phases try for (111) ordering, removing the ambiguity. Therefore, the intermediate-T_c phases of $La_2MnCo_{1-x}Ni_xO_6$ having tetravalent Mn corresponding to Co^{+2}, and trivalent Mn corresponding to

Ni^{+3} are considered to be (111) ordered. The T_c decreases with increasing Co content because of the lower strength of Mn^{+4}-O-Co^{+2} interaction, compared to the Mn^{+3}-O-Mn^{+3} isotropic interaction.

5.1.6 Conclusions

All the compositions, except the end-members of the series $La_2MnCo_{1-x}Ni_xO_6$ forms three different ferromagnetic phases, when synthesized by a low-temperature method and annealed at different temperatures in the range 200–1300 °C. The difference between the magnetic behaviour of the end-members and the other compositions is that the former have only two ferromagnetic phases, whereas all the intermediate compositions have three ferromagnetic phases. The crystal structures of the compositions formed after annealing at 1300-1350 °C show a continuous transition from monoclinic (structure of La_2MnCoO_6) to rhombohedral (structure of La_2MnNiO_6). Multiple ferromagnetic phases are possible due to the different combinations of possible spin-states of Mn, Co and Ni. The ionic ordering and charge disproportionation in the Mn-site facilitates the formation of different ferromagnetic phases. The present study on $La_2MnCo_{1-x}Ni_xO_6$ shows that the ferromagnetic transition temperatures of different phases of the compositions ($0 < x < 1$), obtained by annealing the low-temperature synthesized samples at different temperatures in the range 200–1350°C, can be predicted on the basis of the T_cs of the different phases of the end members La_2MnCoO_6 ($x = 0$) and La_2MnNiO_6 ($x = 1$), assuming a combination of different spin-states of Mn, Co and Ni in these compositions. The results also further confirms the validity of the conclusion of different spin-states of these ions and the concept of charge disproportionation during the formation of different ferromagnetic phases in the end members.

5.2 $La_2MnCo_{1-x}Fe_xO_6$

5.2.1 Background

It is interesting to note that, though $LaMn_{1-x}M_xO_3$ ($x \leq 0.5$) with M = Cr, Co, and Ni are ferromagnetic, the corresponding compositions when M = Fe are not. Thus, it appears that M plays a crucial role in determining the ferromagnetic exchange interactions in the B-site substituted compositions. The effect of doping Fe, in the Mn-site, on the magnetic, transport and magnetoresistive properties of $R_{1-x}D_xMnO_3$ type systems have been studied by several authors [Ahn96, Gho99, Cha02]. Interestingly, all these studies gave similar results. That is, as the concentration of Fe increases, the spontaneous magnetization, the Curie temperature and the metal-insulator transition temperature decreases, the resistivity increases and magnetoresistance increases up to a doping level of 10% of Fe. In the doped compounds, Fe is found to be present in the high-spin Fe^{+3} ($t_{2g}^3e_g^2$) state [Pis97]. The consequences of substituting Fe for Mn in $R_{1-x}D_xMnO_3$ are explained on the basis of a) the break down of long range ferromagnetic order in the system, as Fe^{+3} occupy the Mn-sites randomly, b) the increased strength of Fe^{+3}-O-Fe^{+3} antiferromagnetic superexchange interactions, and c) the weakening of Mn^{+3}-O-Mn^{+4} double exchange mechanism. Hebert *et al* [Heb02b], from a recent study on the effect of doping different elements in the Mn-site of $Pr_{0.5}Ca_{0.5}MnO_3$, found spin glass like insulating properties for dopants without d orbitals or with d^0 and d^{10} configurations and Fe^{+3}, with a half-filled d^5 configuration, is also found to belong to this category in spite of the five unpaired electrons.

Though polycrystalline La_2MnFeO_6 ($LaMn_{0.5}Fe_{0.5}O_3$) was found to be not truly ferromagnetic unlike its counter parts, La_2MnCoO_6 and La_2MnNiO_6, the recent study by Ueda *et al* [Ued01] found ferromagnetism in thin film samples of La_2MnFeO_6 with T_c as high as 380 K, compared to the Curie temperatures of 225 and 273 K,

respectively, observed for the polycrystalline Co and Ni compounds. The thin film samples of La_2MnFeO_6 were prepared as an ordered array (artificial superlattice) of Mn and Fe ions in the <111> direction of the perovskite lattice. Similarly, ordered La_2CrFeO_6 superlattice films were also shown to be ferromagnetic when compared to the antiferromagnetic behaviour of the polycrystalline specimen [Ued98]. According to Goodenough [Goo55] and Kanamori [Kan59], Mn^{+3}-O-Fe^{+3} is one of the strongest ferromagnetic superexchange interactions, where a d^4-O-d^5 type exchange occurs. So, the contradictory effect due to Fe doping in $LaMnO_3$, found in the polycrystalline and thin film samples, can be due to the lack of sufficiently long range Mn^{+3}-O-Fe^{+3} superexchange interactions in the polycrystalline material.

To understand why ferromagnetism is not observed in polycrystalline La_2MnFeO_6, a thorough investigation on the magnetic properties of $La_2MnCo_{1-x}Fe_xO_6$ is carried out by gradually substituting increasing amounts of Co by Fe up to $x = 1$ in the high-T_c phase of La_2MnCoO_6.

5.2.2 Synthesis

Polycrystalline $La_2MnCo_{1-x}Fe_xO_6$ (LMCF) samples, where $0.0 \leq x \leq 1$, were prepared by a low-temperature method as described previously. Since it was found that the high-T_c phase of La_2MnCoO_6, in single phase form, is formed only if heated close to 700 °C, all the samples were heated in air at 700 °C for 12 hours each and then furnace cooled to room temperature. The samples were characterized by magnetic measurements and powder x-ray diffraction studies. Zero field cooled (ZFC) magnetization, in the temperature range 80–300 K and using a low magnetic field of 50 Oe, was measured while warming after cooling the sample from 300 K to 80 K in zero applied field. Field cooled (FC) magnetization was measured at 50 Oe after cooling the sample in this field. The field dependence of magnetization was measured at 82 K with a maximum applied field of 15 kOe.

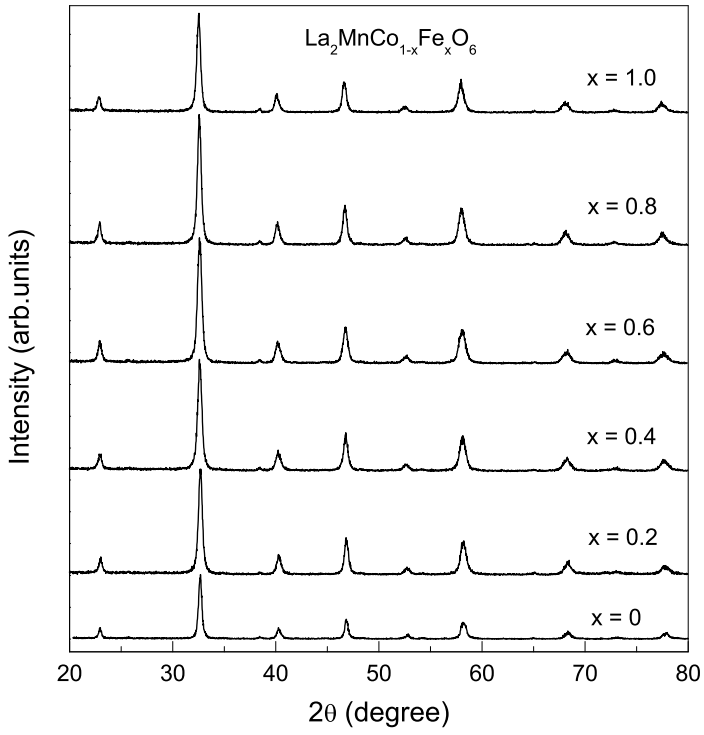

Figure 5.13: Powder x-ray diffraction patterns of different compositions in $La_2MnCo_{1-x}Fe_xO_6$.

5.2.3 Powder XRD studies

XRD patterns of the different compositions in the series $La_2MnCo_{1-x}Fe_xO_6$ ($0 \leq x \leq 1$) are shown in Figure 5.13. All the reflections in the XRD patterns correspond to a perovskite structure, indicating the formation of single phase compounds. The reflections could be indexed on a $GdFeO_3$ type orthorhombic perovskite lattice with the space group *Pbnm*. Variation of the lattice parameters, as a function of x, is shown in Figure 5.14. A linear variation of the lattice parameters, with concentration, is observed for the Fe containing compositions ($x > 0$). Formation of single phase

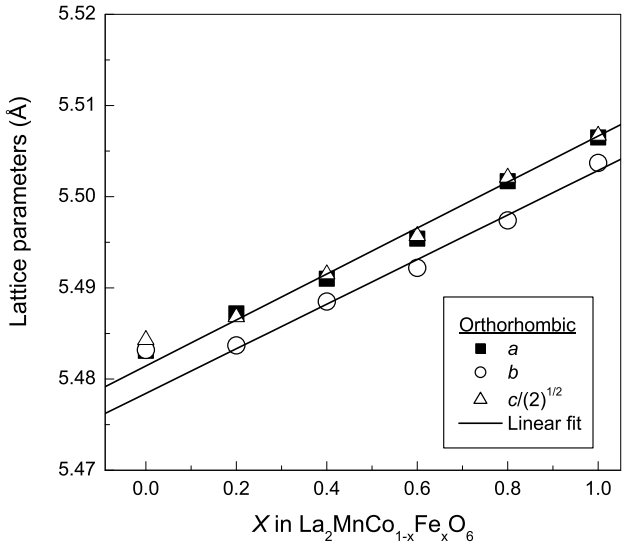

Figure 5.14: Variation of the lattice parameters as a function of x in $La_2MnCo_{1-x}Fe_xO_6$.

solid solution is further confirmed by this linear increase in the orthorhombic lattice parameters when low-spin Co^{+3}, having a lower ionic radius ($r_{Co^{+3}}$ = 0.545 Å), is replaced by Fe^{+3} having a larger ionic radius ($r_{Fe^{+3}}$ = 0.645 Å) [Sha76].

5.2.4 Magnetic measurements

Figure 5.15 shows the temperature dependence of zero field cooled magnetization (M_{ZFC}) of $La_2MnCo_{1-x}Fe_xO_6$ for different values of x. A sharp magnetic transition is observed for x = 0.0-0.3, without any change in the transition temperature. The temperature at which a peak in M_{ZFC} is observed, T_p, also remains the same up to x = 0.3 (T_p was found to be less for a composition with x = 0.35, see Figure 5.18). Only the magnitude of magnetization decreases with increasing x in this range. As the Fe content increases further, there are four parameters changing monotonously, namely, the magnitude of maximum magnetization decreases, T_p decreases, the peak

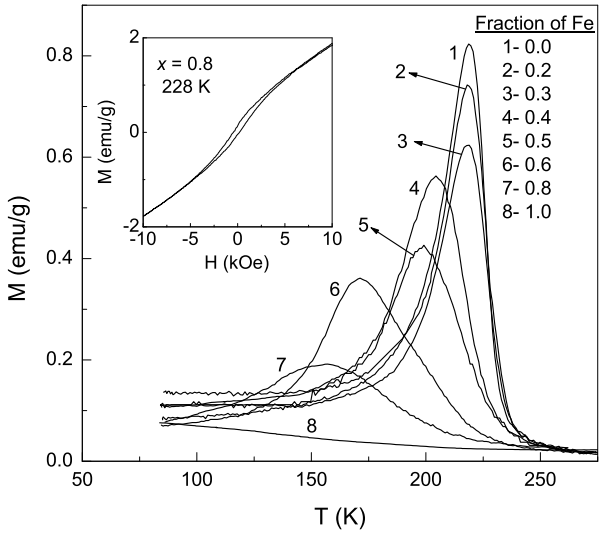

Figure 5.15: ZFC magnetization (H = 50 Oe) curves of different compositions in $La_2MnCo_{1-x}Fe_xO_6$. Inset: magnetic hysteresis of the $x = 0.8$ composition measured at 228 K.

at T_p broadens, and the magnetic transition becomes increasingly broad. Finally, no sign of a magnetic transition is observed for $x = 1$, i.e., for the composition $La_2MnCo_{1-x}Fe_xO_6$, down to 80 K.

The field cooled (FC) and zero field cooled (ZFC) magnetization (measured at H = 50 Oe) curves of the $x = 0$ and 0.6 compositions are compared in Figure 5.16. For both compositions, thermomagnetic irreversibility ($M_{FC} > M_{ZFC}$) is observed at low temperatures. The FC and ZFC curves meet at a certain temperature between T_c and T_p and the magnetization behaviours of both samples are comparable.

The magnetic hysteresis curves, recorded at 82 K, of all compositions are shown in Figure 5.17. Though no clear magnetic transition is observed for $x = 1$, a well-defined hysteresis loop is obtained for this composition at 82 K. This indicates that La_2MnFeO_6 is not truly paramagnetic at low temperatures.

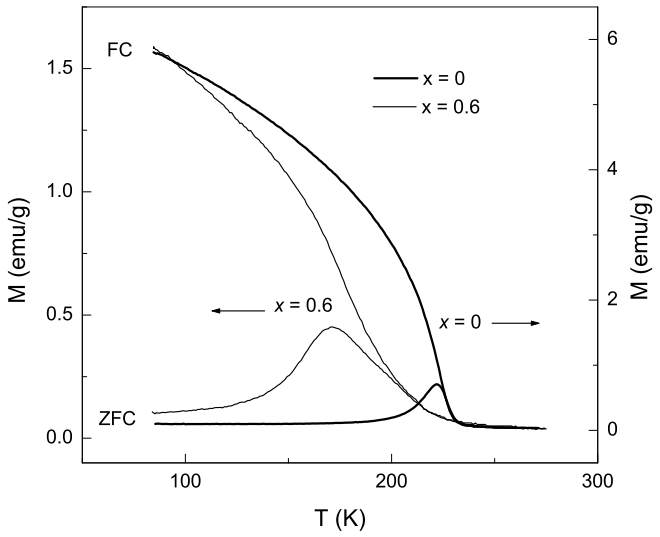

Figure 5.16: Field cooled (FC) and zero field cooled (ZFC) magnetization for $x = 0$ and 0.6 in $La_2MnCo_{1-x}Fe_xO_6$.

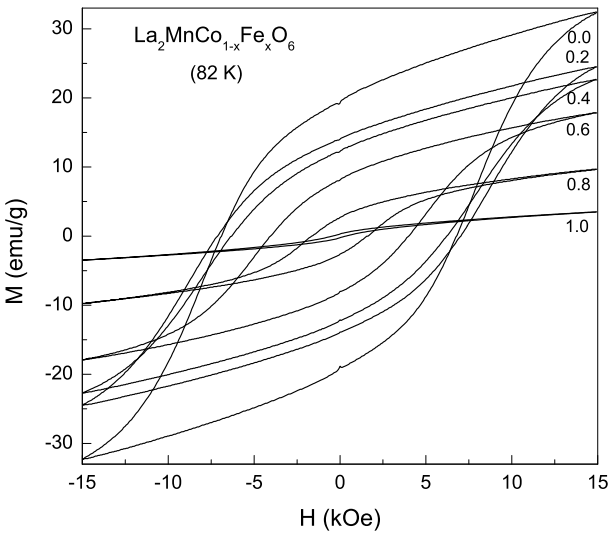

Figure 5.17: Magnetic hysteresis, recorded at 82 K, for different values of x in $La_2MnCo_{1-x}Fe_xO_6$.

The variations of T_p as well as the coercivity (H_c) and the magnetization (M) at 82 K, as a function of x, are shown in Figure 5.18. T_p remains constant up to $x = 0.3$ and then decreases suddenly for $x = 0.35$ and varies non-linearly with x. Similarly, the coercivity remains almost constant below $x = 0.4$ and then decreases sharply to a low value by one order of magnitude for $x = 1$. The magnetization (M) at 82 K, measured at a field of 15 kOe, decreases as x is increased in $La_2MnCo_{1-x}Fe_xO_6$ from $x = 0$ to 1. After an initial linear decrease of M at the rate of 10%, up to $x = 0.3$, a small slope change is observed between $x = 0.3$ and 0.4 and M then decreases again linearly by approximately at the rate of 10% up to $x = 1$.

The linear increase in the lattice parameters of $La_2MnCo_{1-x}Fe_xO_6$, when Co is replaced by Fe, is in accordance with Végard's law [Veg21]. It is known that a linear variation of the lattice parameter as a function of concentration is associated with a random distribution of the constituents in the lattice. i.e., deviations from the linear Végard's law dependence of lattice parameter versus concentration are associated with tendencies towards ordering [Ice99].

In the $A_2BB'O_6$ perovskite lattice, the ordered state is established due to a charge difference or a substantial difference in the ionic radii between the two B-site ions, and the size difference is found to be more critical [Gal62, Gal69, Che96]. For example, for the ordered double perovskite Sr_2FeMoO_6, ordering is possible because of the charge and ionic size differences between Fe^{+3} (r = 0.645 Å) and Mo^{5+} (r = 0.61 Å). When Mo^{5+} is gradually substituted by W^{5+} with comparable ionic radius (0.62 Å), a non-linear change in the lattice parameters is observed [Das01]. On the other hand, when Fe^{+3} is substituted by Cr^{+3} (r = 0.615 Å), having comparable ionic radius with that of Mo^{5+} (r = 0.61 Å), a total disorder is observed in the B-site and the lattice parameters follow a linear variation, even though the charge difference remains the same [Bla02c].

In the case of $La_2Mn MO_6$, where M = Co or Ni, ordering of Mn^{+3} and M^{+3} ions

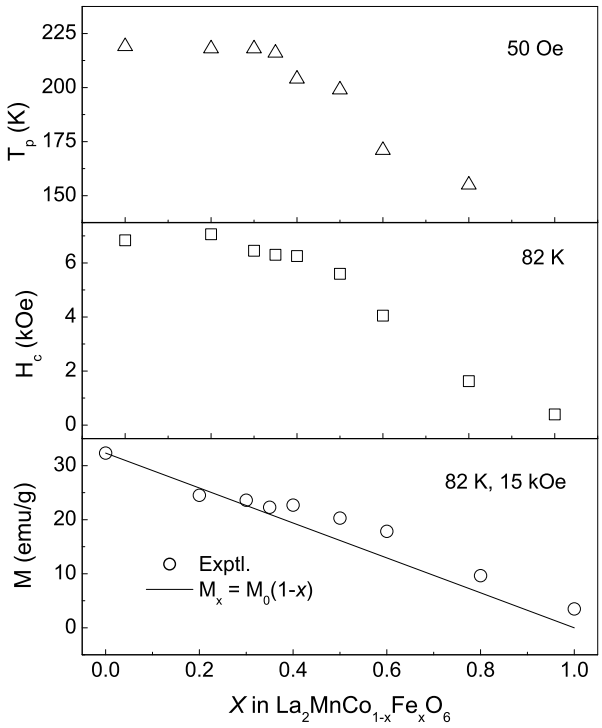

Figure 5.18: Variation of T_p (top), H_c (middle), and M (bottom) as a function of x in $La_2MnCo_{1-x}Fe_xO_6$. The solid line in the bottom panel is the estimated reduction in M from that of the $x = 0$ composition, $M_x = M_0(1 - x)$.

in the B-site is expected because of the considerable ionic size difference of Mn^{+3} (0.645 Å) from that of low-spin Co^{+3} (0.545 Å) or Ni^{+3} (0.56 Å) ions. Goodenough *et al* [Goo61] considered the case of ordering of Mn^{+3} and the non-magnetic Ga^{+3} ions in the lattice of $LaMn_{1-x}Ga_xO_3$, because of the ionic size differences between Mn^{+3} and Ga^{+3}, to explain the origin of ferromagnetism in this series. So, it may be considered that the Mn and Co ions are ordered in the alternate *ab* planes of La_2MnCoO_6 lattice, as in the case of the double perovskite Sr_2FeMoO_6 [Tom00]. It is difficult to observe superlattice reflections of ordered structure in the powder x-ray spectrum of the Co and Ni compounds, due to the similarity in the scattering factors

of the B-site ions in the perovskite structure. This ordered model can explain the charge disproportionation, $Mn^{+3} + Co^{+3} \longrightarrow Mn^{+4} + Co^{+2}$, when the high-$T_c$ phase of the compound is converted to a low-T_c phase on processing at higher temperatures. Based on these arguments, it can be expected that La_2MnFeO_6 will be a disordered system because of the identical sizes of Mn^{+3} and Fe^{+3} (0.645 Å) ions, as in the case of Sr_2CrMoO_6.

In the present case, the variation of lattice parameters as a function of x ($x > 0$) is almost linear, indicating the possibility for a random distribution of the B-site ions. Then there are two different ways for random distribution of the ions in the B-site of the $La_2MnCo_{1-x}Fe_xO_6$ perovskite lattice. Either the Co and Fe ions are randomly distributed in a plane containing the Co and Fe ions (Co sublattice of the pristine compound) since only Co is replaced by Fe in the ordered structure or all the three ions, Mn, Fe and Co, are randomly distributed throughout the B-sites. The chances for the first case are less due to the large difference in the ionic sizes of Co^{+3} and Fe^{+3}. More over, such a distribution is expected to show large anisotropy in the lattice parameters. On the other hand, because of the identical ionic sizes of Mn^{+3} and Fe^{+3} (0.645Å), a total disorder in the B-site can be expected, as found in the case of $Sr_2(FeCr)MoO_6$.

In the high-T_c ferromagnetic phase of La_2MnCoO_6, the Mn and Co ions are in their trivalent states. More over, the trivalent Co ion is present in the low-spin ($S = 0$) state with the electronic configuration $t_{2g}^6 e_g^0$. This ion is non-magnetic and therefore the contribution to ferromagnetism comes mainly from Mn^{+3} ions. Here, considering the ordering of Mn and Co ions in the alternate ab planes, it is possible that ferromagnetism arises from Mn-O-Mn superexchange interactions within the Mn planes, and three dimensional ordering is possible through Mn-O-Co-O-Mn exchange interactions along c-axis. If it is assumed that the substituted Fe ions are distributed within the Co planes only, then the effect of substitution is to weaken the latter inter-

planar magnetic interactions, even if the Fe and Co ions are randomly distributed within this plane. This will effectively alter the magnetic transition temperature on Fe substitution. However, instead of a shift in T_c, a broadening of the magnetic transition is observed on Fe substitution. On the other hand, if all the three ions; Mn, Co, and Fe, are randomly distributed as soon as a small amount of Co is replaced by Fe in La_2MnCoO_6, a different scenario is expected. If the role of Fe^{+3} is similar to that observed in $Pr_{0.5}Ca_{0.5}MnO_3$, by Hebert *et al* [Heb02b], it may be assumed that ferromagnetic clusters (containing Mn and Co ions) will be formed which are blocked from long range ordering by the Fe ions and Fe^{+3}-O-Fe^{+3} antiferromagnetic exchange interactions will be more predominant. In this case, it is expected that the magnetic transition of La_2MnCoO_6 will be broadened with Fe substitution and a cluster-glass-like or spin-glass-like behaviour will be observed depending on the Fe concentration. Kuznetsov *et al* recently reported Mössbauer spectral evidence for disorder in the *B*-site of the perovskite series $LaFe_{1-x}Cr_xO_3$ whose lattice parameters vary linearly as a function of x [Kuz01]. Similarly, Blasco *et al* [Bla02c], from neutron diffraction studies, found that the ordered structure of the double perovskite Sr_2FeMoO_6 becomes disordered on substitution of Fe by Cr, and the Mo, Fe and Cr ions are distributed randomly over the Fe and Mo sites due to the comparable sizes of Mo^{5+} and Cr^{+3}.

The magnetic hysteresis loop, shown in the inset of Figure 5.15, is recorded for the $x = 0.8$ composition, at 228 K, just below the magnetic transition temperature of the $x = 0$ composition. The well-defined hysteresis loop indicates that still spontaneous magnetization is present at this temperature for this composition and confirms that there is no shift in the Curie temperature with increasing x. The continuously increasing magnetization at higher fields, for $x = 0.8$, may be from the presence of a large paramagnetic component due to the spins which are not ordered.

Thermomagnetic irreversibility ($M_{FC} > M_{ZFC}$) and a peak in M_{ZFC} are generally considered as the peculiar characteristics of spin glass or superparamagnetic

systems. However, many long range ordered systems, including high-T_c ferrimagnetic systems, have been shown to exhibit similar behaviour due to domain wall pinning effects [Roy97, Kum99, Kum00, Joy00, Sok02]. For ferromagnetic systems, such as La_2MnCoO_6 ($x = 0$), the sharp peak in M_{ZFC} close to T_c and the thermomagnetic irreversibility below T_c originate from the magnetocrystalline anisotropy. A peak is observed at a temperature below which the anisotropy field overcomes the applied magnetic field [Joy00]. Similarly, thermomagnetic irreversibility is observed below a certain temperature if M_{FC} and M_{ZFC} are measured with magnetic fields less than the field below which irreversibility of magnetization is observed in M vs. H measurements at a certain temperature [Kum99]. The thermomagnetic irreversibility behaviour observed for the $x = 0.6$ in $La_2MnCo_{1-x}Fe_xO_6$ is much different from those of spin glass or superparamagnetic characteristics [Sen95]; the FC magnetization in the present case decreases continuously from the lowest temperature through T_p and no anomaly is observed in the M_{FC} curve at T_p.

The magnetic behaviour of $La_2MnCo_{1-x}Fe_xO_6$, i.e., increasing the broadness of the magnetic transition with increasing value of x and the observation of spontaneous magnetization up to $x = 1$, are indicative of dilution of the magnetic lattice randomly. This is in accordance with the conclusions derived from the structural studies. Therefore, it can be assumed that Mn, Fe, and Co occupy the B-site in an absolutely random manner, as it was found in similar systems [Bla02c], and hence the magnetic behaviour of Fe substituted compound may be explained in terms of random percolation [Sta85]. However, in the present case, the change in the magnetic behaviour on substitution of Co by Fe in La_2MnCoO_6 is unlike the usual case of substitution of a magnetic lattice with non-magnetic atoms, i.e., dilution of the magnetic lattice. The original compound $LaMnO_3$ is not ferromagnetic because of the antiferromagnetic ordering of the adjacent ferromagnetic planes. In La_2MnCoO_6, Co is a diamagnetic ion and the magnetic Mn and non-magnetic Co ions are ordered in differ-

ent planes (Mn and Co sublattices) so that the inter-layer antiferromagnetic ordering found in $LaMnO_3$ is destroyed. Then the role of Co ions in determining ferromagnetism of the compound is to support 3-dimensional magnetic ordering through 180° Mn-O-Co-O-Mn type superexchange interactions. When Fe, which is a magnetic ion, is substituted for Co, instead of favoring a strong Mn-O-Fe ferromagnetic exchange, the effect is the 'dilution' of the magnetic Mn sublattice by a random distribution of Mn, Co, and Fe on the *B*-site of the perovskite. Blasco *et al* have shown the evidence for such a distribution when Fe in the ordered perovskite Sr_2MoFeO_6 is substituted by Cr [Bla02c]. The results reported by these authors show that nearly 65% of the substituted Cr and 10% of the remaining Fe goes to the Mo sublattice. Therefore, in the present case, Fe^{+3} with a d^5 configuration is behaving like a non-magnetic ion, similar to that observed by Hebert *et al* [Heb02b].

$La_2MnCo_{1-x}Fe_xO_6$ (LMCF) may be considered as made of the end members La_2MnCoO_6 (LMC) and La_2MnFeO_6 (LMF). LMC is an ordered double perovskite whereas LMF is a completely disordered system. Thus, LMC can be considered as an infinite ferromagnetic lattice in the sense that ferromagnetic interactions in it is extendible to infinity. Now, consider the substitution of a fraction x of the Co ions by Fe in LMC. In effect, such a substitution removes x Co ions which are prone to order and introduces x Fe ions which are prone to disorder. That is, totally it will generate x disorder in the *B*-site ions of LMCF. In other words, it will destroy 10% of the ferromagnetic Mn-O-Mn interactions in the LMC lattice when substituted by 10% Fe. In effect, a corresponding decrease in the magnetization is observed for this composition. Assuming a random distribution of the Fe ions in the *B*-lattice, then the magnetization of LMC should decrease by 10% for every 10% substitution. The calculated values, $M_x = M_0(1-x)$, are almost comparable to the experimental values based on this assumption, as shown in Figure 5.18.

The observations that the sharp magnetic transition at the T_c of the infinite

ferromagnetic lattice of La_2MnCoO_6 remains unaffected, T_p and H_c are independent of x, and M decreases initially as expected, up to a doping level of $x = 0.3$, in $La_2MnCo_{1-x}Fe_xO_6$, suggest the presence of infinite ferromagnetic clusters comprising of Mn-O-Mn and Mn-O-Co-O-Mn exchange interactions below this value of x. In the perovskite structure, the B-site ions form a simple cubic lattice. For a simple cubic ferromagnetic lattice, the percolation threshold, $x_c = 0.31$ [Sta85]. That is, a material will not show spontaneous magnetization if the fraction of nonmagnetic atoms is greater than 1-$x_c = 0.69$. In the case of La_2MnCoO_6, this may not be directly applicable because already 50% of the lattice is occupied by nonmagnetic trivalent low-spin Co ions and these ions ordered in alternate layers are responsible for ferromagnetism when compared to the antiferromagnetic behaviour of $LaMnO_3$. However, in the present case, a fraction of Mn^{+3} ions from the ferromagnetic layers is removed and distributed in the nonmagnetic Co layers and their position is occupied by Fe and Co which are randomly distributed in the Mn layer, when Fe is substituted for Co. So, effectively, the concentration of the 'magnetic ions' in the ferromagnetic layer is decreased.

In LMC, Co is acting as a catalyst which help Mn ions to order in such a way that the Mn-O-Mn ferromagnetic exchange is possible to a maximum extent in a plane. As Co in LMC is substituted by Fe, a random distribution of Fe in the Mn and Co planes weaken the Mn-O-Mn interactions within a plane as well as the Mn-O-Co-O-Mn inter-planar ferromagnetic interactions. That is, the Mn-O-Mn interactions are broken randomly, producing broadening and weakening of the ferromagnetic transition. Data shown in Figure 5.17 indicate that even for the fully substituted compound, La_2MnFeO_6, magnetic hysteresis is observed at low temperatures. This implies the spontaneous magnetization present in the sample, as observed in the case of Sr_2CrMoO_6 [Bla02c]. Therefore, it may be concluded that, on substitution of Fe for Co in La_2MnCoO_6, the Mn and Co sites are randomly occupied by Fe. The ob-

served magnetic behaviour of $La_2MnCo_{1-x}Fe_xO_6$ is, therefore, a case of random site percolation.

5.2.5 Conclusions

La_2MnCoO_6 is a ferromagnetic compound whereas the related compound La_2MnFeO_6 is not. We have studied the magnetic properties of $La_2MnCo_{1-x}Fe_xO_6$, by gradually substituting increasing amounts of Co by Fe up to $x = 1$, to understand the role of Fe in determining the magnetic properties of La_2MnFeO_6. It was found that the magnetic transition remains sharp, the temperature at which a peak in the ZFC magnetization curve is obtained and the coercivity at low temperatures are found to be independent of x, up to a value of $x = 0.3$ in $La_2MnCo_{1-x}Fe_xO_6$. A broadening of the magnetic transition is observed for x above 0.3. A 10% decrease in the magnetization is observed for every 0.1 increment in x, in the entire range of substitution. This decrease in magnetization is in accordance with $M_x = M_0(1 - x)$, based on the assumption that the Mn, Co and Fe ions are randomly distributed in the B-site of the perovskite lattice. The observed magnetic properties of $La_2MnCo_{1-x}Fe_xO_6$ can be explained in terms of random site percolation behaviour.

5.3 $La_2MnCo_{1-x}Al_xO_6$

5.3.1 Background

It is interesting to note that, though non-magnetic ions, Ga^{+3} substituted compositions, $LaMn_{1-x}Ga_xO_3$, are ferromagnetic [Ver02] whereas Al^{+3} substituted compositions, $LaMn_{1-x}Al_xO_3$, are not [Jon56]. Hebert *et al*, from the studies on the substitution of Mn in $Pr_{0.5}Ca_{0.5}MnO_3$ with 5% of different elements showed that the dopants without d orbitals such as Al^{+3} or with d^{10} configuration such as Ga^{+3}, induce orbital disordering, partially destroying the orbital ordering of Mn^{+3} [Heb02b]. From

neutron diffraction studies, Cussen *et al* found that the Ga^{+3} ions are distributed randomly in the Mn lattice of La_2MnGaO_6 and ferromagnetism in the compound is due to the ferromagnetic coupling of the ferromagnetic Mn^{+3} layers as in the parent compound $LaMnO_3$ [Cus01].

If Co ions in La_2MnCoO_6 is present as low-spin Co^{+3}, which is a diamagnetic ion ($t_{2g}^6 e_g^0$, S = 0), along with Mn^{+3}, in the high-T_c phase, it is not known what is the role of the Co ions in determining the ferromagnetic properties of the compound. To understand this, the Co^{+3} ion in La_2MnCoO_6 is partially replaced by Al^{+3} which is a non-magnetic ion having no *d* orbitals. More over, the sizes of these two ions are comparable (0.545 and 0.535 Å, respectively [Sha76], for low-spin Co^{+3} and Al^{+3} ions, in six-fold coordination) and therefore not much structural distortions are expected on substitution of Co by Al.

5.3.2 Synthesis

Different compositions in $La_2MnCo_{1-x}Al_xO_6$ ($0 \leq x \leq 1$) were synthesized by a low-temperature combustion method, as described previously, from stoichiometric mixture of the water solutions of the nitrates of La, Mn, Co and Al and two moles of glycine for one mole of metal ion. Powder formed, from the combustion reaction, were further annealed in air at 700 °C for 12 hours each, as it was found earlier that the high-T_c phase of the parent compound, in single phase form, is obtained after annealing at this temperature. The powder samples were characterized using powder x-ray diffraction and magnetic measurements.

5.3.3 Powder XRD studies

Figure 5.19 shows the powder x-ray diffraction patterns of different compositions in $La_2MnCo_{1-x}Al_xO_6$. All the reflections are some what broad, and this is due to the

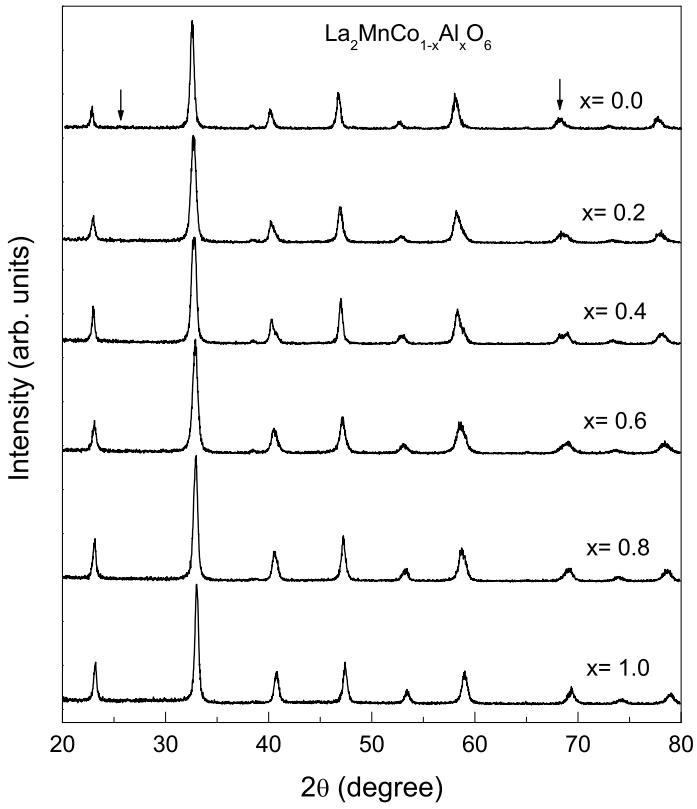

Figure 5.19: Powder XRD patterns for different compositions in $La_2MnCo_{1-x}Al_xO_6$.

smaller particle sizes of the powder samples, as the different compositions synthesized by the low-temperature method are annealed at 700 °C only. The particle sizes, calculated using the Scherrer formula, were found to be ∼40 nm for all samples. All the diffraction patterns are almost identical, showing not much variation in the positions or intensities of the corresponding reflections. The XRD patterns are almost similar to that reported by Dass and Goodenough for a low-temperature synthesized sample annealed at 600 °C [Das03], except for the absence of few weak reflections.

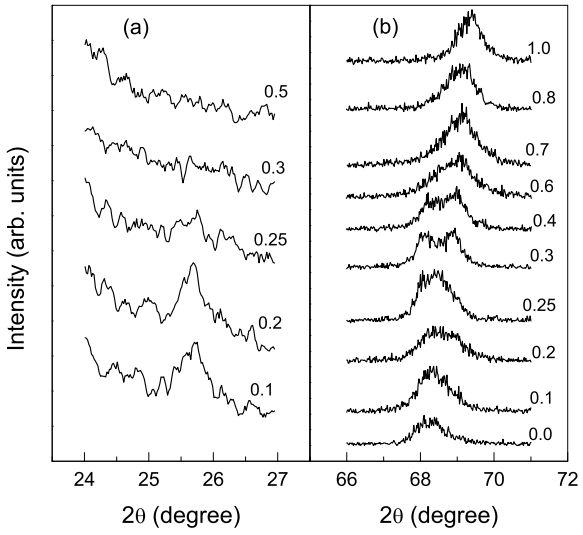

Figure 5.20: Evolution of peaks in two different 2θ regions (indicated by arrows in the previous figure) in the powder XRD patterns of $La_2MnCo_{1-x}Al_xO_6$, with x.

A close examination of the XRD patterns in Figure 5.19 reveals splitting of the reflections at higher diffraction angles, especially for $x = 0.4$. Such splitting is expected for a rhombohedral perovskite structure. Hence, the XRD patterns of all compositions in $La_2MnCo_{1-x}Al_xO_6$ were closely examined to look for any noticeable differences in the patterns, with respect to the monoclinic and rhombohedral structures reported for La_2MnCoO_6 by Bull *et al* [Bul03]. Figure 5.20 shows the powder XRD patterns, recorded at a very slow scan rate, in the two-theta region where the (111) reflection from the monoclinic perovskite lattice of La_2MnCoO_6 is expected and also the expanded pattern in the two-theta region where a clear splitting of the peak is expected for the rhombohedral lattice (as indicated by arrows in Figure 5.19). It may be seen that the (111) reflection from the monoclinic structure is observed for $x \leq 0.25$. This reflection is observed with almost equal intensity for $x \leq 0.2$, is absent for $x \geq 0.3$ and partially present for $x = 0.25$. This implies that compositions with $x > 0.25$ are

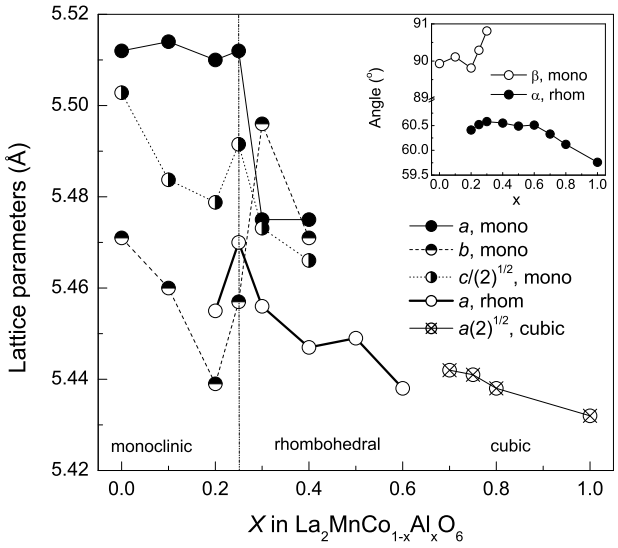

Figure 5.21: Variation of the lattice parameters, as a function of x in $La_2MnCo_{1-x}Al_xO_6$. inset: variation of monoclinic and rhombohedral angles, as a function of x.

having rhombohedral structure, compositions with $x < 0.25$ are monoclinic and for $x = 0.25$, there is a possibility of formation of mixed phases with the two structures. Similarly, at higher diffraction angles, a single peak initially observed for $x < 0.25$ splits in to two for intermediate values of x and again converged in to a single peak for $x > 0.6$. The diffraction angle increases with increasing x, indicating a decrease in the lattice parameter and this is due to the replacement of Co^{+3} ions by the slightly smaller Al^{+3} ions.

A change over of the structure from monoclinic to rhombohedral is clearly evident from Figure 5.20. Based on these observations, the diffraction patterns of the low Al containing compositions are indexed to a monoclinic structure and those of the high Al containing compositions are indexed on the rhombohedral structure, initially, as reported for the ordered structure of La_2MnCoO_6, by Bull *et al.* However, for

$x \geq 0.6$, only single peaks are observed in the XRD patterns, in the high 2θ region as shown in Figure 5.20. The XRD patterns for these compositions could be fitted well to a cubic perovskite structure. Figure 5.21 shows the variation of the lattice parameters of the compositions, as a function of x, in $La_2MnCo_{1-x}Al_xO_6$. Lattice parameters were calculated based on both the monoclinic and rhombohedral structures for compositions close to $x = 0.25$. Similarly, parameters were calculated for both rhombohedral and cubic structures in the vicinity of $x = 0.6$. Large deviations in the monoclinic lattice parameters are observed for $x > 0.25$ and rhombohedral lattice parameters for $x < 0.25$. Similarly, large variation in the rhombohedral angle is observed for $x > 0.6$. The rhombohedral angle varies very little for $x = 0.25$ to 0.6 and large deviation is observed for $x > 0.6$, indicating the cubic structure at larger x values. These observations clearly show that the structure of fig5c-3cel changes from monoclinic to rhombohedral above $x = 0.25$ and from rhombohedral to cubic above $x = 0.6$. There is an over all decrease in the size of the unit cell with increasing x and this is in accordance with the smaller ionic size of Al^{+3}. The difference in the lattice parameters of the compositions with $x = 0$ and 1 are comparable to that between $LaCoO_3$ and $LaAlO_3$ [Gal69].

5.3.4 Magnetic measurements

Figure 5.22 shows the temperature variation of zero field cooled magnetization of different compositions in $La_2MnCo_{1-x}Al_xO_6$. A ferromagnetic transition below 230 K is observed for $x = 0$. The ferromagnetic transition temperature is decreased as the concentration of Al is increased. The magnetic transition remains almost sharp for lower concentrations of Al, up to $x = 0.4$. The magnetic transition becomes broader when more than 50% of Co is replaced by Al, and finally no magnetic transition is observed for $x = 1$, i.e., for the composition La_2MnAlO_6.

The magnetization behaviour of different compositions in $La_2MnCo_{1-x}Al_xO_6$, as

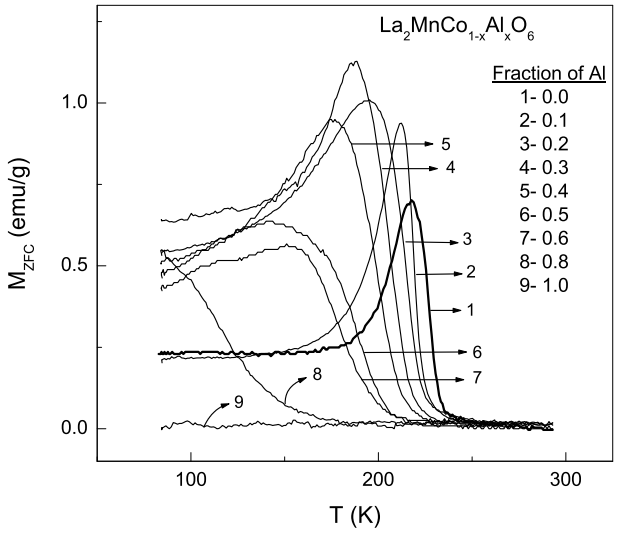

Figure 5.22: Zero field cooled magnetization curves of different compositions in the series $La_2MnCo_{1-x}Al_xO_6$, measured at 50 Oe.

a function of magnetic field, measured at 82 K, are shown in Figure 5.23. Though no magnetic saturation is obtained even at the highest measuring field of 15 kOe, there are some interesting observations. First of all, the magnetization, at 15 kOe, decreases only marginally for values of x up to 0.2. The magnetization is further increased to a larger value for $x = 0.3$ and then decreases with increasing x. True paramagnetic behaviour is observed for $x = 1$. Apart from the above observations, it is seen that the shape of the initial magnetization curves is also affected by Al substitution. The curve for $x = 0$ is more S-shaped, with no magnetic saturation at all. The degree of magnetic saturation increases and the S-shaped behaviour decreases with increasing Al concentration.

The variation of the magnetic transition temperature and the ferromagnetic moment, measured at 15 kOe and 82 K, as a function of Al content, is shown in Figure 5.24. The magnetic transition temperature decreases almost linearly with x (T_c

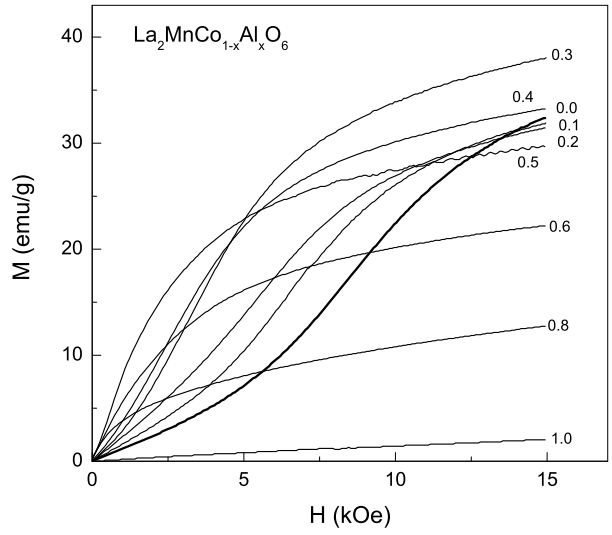

Figure 5.23: Magnetization as a function of field, measured at 82 K, for different compositions in $La_2MnCo_{1-x}Al_xO_6$.

is obtained as the temperature at which dM/dT is maximum), which is expected, because of the increasing concentration of the non-magnetic ion Al^{+3}. Though the concentration of the magnetic ions, Mn^{+3}, is not affected on the substitution of Co^{+3} by Al^{+3}, the magnetization remains almost constant up to $x = 0.2$, jumped to a higher value for $x = 0.3$ and then decreases linearly further with increasing concentration of Al. It may be seen that the magnetic moment, even after substitution of 50% of Co by Al, is comparable to that of the pristine compound La_2MnCoO_6.

The above observations can be explained if it is assumed that only Mn^{+3} ions are responsible for ferromagnetism and the three dimensional ferromagnetic exchange interaction between the ferromagnetically ordered manganese layers is facilitated through the empty e_g d-orbitals of Co^{+3} ions. This explains why ferromagnetism is not observed when Co is replaced completely by Al which contains no d orbitals. The fact that La_2MnAlO_6 is not magnetic, indicates that the presence of Co is es-

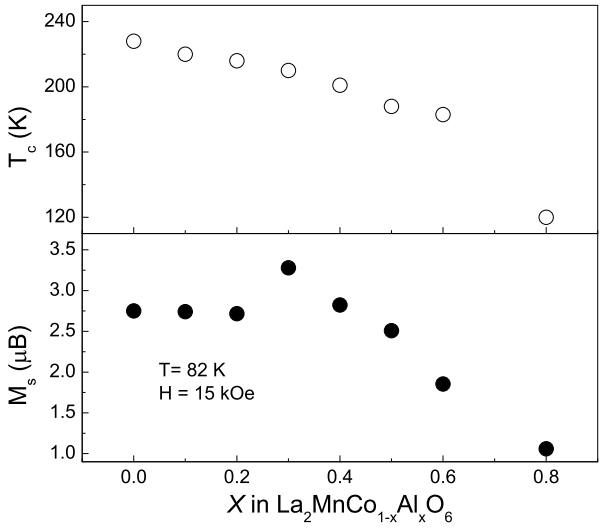

Figure 5.24: Variation of Curie temperature and saturation magnetization at 82 K and 15 kOe, as a function of x in $La_2MnCo_{1-x}Al_xO_6$.

sential in inducing ferromagnetism. Jonker earlier reported that all compositions in the $LaMn_{1-x}Al_xO_3$ system are not ferromagnetic [Jon56]. This is an indication for the fact that mere removal of part of the Jahn-Teller Mn^{+3} ions alone is not a prerequisite for inducing ferromagnetism in $LaMnO_3$. It may be recalled that, in the colossal magnetoresistive manganites, $La_{1-x}D_xMnO_3$, where D is a divalent ion, ferromagnetism arises due to the double exchange ferromagnetic interactions between Mn^{+3} and the Mn^{+4} ions and this ferromagnetism is destroyed on the substitution of Mn by Al [Bla97].

For $La_2Mn^{+3}Co^{+3}O_6$, the theoretically expected spin-only value of saturation moment is 4 μ_B (Mn^{+3}: S = 2, Co^{+3}: S = 0). For $La_2Mn^{+3}Co^{+3}O_6$, a ferromagnetic moment close to this value is obtained at 5 K under a magnetic field of 5.5 T [Ver02]. The lower experimental values for La_2MnCoO_6 may be due to large orbital moment contribution from Co. As the amount of Co is decreased initially (increasing Al

concentration) this orbital contribution is decreased, as evidenced by the decreasing S-shape of the initial magnetization curves and the saturation magnetization increases toward the theoretical value, with a maximum experimental value for $x = 0.3$. The increasing magnetic moment, for $x > 0.2$, may also be due to the structural change from monoclinic to rhombohedral above this concentration. Compared to the monoclinic structure, the rhombohedral structure is less distorted for perovskites and this causes an increase in the B-O-B angle thereby increasing the strength of the magnetic exchange interactions. Further increasing the Al concentration has a negative impact, the dilution effect overtakes the positive contribution of decreasing orbital contribution, by effectively reducing the strength of the magnetic exchange interactions.

5.3.5 Conclusions

The present study on $La_2MnCo_{1-x}Al_xO_6$ reveals the large orbital contribution to the magnetic moment, making the system very difficult to saturate. A structural change from monoclinic to rhombohedral is observed for $x > 0.2$. Higher saturation magnetic moments are obtained above this composition, when Co^{+3} is partially replaced by the non-magnetic Al^{+3} ions and this may be due to the decreasing orbital contribution from Co or due to the transition to a less distorted structure (or a combination of both). At higher concentrations of Al, the dilution effect is the dominant factor and therefore saturation magnetization decreases.

Chapter 6

Studies on $RE_2\mathrm{Mn}M\mathrm{O}_6$

Though the rare-earth perovskites, $REMO_3$ (RE=rare-earth ion, M=transition metal ion), are known since 1950 [Gal69, Goo70], the double perovskite compositions of the rare-earth ions $RE_2\mathrm{Mn}M\mathrm{O}_6$ (M=transition metal ions) are rarely studied. Because of the decreasing ionic radius of the trivalent rare-earth ions across the lanthanide series, it is expected that such a change in the size of A-site ion in the double perovskites will be sensitive to the crystal structures as well as to the magnetic properties. In the case of extremely smaller ionic sizes, the perovskite structure as such will collapse and hexagonal structures will be formed. The validity of such arguments can be checked by the studies on $RE_2\mathrm{Mn}M\mathrm{O}_6$.

6.1 Background

As described in the previous chapters, for $\mathrm{La_2MnNiO_6}$ with M = Co or Ni, two ferromagnetic phases are possible with different spin-states of Mn and M ions. These phases can be obtained in single phase forms by a low-temperature method of synthesis. For $\mathrm{La_2MnCoO_6}$, the phases with a higher Curie temperature (high-T_c phase) is stable only below 700 °C which is converted to another phase (low-T_c phase) after repeatedly heating at higher temperatures (1300 °C). In the case of $\mathrm{La_2MnNiO_6}$, the low-T_c phase is stable only up to 400 °C and a high-T_c phase is formed in the pure

form when heated above 1200 °C. In high-T_c phases of $La_2Mn$$MO_6$, Mn ion is present in the high-spin trivalent state and Co or Ni ion is present in the low-spin trivalent state. Though the ionic sizes of low-spin Co and Ni ions are almost comparable (0.545 and 0.56 Å, respectively [Sha76]), the T_c of Ni compound is higher than that of the corresponding Co compound due to the additional strength of Mn^{+3}-O-Ni^{+3} ferromagnetic exchange interactions in La_2MnNiO_6. This difference stems from the fact that low-spin Co^{+3} is a diamagnetic ion ($t_{2g}^6 e_g^0$, S = 0) whereas low-spin Ni^{+3} contains one unpaired electron in the e_g orbital ($t_{2g}^6 e_g^1$, S = 1/2) which can take part in the superexchange process.

It is reported that the magnetic ordering in some of the rare-earth containing compositions (RE = Pr, Nd, etc. in RE_2MnCoO_6), synthesized by the ceramic method, occurs in a wide temperature interval [Tro97]. This is comparable to the case of insufficiently heat treated La_2MnCoO_6, where the partial formation of the phases broadens the magnetic transition temperature. Therefore, to investigate whether more than one ferromagnetic phase is possible in other rare-earth containing compositions also, $RE_2Mn$$MO_6$ (M = Co, Ni) is synthesized by the low-temperature method, which facilitate the formation of any metastable phases if exists.

It is reported that in the double perovskites containing Mn^{+3} and other nonmagnetic ions Ti, Nb, or Ta, ferromagnetism originates from Mn^{+3}-O-Mn^{+3} superexchange interactions when the Mn-O-Mn angle is greater than 150 degrees [Hav66], and the same interaction become antiferromagnetic for lower angles. In other words, this angle decides the strength and nature (sign) of the superexchange interactions. This is because the extent of overlap between O2p and M3d orbitals depends up on the M-O-M angle which in turn determines the strength of the corresponding superexchange interactions. Naturally, the more this bond angle nearer to 180°, the overlapping is more and results in stronger ferromagnetism [Ega01]. In perovskites, the ideal value of 180° (corresponds to a cubic crystal structure) for ferromagnetic

Mn^{+3}-O-Mn^{+3} exchange , is rarely encountered . In manganates, the Mn-O-Mn (or generally M-O-M) bond angle is less than 180°, due to the tilting of the $Mn^{+3}O_6$ octahedra, caused by the ionic-size mismatch (see Section 1.2.1) and also slightly due to the distortion of the $Mn^{+3}O_6$ octahedra from Jahn-Teller effect (as described in Section 1.2.2). The above two effects lead to the puckering of the M-O-M angle and thereby lessening the overlap between O2p and $M3d$ orbitals which in turn weakens the ferromagnetic exchange interaction and supposedly reduce the ferromagnetic ordering temperature.

In the perovskite oxides, ABO_3, the tolerance factor, t, calculated using Equation 1.1, gives an account of the degree of distortion of the unit cell structure from cubic symmetry of $t = 1$. So, a decrease in the ferromagnetic transition temperature is expected, as the tolerance factor is decreased. The tolerance factor can be decreased by decreasing the ionic radius of A for a given B ion. This is happening when La, in $LaMnO_3$ (La^{+3} is the largest trivalent rare-earth ion), is replaced by rare earth ions. The ionic size decreases continuously from the left to the right in the lanthanide series, and therefore, the strain associated with the reduction of ionic-size of RE^{+3} increases, consequently increasing the octahedral tilting [Alo00]. Therefore, the T_c of a ferromagnetic perovskite manganate is expected to decrease with decreasing $< r_A >$, which is the average ionic radius of the A-site cation(s), or with decreasing tolerance factor. This behaviour has already been observed for the A-site substituted manganates and the importance of the role of crystal chemistry on the properties of the A-site substituted manganates has been studied in great detail [Rav98].

The effect of the size of rare-earth ion (RE = Pr, Nd, Sm, Eu, Gd, Tb, Dy, Er and Yb) on the ferromagnetic exchange interactions, and therefore, the T_cs of the double perovskite composition RE_2MnMO_6 is investigated. Based on the results on La_2MnCoO_6 and La_2MnNiO_6 (on the different ferromagnetic phases obtained, after annealing the low-temperature synthesized samples at different temperatures) the RE

compositions were also studied under similar conditions to look for new metastable phases. Such a study is expected to enhance the understanding of the structural-magnetic property correlation of double-perovskites.

6.2 Synthesis

The few reports in the literature on rare-earth containing double perovskite manganese compounds are based on the samples synthesized by the conventional solid-state reaction method. As observed in the case of La_2MnMO_6, when synthesized by the low-temperature method, there is a possibility of formation of metastable phases, which can not be stabilized by the ceramic route. In addition, the pure ferromagnetic phases are not formed with the solid-state method of synthesis due to the extra stability of the metastable phases. Therefore, the RE_2MnMO_6 (M = Co, Ni) compositions were synthesized by the low-temperature method, as followed in the case of the La compounds. The extremely fine powder samples obtained after the combustion process were heated in air at different temperatures. All Co containing samples are annealed between 700 °C and 1350 °C, since the high-T_c and low-T_c phases of La_2MnCoO_6 are formed at these temperatures, respectively. Similarly, all the Ni containing compositions were heated at 1350 °C to trace any high-T_c phase formation. The samples are assumed to be stoichiometric in oxygen because of the lesser tendency found in the heavier rare-earth containing manganates to have excess Mn^{+4} [Gun96]. This is supported by the observation of negligibly small δ values (nearly +0.02) in the Pr, Nd and Sm containing $RE_2MnCoO_{6\pm\delta}$, after annealing at 1350 °C. Those samples annealed at 700 °C showed slightly higher δ values ($\approx +0.07$), which can be due to the error in the calculation, because of carbon contamination.

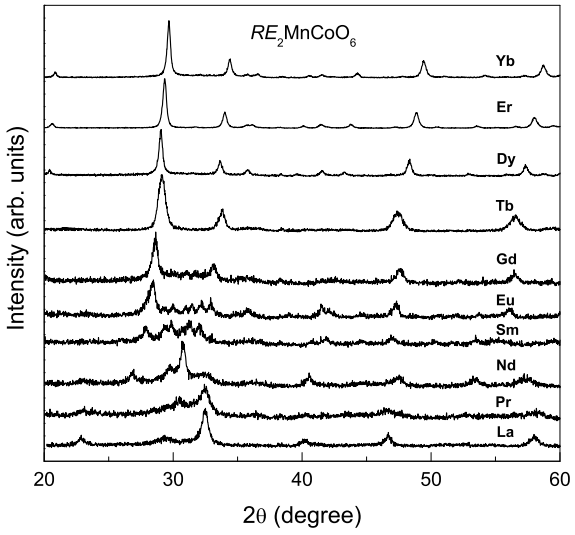

Figure 6.1: Powder XRD patterns of low-temperature synthesized RE_2MnCoO_6, including that of La_2MnCoO_6, annealed at 200 °C.

6.3 Powder XRD studies

The crystal structure of $REMnO_3$ is O′-orthorhombic ($c/a < \sqrt{2}$) [Goo70]. The O′-orthorhombic structure results from static cooperative Jahn-Teller distortion of Mn ion, superimposed on the O-orthorhombic structure. But when 50% of Mn is replaced by Co, this cooperative structural distortion vanishes. Therefore an O′-orthorhombic structure is not expected in these compounds, instead an O-orthorhombic structure is probable. Since pure ferromagnetic phases are obtained in the case of La_2MnCoO_6 after annealing at three different temperatures, viz. 200, 700 and 1300 °C, the rare-earth counter parts are also investigated by powder XRD studies, after annealing at the above three temperatures. Figure 6.1 and Figure 6.2 show the powder XRD patterns of RE_2MnCoO_6 and RE_2MnNiO_6, respectively, annealed at 200 °C. The profiles are comparatively broad due to the smaller particle sizes (∼30 nm) of the

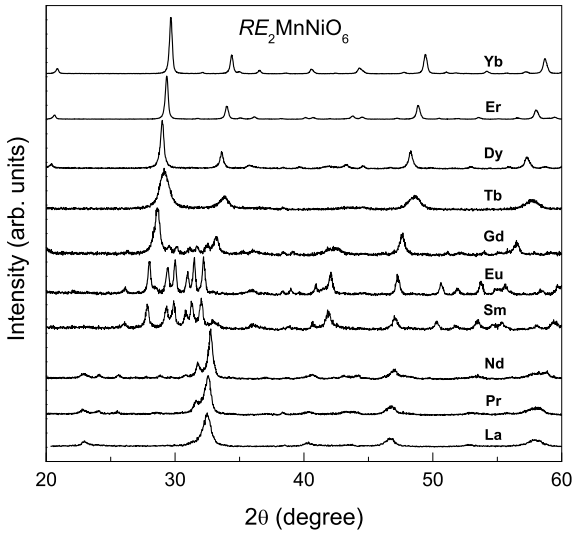

Figure 6.2: XRD patterns of low-temperature synthesized RE_2MnNiO_6,including that of La_2MnNiO_6, annealed at 200 °C.

samples, when synthesized by the low-temperature method. The interesting observation is that except for the La and Pr compounds, all the Ni and Co samples show the presence of respective rare-earth oxides, in addition to the perovskite phase. The amount of the perovskite phase decreases with the decreasing ionic-size and for the extreme members, only the corresponding rare-earth oxides are formed initially. However, after annealing at 700 °C, pure perovskite phases are formed for compounds of Pr, Nd, Sm, and Eu and the compounds of Gd and beyond were annealed up to 1000 °C to obtain single phases. Even after annealing at this temperature, the Yb compound showed the presence of minor amounts of Yb_2O_3. The XRD patterns of RE_2MnCoO_6 annealed in the temperature range 700-1000 °C are shown in Figure 6.3. Here, all the patterns indicate orthorhombic perovskite phase formation, even though the reflections are slightly broader.

Figure 6.4 and 6.5 show the XRD patterns of the Co and Ni samples annealed

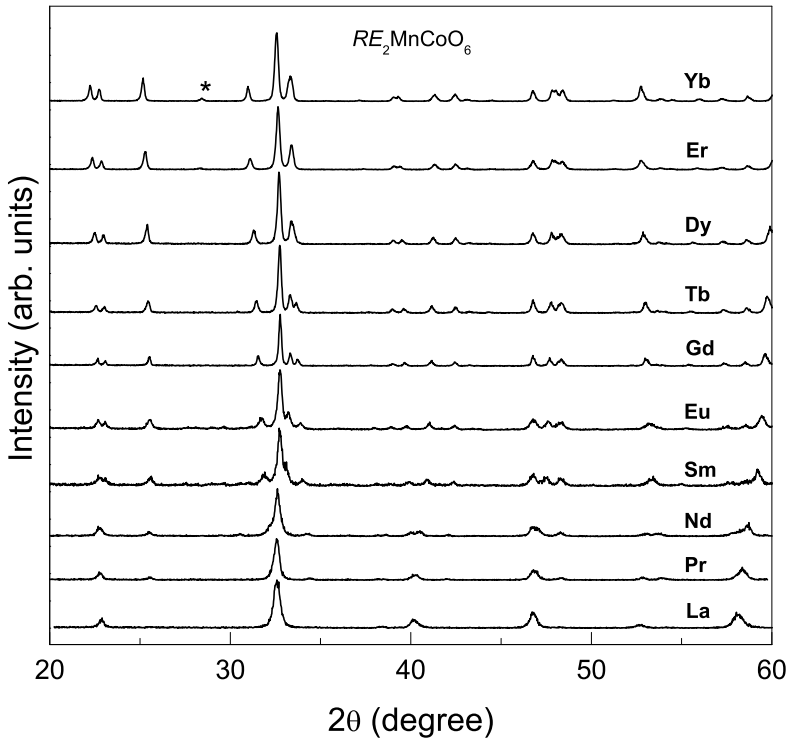

Figure 6.3: Powder XRD patterns of low-temperature synthesized RE_2MnCoO_6, including that of La_2MnNiO_6, annealed at 700–1000 °C. * - Yb_2O_3.

at 1300-1350 °C. Some additional weak reflections due to the corresponding rare-earth oxides are seen in the patterns of RE = Tb and beyond, as indicated in the figures. All the XRD patterns could be indexed into an orthorhombic *Pbnm* space group. The most intense peak around the 2θ region of 32 ° and the 'satellite' peaks on its both sides illustrate the degree of orthorhombic distortion. As the ionic-size of RE decreases, more and more 'satellite' peaks are evolved and their separation from the main peak also increases. The degree of orthorhombic distortion increases as in the case of the corresponding unsubstituted manganites [Alo00]. This can be taken as the direct evidence for the reduction in crystal symmetry, produced by the

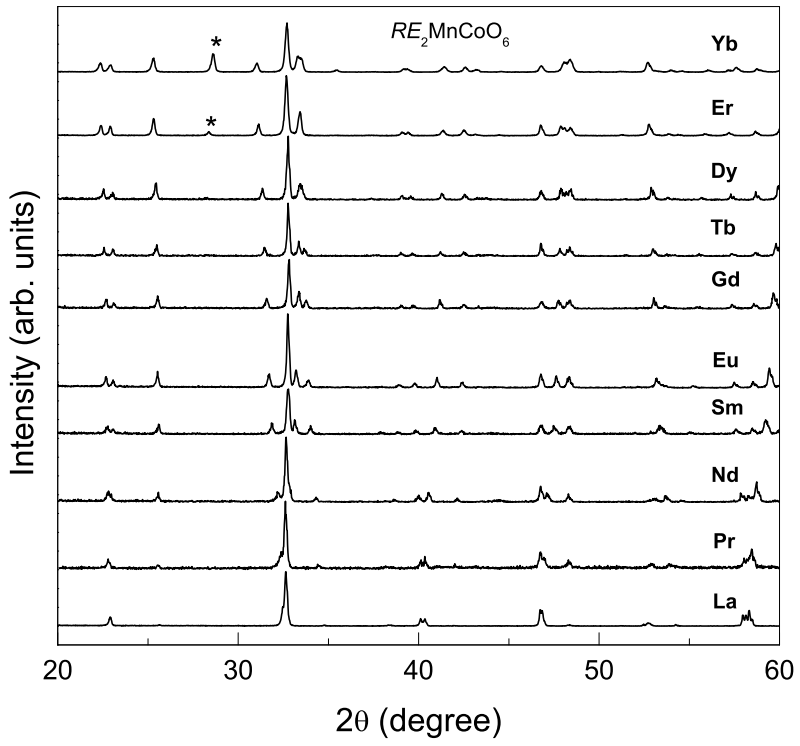

Figure 6.4: Powder XRD patterns of low-temperature synthesized RE_2MnCoO_6, including that of La_2MnCoO_6, annealed at 1300-1350 °C. * - Er_2O_3 and Yb_2O_3.

increasing distortion. For a given RE, the RE_2MnCoO_6 samples annealed at 700 and 1300 °C have almost similar XRD profiles, excluding the possibility of a structural phase transition when heated in the temperature range of 700-1300 °C. However, the heavier rare-earth compositions showed the formation of minor amounts of hexagonal perovskite phases in addition to the normal perovskite phase. Similar observation is reported in the case of $REMnO_3$ compounds [Alo00], where, due to the extreme orthorhombic distortion in the heavier members, the perovskite structure gradually collapses to form a hexagonal phase with the space group $P6_3cm$. Here, the hexagonal phases appears for RE heavier than Dy, in the Co compounds, and those heavier than

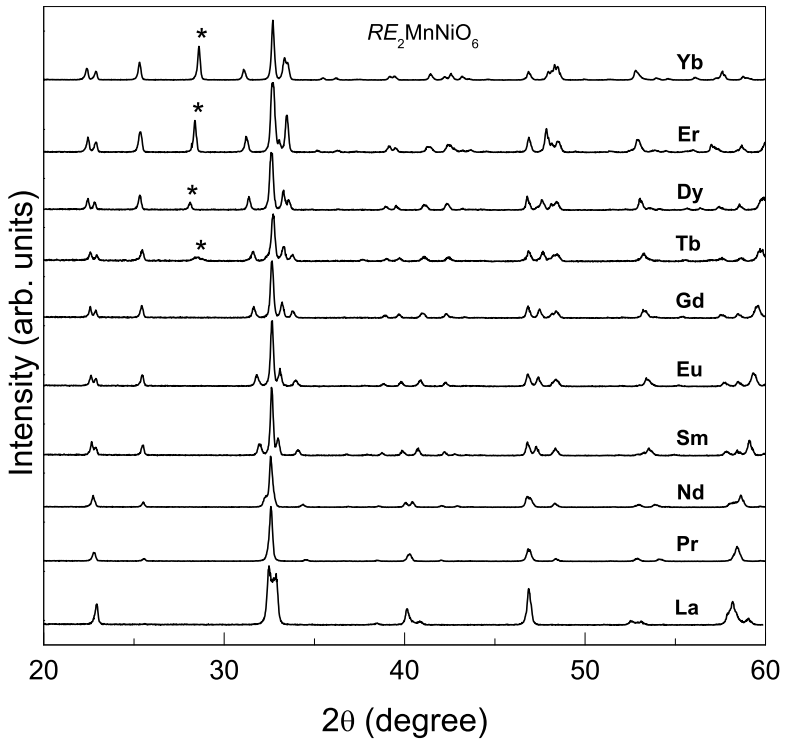

Figure 6.5: XRD patterns of low-temperature synthesized RE_2MnNiO_6, including that of La_2MnNiO_6, annealed at 1300-1350 °C. * - rare-earth oxides.

Gd, in the case of the Ni compounds. That is, for the Ni compounds, the perovskite phases are less tolerable to the structural distortion.

Figure 6.6 and Figure 6.7 show the variation of the orthorhombic ($Pbnm$) lattice parameters (for the samples annealed 1300-1350 °C) of RE_2MnCoO_6 and RE_2MnNiO_6, respectively, as a function of the ionic-size (for nine coordination) of trivalent rare-earth ion, including that of La^{+3}. Both the systems show similar changes in the cell parameters with ionic-size of RE. Here, the b value increases and the a and c values decrease as the size of the rare-earth ion decreases. This type of variation is characteristic of increasing orthorhombic distortion, with increasing ionic-size mismatch,

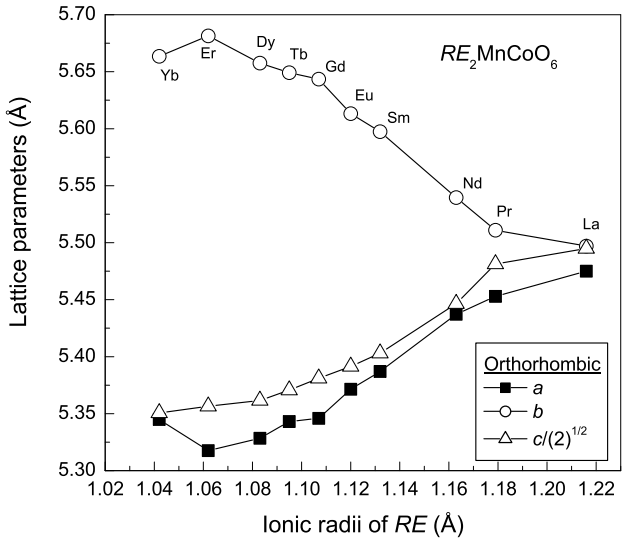

Figure 6.6: Variation of lattice parameters, as a function of the nine-coordinated ionic radii of RE in RE_2MnCoO_6, annealed at 1300-1350 °C.

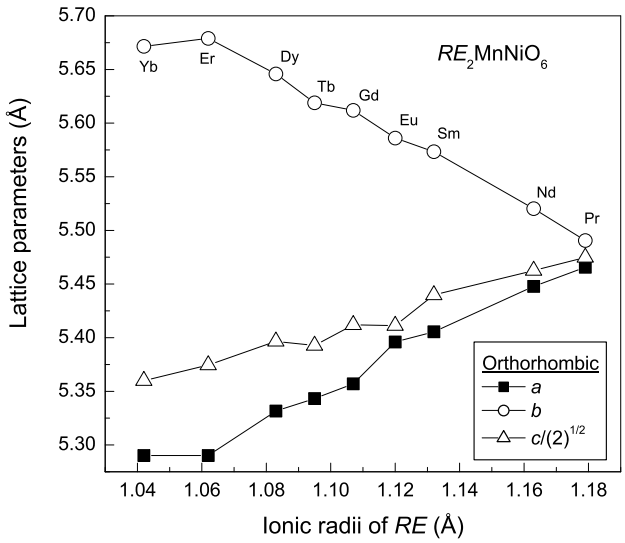

Figure 6.7: Variation of lattice parameters, as a function of the nine-coordinated ionic radii of RE in RE_2MnNiO_6, annealed at 1300-1350 °C.

as observed previously in gallium [Goo61, Top97b, Zho01, Heb02a] and chromium [Dei02] substituted $LaMnO_3$, and $REMnO_3$ [Alo00]. The origin of this behaviour is the increased tilting of BO_6 octahedra [Goo02]. According to the Glazer's classification of octahedral tilting in perovskites, such a variation in lattice parameters of *Pbnm* symmetry originates from a tilting of the type, $a^-a^-c^+$ [Gla72]. This is a three-tilt system, where the total tilt is the combination of three component tilts along the three crystallographic axes. In $a^-a^-c^+$, the tilt along the two axes (x and y) are equal, but different from the third one (z). Also, the tilt is in the opposite directions in the adjacent planes along x and y, whereas the tilt is in the same direction along z direction. For both the Co and Ni compounds of RE_2MnMO_6 annealed at 1300-1350 °C, $c/\sqrt{2} > a$, indicating an O-orthorhombic structure ($c/a > \sqrt{2}$).

6.4 Magnetic measurements

Studies on the low-temperature synthesized La_2MnCoO_6 and La_2MnNiO_6 revealed the formation of a ferromagnetic phase for samples annealed at 200 °C. The high-T_c phase of La_2MnCoO_6 was obtained after annealed at 700 °C and a low-T_c phase after annealed at 1300 °C, as evidenced from the sharp magnetic transitions. Samples annealed at temperatures other than these two temperatures showed either broad magnetic transitions or more than one magnetic transition indicating the mixed phase behaviour. On the other hand, in the case of La_2MnCoO_6, only one phase is obtained with a sharp magnetic transition after annealing at 1300 °C. Samples annealed in the temperature range 400–1300 °C showed mixed phase behaviour. Based on these observations, the magnetic measurements on the rare-earth compositions are also performed on samples annealed at different temperatures. Annealing at 1300-1350 °C were performed several times till the magnetic transitions become sharp and free of any other minor transitions.

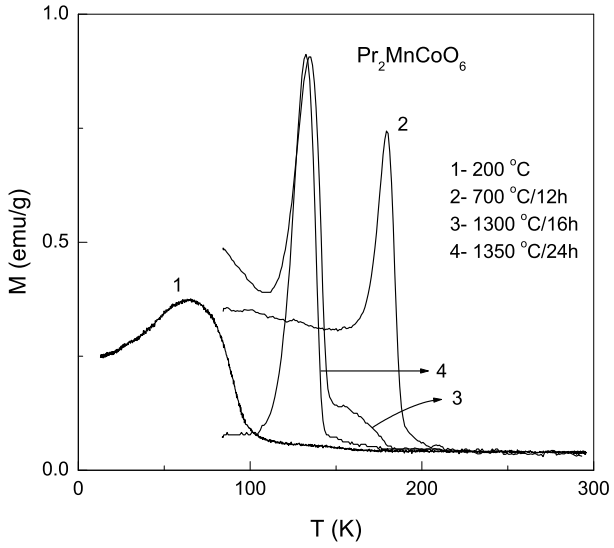

Figure 6.8: ZFC magnetization curves of Pr_2MnCoO_6, annealed at different temperatures.

Powder XRD studies showed that the Pr and Nd compounds form almost pure perovskite phases after annealing at 200 °C. Figure 6.8 and Figure 6.9 show the ZFC magnetization curves of Pr_2MnCoO_6 and Nd_2MnCoO_6, respectively, annealed at 200, 700 and 1300 °C. In the case of both Pr and Nd compositions, broad magnetic transitions are observed in the samples annealed at 200 °C. For the Pr compound, the magnetic transition is below 100 K whereas for the Nd compound, this transition is below 80 K. This may be compared with the similar broad magnetic transition of La_2MnCoO_6 observed below 150 K. For both compounds, the sample heated at 700 °C shows a sharp ferromagnetic transition at a higher temperature, compared to a sharp magnetic transition observed at a lower temperature after heating at 1350 °C. The magnetization curves of the Pr_2MnCoO_6 and Nd_2MnCoO_6 samples, after a single heating at 1300 °C, show a major ferromagnetic transition at the T_cs of the samples heated to 1350 °C, and a weak magnetic transition at the temperatures

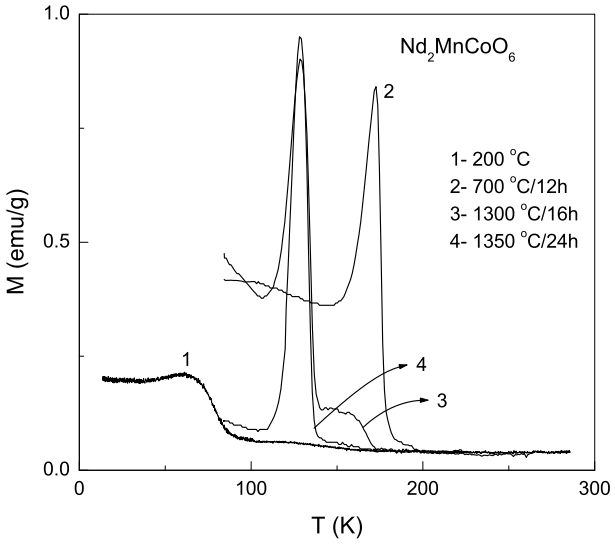

Figure 6.9: ZFC magnetization curves of Nd_2MnCoO_6, annealed at different temperatures.

corresponding to the T_cs of the 700 °C heated samples. This indicates the presence of a major phase and a minor phase in the samples heated at 1300 °C for a short time. This is similar to that observed in the case of La_2MnCoO_6, where two different phases of the compound were obtained after heating at 700 °C and 1300 °C. This indicates that, for each composition, two different phases are formed, a high-T_c phase after heating at 700 °C and a low-T_c phase after heating at 1350 °C.

Temperature dependence of the ZFC magnetization of the RE_2MnCoO_6 compositions synthesized by the low-temperature method and annealed at 200 °C are shown in Figure 6.10. The ZFC magnetization curves of the La and Nd compounds containing both Co and Ni are compared in the inset of Figure 6.10. As discussed in Section 6.3, the Co and Ni compositions show the presence of respective rare-earth oxides for *RE* heavier than Nd, for samples annealed at 200 °C. In agreement with that, the magnetic transition observed in the ZFC magnetization curves of the

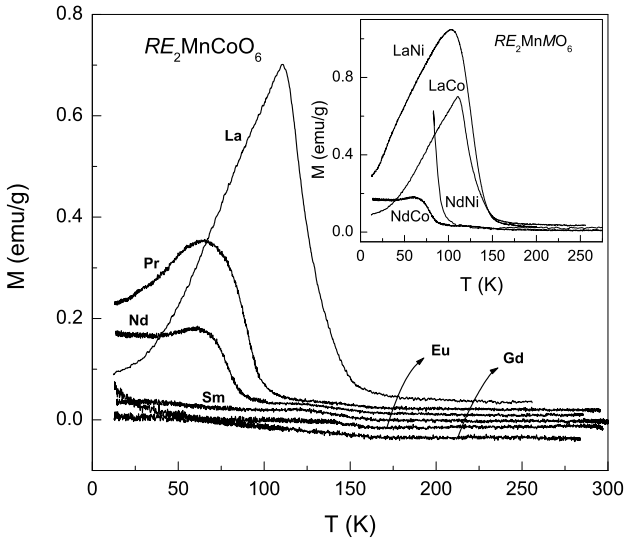

Figure 6.10: ZFC magnetization curves of some RE_2MnCoO_6 compositions, annealed at 200 °C. Inset: comparison of La (labelled LaCo & LaNi) and Nd (labelled NdCo & NdNi) compounds of RE_2MnMO_6

RE_2MnMO_6 compositions gradually shifts to lower temperature and vanishes after Nd among the lanthanoids. The decreasing magnetic transition temperature with the decrease in the ionic-size of RE is due to the increased structural distortion. In the case of La compounds, this transition corresponds to the Mn^{+4}-O-Co^{+2}/Ni^{+2} superexchange (see Section 3.1 and Chapter 4). For the RE compositions also it is due to the same type of superexchanges as evidenced from the results of XPS studies on Nd_2MnNiO_6, where the spin-states Mn and Ni is tetravalent and divalent respectively (see Section 4.5.3).

Figures 6.8 and 6.9 show that two different ferromagnetic phases can be obtained for the rare-earth compositions also, as in the case of the low-temperature synthesized La_2MnCoO_6. Therefore, all rare-earth compounds (RE = Pr, Nd, Sm, Eu, Gd, Tb, Dy, Er and Yb) are investigated for the possible ferromagnetic phases formed at a rela-

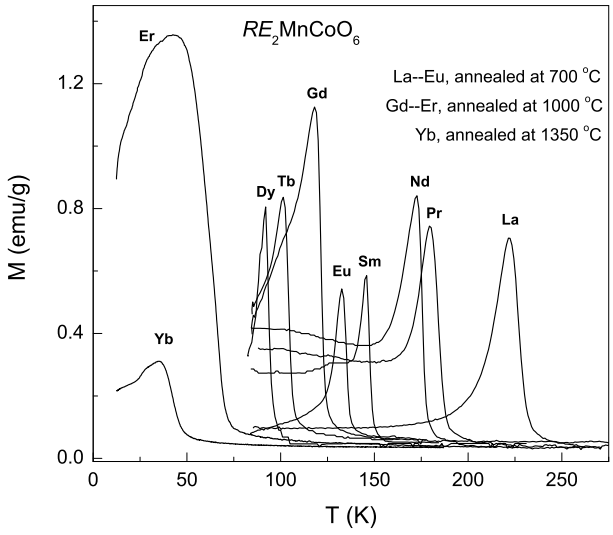

Figure 6.11: ZFC magnetization of the high-T_c phases of RE_2MnCoO_6, obtained after annealing at 700 (for La–Eu), 1000 (for Gd–Er), and 1350 °C (for Yb).

tively lower annealing temperature of 700 °C and for the second phase after annealing at 1350 °C. Figure 6.11 illustrates the magnetization curves of the pure ferromagnetic phases, obtained after annealing at 700 °C, having a higher curie temperature. These phases are called the high-T_c phases and the temperature of formation of this phase is higher for the latter members of rare-earth series. From La to Eu, the high-T_c phase is formed after annealing at 700 °C, whereas for Gd and heavier RE, the annealing temperature required to get this phase, as evidenced by sharp magnetic transitions, is 1000 °C . The Curie temperature of the Er compound annealed at 1000 °C was found to be unaffected after annealing at higher temperatures. Similarly, the Yb compound give a sharp magnetic transition only after annealing at 1350 °C. Therefore it can be assumed that for Er and Yb there is only one ferromagnetic phase.

Similar to the case of La_2MnCoO_6, a low-T_c is phase formed from the high-T_c phase after annealing the RE compositions at 1350 °C. Similar behaviour is obtained

for all the RE_2MnCoO$_6$ compositions, except for the extreme end members Er and Yb which form only one phase. In Figure 6.12, the ZFC magnetization curves of the low-T$_c$ phases of all compositions, including that of La, are compared with that of the corresponding high-T$_c$ phases. Sharp magnetic transitions are observed for both phases of the compounds and the Curie temperatures of the two phases decrease from RE = Pr to Yb.

The variation of the T$_c$s of both phases of RE_2MnCoO$_6$ with the ionic-radius of rare-earth ion and the difference between the T$_c$s (ΔT$_c$) of the two phases, for a given RE^{+3} (the ionic radius is taken for nine-fold coordination [Sha76]) are shown in Figure 6.13. For both the phases, T$_c$ decreases with decreasing ionic radius, but a faster decrease of T$_c$ for the high-T$_c$ phase is observed, so that ΔT$_c$ is small at lower ionic radii. For both the phases, T$_c$ decreases linearly with decreasing ionic radius, up to Gd. A deviation from linearity is observed for both the phases from Tb to Yb.

As shown in Figure 6.14, the ionic-size of trivalent rare-earth ions decreases linearly with number of f-electrons, from Pr to Yb, except for La^{+3}. The less distorted orthorhombic structures observed for the La compounds may be due to the relatively larger size of La^{+3} ion. In fact, in the case of REMnO$_3$, the average Mn-O-Mn angle is affected by the strain associated with the octahedral tilting and the Jahn-Teller distortion of MnO$_6$ octahedra in REMnO$_3$. Alonso *et al.* [Alo00] have calculated the average Mn-O-Mn angle distortion of the MnO$_6$ octahedra in REMnO$_3$ from the <Mn-O-Mn> bond angle $< \theta >$ as $< \omega > = 180 - < \theta >$. Mn-O-Mn angle [Alo00] decreases linearly with the radius of the rare-earth ion (except for LaMnO$_3$, having larger size for La^{+3}), as shown in the inset of Figure 6.14, and the same trend is expected in the case of RE_2MnCoO$_6$ series also. It may be seen that $< \theta >$ decreases almost linearly (excluding La^{+3}), with decreasing r$_{RE}$, indicating that there are no structure-related anomalies for Tb and Dy manganates due to the smaller sizes of these two rare earth ions. Therefore, a linear decrease in the T$_c$ with ionic size of

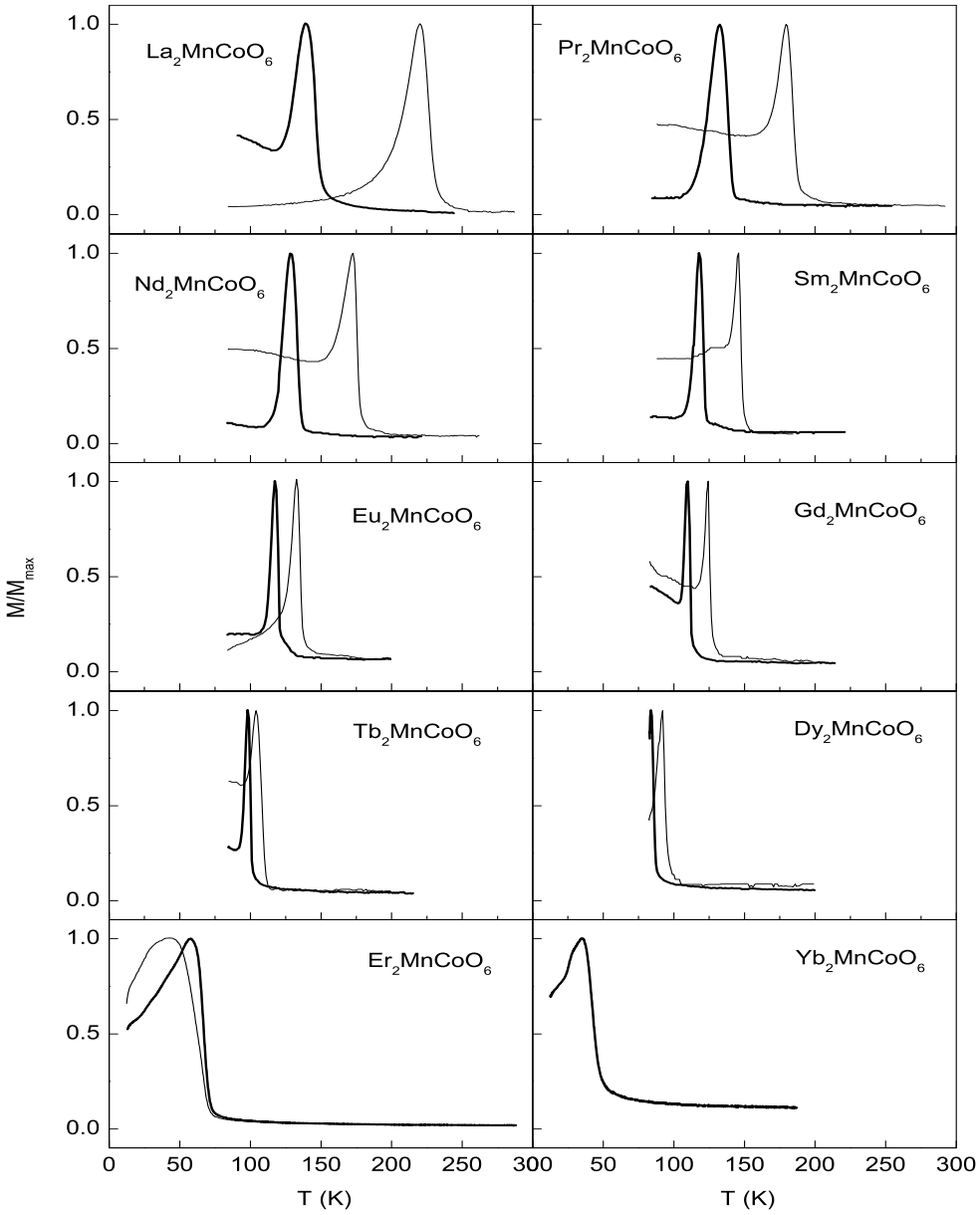

Figure 6.12: Comparison of the ZFC magnetization curves of the high-T_c (thin lines) and low-T_c (thick lines) phases of RE_2MnCoO_6, H = 50 Oe and La_2MnCoO_6.

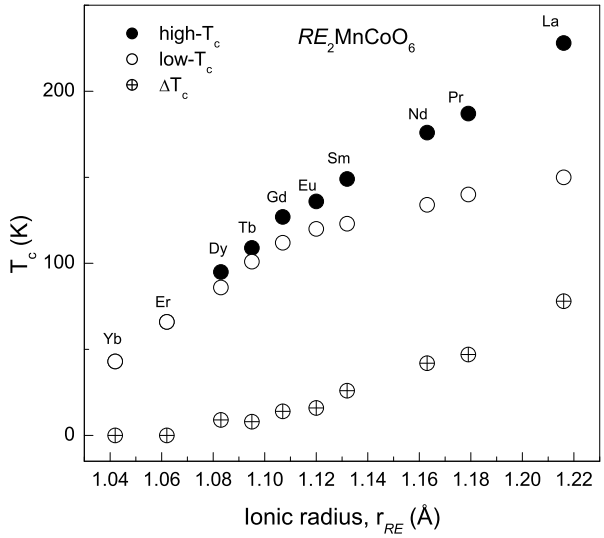

Figure 6.13: Variation of T_cs of the two phases of RE_2MnCoO_6 as a function of ionic radius of RE^{+3}, along with the difference in the T_cs (ΔT_c).

RE^{+3} is expected, based on the linear change in the Mn-O-Mn angle. However, the deviation from linearity, in the variation of T_c with decreasing ionic size, after Gd, and the much faster drop in T_c for the heavier rare-earth compounds, are not expected since the rare earth ionic size decreases almost linearly from Pr to Yb. Therefore, the unexpected lower values of the Curie temperatures of the compositions having RE smaller than that of Gd may be linked to some factors other than those related to the internal pressure effect. The fact that a larger decrease in T_c is observed for the low-T_c phases of the Tb and Dy compounds implies that the change in T_c may be linked to the contribution from B-site ions, Mn^{+4} and Co^{+2}, along with the contribution from RE^{+3}. The lesser structural distortion and relatively larger Mn-O-Mn angle for the La compound is responsible for the comparatively larger T_cs of its two phases. The decrease in T_c with the ionic-size of RE is in good agreement with the fact that the size of the A-site ion in the perovskite ABO_3 affects the strength of the 180°

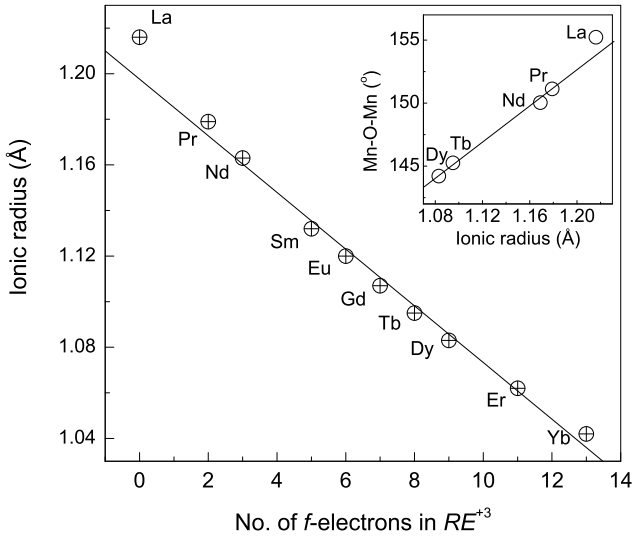

Figure 6.14: Variation of the ionic radius of RE^{+3}, for nine-fold coordination [Sha76], with number of f-electrons. The inset shows the variation of the average Mn-O-Mn angle in $RE\mathrm{MnO_3}$ [Alo00] with the ionic radius of RE^{+3}.

B-O-B ferromagnetic superexchange interactions. For a given crystal structure and B-site ion, the strength of this superexchange interaction is determined by the extent of overlap between the oxygen and B-site ion orbitals.

Since the magnetic transition temperature is determined by the variation of the Mn-O-Mn angle, the structure-magnetic property correlation can be better understood in terms of the tolerance factor which is a direct measure of the structural distortion. Figure 6.15 shows the Curie temperatures of the two phases of $RE_2\mathrm{MnCoO_6}$ as a function of the tolerance factor, t. Tolerance factor is calculated using the nine-fold coordination radii of the rare earth ions, six-fold coordination radii of $\mathrm{Mn^{+3}}$ and low-spin $\mathrm{Co^{+3}}$ for the high-T_c phases and $\mathrm{Mn^{+4}}$ and $\mathrm{Co^{+2}}$ for the low-T_c phases. The spin-states are assumed based on the XPS studies on La and Nd compositions. Therefore, the tolerance factor is different for the two phases of the same compound

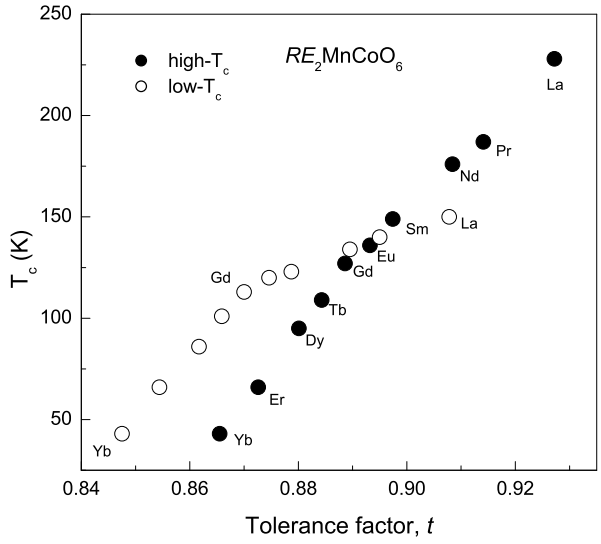

Figure 6.15: Variation of T_cs of the two phases of RE_2MnCoO_6 with tolerance factor, t.

due to the difference in the average ionic radius of the B-site ions. For both the high- and low-T_c phases of RE_2MnCoO_6, the Curie temperature decreases with decreasing tolerance factor. T_c decreases much faster for the high-T_c phase compared to that of the low-T_c phase, similar to the dependence on radius of RE^{+3}. The rate of decrease of T_c of the two phases of RE_2MnCoO_6 with decreasing t or r_{RE} is much slower than that observed [Dam97, Zho99] for the RE-site substituted manganates. T_c of the RE-site substituted compositions, $RE_{0.5}A_{0.5}MnO_3$, decreases very fast and drops below 100 K for $t \approx 0.93$ [Dam97] which is the upper limit of the tolerance factor for RE_2MnCoO_6 phases for which T_c as high as 230 K is observed. This difference in the variation of T_c may be attributed to the larger effect of the variation of the B-O-B angle on Mn^{+3}-O-Mn^{+4} double exchange interactions in the RE-site substituted manganates compared to the effect on Mn^{+3}-O-Mn^{+3} and Mn^{+4}-O-Co^{+2} superexchange interactions in RE_2MnCoO_6. The decrease in T_c with decreasing tolerance factor is

in good agreement with the theoretical predictions based on structural distortions.

Similar to that observed for the the high-T_c phase of La_2MnNiO_6, sharp ferromagnetic transitions are observed for other rare-earth containing RE_2MnNiO_6 compositions annealed at 1350 °C. The ZFC magnetization curves of the high-T_c phases of RE_2MnCoO_6 (containing Mn^{+3} and Co^{+3}) and RE_2MnNiO_6 (RE = Pr, Nd, Sm, Eu, Gd, Tb, Dy, Er and Yb), are compared in Figure 6.16. All the magnetization curves show sharp magnetic transitions, indicating the formation of single phase compositions. The transition temperatures of the Ni compounds are larger than those of the corresponding Co compounds and there is a gradual decrease in the T_cs of both Co and Ni compounds as the rare-earth ion is changed from Pr to Dy. Finally, identical T_cs are observed when RE = Er and the magnetic transition temperature of the Co compound becomes larger than that of the corresponding Ni compound for RE = Yb. Also, there is a significant difference in the shapes of the curves below T_c for the Co and Ni compounds, probably due to the contribution from high anisotropy from Co [Kum98a, Joy00]. Similarly, the contribution from the magnetocrystalline anisotropy of the rare earth ions is visible in the magnetization curves of RE_2MnNiO_6, the broad maximum observed for the La compound becomes sharper with the change in RE, as observed in the case of $RE_{0.7}Ca_{0.3}MnO_3$ [Kum98b].

The changes in the ferromagnetic transition temperatures of RE_2MnCoO_6 and RE_2MnNiO_6, as a function of the ionic-size of RE, are shown in Figure 6.17. T_cs decrease almost linearly up to RE = Gd, except for relatively larger T_cs for the La compounds. There is a sudden change in the rate of decrease of T_c with decreasing ionic-size of RE, after Gd, and again a much faster linear decrease is observed for the heavier rare-earth compounds. Another important observation is that the T_c of the Ni compounds falls relatively faster than that of the corresponding Co compounds, with decrease in the ionic radius of RE.

The higher T_cs for RE_2MnNiO_6 are possibly due to the additional Mn^{+3}-O-Ni^{+3}

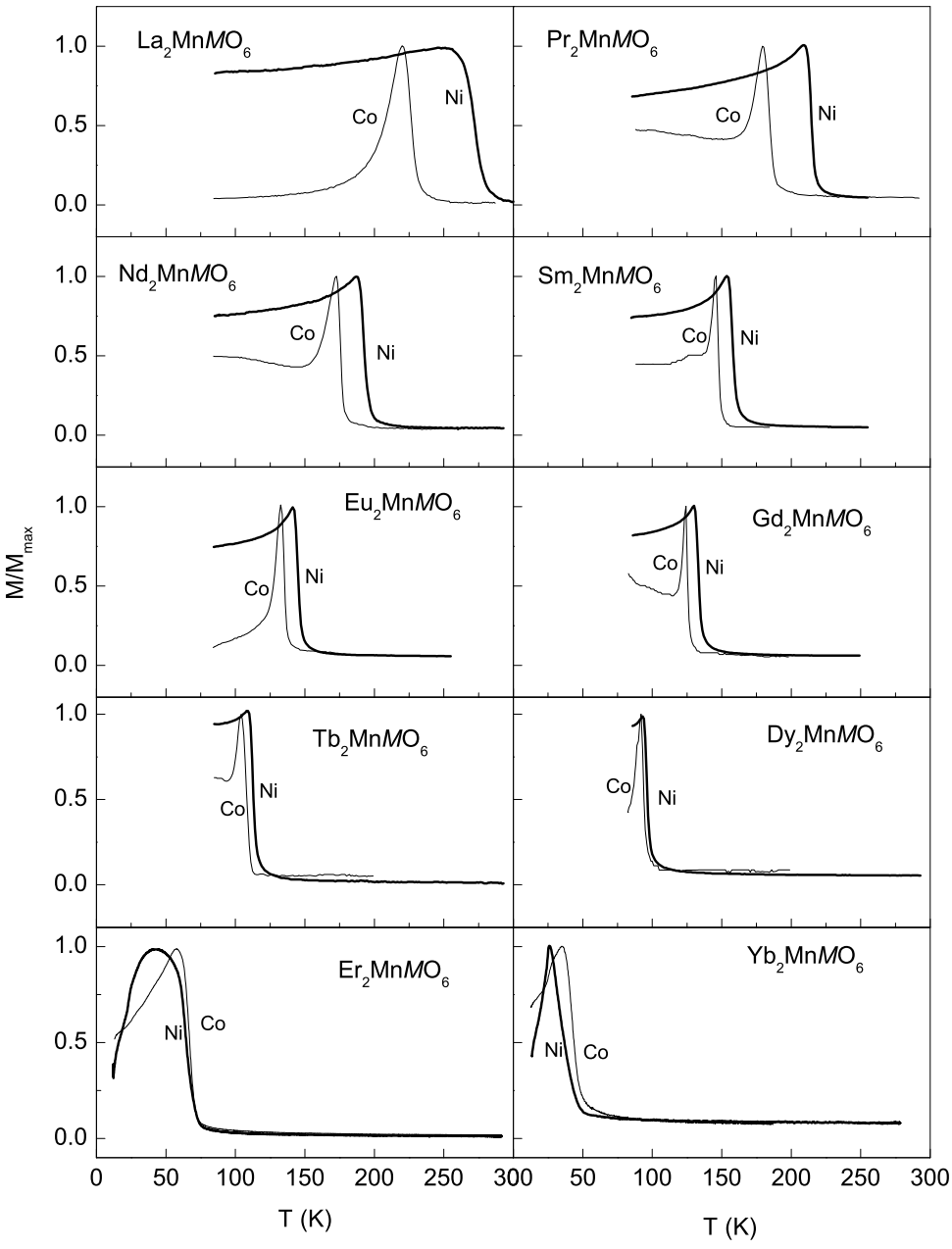

Figure 6.16: Comparison of ZFC magnetization curves of high-T_c phases RE_2MnCoO_6 and RE_2MnNiO_6, H = 50 Oe.

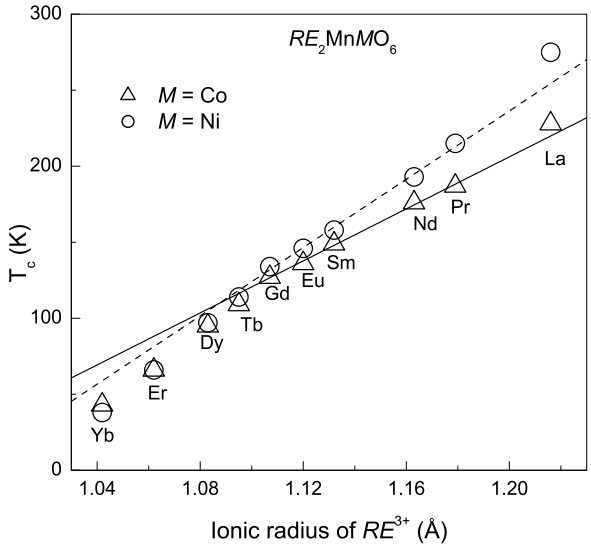

Figure 6.17: Variation of T_cs of the high-T_c phases RE_2MnCoO_6 and RE_2MnNiO_6 with the ionic radius of the rare-earth ions.

superexchange interactions apart from Mn^{+3}-O-Mn^{+3} interactions present in the corresponding high-T_c phase of the Co containing compositions, through the single e_g electron in low-spin Ni^{+3}, as observed for La_2MnNiO_6. Similarly, the comparatively larger T_cs for the La compositions can be understood in terms of the relatively larger size of La^{+3}. The difference between the T_cs of RE_2MnCoO_6 and RE_2MnNiO_6, for a given RE, decreases with the size of RE^{+3} and becomes almost constant for smaller RE ions, indicating that RE ionic size effect overrules the contribution from additional strength of ferromagnetic exchange interactions due to Ni^{+3} ion for the Ni compounds. More over, the higher T_c of the Co compound when compared to that of the Ni compound, for RE = Yb, indicates that the Mn-O-Ni superexchange interactions are greatly affected by the smaller size of RE.

Figure 6.18 shows the variation of the T_c of the high-T_c phases of the Co and Ni compounds with tolerance factor. The tolerance factors are slightly different for the

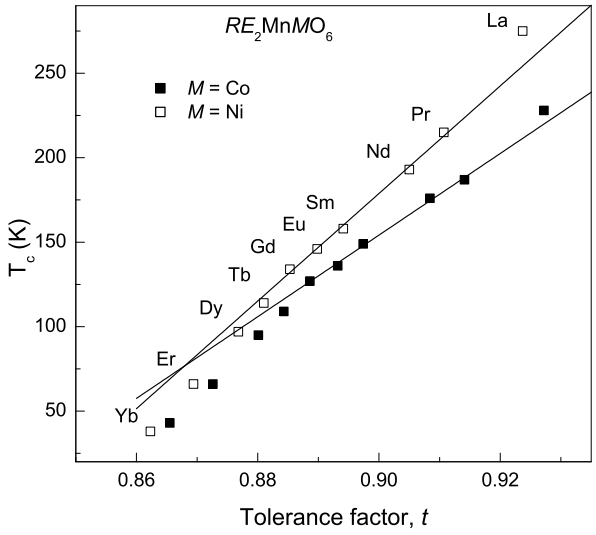

Figure 6.18: Variation of T_cs of high-T_c phases RE_2MnCoO_6 and RE_2MnNiO_6 with tolerance factor.

Co and Ni compounds due to the slight difference in the six-fold coordination ionic radii of Co^{+3} and Ni^{+3}. The T_cs decrease with decreasing tolerance factor and this is in good agreement with the theoretical predictions based on structural distortions. T_c of RE_2MnMO_6 decrease linearly with t from Pr to Gd and larger rate of decrease is observed for RE beyond Gd, indicating another contribution to the strength of the magnetic exchange interactions.

There is a large slope change in the variation of the T_cs of both the low-T_c and high-T_c phases of RE_2MnCoO_6 as well as for the high-T_c phase of RE_2MnNiO_6, beyond Gd. Since the variation of the ionic radius of the rare-earth ion is almost linear, there seems to be another contribution from the rare-earth ion which affects the T_c in the case of the heavier rare-earth compositions. There are two possible contributions from the rare earth ions, apart from structural distortions due to the smaller size of RE^{+3}, which are expected to influence the strength of the magnetic

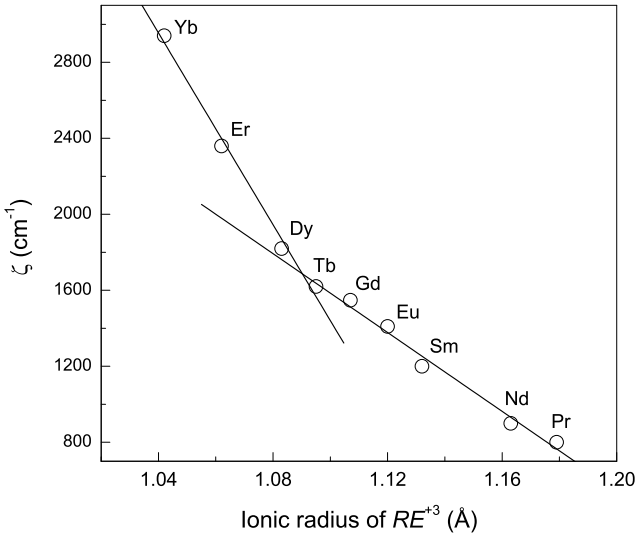

Figure 6.19: Variation of the one-electron spin-orbit coupling coefficient [The76], ζ, with the ionic radius of RE^{+3}.

exchange interactions and therefore, the ordering temperature of RE_2MnCoO$_6$. These are the high magnetocrystalline anisotropy of the rare-earth ions and the larger values of the magnetic moments of the heavier RE ions. Though no ordering of the rare earth spins is observed in REMnO$_3$ down to lowest temperatures [Coe99], the large magnetocrystalline anisotropy of RE^{+3} may influence the ferromagnetic ordering of Mn and Co spins. The effect of the magnetocrystalline anisotropy on the ordering temperature is expected to be identical for both Co and Ni containing compositions as well as for different phases as the rare-earth ions are located in identical environments in the structure of both the phases. This is what is observed in all cases.

It has been shown that the increasing magnetocrystalline anisotropy of the heavier rare-earth ions do not contribute any associated magnetic interactions with the Mn lattice, as evidenced from neutron diffraction studies on TbMnO$_3$ [Bla00]. However, Cheng etal have reported unusually large shift in the magneto-optical Kerr rotation

in thin films of $CoFe_2O_4$ doped with Tb and Dy [Che99]. Similarly, Kahn and Zhang found unusually large blocking temperatures and coercivities for $CoFe_2O_4$ spinel ferrite nanoparticles doped with Gd^{+3} and Dy^{+3} ions when compared to the effect of other lanthanide ions [Kah01]. The authors concluded that the single ion anisotropy of the lanthanide ions may be the controlling factor, but found that the effect of the lanthanide ion is very complex on the modulation of the magnetic properties of the system.

The variation of the one-electron spin-orbit coupling constant, which leads to single ion anisotropy, of the lanthanide ions, as a function of the ionic radius, is shown in Figure 6.19. The spin-orbit coupling constant increases almost linearly from Pr to Gd and then increases much faster, linearly, beyond Tb, showing a slope change between Gd and Dy. The change in the slope of the variation of T_c with ionic-size is exactly in accordance with the variation of the spin-orbit coupling constant, indicating that single-ion anisotropy of the heavier rare-earth ions may be responsible for the anomaly (relatively lower T_cs for the heavier rare-earth ions after Gd) observed.

The present studies demonstrate that single-ion anisotropy of the heavier rare-earth ions marginally affects the magnetic exchange interactions in the ferromagnetic compositions in RE_2MnCoO_6 and RE_2MnNiO_6, apart from the contributions from structural distortions associated with the decreasing ionic size of the rare-earth ions.

6.5 Conclusions

Two distinct ferromagnetic phases of RE_2MnCoO_6 (RE = Pr, Nd, Sm, Eu, Gd, Tb, Dy, Er and Yb) have been synthesized in single-phase forms by a low-temperature method. A phase with a higher Curie temperature is obtained for samples heated in the range 700-1000 °C and another phase with a lower Curie temperature is obtained after heating the samples at 1350 °C. The high-T_c phases of Co compounds are slowly

converted to the low-T_c phase when heated above 1000 °C, so that mixed phase behaviour is observed in magnetic measurements for samples heated in the range 1000-1300 °C. Similarly the high-T_c phases of RE_2MnNiO_6 are also synthesized, but they are formed after annealing at 1350 °C.

The effect of RE^{+3} on the magnetic transition temperatures of two different phases of RE_2MnCoO_6, containing Mn^{+3} and low-spin Co^{+3} in one phase (high-T_c) and Mn^{+4} and Co^{+2} in the second phase (high-T_c) has been studied. The decreasing T_c of both phases with decreasing ionic size of RE^{+3}, r_{RE}, or decreasing tolerance factor, t, is similar to that found for the RE-site substituted CMR manganates. However, in the case of RE_2MnCoO_6, T_c decreases much slowly with decreasing r_{RE} and t, compared to the RE-site substituted manganates. This indicates that superexchange ferromagnetic interactions in RE_2MnCoO_6 are less susceptible to the decreasing B-O-B angle when compared to the double exchange ferromagnetic interactions in the RE-site substituted manganates. The results indicate that the magnetic transition temperature of the two different phases of RE_2MnCoO_6 is mainly affected by the decreasing ionic radius of RE^{+3}, caused by the 'internal pressure effect' due to the smaller size of the rare earth ions. This internal pressure effect is more pronounced in the case of the high-T_c phases containing Mn^{+3} and Co^{+3}, due to the combined effect of Jahn-Teller distortion and tilting of $Mn^{+3}O_6$ octahedra.

Between the Mn^{+4}-O-Co^{+2} and Mn^{+3}-O-Mn^{+3} exchanges present in low-T_c and high-T_c phases, respectively, the latter is more sensitive to the structural distortion. For a particular RE with larger ionic size, the T_c of RE_2MnNiO_6 is larger than that of RE_2MnCoO_6 and vice versa for smaller ionic size, though the ionic sizes of trivalent low-spin Co and Ni ions are comparable. T_cs of both Co and Ni containing compositions decrease with the decrease in the ionic size of RE^{+3}, showing a faster decrease for heavier rare-earth ions beyond Gd. Though the decreasing size of the rare-earth ion is responsible for the decrease in the magnetic transition temperature,

due to structural distortions, an anomalous change in rate of decrease of T_c, beyond Gd, is due to contributions from the single-ion anisotropy of the heavier rare-earth ions. The rapid decrease of T_cs of the Ni compounds indicates that the Mn^{+3}-O-Ni^{+3} exchange present in the Ni compositions are more affected by structural distortion than the Mn^{+3}-O-Mn^{+3} or Mn^{+3}-O-Co^{+3} exchanges present in the Co containing compositions.

Bibliography

[Abb93] Abbate, M., Fuggle, J. C., Fujimori, A., Tjeng, L. H., Chen, C. T., Potze, R., Sawatzky, G. A., Eisaki, H., Uchida, S., *Phys. Rev.B* **47**, 16124 [1993].

[Abr70] Abragam, A., Bleaney, B., in: *Electron Paramagnetic Resonance of Transition Ions*, Clarendon Press, Oxford [1970].

[Ahn96] Ahn, K. H., Wu, X. W., Liu, K., Chien, C. L., *Phys. Rev.B* **54**, 15299 [1996].

[Alo00] Alonso, J. A., Martínez-Lope, M. J., Casais, M. T., Fernández-Díaz, M. T., *Inorg. Chem.* **39**, 917 [2000].

[And50] Anderson, P. W., *Phys. Rev.* **79**, 350 [1950].

[And02] Androulakis, J., Katsarakis, N., Giapintzakis, J., *Solid State. Commun.* **124**, 77 [2002].

[Ani98] Anil, K. P. S., Alias, J. P.,Date, S. K., *J. Mater. Chem.* **8**, 1219 [1998].

[Aru00] Aruna, S. T., Muthuraman, M., Patil, K. C., *Mater. Res. Bull.* **35**, 289 [2000].

[Asa79] Asai, K., Sekizawa, H., Iida, S., *J. Phys. Soc. Jpn.* **47**, 1054 [1979].

[Bar02] Barilo, S. N., Gatal'skaya, V. I., Shiryaev, S. V., Kurochkin, L. A., *Low Temp. Phys.* **28**, 853 [2002].

[Bay82] Baythoun, M. S. G., Sale, F. R., *J. Mater. Sci.* **17**, 2757 [1982].

[Bed86] Bednorz, J. G., Müller, K. A., *Z. Phys. B: Condens. Matter* **64**, 189 [1986].

[Ben57] Bents, U. H., *Phys. Rev.* **106**, 225 [1957].

[Bla65] Blasse. G., *J. Phys. Chem. Solids* **26**, 1969 [1965].

[Bla97] Blasco, J., García, J., De Teresa, J. M., Ibarra, M. R., Perez, J., Algarabel, P. A., Marquina, C., *Phys. Rev. B* **55**, 8905 [1997].

[Bla00] Blasco, J., Ritter, C., García, J., De Teresa, J. M., Pérez-Cacho, J., Ibarra, M. R., *Phys. Rev. B* **62**, 5609 [2000].

[Bla01] Blasco, J., García, J., Sánchez, M. C., Larrea, A., Campo, J., Subías, G., *J. Phys.: Condens. Matter* **13**, L729 [2001].

[Bla02a] Blasco, J., Sánchez, M. C., Pérez-Cacho, J., García, J., Subías, G., Campo, J., *J. Phys. Chem. Solids* **63**, 781 [2002].

[Bla02b] Blasco, J., García, J., Sánchez, M. C., Campo, J., Subías, G., Pérez-Cacho, J., *Eur. Phys. J. B* **30**, 469 [2002].

[Bla02c] Blasco, J., Ritter, C., Morellon, L., Algarabel, P. A., De Teresa, J. M., Serrate, D., García, J., Ibarra, M. R., *Solid State Sciences* **4**, 651 [2002].

[Bri74] Briggs, D., Gibson, V. A., *Chem. Phys. Lett.* **25** 493 [1974].

[Bul01] Bull, C. L., Mortimer, R., Sankar, G., Gleeson, D., Catlow, C. R. A., Wood, I. G., Price, G. D., *Synthetic Metals* **121**, 1467 [2001].

[Bul03] Bull, C. L., Gleeson, D., Knight, K. S., *J. Phys.: Condens. Matter* **15**, 4927 [2003].

[Bus03] Buschow, K. H. J., De Boer, F. R., in: *Physics of Magnetism and Magnetic Materials*, Kluwer Academic/Plenum Publishers, New York [2003].

[Cas76] Casey, A. T., in: *Theory and Applications of Molecular Paramagnetism*, Boudreaux, E. A., Mulay, L. N., (Eds.), John Wiley & Sons, New York [1976].

[Cha92] Chainani, A., Mathew, M., Sarma, D. D., *Phys. Rev. B* **46**, 9976 [1992].

[Cha02] Chang, Y. L., Huang, Q., Ong, C. K., *J. Appl. Phys.* **91**, 789 [2002].

[Che96] Chen, I-W., Li, P., Wang, Y., *J. Phys. Chem. Solids.* **57**, 1525 [1996].

[Che99] Cheng, F., Liao, C., Kuang, J., Xu, Z.,Yan, C., Chen, L., Zhao, H., Liu, Z., *J. Appl. Phys.* **85**, 2782 [1999].

[Che00] Cheong, S.-W., Hwang, H. Y., in: *Colossal Magnetoresistive Oxides*, Tokura, Y., (Ed.), Gordon and Breach Science Publishers, The Netherlands [2000].

[Chi90] Chick, L. A., Pederson, L. R., Moupin, G. D., Bates, D. L., Thomas, L. E., Exarhos, G. J., *Mater. Lett.* **10**, 6 [1990].

[Coe99] Coey, J. M. D., Viret, M., von Molnar, S., *Adv. Phys.* **48**, 167 [1999].

[Col98] *Colossal Magnetoresistance, Charge Ordering and Related Properties of Manganese Oxides*, Rao, C. N. R., Raveau, B., (Eds.), World Scientific, Singapore [1998].

[Col00] *Colossal Magnetoresistive Oxides*, Tokura, Y., (Ed.), Gordon and Breach Science Publishers, The Netherlands [2000].

[Cul56] Cullity, B. D., in: *Elements of X-ray Diffraction*, Addison-Wesley Publishing Company, Inc., Massachusetts, [1956].

[Cul72] Cullity, B. D., in: *Introduction to Magnetic Materials*, Addison-Wesley Publishing Company, Inc., Massachusetts, [1972].

[Cus01] Cussen, E. J., Rosseinsky, M. J., Battle, P. D., Burley, J. C., Spring, L. E., Vente, J. F., Blundell, S. J., Coldea, A. I., Singleton, J., *J. Am. Chem. Soc.* **123**, 1111 [2001].

[Dam97] Damay, F., Maignan, A., Martin, C., Raveau, B., *J. Appl. Phys.* **81**, 1372 [1997].

[Das01] Dass, R. I., Goodenough, J. B., *Phys. Rev. B* **63**, 064417 [2001].

[Das03] Dass, R. I., Goodenough, J. B., *Phys. Rev. B* **67**, 014401 [2003].

[Dei02] Deisenhofer, J., Paraskevopoulos, M., von Nidda, H.-A. K., Loidl, A., *Phys. Rev. B* **66**, 054414 [2002].

[Dem94] Demazeau, G., Siberchicot, B., Matar, S., Gayet, C., Largeteau, A., *J. Appl. Phys.* **75**, 4617 [1994].

[Dey67] Dey, S. K., *Phil. Mag.* **16**, 1097 [1967].

[Dou02] Douvalis, A. P., Venkatesan, M., Coey, J. M. D., Grafoute, M., Greneche, J-M., Suryanarayanan, R., *J. Phys.: Condens. Matter* **14**, 12611 [2002].

[Ear68] Earnshaw, A., in: *Introduction to Magnetochemistry*, Academic press, London [1968].

[Ega01] Egami, T., in: *Localized to Itinerant Electronic Transition in Perovskite Oxides*, Goodenough, J. B., (Ed.), Springer-Verlag, Berlin [2001]

[Elf00] El-Fadli, Z., Metni, M. R., Sapiña, F., Martinez, E., Folgado, J. V., Beltrán, D., Beltrán, A. *J. Mater. Chem.* **10**, 437 [2000].

[Fal97] Falcon, H., Goeta, A. E., Punte, G., Carbonio, R. E., *J. Solid State Chem.* **133**, 379 [1997].

[Fla99] Flavell, W. R., Thomas, A. G., Hollingworth, J., Warren, S., Grice, S. C., Dunwoody, P. M., Mitchell,C. E. J., Marr, P. G. D., Teehan,D., Downes, S., Seddon, E. A., Dhanak, V.R., Asai, K., Koboyashi, Y., Yamada, N., *Faraday Discuss.* **114**, 407 [1999].

[Fro72] Frost, D. C., McDowell, C. A., Woolsey, I. S., *Chem. Phys. Lett.* **17**, 320 [1972].

[Fuj67] Fujiki, H., Nomura, S., *J. Phys. Soc. Jpn.* **23**, 648 [1967].

[Gal62] Galasso, F., Darby, W., *J. Phys. Chem.* **66**, 131 [1962].

[Gal65] Galasso, F., Darby, W., *Inorg. Chem.* **4**, 71 [1965].

[Gal69] Galasso, F. S., in: *Structure, Properties and Preparation of Perovskite-type Compounds*, Pergamon Press, Oxford [1969].

[Gal70] Galasso, F. S., in: *Structure and Properties of Inorganic Solids* , Pergamon Press, Oxford, [1970].

[Gal77] Gallagher, P. K., Johnson, JR., D. W., Vogel, E. M., *J. Am. Ceram. Soc.* **60**, 28 [1977].

[Gho99] Ghosh, K., Ogale, S. B., Ramesh, R., Greene, R. L., Venkatesan, T., Gapchup, K. M., Bathe, R., Patil, S. I., *Phys. Rev. B* **59**, 533 [1999].

[Gil57] Gilleo, M. A., *Acta. Cryst.* **10**, 161 [1957].

[Gla72] Glazer, A. M., *Acta. Cryst. B* **28**, 3384 [1972].

[Gol26] Goldschimdt, V. M., *Akad. Oslo. J. Natur.* **2**, 7 [1926].

[Gon01] Gönen, Z. S., Gopalakrishnan, J., Sirchio, S. A., Eichhorn, B. W., Smolyaninova, V., Greene, R. L., *J. Solid State Chem.* **159**, 68 [2001].

[Gon02] Gönen, Z. S., Gopalakrishnan, J., Eichhorn, B. W., *Solid State Sciences* **4**, 773 [2002].

[Goo55] Goodenough, J. B., *Phys. Rev.* **100**, 564 [1955].

[Goo61] Goodenough, J. B., Wold, A., Arnott, R. J., Menyuk. N., *Phys. Rev.* **124**, 373 [1961].

[Goo63] Goodenough, J. B., in: *Magnetism and the Chemical Bond*, Interscience Publishers, New York [1963].

[Goo70] Goodenough, J. B., Longo, J.M., in: *Magnetic and Other Properties of Oxides and Related Compounds*, Hellwege, K. -H., Hellwege, A. M., (Eds.), Landolt-Börnstein New Series, Springer-Verlag, Berlin, **III/4a**, 126 [1970].

[Goo98] Goodenough, J. B., *Annu. Rev. Mater. Sci.* **28**, 1 [1998].

[Goo00] Goodenough, J. B., Dass, R. I., *Int. J. Inorg. Mater.* **2**, 3 [2000].

[Goo02] Goodenough, J. B., Dass, R. I., Zhou, J., *Solid State Sciences* **4**, 297 [2002].

[Gre01] Greneche, J. M., Venkatesan, M., Suryanarayanan, R., Coey, J. M. D., *Phys. Rev. B* **63**, 174403 [2001].

[Gun96] Gundakaram, R., Arulraj, A., Vanitha, P. V., Rao, C. N. R., Gayathri, N., Raychaudhuri, A. K., Cheetham, A. K., *J. Solid State Chem.* **127**, 354 [1996].

[Hav66] Havinga, E. E., *Philips Res. Repts.* **21**, 432 [1966].

[Haz88] Hazen, R. M., *Scientific American* **258**, 52 [1988].

[Heb02a] Hébert, S., Martin, C., Maignan, A., Retoux, R., Hervieu, M., Nguyen, N., Raveau, B., *Phys. Rev. B* **65**, 104420 [2002].

[Heb02b] Hébert, S., Maignan, A., Martin, C., Raveau, B., *Solid State Commun.* **121**, 229 [2002].

[Hol70] Hollander, J. M., Jolly, W. L., *Accounts Chem. Res.* **3**, 193 [1970].

[Hro97] Hrovat, M., Bernik, S., Holc, J., Kuščer, D., Kolar, D., *J. Mater. Sci. Lett.* **16**, 143 [1997].

[Hu03] Hu, L., Tong, W., Zhu, H., Zhang, Y., *J. Phys.: Condens. Matter* **15**, 2033 [2003].

[Ice99] Ice, G. E., Sparks, C. J., *Annu. Rev. Mater. Sci.* **29**, 25 [1999].

[Jef89] Jeffery, G. H., Bassett, J., Mendham, J., Denney, R. C., in: *Vogel's Textbook of Quantitative Chemical Analysis*, 5^{th} ed., ELBS with Longman, Singapore, [1989].

[Jia94] Jia, Y. Q., Liu, S. T., Wu, Y., *J. Solid State Chem.* **113**, 215 [1994].

[Jin94] Jin, S., Tiefel, T. H., McCormack, M., Fastnacht, R. A., Ramesh, R., Chen, L. H., *Science* **264**, 413 [1994].

[Jon50] Jonker, G. H., Van Santen, J. H., *Physica* **16**, 337 [1950].

[Jon56] Jonker, G. H., *Physica* **22**, 707 [1956].

[Jon66] Jonker, G. H., *J. Appl. Phys.* **37**, 1424 [1966].

[Jon89] Jones, R. W., in: *Fundamental Principles of Sol-Gel Technology*, The Institute of Metals, London [1989].

[Jor71] Jorgensen, C. K., *Chimia* **25**, 213 [1971].

[Joy97] Joy, P. A., Date, S. K., Kumar, P. S. A., *Phys. Rev. B* **56**, 2324 [1997].

[Joy98] Joy, P. A.,Date, S. K., Kumar, P. S. A., *J. Appl. Phys.* **83**, 6536 [1998].

[Joy00] Joy, P. A., Date, S. K., *J. Magn. Magn. Mater.* **218**, 229 [2000].

[Joy02] Joy, P. A., Sankar, C. R., Date, S. K., *J. Phys.: Condens. Matter* **14**, 4985 [2002].

[Jun97] Jung, W. H., Nakatsugawa, H., Iguchi E., *J. Solid State Chem.* **133**, 466 [1997].

[Kah01] Kahn, M. L., Zhang, Z. J.,*Appl. Phys. Lett.* **78**, 3651 [2001].

[Kam00] Kamegashira, N., Mori, T., Imamura, A., Hinatsu, Y., *J. Alloys Comp.* **302**, L6 [2000].

[Kan59] Kanamori, J., *J. Phys. Chem. Solids* **10**, 87 [1959].

[Kan60] Kanamori, J., *J. Appl. Phys.* **31**, 14S [1960].

[Kan96] Kang, Z.-J., Li, L.-P., Wei, Q., *Chem. Res. Chin. Univ.* **12**, 280 [1996].

[Kit03] Kittel, C., in: *Introduction to Solid State Physics*, 7^{th} ed., John Wiley & Sons, Singapore, [2003]

[Klu54] Klug, H. P., Alexander, L. E., in: *X-ray Diffraction Procedures*, John Wiley & Sons, New York, [1954].

[Kni98] Knizek, K., Daturi, M., Busca, G., Michel, C., *J. Mater. Chem.* **8**, 1815 [1998].

[Kob98] Kobayashi, K. -I., Kimura, T., Sawada, H., Terakura, K., Tokura, Y., *Nature* **395**, 677 [1998].

[Kor96] Korotin, M. A., Ezhov, S. Y., Solovyev, I. V., Anisimov, V. I., Khomskii, D. I., Sawatzky, G. A.,*Phys. Rev. B* **54**, 5309 [1996].

[Kri00a] Krishnan, R. V., Banerjee, A., *J. Phys.: Condens. Matter* **12**, 7887 [2000].

[Kri00b] Krishnan, R. V., Banerjee, A., *J. Phys.: Condens. Matter* **12**, 3835 [2000].

[Kum98a] Kumar, P. S. A., Joy, P. A., Date, S. K., *J. Phys.: Condens. Matter* **10**, L487 [1998].

[Kum98b] Kumar, P. S. A., Joy, P. A., Date, S. K., *Solid State Commun.* **108**, 67 [1998].

[Kum99] Kumar, P. S. A., Joy, P. A., Date, S. K., *Physica B* **269**, 356 [1999].

[Kum00] Kumar, P. S. A., Joy, P. A., Date, S. K., *Bull. Mater. Sci.* **23**, 97 [2000].

[Kut00] Kutty, T. R. N., Philip, J., *J. Phys.: Condens. Matter* **12**, 7747 [2000].

[Kuz01] Kuznetsov, M. V., Pankhurst, Q. A., Parkin, I. P., Morozov, Y. G., *J. Mater. Chem.* **11**, 854 [2001].

[Kyo03] Kyômen, T., Yamazaki, R., Itoh, M., *Chem. Mater.* **15**, 4798 [2003].

[Kyo04] Kyômen, T., Yamazaki, R., Itoh, M., *Chem. Mater.* **16**, 179 [2004].

[Li99] Li, X.-G., Fan, X. J., Ji, G., Wu, W. B., Wong, K. H., Choy, C. L., Ku, H. C., *J. App. Phys.* **85**, 1663 [1999].

[Lom83] Lombardo, E. L., Tanaka, K., Toyoshima, I., *J. Catal.* **80**, 340 [1983].

[Mah96] Mahl, S., Neumann, M., Borstel, G., Zygmunt, A., Jezierski, A., Slebarski, A., *J. Magn. Magn. Mater.* **159**, 179 [1996].

[Mah03] Mahendiran, R., Bréard, Y., Hervieu, M., Raveau, B., Schiffer, P., *Phys. Rev. B* **68**, 104402 [2003].

[Meg73] Megaw, H. D., in: *Crystal Structures: A Working Approach*, W. B. Saunders Company, Philadelphia [1973].

[Mil95] Millis, A. J., Littlewood, P. B., Shraiman, B. I., *Phys. Rev. Lett.* **74**, 5144 [1995].

[Min03] Minh, N. V., Kim, S.-J., Yang, I.-S. *Physica B* **327**, 208 [2003].

[Mit00] Mitchell, T. F., Argyriou, D. N.,Jorgensen, J. D., in: *Colossal Magnetoresistive Oxides*, Tokura, Y., (Ed.), Gordon and Breach Science Publishers, The Netherlands [2000].

[Miw00] Miwa, Y., Yamamoto, A., Oda, K., Otsuka, H., *Trans. Mater. Res. Soc. Jpn.* **25**, 1057 [2000].

[Mor01] Morales, L., Caneiro, A., Sánchez, R. D., Vega, D., *J. Magn. Magn. Mater.* **226-230**, 806 [2001].

[Mor02a] Morales, L., Caneiro, A., Vega, D., Zysler, R., Lanza, H., Mercader, R. C., *J. Solid State Chem.* **168**, 100 [2002].

[Mor02b] Morales, L., Zysler, R., Caneiro, A., *Physica B* **320**, 100 [2002].

[Mul74] Muller, O., Roy, R., in: *The Major Ternary Structural Families*, Springer-Verlag, Heidelberg [1974].

[Mul76] Mulay, L. N., in: *Theory and Applications of Molecular Paramagnetism*, Boudreaux, E. A., Mulay, L. N., (Eds.), John Wiley & Sons, New York [1976].

[Myd93] Mydosh, J. A., in: *Spin Glasses: An Experimental Introduction*, Taylor & Francis, London, [1993].

[Nak68] Nakayama, S., Nakagawa, T., Nomura, S., *J. Phys. Soc. Jpn.* **24**, 219 [1968].

[Nar82] Narasimhan, V., Seshan, K., Chakrabarty, D. K., Keer, H. V., *phys. stat. sol. (a)* **70**, K155 [1982].

[Nar85] Narasimhan, V., Keer, H. V., Chakrabarty, D. K., *phys. stat. sol. (a)* **89**, 65 [1985].

[Nis95] Nishimori, N., Asai, K., Mizoguchi, M., *J. Phys. Soc. Jpn.* **64**, 1326 [1995].

[Ng76] Ng, K. T., Hercules, D. M., *J. Phys. Chem.* **80**, 2094 [1976].

[Oda02] Oda, K., Miwa, Y., Ohtsuka, H., *Hyperfine Interactions* **139/140**, 569 [2002].

[Oku75] Oku, M., Hirokawa, H., Ikeda, S., *J. Electron Spectrosc. Relat. Phenom.* **7**, 465 [1975].

[Par97] Park, J.-H., Cheong, S-W., Chen, C. T., *Phys. Rev. B* **55**, 11072 [1997].

[Par99] Park, J.-H., *Phys. Rev. B* **60**, 7651 [1999].

[Pat02] Patil, K. C., Aruna, S. T., Mimani, T., *Curr. Opin. Solid State Mater. Sci.* **6**, 507 [2002].

[Pau00] Paulsen,J. M., Thomas, C. L., Dahna, J. R., *J. Electrochem. Soc.* **147**, 861 [2000].

[Pen01] Peña, A., Gutiérrez, J., Rodríguez-Martínez, L. M., Barandiarán, J. M., Hernández, T., Rojo, T., *J. Phys.: Condens. Matter* **13**, 6535 [2001] .

[Pic98] Pickett, W. E., *Phys. Rev. B* **57**, 10613 [1998].

[Pis97] Pissas, M., Kallias, G., Devlin, E., Simopoulos, A., Niarchos, D., *J. Appl. Phys.* **81**, 5770 [1997].

[Por99] Porta, P., Rossi, S. D., Faticanti, M., Minelli, G., Pettiti, I., Lisi, L., Turco, M., *J. Solid State Chem.* **146**, 291 [1999].

[Ram00] Ramesha, K., Thangadurai, V., Sutar, D., Subramanyam, S. V., Subbanna, G. N., Gopalakrishnan, J., *Mater. Res. Bull.* **35**, 559 [2000].

[Rao94] Rao, C. N. R., in: *Chemical Approaches to the synthesis of Inorganic Materials*, Wiley Eastern Ltd., New Delhi, [1994].

[Rav98] Raveau, B., Maignan, A., Martin, C., Hervieu, M., in: *Colossal Magnetoresistance, Charge Ordering and Related Properties of Manganese Oxides*, Rao, C. N. R., Raveau, B., (Eds.), World Scientific, Singapore [1998].

[Rit97] Ritter, C., Ibarra, M. R., De Teresa, J. M., Algarabel, P. A., Marquina, C., Blasco, J., García, J., Oseroff, S., Cheong, S-W., *Phys. Rev. B* **56**, 8902 [1997].

[Roy97] Roy, S. B., Pradhan, A. K., Chaddah, P., Park, J. G., *Phil. Mag. B* **75**, 303 [1997].

[Sah02] Sahu, R. K., Rao, M. L., Manoharan, S. S., Dörr, K., Müller, K.-H., *Solid State Commun.* **123**, 217 [2002].

[Sah03] Sahana, M., Venimadhav, A., Hegde, M. S., Nenkov, K., Rößbler, U. K., Dörr, K., Müller, K.-H., *J. Magn. Magn. Mater.* **260**, 361 [2003].

[Sai95] Saitoh, T., Bocquet, A. E., Mizokawa, T., Namatame, H., Fujimori, A., Abbate, M., Takeda, Y.,Takano, M., *Phys. Rev. B* **51**, 13942 [1995].

[Sai97a] Saitoh, T., Mizokawa, T., Fujimori, A.,Abbate, M., Takeda, Y.,Takano, M., *Phys. Rev. B* **55**, 4257 [1997].

[Sai97b] Saitoh, T., Mizokawa, T., Fujimori, A., Abbate, M., Takeda, Y., Takano, M., *Phys. Rev. B* **56**, 1290 [1997].

[Sam01] Ray, S., Kumar, A., Majumdar, S., Sampathkumaran E. V., Sarma, D. D., *J. Phys.: Condens. Matter 13*, 607 [2001].

[San01] Sánchez, M. C., Subías, G., Pérez-Cacho, J., García, J., Blasco, J., *J. Synchrotron Rad.* **8**, 901 [2001].

[San02] Sánchez, M. C., García, J., Blasco, J., Subías, G., Pérez-Cacho, J., *Phys. Rev. B* **65**, 144409 [2002].

[Sar94] Sarma, D. D., Rader, O., Kachel. T., Chainani, A., Mathew, M., Holldack, K., Gudat, W., Eberhardt, W., *Phys. Rev. B* **49**, 14238 [1994].

[Sar96] Sarma, D. D., *J. Electron Spectrosc. and Relat. Phenom.* **78**, 37 [1996].

[Sch00] Schinzer, C., *J. Phys. Chem. Solids* **61**, 1543 [2000].

[Sen95] Señarís-Rodríguez, M. A., Goodenough, J. B., *J. Solid State Chem.* **118**, 323 [1995].

[Sha76] R.D. Shannon, *Acta Crystallogr. A* **32**, 751 [1976].

[Sle72] Sleight, A. W., Weiher, J. F., *J. Phys. Chem. Solids* **33**, 679 [1972].

[Sma66] Smart, J. S., in: *Effective Field Theories of Magnetism*, W. B. Saunders Company, Philadelphia [1966].

[Sok02] Sokhey, K. J. S., Chaudhary, S., Chattopadhyay, M. K., Roy, S. B., *Solid State Commun.* **121**, 543 [2002].

[Son92] Sonobe, M., Asai, K., *J. Phys. Soc. Jpn.* **61**, 4193 [1992].

[Sta85] Stauffer, D., in: *Introduction to Percolation Theory*, Taylor and Francis, London [1985].

[Sto97] Stojanovic, M., Haverkamp, R. G., Mims, C. A., Moudallal, H., Jacobson, A. J., *J. Catal.* **166**, 315 [1997].

[Sun00] Sun, Y., Xu, X., Tong, W., Zhang, Y., *Appl. Phys. Lett.* **77**, 2734 [2000].

[Sun01] Sun, Y., Tong, W., Xu, X., Zhang, Y., *Phys. Rev. B* **63**, 174438 [2001].

[Tab98] Tabata, K., Hirano, Y., Suzuki, E., *Appl. Catal. A:* **170**, 245 [1998].

[Tag78] Taguchi, H., Shimada, M., Koizumi, M., *Mater. Res. Bull.* **13**, 1225 [1978].

[Tag99] Taguchi, H., Matsu-ura, S.-I., Nagao, M., Kido, H., *Physica B* **270**, 325 [1999].

[Tal01] Talik, E., Novosselov, A., Kulpa, M., Pajaczkowska, A., it J. Alloys Comp. **321**, 24 [2001].

[Tan99] Tanaka, H., Okawa, N., Kawai, T., *Solid State Commun.* **110**, 191 [1999].

[Tan02] Tan, R., Zhu, Y., Feng, J., Ji, S., Cao, L., *J. Alloys Comp.* **337**, 282 [2002].

[Tep00a] Teplykh, A. E., Pirogov, A. N., Men'shikov, A. Z., Bazuev, G. V., *Physica B* **276-278**, 574 [2000].

[Tep00b] Teplykh, A. E., Pirogov, A. N., Men'shikov, A. Z., Bazuev, G. V., *Phys. Solid State* **42**, 2241 [2000].

[Ter00] Terakura, K., Solovyev, I. V., Sawada, H., in: *Colossal Magnetoresistive Oxides*, Tokura, Y., (Ed.), Gordon and Breach Science Publishers, The Netherlands [2000].

[The76] *Theory and Applications of Molecular Paramagnetism*, Boudreaux, E. A., Mulay, L. N., (Eds.), John Wiley & Sons, New York [1976].

[Tho00] Thomas, A. G., Flavell, W. R., Dunwoody, P. M., Mitchell, C. E. J., Warren, S., Grice, S. C., Marr, P. G. D., Jewitt, D. E., Khan, N., Dhanak, V. R., Teehan, D., Seddon, E. A., Asai, K., Koboyashi, Y., Yamada, N., *J. Phys.: Condens. Matter* **12**, 9259 [2000].

[Tom00] Tomioka, Y., Okuda, T., Okimoto, Y., Kumai, R., Kobayahi, K. -I., Tokura, Y., *Phys. Rev. B* **61**, 422 [2000].

[Top97a] Töpfer, J., Goodenough, J. B., *J. Solid State Chem.* **130**, 117 [1997].

[Top97b] Töpfer, J., Goodenough, J. B., *Eur. J. Solid State Inorg. Chem.* **34**, 467 [1997].

[Tro97] Troyanchuk, I. O., Samsonenko, N. V., Shapovalova, E. F., Szymczak, H., Nabialek, A., *Mat. Res. Bull.* **32**, 67 [1997].

[Tro00] Troyanchuk, I. O., Lobanovsky,L. S., Khalyavin, D. D., Pastushonok, S. N., Szymczak, H., *J. Magn. Magn. Mater.* **210**, 63 [2000].

[Ued98] Ueda, K., Tabata, H., Kawai, T., *Science* **280**, 1064 [1998].

[Ued99] Ueda, K., Tabata, H., Kawai, T., *Phys. Rev. B* **60**, R12561 [1999].

[Ued01] Ueda, K., Muraoka, Y., Tabata, H., Kawai, T., *Appl. Phys. Lett.* **78**, 512 [2001].

[Van39] van Vleck, J. H., *J. Chem. Phys.* **7**, 72 [1939].

[van82] van Duyneveldt, A. J., J. Appl. Phys. **53**, 8006 [1982].

[Van91] van Elp, J., Wieland, J. L., Eskes, H., Kuiper, P., Sawatzky, G. A., de Groot, F. M. F., Turner, T. S., *Phys. Rev. B* **44**, 6090 [1991].

[Van99] van Elp, J., *Phys. Rev. B* **60**, 7649 [1999].

[Vas84] Vasanthacharya, N. Y., Ganguly, P., Goodenough, J. B., Rao, C. N. R., *J. Phys. C: Solid State Phys.* **17**, 2745 [1984].

[Vas89] Vasanthacharya, N. Y., Raychaudhuri, A. K., Ganguly, P., Rao, C. N. R., *J. Magn. Magn. Mater.* **81**, 133 [1989].

[Veg21] Vegard, L., *Z. Kristallogr.* **6**, 239 [1921].

[Ver02] Vertruyen, B., Hébert, S., Maignan, A., Martin, C., Hervieu, M., Raveau, B., *Cryst. Engineering* **5**, 299 [2002].

[Vog77] Vogel, E. M., Johnson, JR., D. W., Gallagher, P. K., *J. Am. Ceram. Soc.* **60**, 31 [1977].

[Wak01] Wakeshima, M., Izumiyama, Y., Doi, Y., Hinatzu, Y., *Solid State Commun.* **120**, 273 [2001].

[Was97] Washburn, N. R., Stacy, A. M., Portis, A. M., *Appl. Phys. Lett.* **70**, 1622 [1997].

[Was00] Washburn, N. R., Stacy, A. M., Portis, A. M., *J. Phys. Chem. B* **104**, 1447 [2000].

[Wol55] Wollan, E. O., Koehler, W. C., *Phys. Rev.* **100**, 545 [1955].

[Wol58] Wold, A., Arnott, R. J., Goodenough, J. B., *J. Appl. Phys.* **29**, 387 [1958].

[Wol59] Wold, A., Arnott, R. J., *J. Phys. Chem. Solids* **9**, 176 [1959].

[Won85] Wong, Po-zen., von Molnar, S., Palstra, T. T. M., Mydosh, J. A., Yoshizawa, H., Shapiro, S. M., Ito, A., *Phys. Rev. Lett.* **55**, 2043 [1985].

[Wu94] Wu, Y., Yu, Z., Liu, S., *J. Solid State Chem.* **112**, 157 [1994].

[Yak55] Yakel, H. L., Acta Cryst. **8**, 394 [1955].

[Yam02] Yamamoto, A., Oda, K., *J. Phys.: Condens. Matter* **14**, 1075 [2002].

[Yan99] Yang, Z., Ye, L., Xie, X., *Phys. Rev. B* **59**, 7051 [1999].

[Yan00a] Yang, Z., Ye, L., Xie, X., *phys. stat. sol. (b)* **220**, 885 [2000].

[Yan00b] Yang, Z., Ye L., Xie, X., *J. Phys.: Condens. Matter* **12**, 2737 [2000].

[Zen51] Zener, C., *Phys. Rev.* **82**, 403 [1951].

[Zha00] Zhang, L.W., Feng, G., Liang, H., Cao, B.S., Meihong Z., Zhao, Y.G., *J. Magn. Magn. Mater.* **219**, 236 [2000].

[Zho99] Zhou, J. P., McDevitt, J. T., Zhou, J. S., Yin, H. Q., Goodenough, J. B., Gim, Y., Jia, Q. X., *Appl. Phys. Lett.* **75**, 1146 [1999].

[Zho01] Zhou, J.-S., Yin, H. Q., Goodenough, J. B., *Phys. Rev. B* **63**, 184423 [2001].

List of Publications

1. Joly, V. L. J., Joy, P. A., Date, S. K., Gopinath, C. S., "The Origin of ferromagnetism in two different phases of $LaMn_{0.5}Co_{0.5}O_3$ evidence from x-ray photoelectron spectroscopic studies" *J.Phys.:Condens.Matter* **13**, 649 [2001].

2. Joly, V. L. J., Joy, P. A., Date, S. K., "Magnetic properties of Co-rich compositions ($x > 0.5$) in the$LaMn_{1-x}Co_xO_3$ Series" *J.Phys.:Condens.Matter* **13**, L841 [2001].

3. Joly, V. L. J., Khollam, Y. B., Joy, P. A., Gopinath, C. S., Date, S. K., "Unusual charge disproportionation and associated magnetic behavior in nanocrystalline $LaMn_{0.5}Co_{0.5}O_3$" *J.Phys.:Condens.Matter* **13**, 11001 [2001].

4. Joly, V. L. J., Joy, P. A., Date, S. K., "Synthesis of two different ferromagnetic phases of $RMn_{0.5}Co_{0.5}O_3$ (R=Pr,Nd,Sm) by a low temperature method" *Mater. Lett.* **51**, 172 [2001].

5. Joly, V. L. J., Joy, P. A., Date, S. K., "Comment on '$La_{0.95}Mg_{0.05}MnO_3$: an ideal ferromagnetic system?'" *J.Phys.:Condens.Matter* **13**, 6433 [2001].

6. Joly, V. L. J., Joy, P. A., Date, S. K., "Comment on 'Giant magnetoresistance of the $La_{1-x}Ag_xMnO_3$ polycrystalline inhomogeneous granular system' [Appl. Phys. Lett. 77, 723 (2000)]" *Appl. Phys. Lett.* **78**, 3747 [2001].

7. Joly, V. L. J., Joy, P. A., Date, S. K., "Effect of R on the magnetic transition temperature of $RMn_{0.5}Co_{0.5}O_3$" *Solid State Commun.* **121**, 219 [2002].

8. Joly, V. L. J., Joy, P. A., Date, S. K., "Studies on the effect of substitution of tetravalent ions for La^{3+} in $LaMnO_3$" *J.Magn. Magn. Mater.* **247**, 316 [2002].

9. Joly, V. L. J., Joy, P. A., Date, S. K., Gopinath, C. S., "Two ferromagnetic phases with different spin states of Mn and Ni in $LaMn_{0.5}Ni_{0.5}O_3$" *Phys. Rev. B* **65**, 184416 [2002].

10. Joly, V. L. J., Joy, P. A., Date, S. K., "Observation of three different ferromagnetic phases with predictable T_cs in $La_2MnCo_{0.5}Ni_{0.5}O_6$" *J.Phys.:Condens. Matter* **15**, L243 [2003].

11. Joly, V. L. J., Bhame, S. D., Joy, P. A., Date, S. K., "Magnetic properties of $La_2MnCo_{1-x}Fe_xO_6$" *J.Magn. Magn. Mater.* **261**, 433 [2003].

12. Joly, V. L. J., Date, S. K., Joy, P. A., "Role of the rare-earth ion on the strength of the ferromagnetic exchange interactions in $RMn_{0.5}M_{0.5}O_3$(M=Co, Ni)" *J.Phys.:Condens. Matter* **16**, 155 [2004].

13. Joly, V. L. J., Date, S. K., Joy, P. A., "Metastable ferromagnetic phases with predictable T_cs in $La_2MnCo_{1-x}Ni_xO_6$" *Solid State Commun.* **130**, 547 [2004].

Awards

"Keerti Sangoram Endowment Award" by the National Chemical Laboratory Research Foundation, for the best research scholar of the year 2003, of NCL, in Physical/Material Sciences.

Symposia and Conferences

1. Joly, V. L. J., Joy, P. A., Date, S. K., "Existence of Two Ferromagnetic Phases in $RMn_{0.5}Co_{0.5}O_3$ (R = rare earth ion)", Oral presentation, National Conference and Symposium on Solid State Chemistry and Allied areas, Dept. of Chemistry, IIT Kanpur, India, December [2001].

2. Joly, V. L. J., Joy, P. A., Date, S. K., "Rare-earth ionic size effect on the strength of ferromagnetic exchange in $REMn_{0.5}$ $M_{0.5}O_3$ (M = Co, Ni)", Poster presentation, International Symposium on Recent Advances in Inorganic Materials, IIT Bombay, India, December [2002].

3. Joly, V. L. J., Joy, P. A., Date, S. K., "Unusual effects of Fe and Ni ions on the strength of ferromagnetism in $La_2MnCo_{1-x}M_xO_6$ (M = Fe, Ni)", Oral presentation, RSC-West India Section Students Symposium, NCL Pune, India, September [2003].

4. Joly, V. L. J., Joy, P. A., Date, S. K., "Tunable Ferromagnetism in the La_2Mn $Co_{1-x}Ni_xO_6$ Series", Oral presentation, Raman Memorial Conference, Dept. of Physics, University of Pune, India, February [2004].

5. Joly, V. L. J., Date, S. K., Joy, P. A.,"Tunable Ferromagnetism in the La_2Mn $Co_{1-x}Ni_xO_6$ Series", Poster presentation, Condensed Matter and Materials Physics Conference(CMMP04), University of Warwick, United Kingdom, April [2004].

Workshops

1. IUPAC Workshop on "Advanced Materials-II: Nanostructured advanced materials", JNCASR Bangalore, India, February [2002].

2. X^{th} Workshop on "Neutrons as Probes of Condensed Matter", BARC Bombay, India, March [2002].